The synthesis of one-dimensional platinum complexes : mechanistic studies from multinuclear NMR
by Stephen Oliver Dunham

A thesis submitted in partial fulfillment of the requirements for the degree of Doctor of Philosophy in . Chemistry
Montana State University

Abstract:
When aqueous solutions of Pt(IV) and Pt(II) oxalato or cyanato complexes are allowed to react, polymeric chains of mixed valence Pt compounds are formed. The polymeric chains are one-dimensional conductors with Pt-Pt distances of 2.7-2.8 Å. Solutions of these polymeric complexes also contain mixed valence chains. The synthesis and characterization of Pt(II) and Pt(IV) complexes used in the synthesis of onedimensional platinum complexes has been determined by multinuclear 195Pt, 13C and 31P NMR, and x-ray crystallography. Kinetic intermediates in the formation of bis(oxalato) and bis(malonato) complexes include monodentate complexes. Isotopic labeling studies with H2^180 have shown that the oxidation mechanism for Pt(II) complexes by hydrogen peroxide is a rapid two electron transfer. The trans dihydroxobis(oxalato)platinate(IV) complexes gain one hydroxyl from hydrogen peroxide, and the trans hydroxyl from solvent. 180 labeling studies have shown that the trans dihydroxo Pt(IV) complex isomerize to cis dihydroxo Pt(IV) by an intramolecular twist. H20 exchange rates have been measured for trans-diaquobis(oxalato)platinum(IV) by isotopic dilution with H2^18O Kex^298 = 4.4 x 10^-6 sec^-1. This exchange rate is much slower than the polymerization rate for bis(oxalato)platinate one-dimensional complexes. The Pt(IV) complex is not initiating polymerization by H20 exchange for a Pt(H) complex as has been proposed by Krogmann and others. The polymerization of bis(oxalato)platinates is a pH dependent redox process Oxidative titration of bis(oxalato)platinate(II) reveals four stable polynuclear complexes in solution. The complexes have the average oxidation states of +2.25, +2.5, +2.75, and +3.0. The +3.0 species has been identified as a binuclear Pt(III) complex from multinuclear NMR. A facile electron transfer reaction to form Pt(III) complexes is proposed as the key step in initiation of one dimensional polymerization of Pt oxalato complexes.

THE SYNTHESIS OF ONE-DIMENSIONAL PLATINUM COMPLEXES; MECHANISTIC STUDIES FROM MULTINUCLEAR NMR

by

Stephen Oliver Dunham

A thesis submitted in partial fulfillment
of the requirements for the degree

of

Doctor of Philosophy

in

Chemistry

MONTANA STATE UNIVERSITY
Bozeman, Montana

June 1992

APPROVAL

of a thesis submitted by

Stephen Oliver Dunham

This thesis has been read by each member of the thesis committee and has been found to be satisfactory regarding content, English usage, format, citations, bibliographic style, and consistency, and is ready for submission to the College of Graduate Studies.

June 26, 1992
Date

Edwin H. Abbott
Chairperson, Graduate Committee

Approved for the Major Department

June 26, 1992
Date

John R Ames
Head, Major Department

Approved for the College of Graduate Studies

June 30, 1992
Date

Henry J Parsons
Graduate Dean

STATEMENT OF PERMISSION TO USE

In presenting this thesis in partial fulfillment of the requirements for a doctoral degree at Montana State University, I agree that the Library shall make it available to borrowers under rules of the Library. I further agree that copying of this thesis is allowable only for scholarly purposes, consistent with "fair use" as prescribed in the U.S. Copyright Law. Requests for extensive copying or reproduction of this thesis should be referred to University Microfilms International, 300 North Zeeb Road, Ann Arbor, Michigan 48106, to whom I have granted "the exclusive right to reproduce and distribute copies of the dissertation in and from microfilm and the right to reproduce and distribute by abstract in any format."

Signature Stephen O. Jenkins

Date June 26, 1992

TABLE OF CONTENTS

Page

LIST OF TABLES x

LIST OF FIGURES xiii

ABSTRACT xviii

INTRODUCTION 1

Platinum Chemical Reactions 3
Chemistry of Metal-Metal Bond Formation 5
Theoretical Descriptions 5
Experimental Evidence for Metal-Metal Bond 12
Metal-Metal Bonded Platinum Complexes 16
Binuclear Platinum Complexes 16
Polynuclear Platinum Complexes 21
Platinum Cluster Complexes 21
Linear Chain Platinum Blues 24
One Dimensional Platinum Polymers 27
Platinum (II) Polymers 27
Platinum(II) and Platinum(IV) Polymers 33
Platinum(II) and Platinum(III) Polymers 35
Partially Oxidized Pt(II) Polymers 37

EXPERIMENTAL 46

Preparation of Compounds 46
Starting Materials 46
Synthesis of Complexes 46
Potassium Bis(oxalato)platinate(II) Dihydrate(**5**) 46
Potassium Dichlorooxalatoplatinate(II) Hydrate(**3**) 46
Sodium Dichlorooxalatoplatinate(II)(**3**) 47
Tetra-n-butyl Ammonium Salts 47
Potassium and Sodium Bis(malonato)platinate(II)(**13**) 47
Potassium and Sodium *syn*- and *anti*-Bis(2-methylmalonato)platinate(II)(**22,23**) 48
Potassium *trans*-dihydroxobis(oxalato)platinate(IV) Hexahydrate(**28**) 48
Potassium *cis*-dihydroxobis(oxalato)platinate(IV) Hydrate(**40**) 49
Sodium *trans*-dihydroxobis(malonato)platinate(IV) Hexahydrate(**31**) . 49

TABLE OF CONTENTS (continued)

Page

Spectroscopy 49
Nuclear Magnetic Resonance 49
Ultraviolet and Visible 51
Oxidative Titrations 52
X-Ray Crystallography 52

RESULTS AND DISCUSSION 54

Reactions of Pt(II) with Dicarboxylic Acids 54
Reaction of Oxalic acid and $K_2[PtCl_4]$(**1**) 56
Nuclear Magnetic Resonance 56

X-Ray Crystallography 61
$K_2[Pt(Ox)Cl_2].H_2O$(**3**) 61
$K_2[Pt(Ox)_2].2\ H_2O$(**5**) 65

Reaction of Oxalic Acid and $[Pt(H_2O)_4]^{2+}$(**6**) 65
Nuclear Magnetic Resonance 65
$[Pt(OxH\text{-}O)(H_2O)_3]^{+}$(**7**) 67
$[Pt(Ox)(H_2O)_2]$(**8**) 67
$[Pt(Ox)(OxH\text{-}O)(H_2O)]^{-}$(**9**) 67

Reaction of Malonic Acid and $K_2[PtCl_4]$(**1**) 70
Nuclear Magnetic Resonance 70
$[Pt(MalH\text{-}O)Cl_3]^{2-}$(**10**) 70
$[Pt(Mal)Cl_2]^{2-}$(**11**) 70
$[Pt(Mal)(MalH\text{-}O)Cl]^{2-}$(**12**) 72
$[Pt(Mal)_2]^{2-}$(**13**) 72

Reaction of Malonic Acid and $[Pt(H_2O)_4]^{2+}$(**6**) 76
Nuclear Magnetic Resonance 76
$[Pt(MalH\text{-}O)(H_2O)_3]^{+}$(**14**) 76
trans-$[Pt(MalH\text{-}O)_2(H_2O)_2]$(**15**) 76
$[Pt(Mal)(H_2O)_2]$(**16**) 78
$[Pt(Mal)(MalH\text{-}O)(H_2O)]^{-}$(**17**) 78

TABLE OF CONTENTS (continued)

Page

Reaction of 2-Methylmalonic Acid and $K_2[PtCl_4]$(1) 78
Nuclear Magnetic Resonance 78
$[Pt(Mmal)Cl_2]^{2-}$(**19**) 79
$[Pt(Mmal)(MmalH\text{-}O)Cl]^{2-}$(**20**) 79
$[Pt(Mmal)(MmalH\text{-}O)Cl]^{2-}$(**21**) 79
syn-$[Pt(Mmal)_2]^{2-}$(**22**) 81
anti-$[Pt(Mmal)_2]^{2-}$(**23**) 81

X-Ray Crystallography 85
K_2*anti*-$[Pt(Mmal)_2].2H_2O$(**23**) 85

Reaction of 2-Methylmalonic Acid and $[Pt(H_2O)_4]^{2+}$(**6**) 90
Nuclear Magnetic Resonance 90
$[Pt(MmalH\text{-}O)(H_2O)_3]^{+}$(**24**) 90
trans-$[Pt(MmalH\text{-}O)_2(H_2O)_2]$(**25**) 90
$[Pt(Mmal)(H_2O)_2]$(**26**) 90
$[Pt(Mmal)(MmalH\text{-}O)(H_2O)]^{-}$(**27**) 90

OXIDATION REACTIONS OF PLATINUM(II) COMPLEXES 93

Hydrogen Peroxide Oxidation 94

Bis(oxalato)platinate(II) 94
Nuclear Magnetic Resonance 94
trans-$[Pt(OH)_2(Ox)_2]^{2-}$(**28**) 94
trans-$[Pt(OH)(OMe)(Ox)_2]^{2-}$(**29**) 97
trans-$[Pt(OH)(OEt)(Ox)_2]^{2-}$(**30**) 97

X-Ray Crystallography 99
Na_2*trans*-$[Pt(OH)_2(Ox)_2].6\ H_2O$(**28**) 99
K_2*trans*-$[Pt(OH)_2(Ox)_2].x\ H_2O$(**28**) 104

Bis(malonato)platinate(II) 105
Nuclear Magnetic Resonance 105
trans-$[Pt(OH)_2(Mal)_2]^{2-}$(**31**) 105

X-Ray Crystallography 105
Na_2*trans*-$[Pt(OH)_2(Mal)_2].6\ H_2O$(**31**) 105

TABLE OF CONTENTS (continued)

Page

Syn- and *Anti*-Bis(2-methylmalonatoplatinate(II) 110
Nuclear Magnetic Resonance 110
anti-trans-$[Pt(OH)_2(Mmal)_2]^{2-}$(**32**) 110
syn-trans-$[Pt(OH)_2(Mmal)_2]^{2-}$(**33**) 110

Dichlorooxalatoplatinate(II) 113
Nuclear Magnetic Resonance 113
trans-cis-$[Pt(OH)_2Cl_2(Ox)_2]^{2-}$(**34**) 113

Tetrachloroplatinate(II) 115
Nuclear Magnetic Resonance 115
trans-$[Pt(OH)_2Cl_4]^{2-}$(**35**) 115

Chlorine Oxidation of Bis(oxalato)platinate(II) 117
Nuclear Magnetic Resonance 117
trans-$[PtCl_2(Ox)_2]^{2-}$(**36**) 117
trans-$[PtCl(H_2O)(Ox)_2]^{-}$(**37**) 117

Bromine Oxidation of Bis(oxalato)platinate(II) 118
Nuclear Magnetic Resonance 118
trans-$[PtCl_2(Ox)_2]^{2-}$(**38**) 118
trans-$[PtCl(H_2O)(Ox)_2]^{-}$(**39**) 118

ISOMERIZATION OF DIHYDROXO PLATINUM(IV) COMPLEXES 120

Trans-dihydroxobis(oxalato)platinate(IV) 120
Nuclear Magnetic Resonance 120
cis-$[Pt(OH)_2(Ox)_2]^{2-}$(**40**) 120
X-Ray Crystallography 123
K_2*cis*-$[Pt(OH)_2(Ox)_2]\cdot x\ H_2O$(**40**) 123

Trans-dihydroxobis(malonato)platinate(IV) 125
Nuclear Magnetic Resonance 125
cis-$[Pt(OH)_2(Mal)_2]^{2-}$(**41**) 126

Syn- and *anti-trans*-dihydroxobis(2-methylmalonato)platinate(IV) 126
Nuclear Magnetic Resonance 126
Cis-$[Pt(OH)_2(Mmal)_2]^{2-}$(**42**) 129
Cis-$[Pt(OH)_2(Mmal)_2]^{2-}$(**43**) 129
Cis-$[Pt(OH)_2(Mmal)_2]^{2-}$(**44**) 129

TABLE OF CONTENTS (continued)

Page

Rate for Trans-Cis Isomerization
Trans-$[Pt(OH)_2(Ox)_2]^{2-}$(**28**) 131
Anti-trans-$[Pt(OH)_2(Mmal)_2]^{2-}$(**32**) 131
Syn-trans-$[Pt(OH)_2(Mmal)_2]^{2-}$(**33**) 131

Mechanism for Trans-Cis Isomerization 131

HYDROXYL, AQUO, AND OXALATO OXYGEN EXCHANGE FOR BIS(OXALATO)PLATINUM(IV) COMPLEXES 140

pKa Measurements for *trans*-$Pt(OH)_2(Ox)_2$ 141

Hydroxyl Oxygen Exchange Rate for *cis*- and *trans*- dihydroxobis(oxalato)platinate(IV) 143

Hydroxyl Oxygen Exchange Rate for *syn*- and *anti-trans*- dihydroxobis(malonato)platinate(IV) 144

Aquo Oxygen Exchange Rate for diaquobis(oxalato)platinum(IV) 144

Oxalato Oxygen Exchange Rate for diaquobis(oxalato)platinum(IV) . . . 149

OXIDATION REACTIONS OF PLATINUM(II) 152

Bis(oxalato)platinate(II) (**5**) 152
Oxidation by Cerium (IV) 152
Potentiometric Studies 152
Ultraviolet and Visible 153
$[Pt(Ox)_2]_n^{175-}$(**45**) 153
$[Pt(Ox)_2]_n^{15-}$(**46**) 154
$[Pt(Ox)_2]_n^{125-}$(**47**) 154
$[Pt_2(Ox)_2(H_2O)_2]^-$(**48**) 154

Oxidation by Diaquobis(oxalato)platinum(IV) 158
Ultraviolet and Visible Studies 158

TABLE OF CONTENTS (continued)

Page

Nuclear Magnetic Resonance 158
$[Pt_2(Ox)_2(H_2O)_2]^-$(**48**) 159
$[Pt_2(Ox)_2(H_2O)_2]^-$(**49**) 161
$[Pt_2(Ox)_2(H_2O)_2]^-$(**50**) 161
$[Pt_2(Ox)_2(H_2O)_2]^-$(**51**) 161

Effect of pH on Oxidation 165

Oxidation Reactions with *trans*-diaquobis(malonato)plainate(IV) . 167
Nuclear Magnetic Resonance 167
$[Pt_2(Ox)_2(H_2O)_2]^-$(**52**) 167
$[Pt_2(Ox)_2(H_2O)_2]^-$(**49**) 168

Oxidation Reactions with Hexachloroplatinate 168
Ultraviolet and Visible Studies 168
Nuclear Magnetic Resonance 168

Tetra(cyanato)platinate(II) 170

Oxidation by *trans*-dibromotetra(cyanato)platinate(IV) 170
Nuclear Magnetic Resonance 170

Diphosphitoplatinate (II) 173
Oxidation by Hexachloroplatinate(IV) 173
Nuclear Magnetic Resonance 173

SUMMARY 174

Pt(III) Polymerization Mechanism 175

REFERENCES CITED 177

LIST OF TABLES

Table		Page
1.	^{13}C NMR Data for Pt(II) Reactions with Oxalic Acid	60
2.	^{195}Pt NMR Data for Pt(II) Reactions with Oxalic Acid	60
3.	Crystallographic Data for $K_2[Pt(Ox)Cl_2]H_2O$	61
4.	Atomic Coordinates and Isotropic Temperature Factors for $K_2[Pt(Ox)Cl_2]H_2O$	63
5.	Bond Lengths for $K_2[Pt(Ox)Cl_2]H_2O$	63
6.	Bond Angles for $K_2[Pt(Ox)Cl_2]H_2O$	64
7.	Anisotropic thermal parameters for $K_2[Pt(Ox)Cl_2]H_2O$	65
8.	^{195}Pt NMR Data for Pt(II) Reactions with Malonic Acid	73
9.	^{13}C NMR Data for Pt(II) Reactions with Malonic Acid	73
10.	^{195}Pt NMR Data for Pt(II) Reactions with 2-Methylmalonic Acid	84
11.	^{13}C NMR Data for Pt(II) Reactions with 2-Methylmalonic Acid	84
12.	Crystallographic Data for K_2*anti*-$[Pt(Mmal)_2]2H_2O$	87
13.	Atomic Coordinates and Isotropic Temperature Factors for K_2*anti*-$[Pt(Mmal)_2]2H_2O$	87
14.	Bond Lengths for K_2*anti*-$[Pt(Mmal)_2]2H_2O$	88
15.	Bond Angles for K_2*anti*-$[Pt(Mmal)_2]2H_2O$	89
16.	Anisotropic thermal parameters for K_2*anti*-$[Pt(Mmal)_2]2H_2O$	89
17.	^{195}Pt NMR Data for Pt(II) Reactions with Hydrogen Peroxide	99
18.	^{13}C NMR Data for Pt(II) Reactions with Hydrogen Peroxide	99
19.	Crystallographic Data for Na_2*trans*-$[Pt(OH)_2(Ox)_2]\cdot 6H_2O$	101

LIST OF TABLES (continued)

Table		Page
20.	Atomic Coordinates and Isotropic Temperature Factors for Na_2*trans*-$[Pt(OH)_2(Ox)_2]6H_2O$	102
21.	Bond Lengths for Na_2*trans*-$[Pt(OH)_2(Ox)_2]6H_2O$	102
22.	Bond Angles for Na_2*trans*-$[Pt(OH)_2(Ox)_2]6H_2O$	103
23.	Anisotropic thermal parameters for Na_2*trans*-$[Pt(OH)_2(Ox)_2]\cdot 6H_2O$	103
24.	Crystallographic Data for Na_2*trans*-$[Pt(OH)_2(Mal)_2]\cdot 6H_2O$	107
25.	Bond Lengths for Na_2*trans*-$[Pt(OH)_2(Mal)_2]\cdot 6H_2O$	107
26.	Atomic Coordinates and Isotropic Temperature Factors for Na_2*trans*-$[Pt(OH)_2(Mal)_2]\cdot 6H_2O$	108
27.	Bond Angles for Na_2*trans*-$[Pt(OH)_2(Mal)_2]\cdot 6H_2O$	109
28.	Anisotropic thermal parameters for Na_2*trans*-$[Pt(OH)_2(Mal)_2]\cdot 6H_2O$	110
29.	^{195}Pt NMR Data for Pt(II) Reactions with Hydrogen Peroxide	111
30.	^{13}C NMR Data for Pt(II) Reactions with Hydrogen Peroxide	113
31.	^{195}Pt and ^{13}C NMR Data for Pt(II) Reactions with Hydrogen Peroxide	117
32.	^{195}Pt NMR Data for Pt(II) Reactions with Chlorine and Bromine	119
33.	Bond Lengths for K_2*cis*-$[Pt(OH)_2(Ox)_2]xH_2O$	123
34.	Bond Angles for Na_2*cis*-$[Pt(OH)_2(Ox)_2]xH_2O$	124
35.	^{195}Pt NMR Data for *cis*-Pt(IV) complexes	129
36.	^{13}C NMR Data for *cis*-Pt(IV) complexes	131
37.	Temperature dependence for the H_2O exchange rate for *trans*-$[Pt(H_2O)_2(Ox)_2]$	148

LIST OF TABLES (continued)

Table Page

38. H_2O exchange rates for several inert transition metal complexes 149

39. UV-vis Data for bis(oxalato)platinate polymers 157

40. ^{195}Pt NMR Data for Pt(III) dimers 167

LIST OF FIGURES

Figure		Page
1.	Substitution Reactions for Pt Complexes	4
2.	Molecular Orbital Diagram for Metal-Metal Bonding Along the z-axis	8
3.	Molecular Orbital Drawings for Small Molecules	10
4.	Molecular Orbital Drawing for a Band Structure	10
5.	Molecular Orbital Diagram for a One-Dimesional Chain Complex	11
6.	X-ray Crystallographic Structures of $[Re_2Cl_8]^{2-}$ and $[Mo_2Cl_8]^{2-}$	14
7.	Nuclear Spin Coupling Manifested by Electron Spin Coupling	15
8.	Lantern Structures for Sulphato and Phosphato Dimeric Pt(III) Complexes	18
9.	Dimeric Pt(III) Complexes with Methyl and Amine Ligands	20
10.	Pyrophosphite and Thioacetate Bridged Dimers	22
11.	Tetra-nuclear Pt Acetate Complexes	23
12.	General Structures for Pt Blues	26
13.	Stuctures of One-dimensional Pt(II) Complexes	29
14.	Metal-Metal Bonded Molecular Orbital Diagram with Configuration Interaction	30
15.	The Structure of Magnus Green Salt	32
16.	Structure of Wolframs Red Salt	34
17.	Pyrophosphito Halide Bridged Polymers	38
18.	$[Pt(CN)_4]^{2-}$ One-Dimensional Polymers	39
19.	Linear Chain Bis(oxalato)platinate Polymer	41

LIST OF FIGURES (continued)

Figure Page

20. Krogmann Mechanism for Polymerization of One-Dimensional Bis(oxalato)platinates 43

21. Structure Comparisons of One-Dimensional Pt Chain Complexes 45

22. ^{195}Pt NMR of the Reaction of $[PtCl_4]^{2-}$ with Oxalic Acid 57

23. ^{195}Pt NMR of the Reaction of $[Pt(Ox)_2]^{2-}$ with KCl 59

24. Thermal ellipsoid plot of $[Pt(Ox)Cl_2]^{2-}$ 64

25. ^{195}Pt NMR of the Reaction of $[Pt(H_2O)_4]^{2+}$ with Oxalic Acid 66

26. ^{195}Pt NMR of Blue $[Pt(Ox)_2]^{2-}$ Solutions 68

27. ^{195}Pt NMR of the Temperature Dependence of the Line Width of $[Pt(Ox)_2]^{2-}$ Blue Solutions 71

28. ^{195}Pt NMR of the Concentration Dependence for $[Pt(Ox)_2]^{2-}$ Blue Solutions 71

29. ^{195}Pt NMR of the Reaction of $[PtCl_4]^{2-}$ with Malonic Acid 74

30. Reaction of $[Pt(Mal)_2]^{2-}$ with KCl 75

31. ^{195}Pt NMR of the Reaction of $[Pt(H_2O)_4]^{2+}$ with Malonic Acid 77

32. ^{195}Pt NMR of the Reaction of $[PtCl_4]^{2-}$ with 2-Methylmalonic Acid 80

33. Idealized Drawings of 2-Methylmalonato Complexes 82

34. ^{1}H NMR Spectra of the Temperature Dependence for *syn*- and *anti*-$[Pt(Mmal)_2]^{2-}$ in Water 83

35. Thermal ellipsoid plot for *anti*-$[Pt(Mmal)_2]^{2-}$ 86

36. ^{195}Pt NMR of the Reaction of $[Pt(H_2O)_4]^{2+}$ with 2-Methylmalonic Acid . . 91

37. Reactions of Pt(II) with Dicarboxylic Acids 92

LIST OF FIGURES (continued)

Figure Page

38. ^{195}Pt NMR of the Reaction of $H_2{}^{16}O_2$ with $[Pt(Ox)_2]^{2-}$ in 50% $H_2{}^{16}O$ / 50% $H_2{}^{18}O$ 96

39. Mechanism for Hydrogen Peroxide Oxidation Pt(II) Complexes 98

40. Thermal ellipsoid plot of *trans*-$[Pt(OH)_2(Ox)_2]^{2-}$ 104

41. Thermal ellipsoid plot of *trans*-$[Pt(OH)_2(Mal)_2]^{2-}$ 109

42. ^{195}Pt NMR of the Reaction of $H_2{}^{16}O_2$ with *syn*- and *anti*-$[Pt(Mal)_2]^{2-}$ in 60% $H_2{}^{16}O$ / 40% $H_2{}^{18}O$ 112

43. ^{195}Pt NMR of *trans-cis*-$[Pt(OH)_2Cl_2(Ox]^{2-}$ 114

44. ^{195}Pt NMR of *trans*-$[Pt(OH)_2Cl_4]^{2-}$ 116

45. ^{195}Pt NMR for the Trans-Cis Isomerization of *trans*-$[Pt(OH)_2(Ox)_2]^{2-}$ in 50% $H_2{}^{16}O$ / 50% $H_2{}^{18}O$ 122

46. Thermal ellipsoid plot of *cis*-$[Pt(OH)_2(Ox)_2]^{2-}$ 125

47. Idealized structures of 2-Methylmalonato Complexes 128

48. ^{195}Pt NMR for the Trans-Cis Isomerization of *syn*- and *anti-trans*-$[Pt(OH)_2(Mmal)_2]^{2-}$ in 50% $H_2{}^{16}O$ / 50% $H_2{}^{18}O$ 130

49. Trans-Cis Isomerization of *anti-trans*-$[Pt(OH)_2(Mmal)_2]^{2-}$ by a Trigonal-bipyramidal mechanism 134

50. Trans-Cis Isomerization of *syn-trans*-$[Pt(OH)_2(Mmal)_2]^{2-}$ by a Trigonal-bipyramidal mechanism 135

51. Trans-Cis Isomerization of *anti-trans*-$[Pt(OH)_2(Mmal)_2]^{2-}$ by a Bailar twist mechanism 137

52. Trans-Cis Isomerization of *syn-trans*-$[Pt(OH)_2(Mmal)_2]^{2-}$ by a Bailar twist mechanism 138

53. Titration of ^{195} chemical shift for *cis*-and *trans*-$[Pt(OH)_2(Ox)_2]^{2-}$ vs pH . 142

LIST OF FIGURES (continued)

Figure Page

54. ^{195}Pt NMR for the H_2O exchange reaction of *trans*-$[Pt(H_2O)_2(Ox)_2]$ in 1 M $HClO_4$ 146

55. Regression plot of H_2O exchange reaction for *trans*-$[Pt(H_2O)_2(Ox)_2]$ at 300K 147

56. Eyring Plot for the H_2O exchange reaction for *trans*-$[Pt(H_2O)_2(Ox)_2]$ . . 148

57. ^{195}Pt NMR for the oxalato oxygen exchange for *trans*-$[Pt(H_2O)_2(Ox)_2]$ in 1 M $HClO_4$ 150

58. ^{195}Pt NMR for the oxalato oxygen exchange for *cis*- and *trans*-$[Pt(H_2O)_2(Ox)_2]$ in 1 M $HClO_4$ 151

59. UV-vis data for the oxidation of $[Pt(Ox)_2]^{2-}$ by Ce(IV) in 1N H_2SO_4 . . . 155

60. UV-vis spectra for the oxidation of $[Pt(Ox)_2]^{2-}$ by Ce(IV) in 1N H_2SO_4 . 156

61. UV-vis spectra for the oxidation of $[Pt(Ox)_2]^{2-}$ by *trans*-$[Pt(H_2O)_2(Ox)_2]$ in 1N H_2SO_4 160

62. UV-vis spectra of the temperature dependence of bis(oxalato)platinate polymers in 1N H_2SO_4 160

63. ^{195}Pt NMR spectra for the oxidation of $[Pt(Ox)_2]^{2-}$ by *trans*-$[Pt(H_2O)_2(Ox)_2]$ in 1M $HClO_4$ 162

64. ^{195}Pt NMR spectrum of $[Pt_2(Ox)_4(H_2O)_2]^{2-}$ showing the possible structures for the Pt(III) complex 163

65. ^{195}Pt NMR for the H_2O exchange reaction of $[Pt_2(H_2O)_2(Ox)_4]^{2-}$ in 60% $H_2{}^{16}O$ / 40% $H_2{}^{18}O$ 164

66. ^{195}Pt NMR spectra for the reaction of $[Pt(Ox)_2]^{2-}$ and *trans*-$[Pt(H_2O)_2(Ox)_2]$ in 1M $HClO_4$ 166

67. UV-vis spectra for the oxidation of $[Pt(Ox)_2]^{2-}$ by $[PtCl_6]^{2-}$ in 1N H_2SO_4 169

68. ^{13}C NMR spectra of the redox reactions of ^{13}C labeled $[Pt(CN)_4]^{2-}$ and *trans*-$[PtBr_2(CN)_4]^{2-}$ 171

LIST OF FIGURES (continued)

Figure Page

69. ^{195}Pt NMR spectra for the formation of one-dimensional tetra(cyanato)platinate polymers 172

70. ^{31}P NMR spectra for the reaction of $[Pt_2(H_2P_2O_5)_4]^{4-}$ with $[PtCl_6]^{2-}$ 173

71. Platinum(III) polymerization mechanism for bis(oxalto)platinate complexes 176

ABSTRACT

When aqueous solutions of Pt(IV) and Pt(II) oxalato or cyanato complexes are allowed to react, polymeric chains of mixed valence Pt compounds are formed. The polymeric chains are one-dimensional conductors with Pt-Pt distances of 2.7-2.8 Å. Solutions of these polymeric complexes also contain mixed valence chains. The synthesis and characterization of Pt(II) and Pt(IV) complexes used in the synthesis of one-dimensional platinum complexes has been determined by multinuclear ^{195}Pt, ^{13}C and ^{31}P NMR, and x-ray crystallography. Kinetic intermediates in the formation of bis(oxalato) and bis(malonato) complexes include monodentate complexes. Isotopic labeling studies with $H_2{}^{18}O$ have shown that the oxidation mechanism for Pt(II) complexes by hydrogen peroxide is a rapid two electron transfer. The trans dihydroxobis(oxalato)platinate(IV) complexes gain one hydroxyl from hydrogen peroxide, and the trans hydroxyl from solvent. ^{18}O labeling studies have shown that the trans dihydroxo Pt(IV) complex isomerize to cis dihydroxo Pt(IV) by an intramolecular twist. H_2O exchange rates have been measured for trans-diaquobis(oxalato)platinum(IV) by isotopic dilution with $H_2{}^{18}O$ $K_{ex}{}^{298} = 4.4 \times 10^{-6}$ sec^{-1}. This exchange rate is much slower than the polymerization rate for bis(oxalato)platinate one-dimensional complexes. The Pt(IV) complex is not initiating polymerization by H_2O exchange for a Pt(II) complex as has been proposed by Krogmann and others. The polymerization of bis(oxalato)platinates is a pH dependent redox process Oxidative titration of bis(oxalato)platinate(II) reveals four stable polynuclear complexes in solution. The complexes have the average oxidation states of +2.25, +2.5, +2.75, and +3.0. The +3.0 species has been identified as a binuclear Pt(III) complex from multinuclear NMR. A facile electron transfer reaction to form Pt(III) complexes is proposed as the key step in initiation of one dimensional polymerization of Pt oxalato complexes.

INTRODUCTION

Interesting chemical properties can result when two or more transition metal ions are combined into one molecule. These new chemical properties can be attributed to the electronic interactions between the closely spaced transition metals. These metal-metal extended interactions can occur through bridging ligands, or by the formation of metal-metal bonds. Extended interactions between transition metals play an important role in several areas of chemistry. These complexes are important as catalysts in organic and biological systems; conduction pathways in electrical conductors; photochemical models for the conversion and storage of solar energy, and they challenge the descriptions of chemical bonding theory (1-3).

The transition metal that was chosen for this study of metal-metal interactions is platinum (Pt). Several advantageous physical and chemical properties, make Pt a fruitful choice among the transition metals. The isolation of stable kinetic intermediates is important for developing mechanistic theory. Often, the only complexes that are observed in transition metal chemistry are the thermodynamic products. With Pt, the kinetic intermediates have been identified for numerous reactions (4). These kinetic intermediates allow for development of new reactions by providing structure function relationships on the pathway to thermodynamic products. If Pt intermediates could be observed, the understanding of metal-metal bond reactions would be greatly advanced (5). An important physical attribute of Pt is that it has a nuclear magnetic resonance (NMR) isotope with favorable nuclear spin properties (6). ^{195}Pt is 33% naturally

abundant, a spin 1/2 nucleus, and it has a receptivity that is 20 times greater than ^{13}C. These properties make ^{195}Pt NMR spectroscopy a high resolution method for solutions of ca $1x10^{-3}$ M. The ^{195}Pt isotope allows the solution chemistry of Pt complexes to be well characterized, and ^{195}Pt NMR spectroscopy is the primary spectroscopic technique used in this research. ^{195}Pt NMR spectroscopy is a sensitive analytical method for studying the environment of the Pt nucleus. ^{195}Pt NMR can obtain information about the oxidation state of the Pt, the number and type of atoms (ligands) bound to the Pt, and the strength of Pt ligand bonds (6). ^{195}Pt NMR can be used to give high resolution structural information. This is important because the structures of Pt complexes can often be clearly reasoned without the use of x-ray crystallography. A noninvasive technique like NMR is essential to the study of solution reactions. This is a distinct advantage for Pt complexes, because the properties of transition metals can be altered when they are isolated in the solid state. ^{195}Pt NMR can circumvent the inability to obtain x-ray quality crystals and can aid in the understanding of complex mixtures of Pt complexes in solution. With this sensitive spectroscopic method for Pt, complex mixtures in solution could be analyzed to understand the chemistry of metal-metal bond formation. A further advantage to Pt chemistry is the large number of Pt metal-metal bonded complexes that have already been characterized to various degrees in the literature (3,7-13). However, the literature provides little information toward the mechanism of Pt metal-metal bond formation. We are now poised with a powerful analytical technique for determining the structure of Pt complexes, and several examples of Pt metal-metal bonded chemistry which can be further investigated.

Platinum Chemical Reactions

The descriptive chemistry of Pt is largely limited to the reactions of the thermodynamically stable Pt(II) and Pt(IV) complexes (4). Pt(II) complexes have four chemical bonds arranged in a square-planar environment around the Pt. Square-planer Pt(II) complexes form new covalent bonds by an associative substitution mechanism with a ligand (Figure 1). Associative reactions can be viewed as the formation of a new Pt-ligand bond from the top of the square-planar complex. This process dictates that a five coordinate intermediate would be found at the transition state for the reaction. This five coordinate intermediate must lose one of its ligands to once again form the stable square-planar complex. This intermediate can have either a trigonal-bipyramidal or square pyramidal geometry. Pt(IV) complexes have six chemical bonds arranged in an octahedral environment around the Pt. Octahedral Pt(IV) complexes form new covalent bonds by a dissociative substitution mechanism (Figure 1). This means that the Pt must first break a bond with ligand and form a five coordinate intermediate. The Pt(IV) intermediate can also have a trigonal-bipyramidal or a square pyramidal geometry. This intermediate can associate with a new ligand to form the stable octahedral complex. Because Pt(IV) complexes need to break a bond with the Pt before a new bond can be formed, octahedral Pt(IV) complexes react much slower than square-planer Pt(II). It has been observed that Pt(IV) complexes undergo substitution reactions more rapidly in the presence of a reducing agent. This is thought to occur by the Pt(IV) undergoing a two electron reduction to the more reactive Pt(II) species. If Pt(II) complexes are in solution

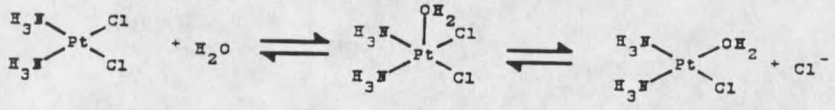

Platinum(II) Substitution Reactions

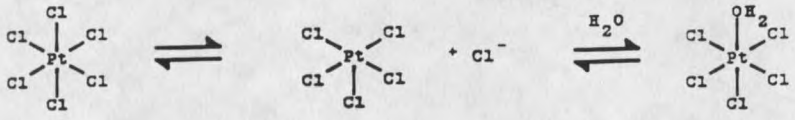

Platinum(IV) Substitution Reactions

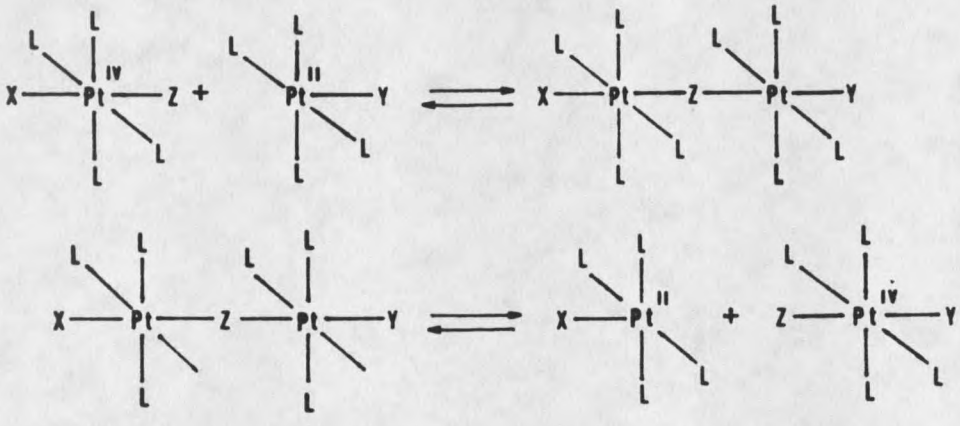

Platinum(IV)::Platinum(II) Catalyzed Reactions

Figure 1 Substitution Reactions for Square Planer Pt(II) and Octahedral Pt(IV) Complexes.

with the Pt(IV), the Pt(II) can act as a two electron reductant for Pt(IV) as shown in Figure 1 (4,5,14) Through this complimentary oxidation/reduction reaction, Pt(II) can catalyze the substitution reactions of Pt(IV).

Chemistry of Metal-Metal Bond Formation

Theoretical Descriptions

The principles of metal-metal bonding are no different than those that are used in main group chemistry. The primary complication in describing metal-metal bond formation is the use of d orbitals, which play the dominant role in transition metal chemistry. There are some common theoretical principles for metal-metal interactions. This theoretical background provides the motivation and protocol for the metal-metal bonding reactions that have been investigated.

When two metals are joined by a bridging ligand or a metal-metal bond, the electronic structure of the single metal complex will be altered. The change in the electronic structure of the metal will be dependent upon the amount of electronic interaction the metal atoms share with each other. More precisely, the electronic interaction between metals is directly related to the amount of orbital overlap between the two metal atoms. A large orbital overlap will delocalize the orbitals of the individual metal complex into a dimer with a unique set of molecular orbitals (MO's). These MO's describe the electronic environment of the metal-metal bonded dimer. If the orbital overlap between metal atoms is less, the electronic structure can be viewed as a hybrid

between the isolated metal complex and the dimeric structure. The hybrid is a linear combination of the two isolated metal complexes with a coefficient that describes the amount of interaction between the metal orbitals. Clearly, the largest coefficients occur when metal atoms are in the dimer, and the smallest coefficients occur when the two metal atoms are monomeric complexes. Complexes which add metal atoms onto the dimer (ie: clusters, linear chains, and colloids) are of great interest because they are intermediate in size between the dimeric complex and the elemental solid. It is important to study complexes of intermediate size. These complexes provide a cohesive link between the chemical properties of molecular solids, and those of the dimer. It is a goal of this work to provide fundamental information toward the synthesis of one-dimensional Pt chain complexes of intermediate size.

The simplest metal-metal interaction to describe would be the interactions of a dimeric species. Metal-metal dimers are known in which the metals are directly bonded to each other, or in which the metals are bridged by an appropriate ligand along the metal-metal axis (15). The direct metal-metal bonded system is of primary importance to these studies. The electronic structures for metal-metal bonded dimer can be depicted by the simplified MO diagram for d orbitals shown in Figure 2 (15). These MO's would result if two metal atoms were allowed to approach each other along the z-axis (ie. M-M < 3Å). The d orbitals of the isolated metal atom will lose their degeneracy and be split into distinct bonding and antibonding levels. The dz^2 orbitals will combine to form σ bonding and σ^* antibonding MO's. The *dxz* and *dxy* orbitals will combine to form two degenerate π bonding and π^* antibonding MO's. The dx^2-y^2 and *dxy* orbitals will form

two degenerate δ bonding and δ^* antibonding MO's. The Pt complexes of interest to this study are not bare metal atoms. The Pt complexes studied will have four to six ligands bonded to Pt. The introduction of four ligands onto each metal will change the symmetry of the dimeric complex to D_4h if the ligands are eclipsed or D_4d if the ligands are staggered. This will affect the MO's of the dimer. The dx^2-y^2 orbital will be stabilized by σ bonds formed with the ligand, and the relative energy will go down for this MO. The metal ligand antibonding orbital dx^2-y^{2*} will replace dx^2-y^2 as the δ bonding orbital between the metals. The dx^2-y^{2*} orbital will be higher in energy than the previous dx^2-y^2 orbital, and it will no longer be degenerate with dxy. By filling the MO's in Figure 2 with valence electrons from each metal, it can be seen that two d^4 metal ions will form the strongest metal-metal bonded complexes. Two d^4 metal atoms will give the electron configuration $\sigma^2\pi^4\delta^2$ which corresponds to a bond order of four (a quadruple bond). Examples of quadruple bonded complexes are $[Re_2Cl_8]^{2-}$ and $[Mo_2Cl_8]^{4-}$ (15). Subsequent addition of electrons to the molecular orbitals of Figure 2 leads to decreasing bond order between the metals until the electron configuration of $\sigma^2\pi^4\delta^2\delta^{*2}\pi^{*4}\sigma^{*1}$ is obtained. This electron configuration would formally have a bond order of 0.5. The simple MO diagram in Figure 2 motivates the following qualitative statements. In general, two transition metals must have seven or fewer electrons in their valence d orbitals to participate in metal-metal bonding interactions. Any metal atom with more than seven electrons must undergo oxidation before metal-metal bonds can be formed. This is important in the reactions of Pt complexes to form metal-metal bonds. Pt(II) complexes have eight d electrons. For Pt(II) complexes to form metal-metal bonded structures, they

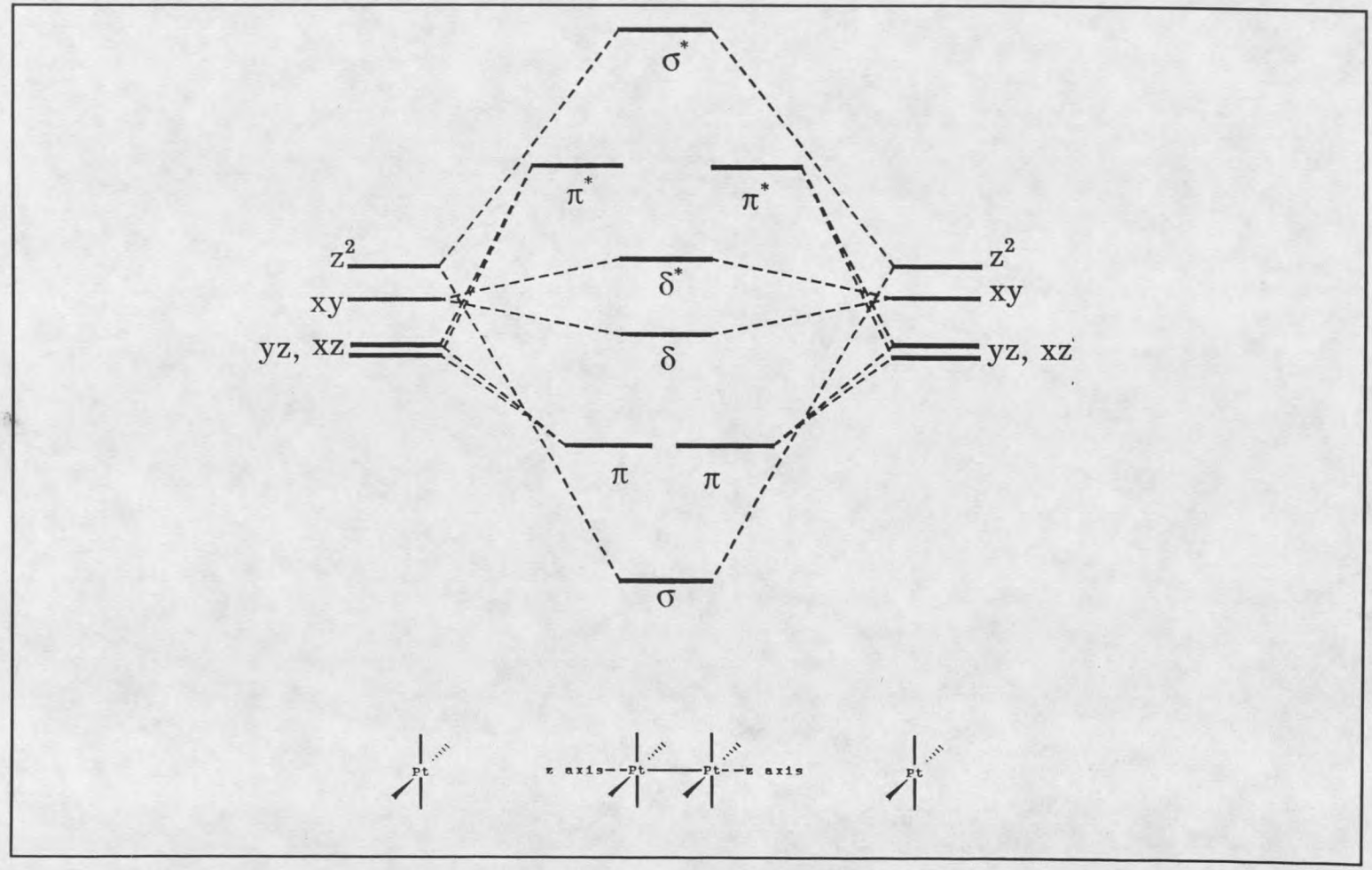

Figure 2 Molecular Orbital Diagram for Metal-Metal Bonding Along the Z-axis (15).

must be oxidized by a minimum of one electron. Pt(IV) complexes have six electrons and do not need to be oxidized to form metal-metal bonded structures.

When more than two metals are joined together in a single complex, the MO's maintain the same general splitting pattern as in Figure 2. The number of MO's that are formed in the multi-atom complex can be obtained from the MO diagram in Figure 2 (16). For the multi atom complex, each MO in Figure 2 is multiplied by the number of atoms that are in the complex. This is somewhat tedious for molecules of intermediate length, but there is nothing different from the dimeric species already described. The complexes of greatest interest to this study are linear chain metal-metal bonded polymers. If the extension of the metal-metal bonds continue in a linear chain of a large number of atoms (Avogadro's number), the d orbitals of the metal will form a series of closely spaced MO's which are known as a band structure (16). Band theory is commonly used to describe electron configurations in molecular solids. If the molecular solid is composed of repeating dimer units along the chain, then the MO's of the band will be a summation of MO's for the dimeric structure. Energy level diagrams for MO band structures are shown in Figures 3, 4, and 5 (16). In Figure 3, the MO band appears as a plot of energy vs MO levels. This representation is often used to describe MO's for small molecules ($<$ 50 atoms). For Avogadro's number of atoms, the drawing in Figure 4 is used. This drawing has the same information as in Figure 3, but it is more practical than drawing the MO's of a solid with an infinite number of atoms. The MO's in Figure 5 represent an idealized one-dimensional chain complex. Again, the polymer is a linear combination of the dimeric units described in Figure 2.

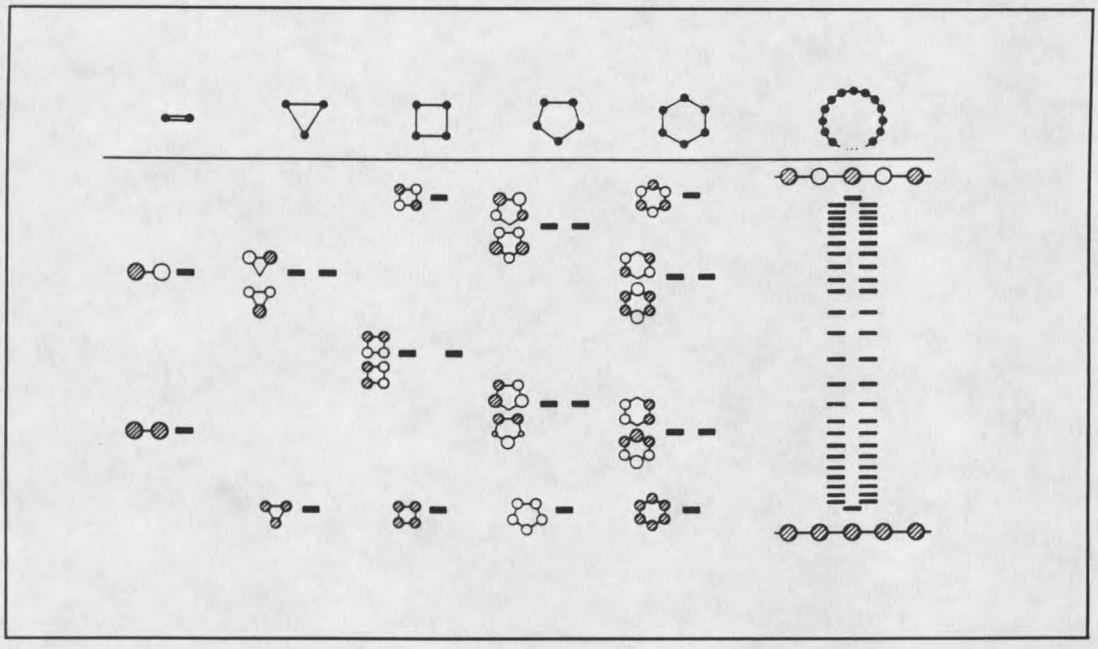

Figure 3 Molecular Orbital Drawings for Small Molecules (16).

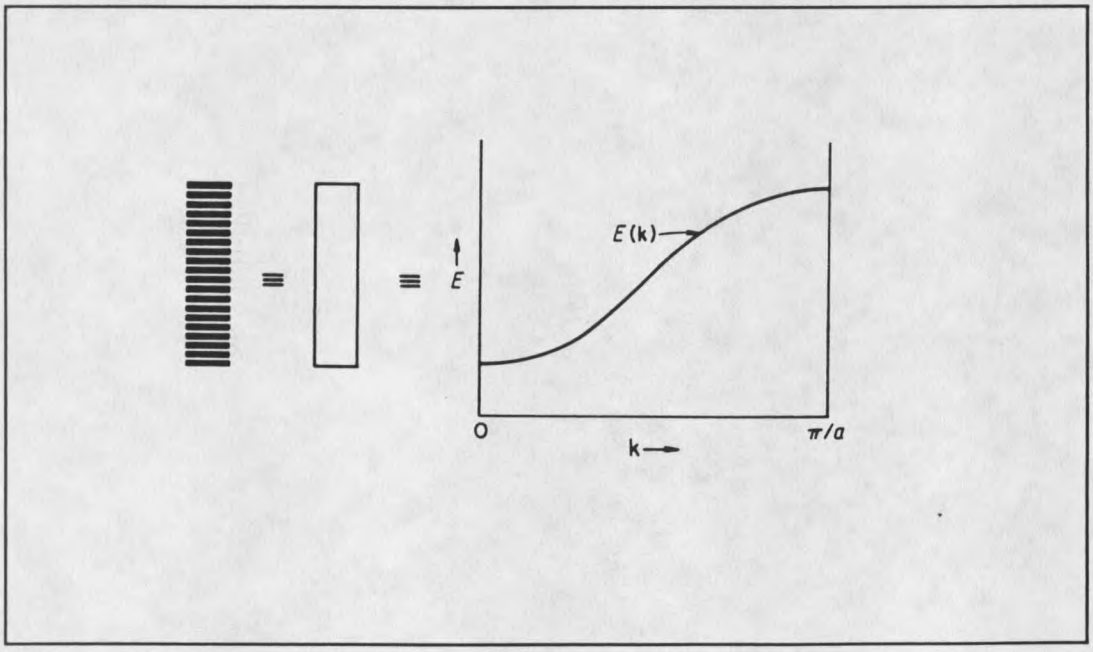

Figure 4 Molecular Orbital Drawing for a Band Structure (16).

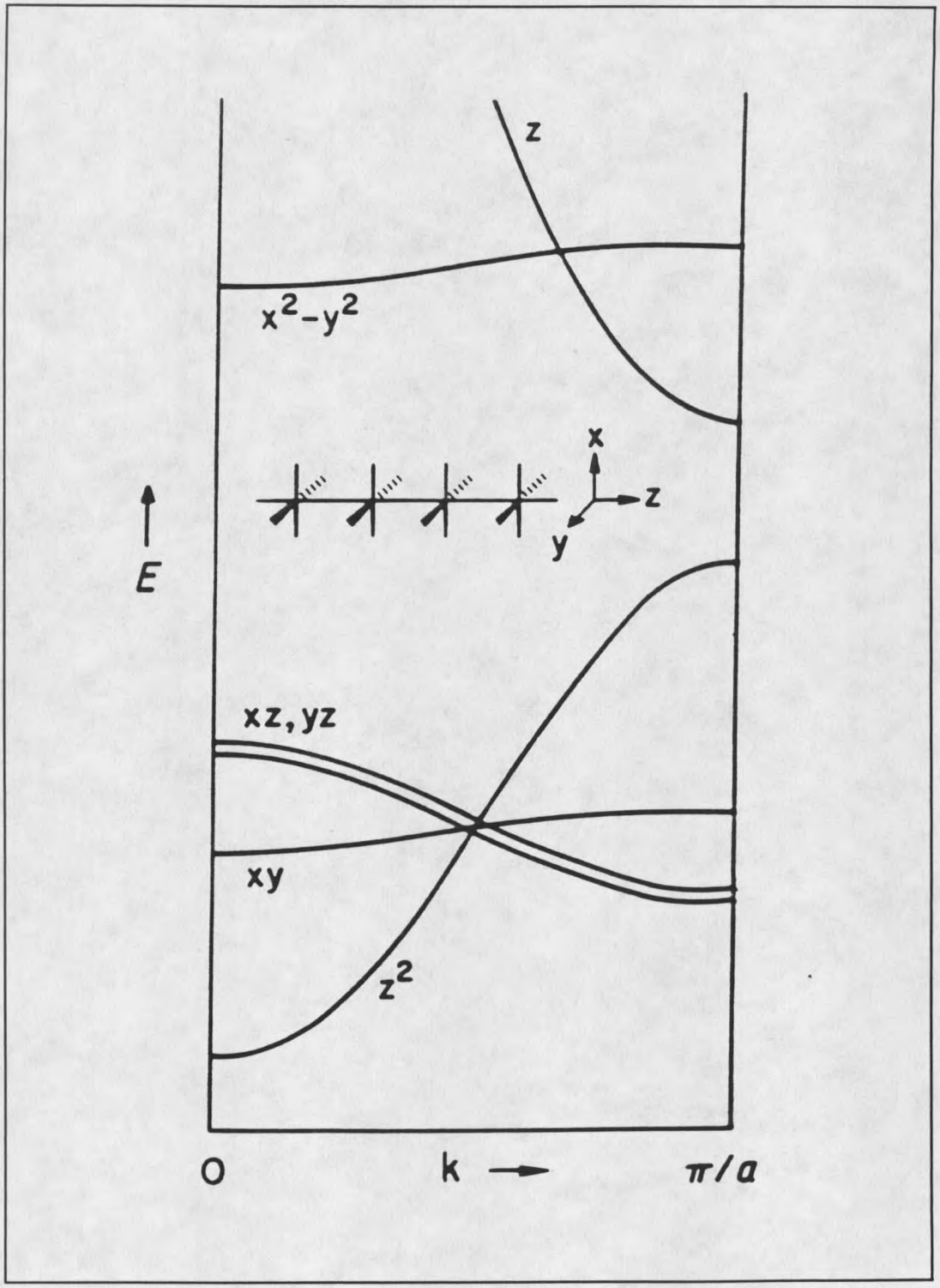

Figure 5 Molecular Orbital Diagram for a One-Dimensional Chain Complex (16)

The presence of low formal charge on the metal is one empirical factor found in highly stabilized transition metal-metal bonded systems. The low formal charge would allow for the maximum expansion of the electrons in the valence orbitals of the metal. As the metal orbitals expand in size, their overlap integral with adjacent metal atom will increase. The metal ligand orbital interactions can also be important to metal-metal bonding. A ligand that can lower the electron density of antibonding orbitals through backbonding can increase the bonding interactions of the metal-metal complex.

Experimental Evidence for
Metal-Metal Bond Formation

Experiments should direct the theory of bonding interactions between metals. Several analytical methods have been used to determine metal-metal interactions. The best indication of a metal-metal bond is the structure of the complex. X-ray crystallography can be used to determine the structure of ordered molecules in a solid. The clearest case for metal-metal bonding is when two metals are adjacent to each other, the metal to metal distance is short, and there are no ligands bridging the two metal centers. $[Re_2Cl_8]^{2-}$ and $[Mo_2Cl_8]^{4-}$ shown in Figure 6 are clear examples of metal-metal bonding (15). Short metal-metal distances are indicative of metal-metal bonding, but one must be cautious about judging metal-metal interactions from distance measurements alone. $[^5n\text{-}CpMo(CO)_3]_2$ has a metal-metal bond of 3.22 Å (15). MoO_2 also has metal-metal bonds between Mo atoms. The MoO_2 complex has Mo-Mo distances of 2.50 Å and 3.10 Å, but the authors assign only one Mo-Mo bond in this complex (15). The short distance of 2.50 Å has been described as the metal-metal bond. The longer Mo-Mo

distance of 3.10 Å is not a metal-metal bond even though the distance is 0.12 Å shorter than in $[^5n\text{-}CpMo(CO)_3]_2$. In general, the length of any metal-metal bond will change as a function of the metal oxidation state, metal-ligand bonds, and steric restraints of the crystal structure.

Measurements of magnetic moment have also been used to describe bonding between two metal atoms. Electron spin pairing between metal atoms is indicative of metal-metal interactions. If the metal atoms form a bond, the spin of the electrons of one metal will be correlated to the electron spin of the other metal. Unfortunately, spin pairing also occurs between metal atoms that are joined by bridging ligands. $[(RuCl_5)_2O]^{4-}$ which has a linear Ru-O-Ru bond has a large interaction between the two metal centers. Cu-O-Cu bridged species are other examples which show antiferomagnetic coupling between the transition metals without the formation of metal-metal bonds.

Nuclear magnetic resonance spectroscopy (NMR) has also been used to indicate the presence of metal-metal interactions. The coupling of nuclear spin angular momenta between two atoms is indicative of the amount of the metal-metal interactions. Nuclear spin coupling is a result of electron correlation between the two atoms (17). It is specific however for electron correlation between s-orbitals of the two spin coupled atoms (Figure 7). The s-orbitals have the greatest non-zero electron integral at the nucleus; and therefore, s-orbital electrons have the greatest interaction with the nuclear spin of the atom. The s-orbital dependence between atoms is known as the "fermi contact integral". The amount of s-orbital overlap between two atoms is expected to be quite significant in cases of metal-metal bonded systems. The presence of large coupling constants between

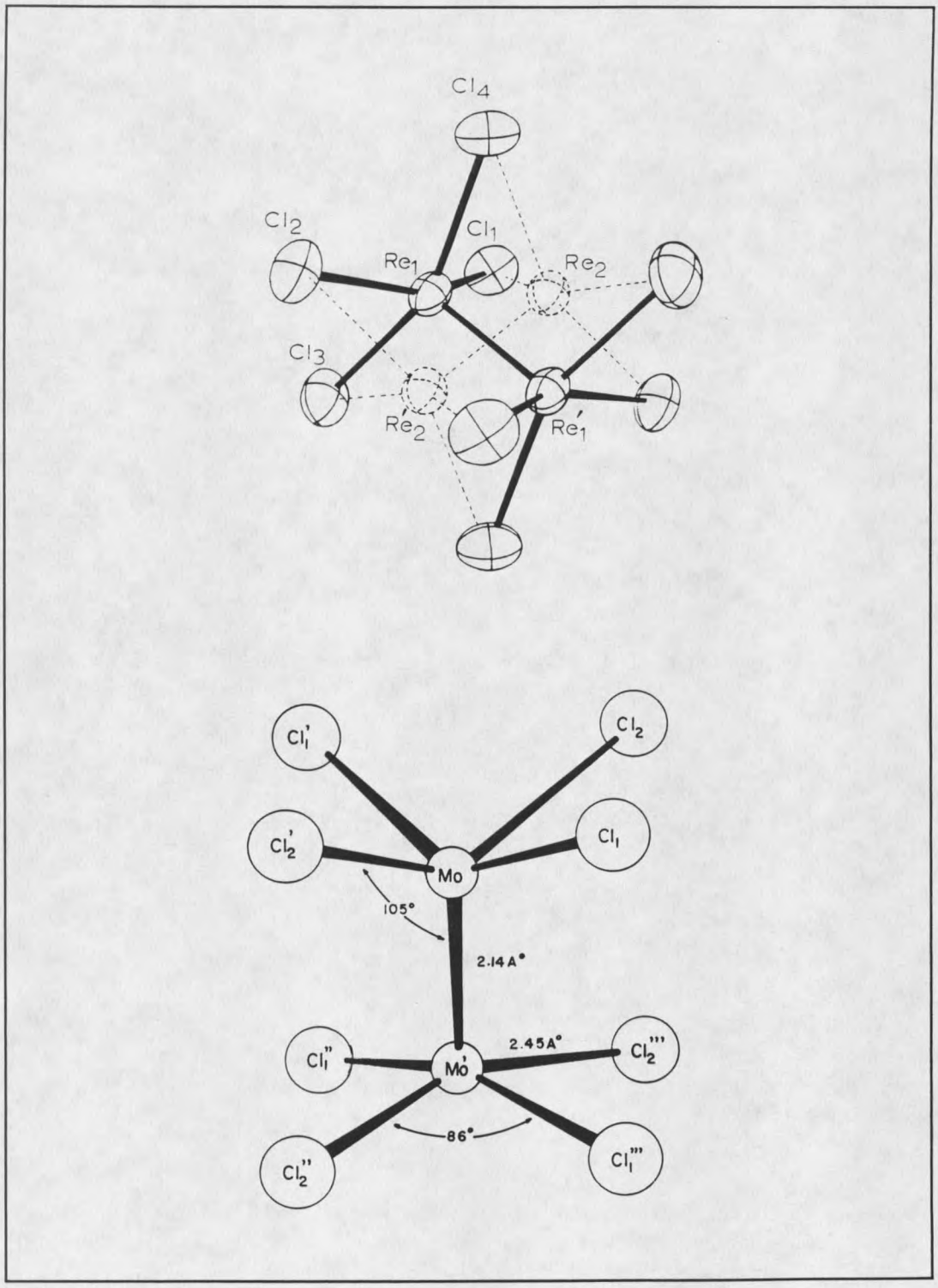

Figure 6 X-ray Crystallographic Structures of $[Re_2Cl_8]^{2-}$ and $[Mn_2Cl_8]^{4-}$ (15).

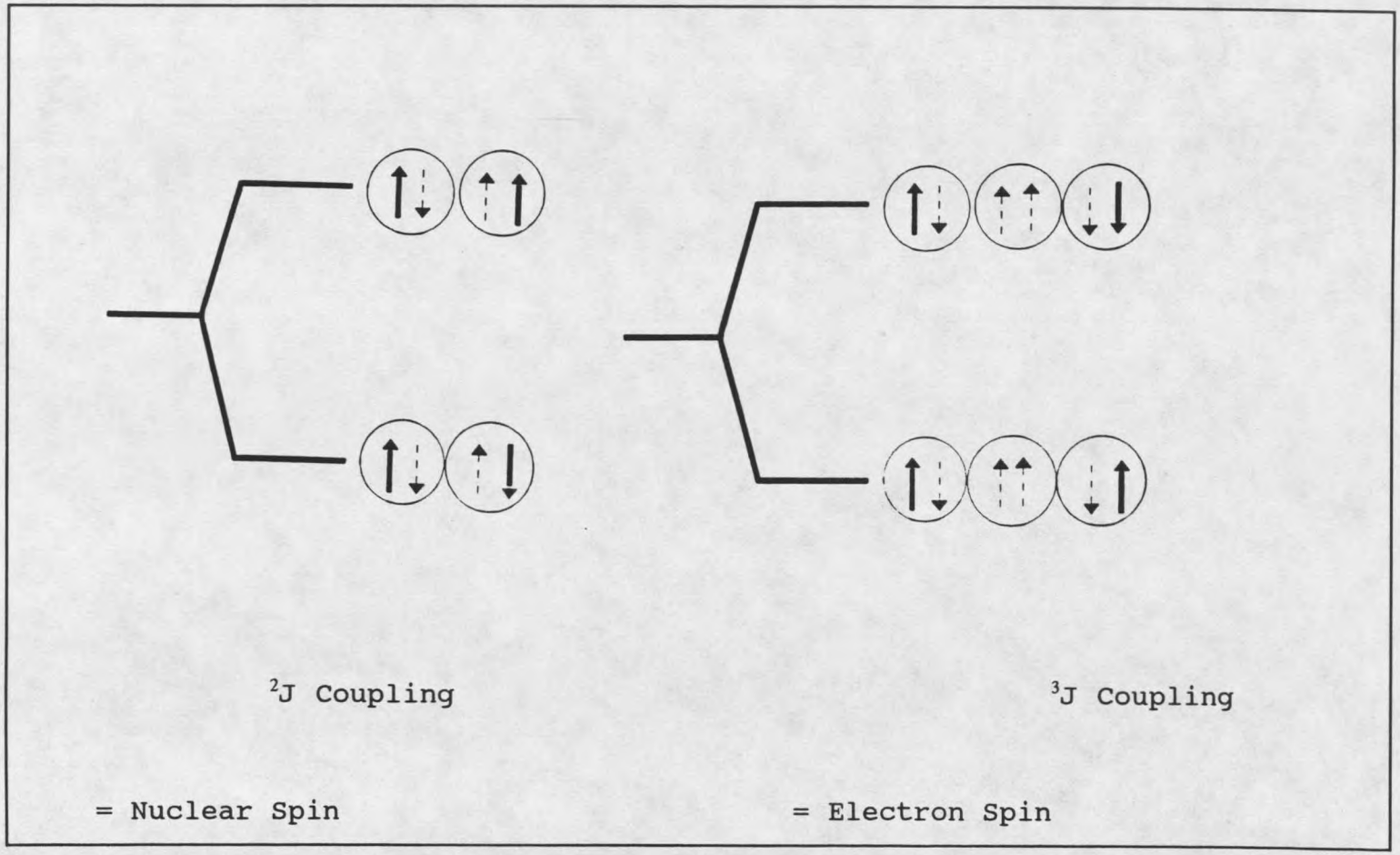

Figure 7 Nuclear Spin Coupling Manifested by Electron Spin Coupling between S Orbital Electrons (17).

nuclear spins is indicative of metal-metal bond formation. ^1J Pt-Pt coupling constants for metal-metal bonded complexes is variable (12,000-3,000 Hz), but the coupling constant is always greater than 3000 Hz for metal-metal bonded Pt complexes (6). However, nuclear spin coupling can also occur through bridging ligands as described earlier for the magnetic moment of the electrons. The interaction between two metal centers is substantially reduced when it occurs through bridging ligands, and the nuclear spin coupling constant for Pt is less than 1000 Hz (6). Metal-metal bonded complexes are intensely colored. $Mn_2(CO)_{10}$ is bright yellow, Re_2Cl_8 is deep blue, $Co_2(CO)_8$ is purple-black, $[Mo_2Cl_8]^{4-}$ is cherry red, and $Fe_2(CO)_9$ is gold (15). The electronic absorption and emission spectra can be informative in the description of metal-metal bonds (18). Electronic transitions between σ-σ^*, π-π^*, and δ-δ^* are all symmetry allowed transitions. These allowed transitions can have large intensities with ϵ values from 10,000-100,000. The absorption often occurs in the ultraviolet and visible region which gives these complexes their intense colors.

Metal-Metal Bonded Platinum Complexes

Binuclear Platinum Complexes

There are several examples of metal-metal interactions between Pt atoms in binuclear and polynuclear complexes. The simplest interaction is the joining of two Pt atoms into a binuclear complex. Binuclear complexes of Pt are found in two varieties. The first type has a metal-metal bond between the Pt atoms. These complexes have the

Pt in the formal oxidation state of Pt(III). A monomeric Pt(III) complex would have the d^7 electron configuration. Combining two isolated Pt(III) complexes into a dimer would fill the molecular orbitals of Figure 2 as $\sigma^2\pi^4\delta^2\delta^{*2}\pi^{*4}$ with a net bond order of one. The first characterized dimeric Pt complexes were the "lantern" structures of $[Pt_2(SO_4)_4(H_2O)_2]^{2-}$, and $[Pt_2(PO_4)_4(H_2O)_2]^{2-}$ shown in Figure 8 (19,20) The term "lantern" is used because the phosphate and sulphate ligands encompass the dimeric unit like the glass flute of a lantern. The axial positions of the Pt(III) dimer are defined to lie along the Pt-Pt bonding axis. These axial positions are labile, and can be readily substituted by ligands in solution (21). When the axial positions are not equivalent, the symmetry of the dimer is broken and each Pt atom of the dimer has unique spectroscopic properties (18,21). The ^{195}Pt NMR readily demonstrates the electron correlation between the Pt atoms in the dimeric structure. The ^1J Pt-Pt coupling constants are 3464 Hz for $[Pt_2(SO_4)_4Cl(H_2O)]^{3-}$, and 5342 Hz for $[Pt_2(PO_4)_4Cl(H_2O)]^{3-}$ (21). The Pt(III) complexes are synthesized by heating $[Pt(NO_2)_4]^{2-}$ in concentrated sulfuric or phosphoric acids in the presence of oxygen. The Pt(II) starting material $[Pt(NO_2)_4]^{2-}$ undergoes oxidation and four sulfate or phosphate ligands bridge the two metal centers. The Pt-Pt bond distance for $[Pt_2(SO_4)_4(H_2O)_2]^{2-}$ is 2.466[?] Å, and the Pt-Pt bond distance for $[Pt_2(PO_4)_4(H_2O)_2]^{2-}$ is 2.486[2] Å (19,20) A "lantern" structure has also been formulated for the tetraacetate bridged Pt(III) dimer. This complex is isolated from a mixture of Pt species formed when $[PtCl_4]^{2-}$ is allowed to react with silver acetate in refluxing acetic acid-H_2O (10:1) (22). Presumably, the silver ion acts as an oxidant on the Pt(II). This complex is different from other known tetraacetates ($[M_2(CH_3COO)_4]$) in that the acetates are not all

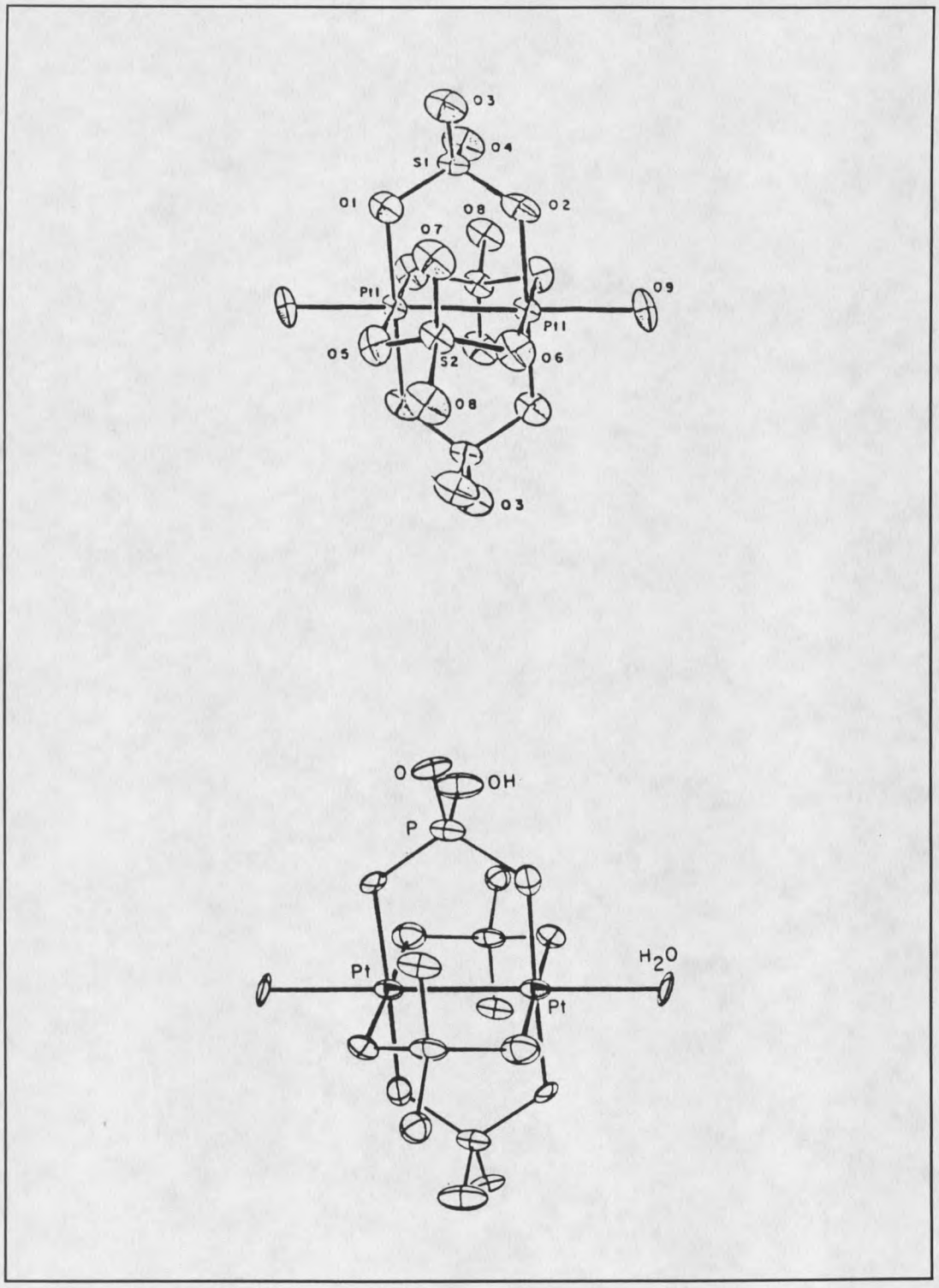

Figure 8 Lantern Structures for Sulphato and Phosphato Dimeric Pt(III) Complexes (19,20).

bound through the oxygen atoms to the Pt (Figure 8). ^{13}C NMR shows two types of "acetate" ligands which is not consistent with a symmetrical "lantern" structure. The authors propose that two acetate ligands are bridging the Pt centers by oxygen and carbon atoms rather than oxygen, oxygen bridging seen for other tetraacetato species. This bridging mode is unique for the Pt-acetates. The Pt-Pt bond distance for $[Pt_2(CH_3COO)_4Cl_2]$ is 2.451[1] Å (22). There is a large class of dimeric Pt(III) complexes which have short metal-metal distances, but do not fit the "lantern" structures. These complexes (Figure 9) have the general formula $[Pt_2(Y)_4(L\text{-}L)_2X_2]$ where Y= NH_3 or CH_3, and L-L is a bridging bidentate nitrogen nitrogen; nitrogen oxygen; or oxygen, oxygen ligand, X= neutral axial ligand, and the Pt is in the 3^+ oxidation state (23,24). The dimethyl complexes are synthesized by allowing the binuclear thiol bridged Pt(II) complex $[(Pt(CH_3)_2)_2(SR_2)_2]$ to react with the silver salt of acetate or hydroxypyriodonate. The silver ion acts as an oxidant and forms a silver mirror on the reaction vessel walls. It is believed that the acetate or hydroxypyridonate bridges the two Pt metal centers before the oxidation takes place. Thallium (Tl) and mercury (Hg) salts have also been used as oxidants in these reactions. The Pt centers will bond two axial ligands if the steric constraints of N-O ligand are not severe (ie. methyl hydroxypyridonate=ligand) (24). The Pt(III) diamine complexes are synthesized by a similar method. These complexes are formed by the oxidation of Pt(II) complexes with the general formula $[Pt_2(NH_3)_4(N\text{-}O)_2]$ by air, or added oxidants (Cl_2, Br_2, or Ce(IV)) (12). Oxidation of binuclear Pt(II) complexes to an oxidation state of less than Pt(III) can result in the formation of tetrameric Pt complexes with variable oxidation states (12).

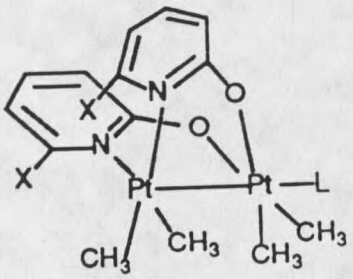

Tetra-methyl Platinum(III) Dimer

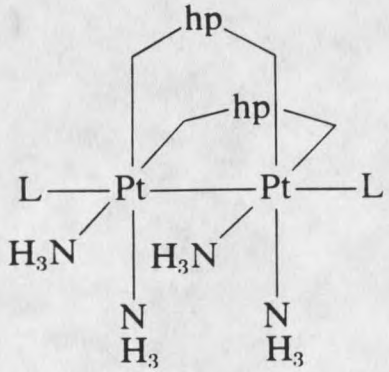

Tetra-amine Platinum(III) Dimer

Figure 9 Dimeric Pt(III) Complexes with Methyl and Amine Ligands (23,24).

These tetrameric Pt complexes will be described later. A further example of dimeric Pt complexes are those formed by the pyrophosphite and thioacetate ligands (Figure 10) (25,26). The pyrophosphite complexes are formed by dehydrating tetrakis-phosphitoplatinum(II) (25). When the phosphite ligands dehydrate, pyrophosphite bonds are formed between two Pt centers. These structures fundamentally fit the "lantern" structure in that there are four pyrophosphite bridges between the two metals. However, the Pt atoms are formally Pt(II), and do not have any significant metal-metal interaction. The Pt-Pt distance for $K_4[Pt_2(H_2P_2O_5)_4].2H_2O$ is 2.925 Å. If the binuclear Pt(II) complex is subjected to oxidizing agents, the Pt atoms undergo a facile electron transfer to form the binuclear metal-metal bonded Pt(III) complex. The Pt-Pt bond length for $K_4[Pt_2(POP)_4Cl_2]$ is 2.695 Å. The binuclear Pt tetra-thioacetates follow a similar chemistry as the Pt pyrophosphites (26). The dinuclear thioacetate complexes are stable as both binuclear Pt(II) complexes, and upon oxidation they form binuclear thioacetate bridged Pt(III) complexes (26).

Polynuclear Platinum Complexes

There are several classifications of Pt complexes which have more than two Pt atoms in the polynuclear complex.

Platinum Cluster Complexes Pt cluster complexes include the tetranuclear Pt acetate species (Figure 11). The tetranuclear Pt acetate complex can be

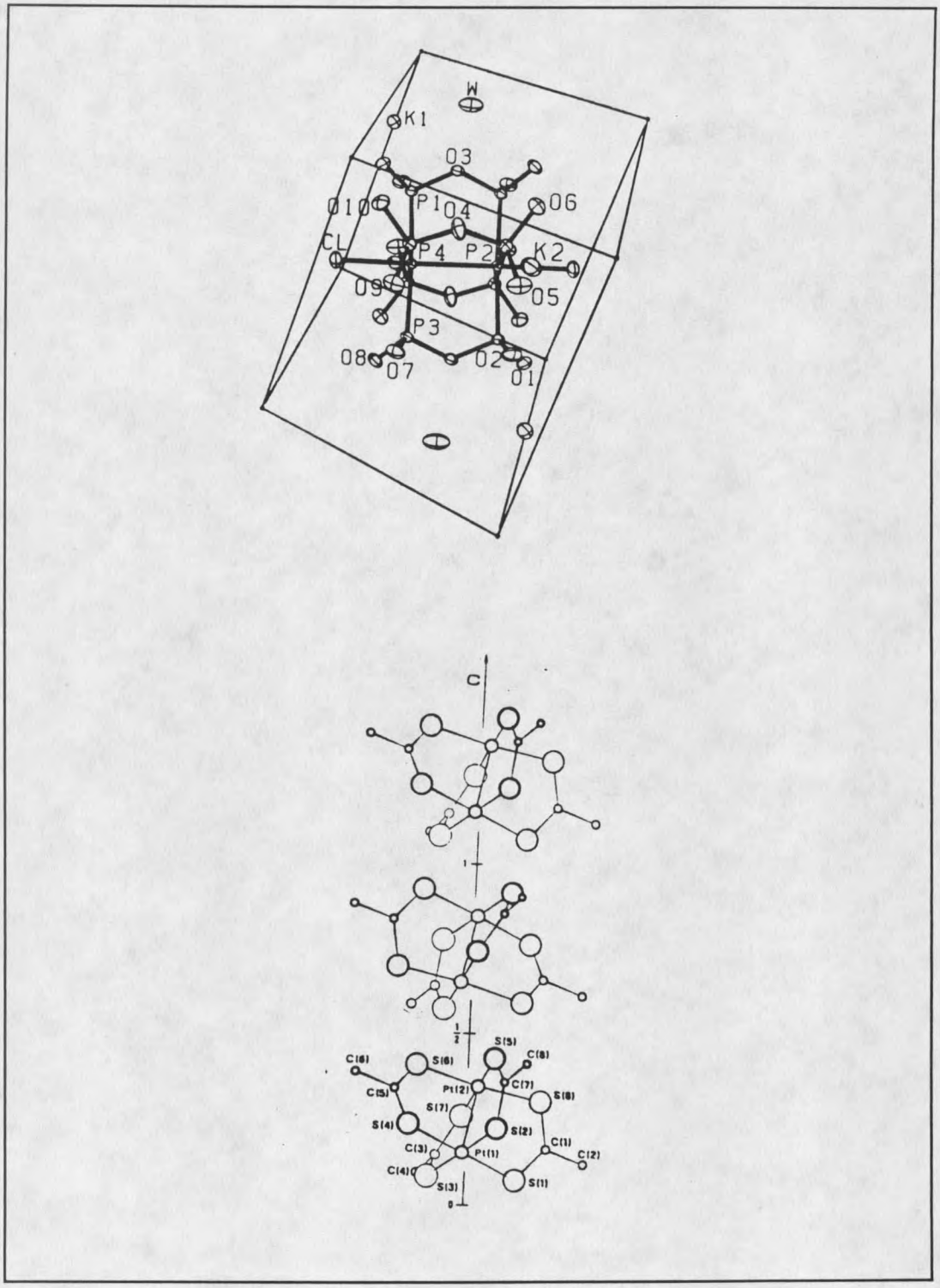

Figure 10 Pyrophosphite and Thioacetate Bridged Pt(II) and Pt(III) Dimers (26).

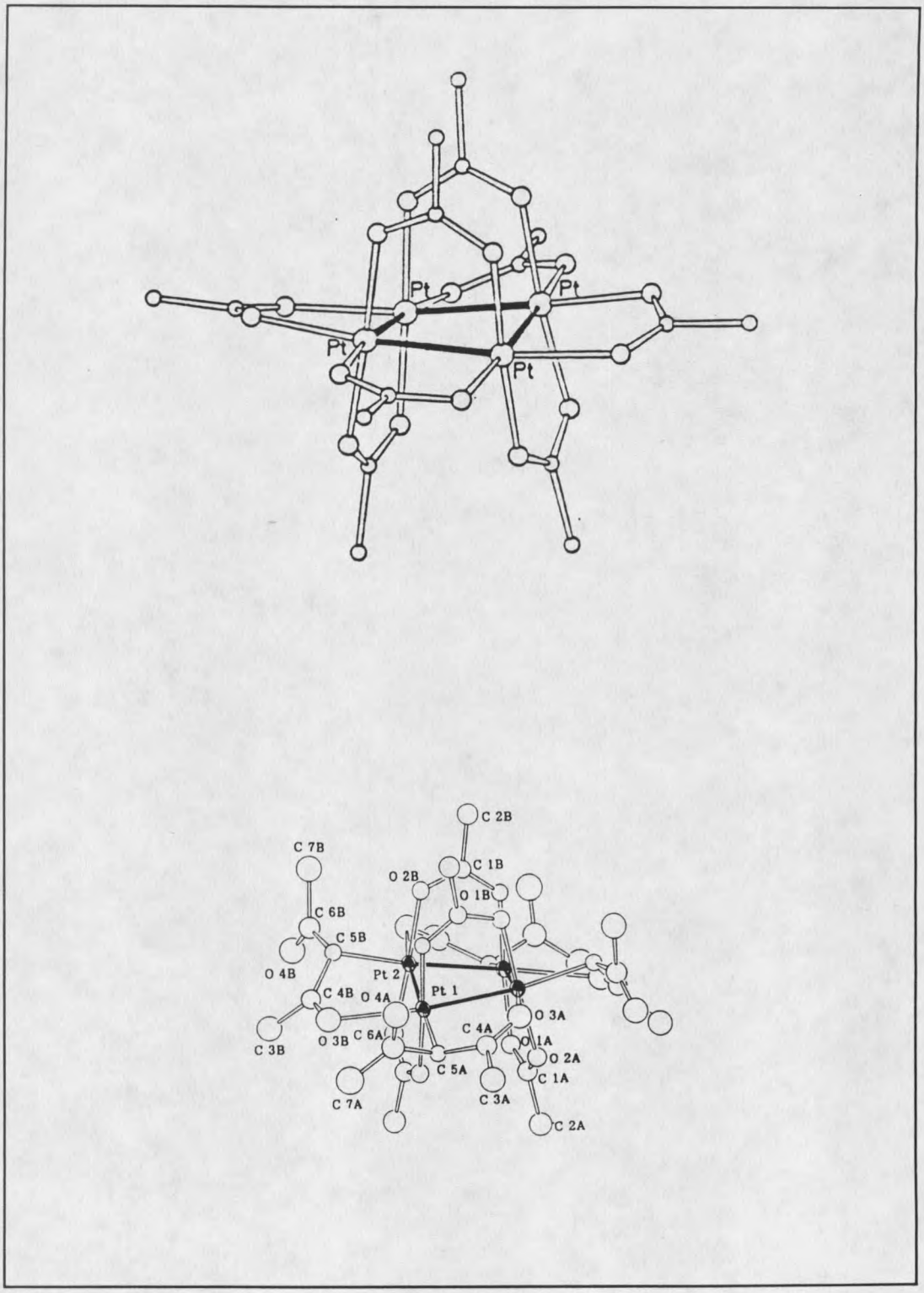

Figure 11 Tetra-nuclear Platinum Acetate Complexes (22).

isolated from the reaction of $[PtCl_4]^{2-}$ with silver acetate in acetic acid (22). This synthesis also yields the dimeric Pt(III) acetate complex described earlier. The complex has four Pt atoms arranged in a square with Pt-Pt distances of 2.495(4) Å. Bridging each Pt atom to its adjacent neighbor around the square are two acetate ligands. Each Pt has a pseudo-octahedral environment with metal-metal bonds to two other Pt atoms. The complex is stable to ligand substitution and one of the acetate bridges to each metal can be substituted with acetoacetonate (acac) (22). Higher nuclearity complexes of Pt acetate have been proposed by molecular weight and colligative properties (vida infra). It has been suggested that these complexes have as many as 50-1000 Pt atoms in a cluster which is surrounded by acetate, but none of these complexes have been isolated or extensively structured by high resolution methods.

Linear Chain Platinum Blues

There is a general class of polynuclear Pt compounds known as the Pt-blues. These complexes are formed in reactions of cis-diamminedichloroplatinum(II) with amides (12,27). Solutions of Pt-blues are thought to contain complex mixtures of metal-metal bonded Pt complexes with different Pt-Pt chain lengths and Pt oxidation states. The dark blue color is attributed to the absorption of low wavelength light along the metal-metal chain. High resolution crystallographic data is available for several of these complexes, although there is a large body of literature mentioning solutions which contain "Pt-blue" species. The tetranuclear complex α-pyridone blue (PPB), $[Pt_4(NH_3)_8(C_5H_4NO)_4](NO_3)_5.H_2O$ was the first well characterized Pt-blue complex (28).

The structure is a tetranuclear Pt chain which has the oxidation state of 2.25 (Figure 12). The oxidation state of PPB corresponds to three Pt(II) atoms and one Pt(III) atom in the chain. However, the electronic structure of PPB is consistent with the delocalization of the electrons over the four Pt atoms in the chain. Further oxidation of platinum blue solutions has resulted in a new complex α-pyrrolidone green, (PPG) $[Pt_4(NH_3)_8(C_5H_6NO)_4](NO_3)_{5.48}\cdot 3H_2O$. PPG is a non-stoichiometric compound with the average oxidation state of 2.37 (29). Further oxidation of PPG results in a new complex α-pyrrolidone tan (PPT), $[Pt_4(NH_3)_8(C_5H_6NO)_4](NO_3)_6\cdot 2H_2O$. PPT is similar to PPB and PPG except the oxidation state is 2.5 (30). This oxidation state corresponds to two Pt(II) atoms and two Pt(III) atoms in the chain. The electrons of the Pt(II) and Pt(III) atoms are not localized. The absence for an electron paramagnetic resonance spectrum (EPR) suggests that the electrons are diamagnetically coupled over the four atom chain. Further oxidation of PPT results in the formation of the dinuclear Pt(III) complex $[Pt_2(NH_3)_4(C_5H_4NO)_2](NO_3)_2$ which was described previously for dinuclear Pt(III) complexes (12). Other chelating ligands have been used in the synthesis of Pt blues. The common theme to Pt-blues is the presence of several stable Pt oxidation states associated with a short (two-four) atom chain. Oxidative titrations with Ce(IV) has shown the presence of a series of favorable oxidation states for these complexes (12,27). The stable Pt oxidation states include 2.0, 2.25, 2.33, 2.5, 2,75, and 3.0 for the tetranuclear molecules. The only Pt-blue complexes that have been crystallized with more than four Pt atoms in a chain are the octanuclear Pt blues (Figure 12). These complexes are synthesized by the same methods as the tetranuclear Pt-blues except

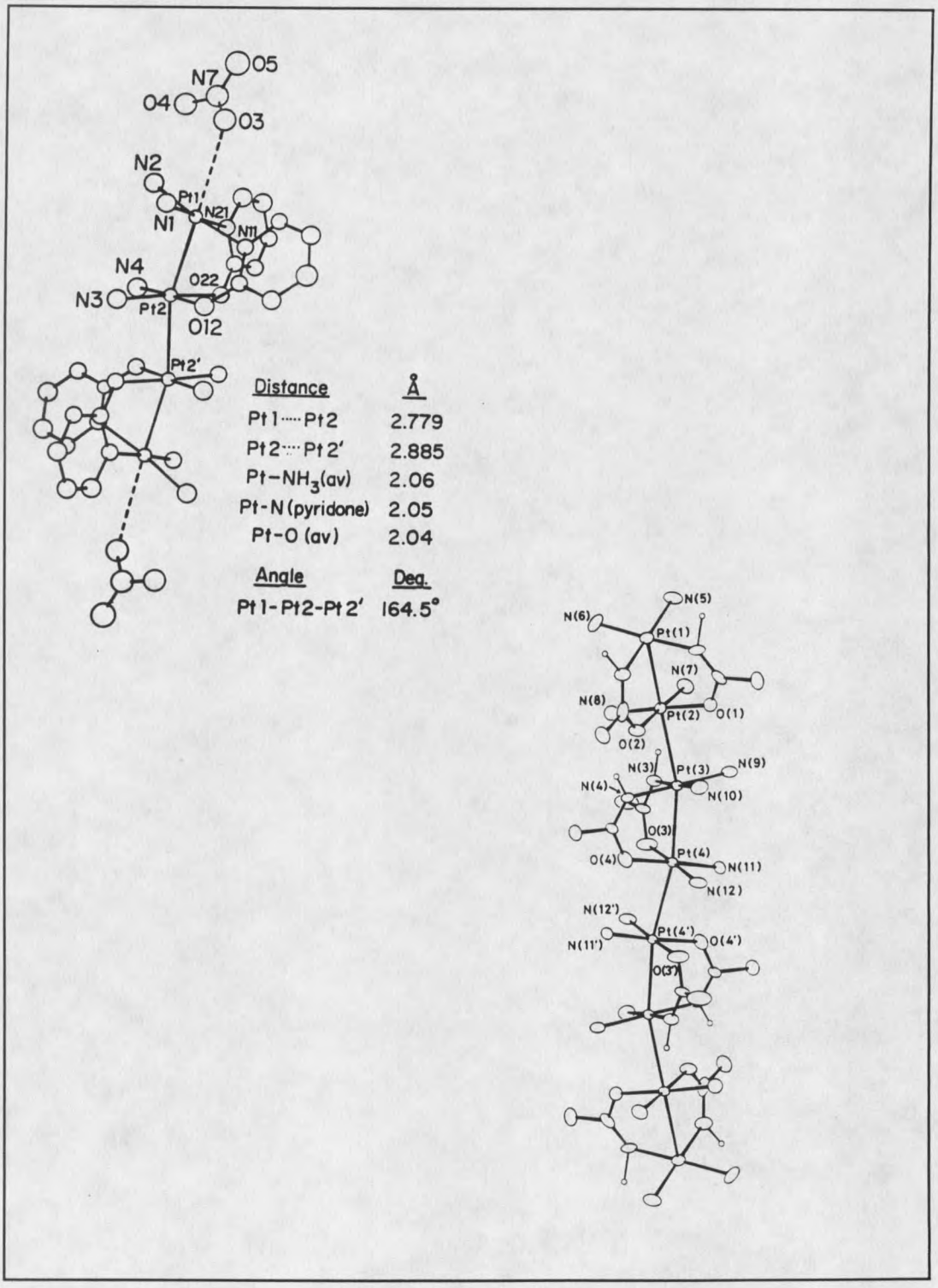

Figure 12 General Structures for Tetranuclear and Octanuclear Platinum Blues (13,28).

acetamide or 2-fluroacetamide is used as the bridging ligand (13,31). It has been proposed that the octanuclear complexes are stable because of the reduced steric interactions between Pt atoms when acetamide is used as a ligand in comparison to α-pyridone. The octanuclear complexes can be viewed as a dimer of Pt-blue tetramers.

One Dimensional Platinum Polymers

There have also been descriptions of several metal-metal bonded Pt polymers in the literatures. Polymeric Pt complexes can be extended in one, two, or three dimensions. The primary interest in this study is in one-dimensional complexes. One-dimensional Pt complexes can be divided into two classifications. The first class has only one common oxidation state of Pt(II). The second class can be described as a mixture of Pt(II), Pt(III) and Pt(IV) complexes, although the oxidation states of the atoms in the polymer may not be localized into Pt(II), Pt(III) and Pt(IV) units.

Platinum(II) Polymers The first type of one-dimensional compound is formed when square planer Pt(II) complexes aggregate along the z orientation axis of the molecules (Figure 13). Pt(II) compounds typically have crystal structures in which the square-planer complexes are stacked along the z axis to form linear chains separated by water molecules and/or counter ions (32,33). With no net bonding between Pt atoms, parallel stacking of square planer complexes would give the closest packing in the solid state. Why then, do these complexes stack in linear chains? When the complexes form a linear chain, the closest packing of molecular complexes cannot be achieved. The loss

of van der Waals energy in linear chain packing is thought to be made up by an increase in the bonding between Pt atoms along the chain. The molecular orbital drawing in Figure 2 for metal-metal bonded complexes would not predict a bond between Pt atoms because of the complete filling of molecular bonding and antibonding orbitals. However, the diagram does not contain effects of mixing orbitals of the same symmetry, which could lower the energy of complexes that aggregated along the z axis (Figure 14) (32). The 5 dz^2 orbitals have the symmetry $a1_g$ will be split to form the bonding $a1_g$ and antibonding $a2_u$ σ orbitals in the molecular complex (Figure 14). The same splitting happens to the 6pz orbitals which have the symmetry $a1_g$ for bonding σ, and $a2_u$ for antibonding σ. The electrons without orbital mixing will fill the σ bonding and antibonding $5dz^2$ orbitals which would result in no net bonding between the Pt atoms. However, the nondegenerate orbitals with the same symmetry for the $5dz^2$ and 6pz will mix with each other and form new hybrid orbitals. Hybridization will result in lowering the energy for the $5dz^2$ orbitals and in raising the energy for the 6pz orbitals as shown in Figure 14. By populating these hybridized orbitals, the metal-metal interaction between Pt atoms can be established.

Pt(II) complexes with four neutral ligands ($[PtL_4]^{2+}$]) (Figure 13) are known to form one-dimensional stacked molecular complexes. Tetraamineplatinum(II)dichloride monohydrate $[Pt(NH_3)_4]Cl_2.H_2O$ is the most studied of $[PtL_4]^{2+}$ stacked complexes (33). The Pt molecules crystallize in chains with Pt atoms eclipsed and separated by 4.21(2) Å. The chloride counter ions stabilize the stacking interactions by forming hydrogen bonds between amine ligands of two $[PtL_4]^{2+}$ complexes. Analogous complexes

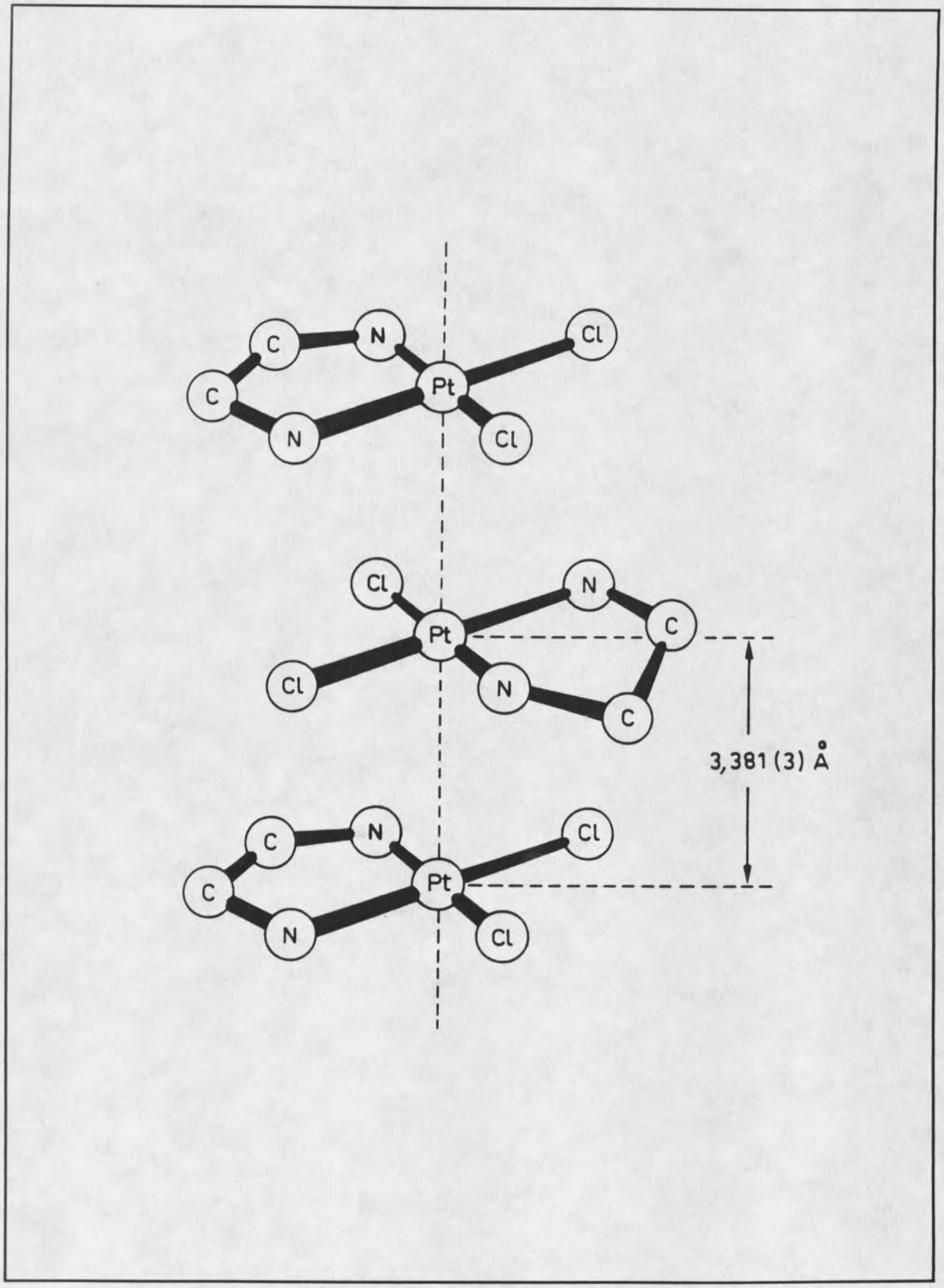

Figure 13 Structures of One-dimensional Platinum(II) Complexes (33).

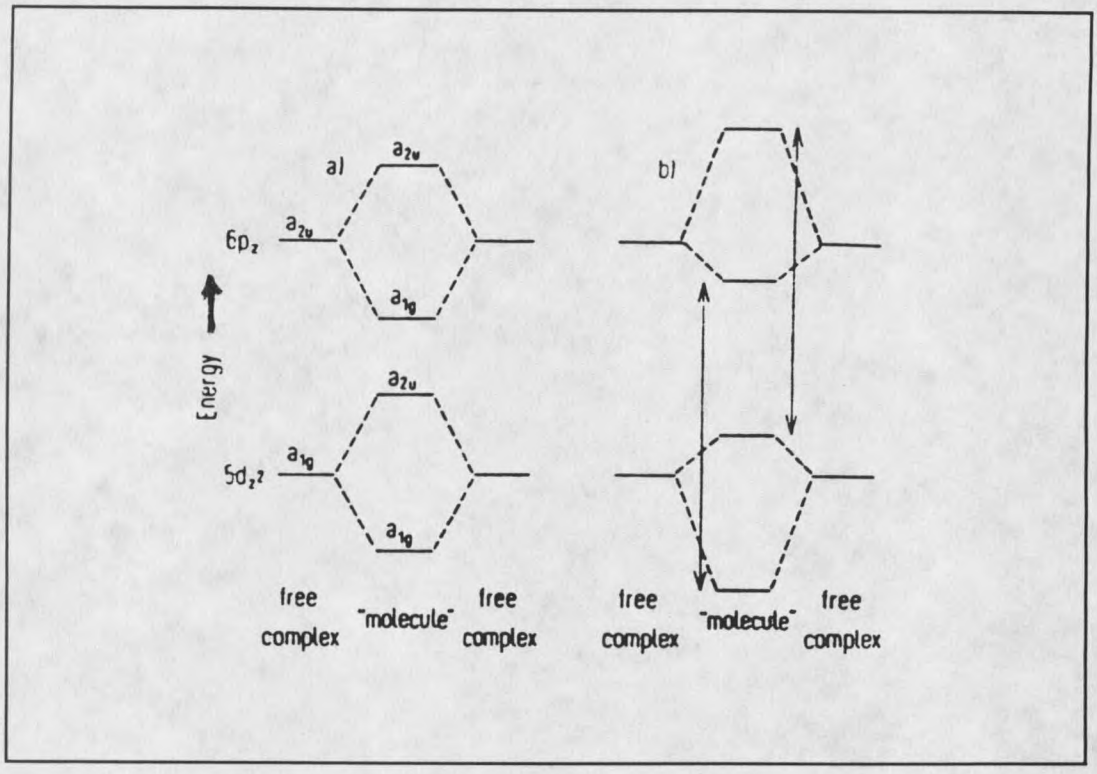

Figure 14 Metal-Metal Bonded Molecular Orbital Diagram with Configuration Interaction (32).

synthesized with larger amines or anions show a progressive increase in the separation of the Pt-Pt distance. The cationic charge of each complex would not favor close approach of the two metal centers. The large Pt-Pt distances in these structures predicts little interaction between metal centers. No conductivity data is available for these complexes. Triammine Pt(II) complexes $[PtL_3X]X$ are also known to stack in the solid state (33). The most interesting of these complexes is chloroterpyridineplatinum(II) cations. $[Pt(terpy)Cl](NO_3)$ forms molecular stacks with a Pt-Pt distance of 3.5721(8) Å. The distance between metal centers is reduced from the Pt tetraammines, but little metal-metal interaction is observed; and no conductivity data is available for these

complexes. Diammine dihalo platinum complexes can be obtained in a number of ionizational isomers. The neutral isomers are planar $[PtL_2X_2]$ complexes. Cis-diamminedichloroplatinum(II) (Peyrone's Chloride) crystallizes in linear chain structure (33). There are two unique Pt-Pt distances 3.372(2)Å and 3.409(2)Å. These distances alternate along the chain of platinum atoms in the crystal. Trans-diamminedichloroplatinum(II) also crystallizes in a linear chain structure. The Pt-Pt distance of 5.0 Å suggests little interaction between the trans-$Pt(NH_3)_2Cl_2$ molecules. Other $[PtL_2X_2]$ complexes will crystallize in columnar stacks if the neutral ligand L is confined to lie in the coordination plane of the Pt. Pt complexes with ethylenediamine (en), 2,2'bipyridine (bipy) and 1,10 phenanthroline (phen) will stack in the solid state because the ligand is required to lie in the plane of the Pt coordination (Figure 13). However, complexes with pyridine (py) as a ligand do not stack because the pyridine ligands are rotated by 55-62° out of the coordination plane of the Pt (33). This rotation prevents close approach of the Pt atoms to form a chain structure. Ionized isomers with the formula PtL_2X_2 are known to stack in the solid state. These complexes are formed by mixing cationic Pt complexes with anionic Pt complexes. Many of these species have not been characterized beyond molecular formula and solubility data. $[Pt(NH_3)_3Cl][Pt(NH_3)Cl_3]$ is one example of a $[PtL_3X][PtLX_3]$ type complex that was described by Peyrone in 1845. Other ionization isomers include $[PtL_3X]_2[PtX_4]$, and $[PtLX_3]_2[PtL_4]$ forms where X can be Cl, Br, or NO_2 and L can be NH_3, 1/2 en, 1/3 terp, 1/3 ten, 1/2 phen, or 1/2 bipy. Magnus' Green Salt (MGS), which was first prepared in 1828 is the most studied example of the ionization isomerism molecules with

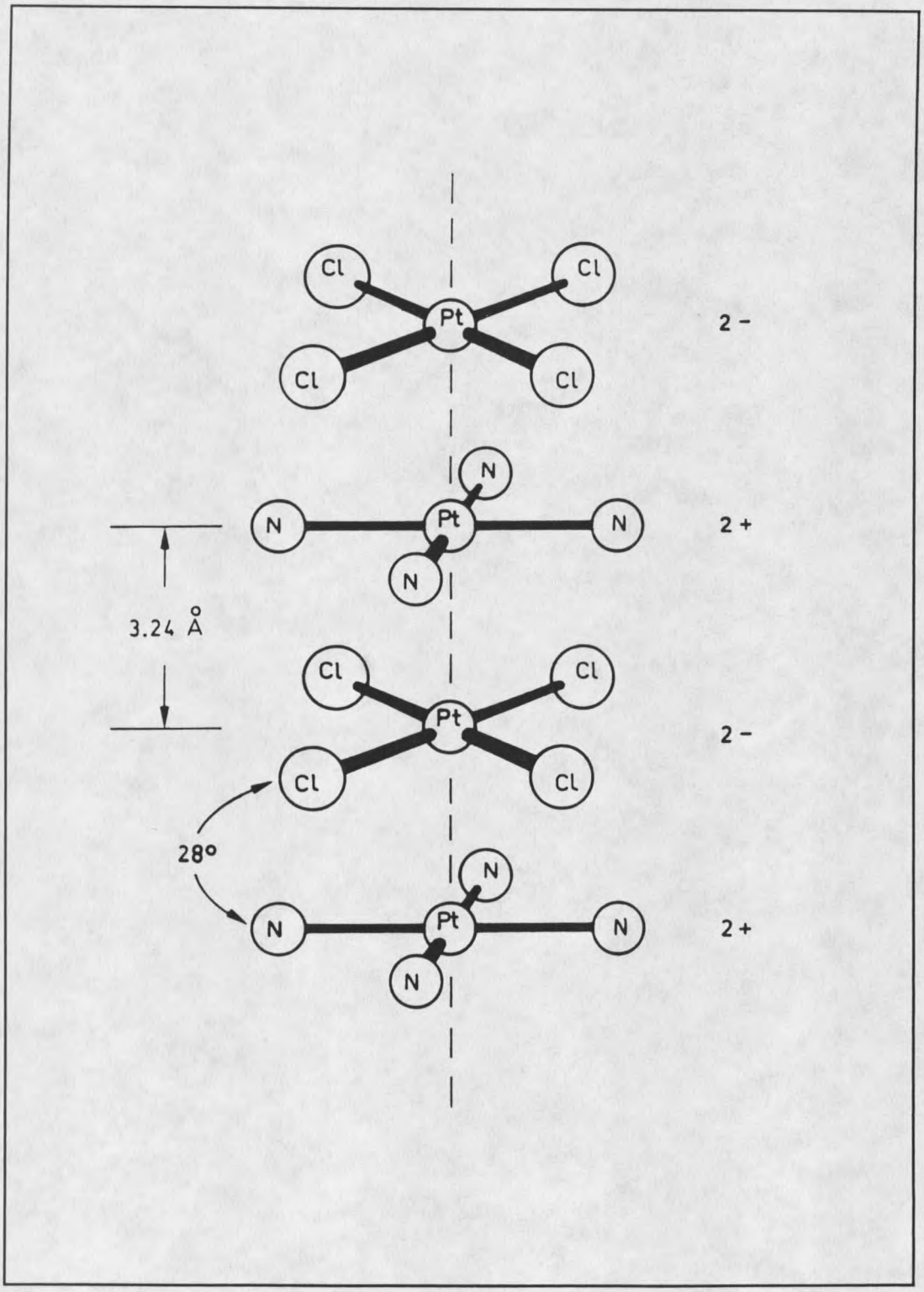

Figure 15 The Structure of Magnus Green Salt (33).

the formula $[PtL_4][PtX_4]$ (Figure 15) (33). The molecular complex Tetraamineplatinum(II)-tetrachloroplatinate(II) ($[Pt(NH_3)_4][Pt(Cl)_4]$) is synthesized by mixing equal molar solutions of $[Pt(NH_3)_4]^{2+}$ and $[Pt(Cl)_4]^{2-}$ complexes. An immediate precipitation of green and pink solids is observed. The bright green molecular complex is a striking difference to the pink $[PtCl_4]^{2-}$ and colorless $[Pt(NH_3)_4]^{2+}$. MGS consists of alternated stacking of cationic $[Pt(NH_3)_4]^{2+}$ and anionic $[Pt(Cl)_4]^{2-}$ where the Pt atoms are separated by a distance of 3.245 Å. The optimal one dimensional conductivity of MGS has been measured to be $2 \times 10^{-9}\ \Omega^{-1}\ cm^{-1}$. Magnus's pink salt (MPS) has a very different structure than MGS even though the salts have the same molecular formula $[Pt(NH_3)_4][Pt(Cl)_4]$. The Pt atoms are not stacked in MPS, and the closest Pt-Pt distance is over 5.0 Å. No conductivity data has been reported for MPS. MGS has a highly anisotropic absorbance of light along the Pt chain axis, while MPS has only the absorbance spectrum of the individual complexes. The difference in optical properties between MGS and MPS has been attributed to the metal-metal interaction in MGS.

Platinum(II) and Platinum(IV) Polymers The second type of Pt polymer can be formulated as a mixture of Pt^{2+} and Pt^{4+} complexes that are bridged by the halide ligands along the metal-metal axis. This type of polymer is exemplified by Wolframs' Red Salt (WR) $[Pt(NH_2Et)_4Cl]^+$ (Figure 16) (33). The formula can also be expressed with distinction of the oxidation states of the Pt atoms as $([Pt^{II}(NH_2Et)_4][Pt^{IV}(NH_2Et)_4Cl_2]Cl_4 \cdot H_2O$. A series of complexes with the WR formula $[PtL_4][PtL_4X_2]Y_4$ have been synthesized where L is a neutral equatorial nitrogen ligand

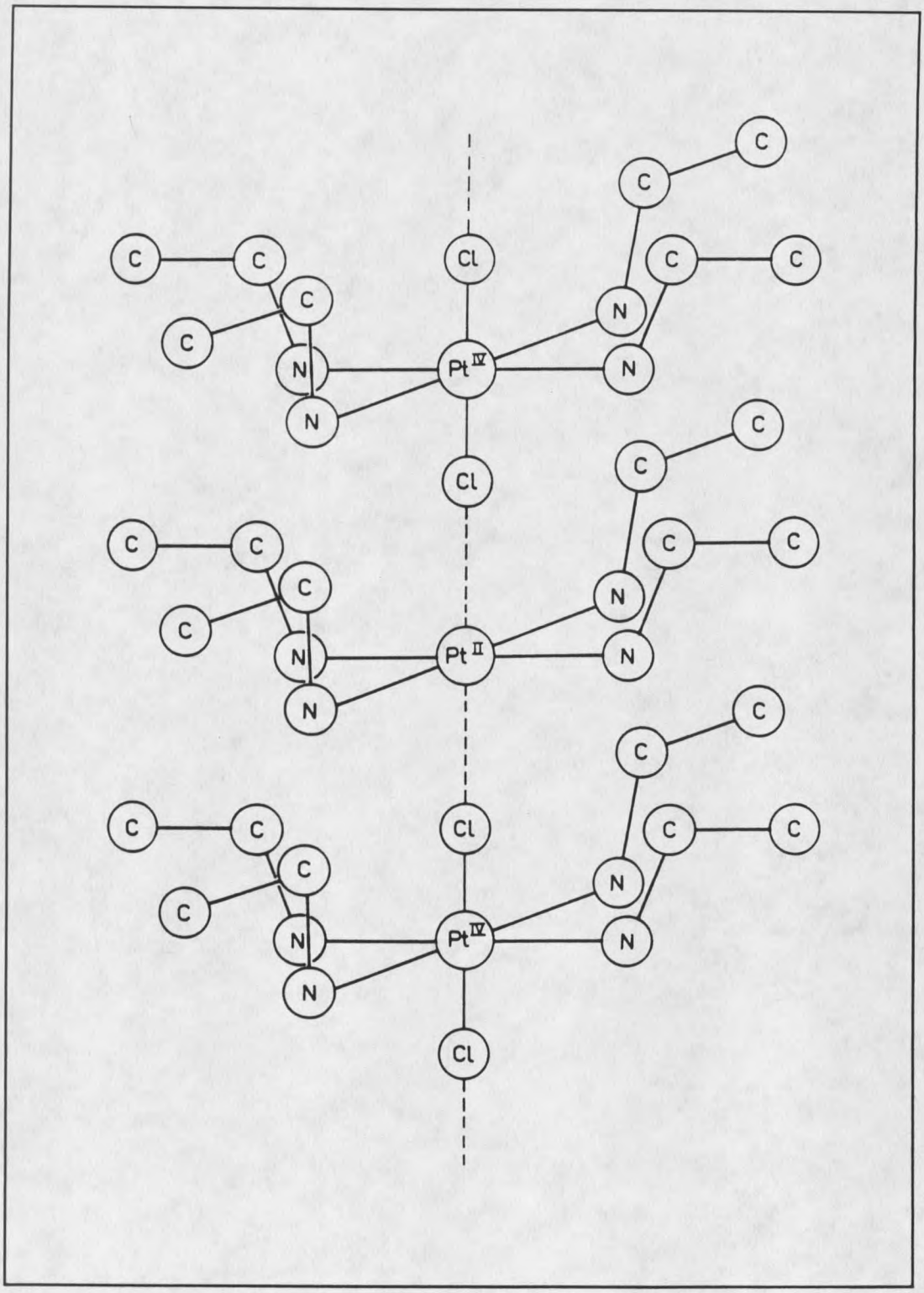

Figure 16 Structure of Wolframs Red Salt (33).

such as NH_3, CH_3NH_2, $C_2H_5NH_2$, 1/2 en, 1/2 pn, 1/2 bipy, 1/2 phen, 1/3 terpy, 1/3 dien, 1/4 trien, or 1/4 cyclam, and X and Y are halides. The colors associated with these complexes have been associated with intervalence charge transfer (IVCT) transitions between Pt(II)----Pt(IV) metal centers polarized in the metal-halide-metal chain direction. The conductivity of WR is 3 X 10^{-10} Ω^{-1} cm^{-1} and the Pt-Pt distance is 5.46 Å. The distance to the bridging halide is different for each Pt. The Pt-halide distance is 3.12 Å to Pt(II) and 2.46 Å to Pt(IV) At ambient conditions WR behaves as separate Pt^{2+} and Pt^{4+} species, but under high pressures (40 kbar), conductivity has been shown to increase as much as nine orders of magnitude as the Pt-X-Pt distance contracts. This contraction of WR can be represented as a contraction of the Pt(II)-X bond distance. The molecule is similar to Pt(III)-X-Pt(III) which has a complete delocalization of electron density when compared to the localized valence structure Pt(II)-X-Pt(IV).

Platinum(II) and Platinum(III) Polymers Another group of Pt complexes fits into the classification of halide bridged polymeric Pt complexes. These are complexes with the molecular formula $[Pt_2(H_2P_2O_5)_2Cl]^{4-}$ (KPOP). The complexes are synthesized by combining equal molar solutions of the Pt(II) complex $[Pt_2(H_2P_2O_5)_2]^{4-}$ and the Pt(III) complex $[Pt_2(H_2P_2O_5)_2Cl_2]^{4-}$(25,34). These pyrophosphate bridged complexes were previously described in the section on metal-metal dimers of Pt complexes. These complexes can then be formulated as a dimeric analog to Wolfram's red complexes. X-ray crystallography of $K_4[Pt_2(H_2P_2O_5Cl]\cdot 3H_2O$ reveals two unique Pt-Pt distances of 2.685 Å and 2.969 Å and two unique Pt-Cl distances of 2.441 Å and 2.809 Å (Figure

17). This bonding is consistent with a ground state of (-Pt(II)-Pt(II)-Cl-Pt(III)-Pt(III)-Cl-)$_n$. This valence localization is consistent with the Wolfram's red formulation. The conductivity of $K_4[Pt_2(H_2P_2O_5Cl]\cdot 3H_2O$ is activated thermally with an activation energy of ~ 0.08 eV. The complex forms gold metallic needles with IVCT transitions in the 10,000-20,000 cm^{-1} region (34). The analogous complexes have been synthesized with bromide and iodide in the chain. These complexes differ from the chloride complex in that the bromide and iodide lie nearly equidistant from the Pt atoms. Because of the equidistant bonding, the bromide and iodide complexes do not support a fixed valence state. Rather, they are best described as a valence delocalized system with $Pt_{2.5+}$ atoms in the halide bridged linear chain. As expected, the valence delocalized chains have even higher conductivity than the valence localized chloride bridged species. An analogous formulation can be applied to the Pt dithioacetate complexes previously described in Pt metal-metal bonded dimers. These complexes have the formula $[Pt_2(CH_3CS_2)_4I]$ and are formed when equal molar solutions of Pt(III) complex $[Pt_2(CH_3CS_2)_4I_2]$ and the Pt(II) complex $[Pt_2(CH_3CS_2)_4]$ are allowed to react. These complexes form linear [-Pt-Pt-I-] chains with a common Pt-Pt distance of 2.677 Å, and a nearly equal Pt-I distance of 2.975 and 2.981 Å (34). This spacing is consistent with a valence delocalized structure. The IVCT bands for this complex occur in the 6000-8000 cm^{-1} region, and the activation energy for conductivity is 0.05 eV. The conductivity of a single crystal of $[Pt_2(CH_3CS_2)_4I]$ increases from 2 Ω^{-1} cm^{-1} at atmospheric pressure to 10 Ω^{-1} cm^{-1} at 7 GPa.

Partially Oxidized Platinum(II) Polymers Anionic Pt(II) complexes with cyanato and oxalato ligands also form stacked linear chain complexes in the solid state (Figure 18) (7,8,32). While aqueous solutions of these complexes are colorless, several different cations can form intensely colored crystals of the anionic complexes. Because the cations and water in the crystal lattice cannot absorb light in the visible regions, the characteristic low energy light absorptions have been assigned to the stacking of the Pt atom chain. The relationship between color and Pt-Pt distance was shown to be a decrease in the wavenumber for absorption bands as the Pt-Pt distance decreases. The absorption band is also polarized along the Pt-Pt axis of the crystal. The Pt-Pt distances in these complexes is dependent upon the solid state phase that is formed. This phase is greatly dependent upon the cation and hydration of the complex (32). For $M_2[Pt(CN)_4]$ the Pt-Pt distance ranges from 3.60 Å for colorless $Sr[Pt(CN)_4].5H_2O$ to 3.09 Å for violet $Sr[Pt(CN)_4 \cdot 3H_2O$ When solutions of Pt(II) oxalato or cyanato complexes are partially oxidized, the same stacked linear structures form upon crystallization. In these oxidized complexes, the Pt-Pt distances are reduced to 2.85-2.78 Å (Figure 19) (7,8,32,36). These mixed valence complexes do not have distinguishable Pt(II) and Pt(IV) units in the solid state. Rather, all Pt-Pt distances are equivalent, or nearly equivalent, which is consistent with a common oxidation state. Partially oxidized compounds have been referred to as "mixed valence" because the formal oxidation state of the Pt is approximately 2.3^+. Gold and bronze colored Pt mixed valence chain complexes were first prepared by Knop in 1842. The structural integrity of these one dimensional polymers was not revealed for more than a century until the work of

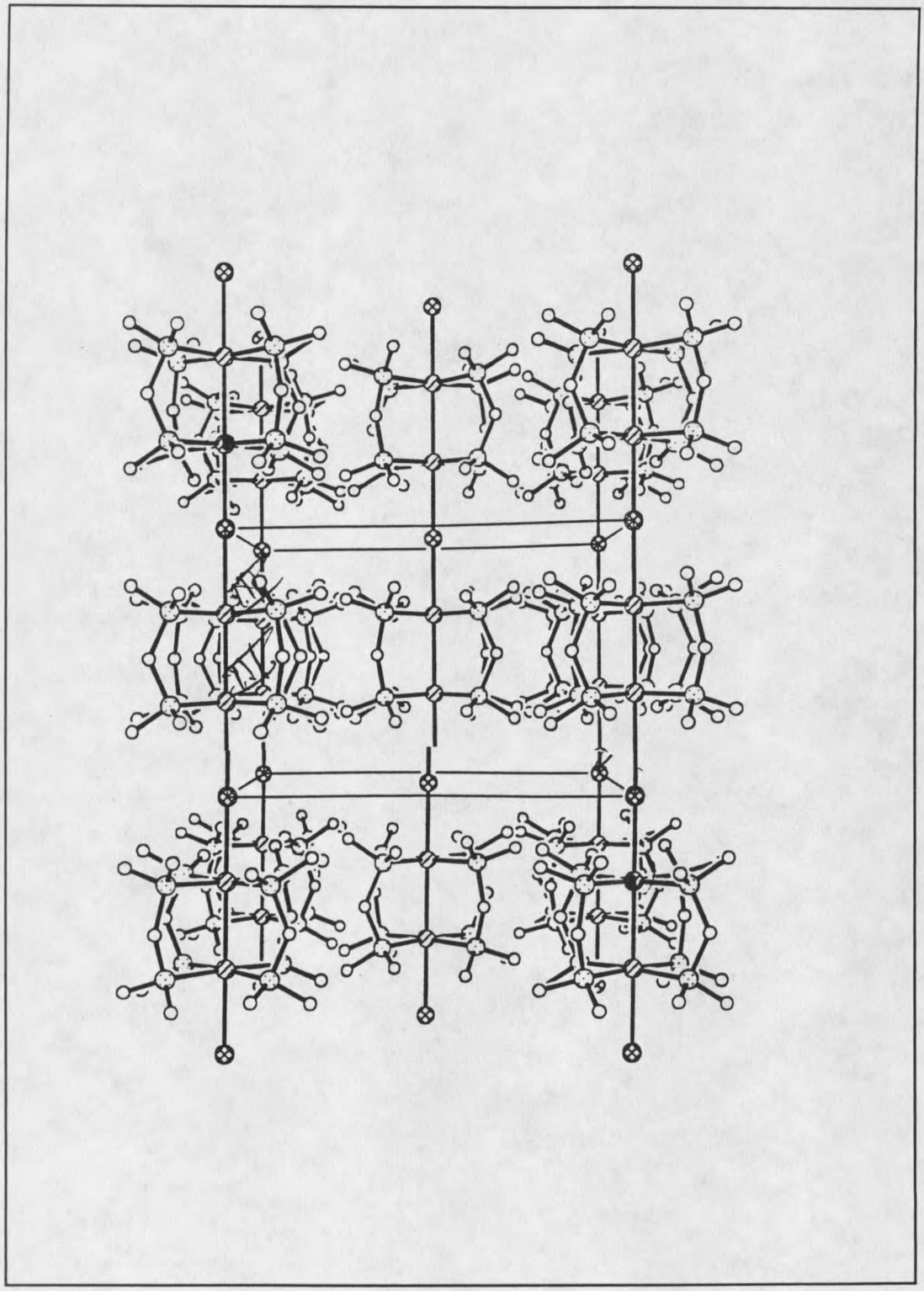

Figure 17 Pyrophosphato Halide Bridged Polymers (34).

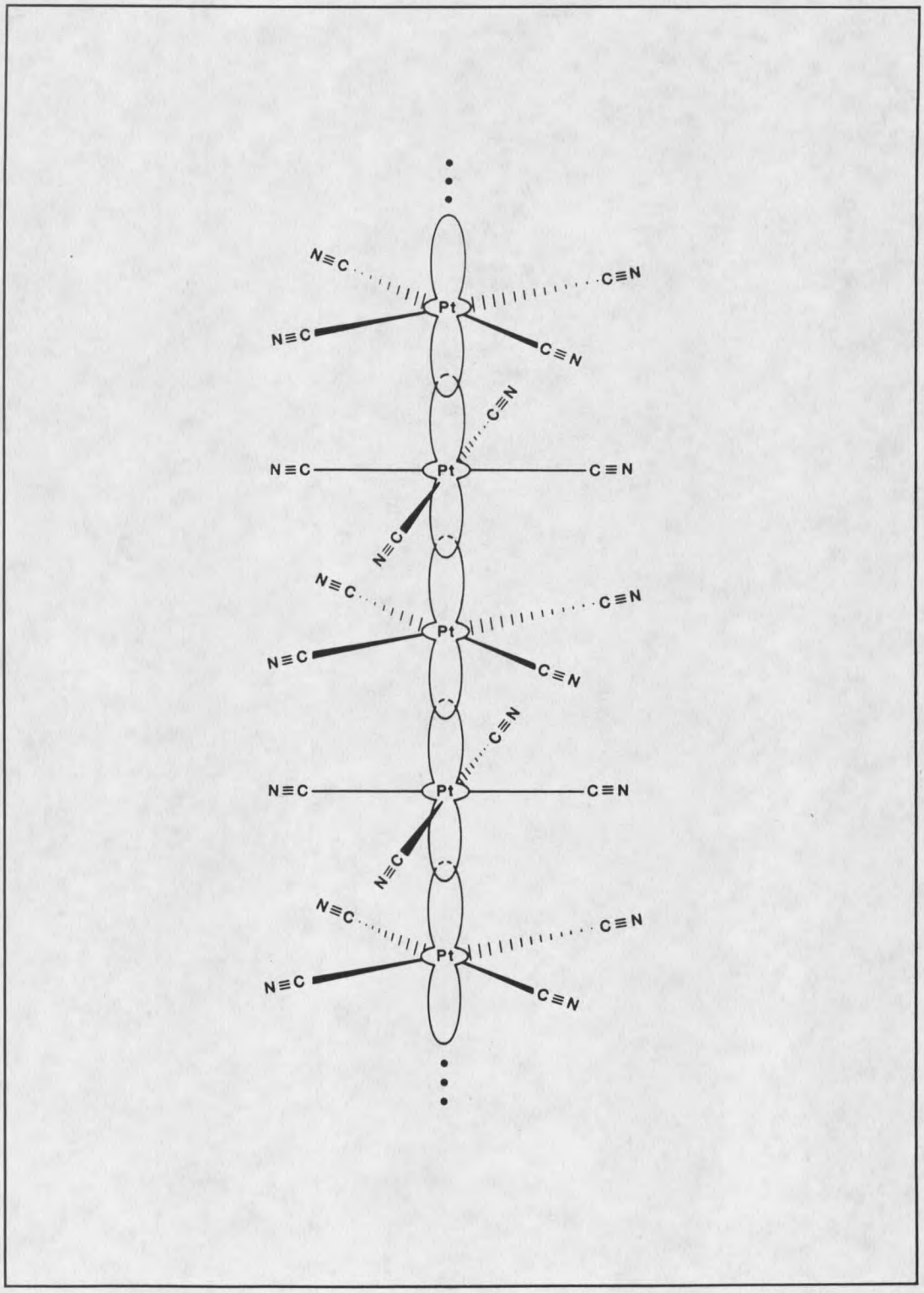

Figure 18 $[Pt(CN)_4]^{2-}$ One-Dimensional Polymers (7).

Krogmann in 1960's. The compound $[K_2Pt(CN)_4X_{0.3}\cdot 3(H_2O)]_n$ (KCP) (X=Cl, Br) with all Pt atoms in the equivalent oxidation state of 2.3 was established by Krogmann (32). The synthesis of KCP is to combine five mole equivalents of the Pt(II) complex $[Pt(CN)_4]^{2-}$ with one mole equivalent of the Pt(IV) complex $[Pt(CN)_4X_2]^{2-}$ (X=Cl, Br). All Pt-Pt distances are equivalent for the oxidized material (2.87 Å), and the halide is not bound to the Pt. Each unit cell contains a site for halide, which is occupied in 64 % of the cells, corresponding to 0.32 X^- per Pt. Subsequent to his pioneering research in this area of Pt chemistry, this type of "mixed valence" complex has become known as a Krogmann salt. The metal-metal bonded polymers have also been prepared by partially oxidizing $[Pt(CN)_4]^{-2}$ with 1/5 of an equivalent of chlorine or bromine, or by electrochemical oxidation of $[Pt(CN)_4]^{-2}$ solutions of KBr or KCl. Krogmann also characterized the first mixed valence compounds of bis(oxalato)platinates (10,11). The bronze colored complex $[Mg_{0.82}Pt(Ox)_2.5H_2O]$ (KOP) can be prepared by the same methods as those for KCP (8,35). The Pt-Pt separation in KOP is 2.85 Å and the average oxidation state for the Pt is +2.36. Eight sites are identified as Mg coordination, but only 40 % of the sites are occupied. The polymerized chains of KCP and KOP display anisotropic (one-dimensional) behavior when optical, magnetic, or electrical properties are measured. Electrical conductivity is 10^5 times greater parallel to the chain axis as it is perpendicular to the chain (8,32). The metal atoms are surrounded by a sheath of organic ligands. Krogmann salts are described as one dimensional metals with conductivities as high as 200 Ω^{-1} cm^{-1} for KCP and 42 Ω^{-1} cm^{-1} for KOP. Conductivity can be compared to Pt metal which has a conductivity

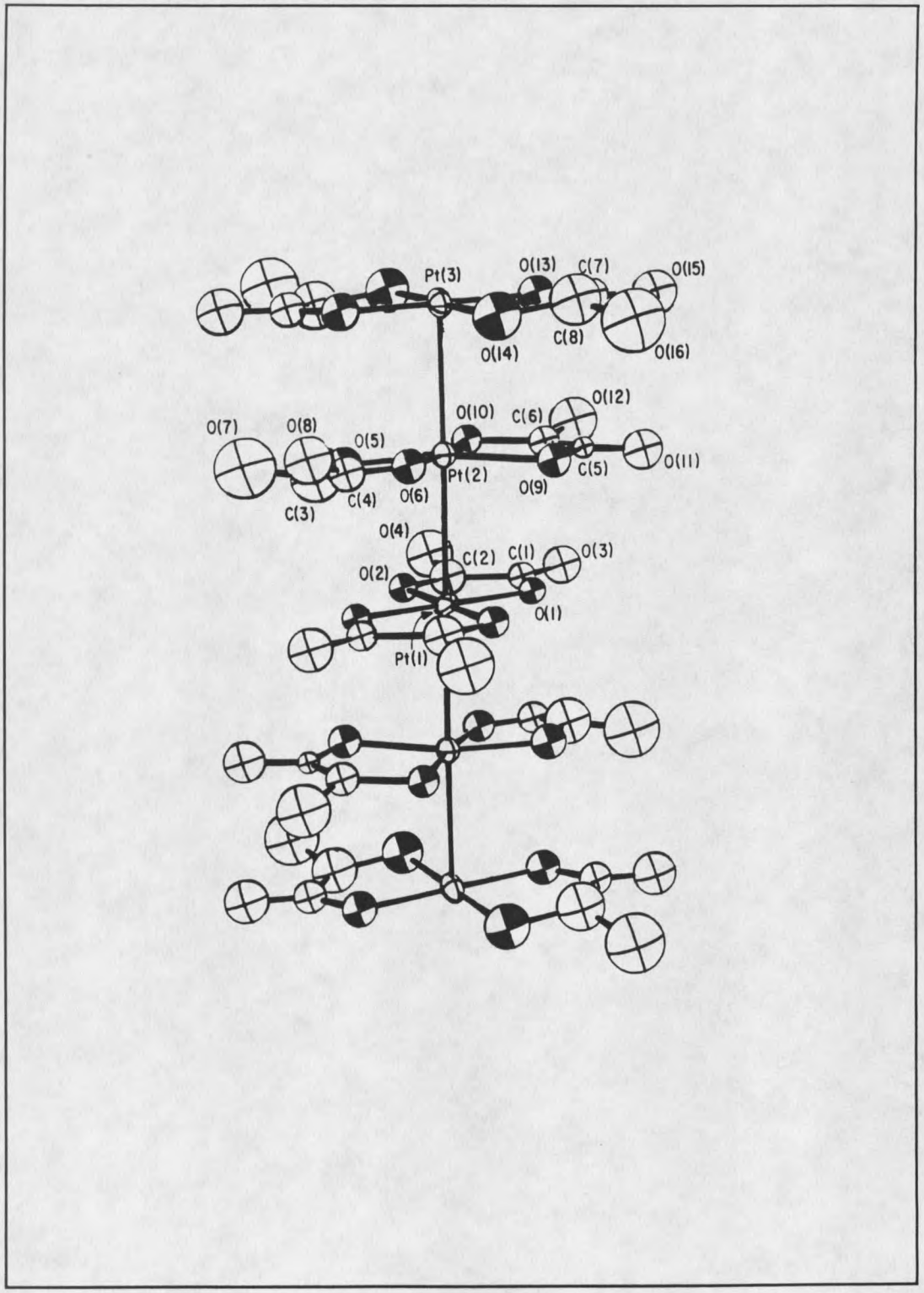

Figure 19 Linear Chain Bis(oxalato)platinate Polymer (8).

of 9,400 Ω^{-1} cm^{-1}.[2] Conductivity measurements are typically performed on single crystals. For a one-dimensional polymer which is 1 mm in length, there are ca $1x10^{23}$ atoms in the chain. Even 1 % impurity levels would provide millions of defects in the Pt-Pt chain. The intrinsic conductivity of these complexes must be much higher than the measured values. Pt bond distances along the one dimensional chain also resemble Pt metal (2.775 A) with 2.87-2.88 Å for KCP, and 2.81-2.85 Å for KOP.

The information for "mixed valence" Pt chain complexes in solution is limited (5,10,11,26,36). Krogmann noted that yellow $H_2[Pt(ox)_2]$ was oxidized by oxygen to form the violet solutions of $H_{1.64}[Pt(ox)_2(H_2O)]_n$ (10,11). Solutions of $H_{1.64}[Pt(ox)_2(H_2O)]_n$ exhibited a pH dependent equilibrium. Krogmann reported that addition of base to polymeric violet solutions results in the formation of monomeric Pt(II) and Pt(IV) oxalato complexes (10,11). Krogmann has suggested that when the linear chain is disrupted, $[Pt^{4+}(Ox)_2]$ separates from the polymeric chain (Figure 20). This Pt(IV) complex is unusual in that it has only four ligands. Pt(IV) complexes typically have six ligands in an octahedral environment, and so the coordinatively unsaturated Pt(IV) complex should add two ligands to its coordination sphere. The most likely ligands will be H_2O in aqueous solution. Krogmann has suggested that if the H_2O ligand is lost from the Pt(IV) complex; the polymerization of the Pt chain will occur. This reaction is the reverse of the base disruption of the polymer, and is the replacement of H_2O ligand on Pt(IV) with the electrons from the dz^2 orbital of bis(oxalato)platinate(II). In base, the polymerization is inhibited by the acid dissociation of the coordinated H_2O ligand of the Pt(IV) to the inert hydroxo ligand. Krogmann has proposed this acid dependent dissociation of

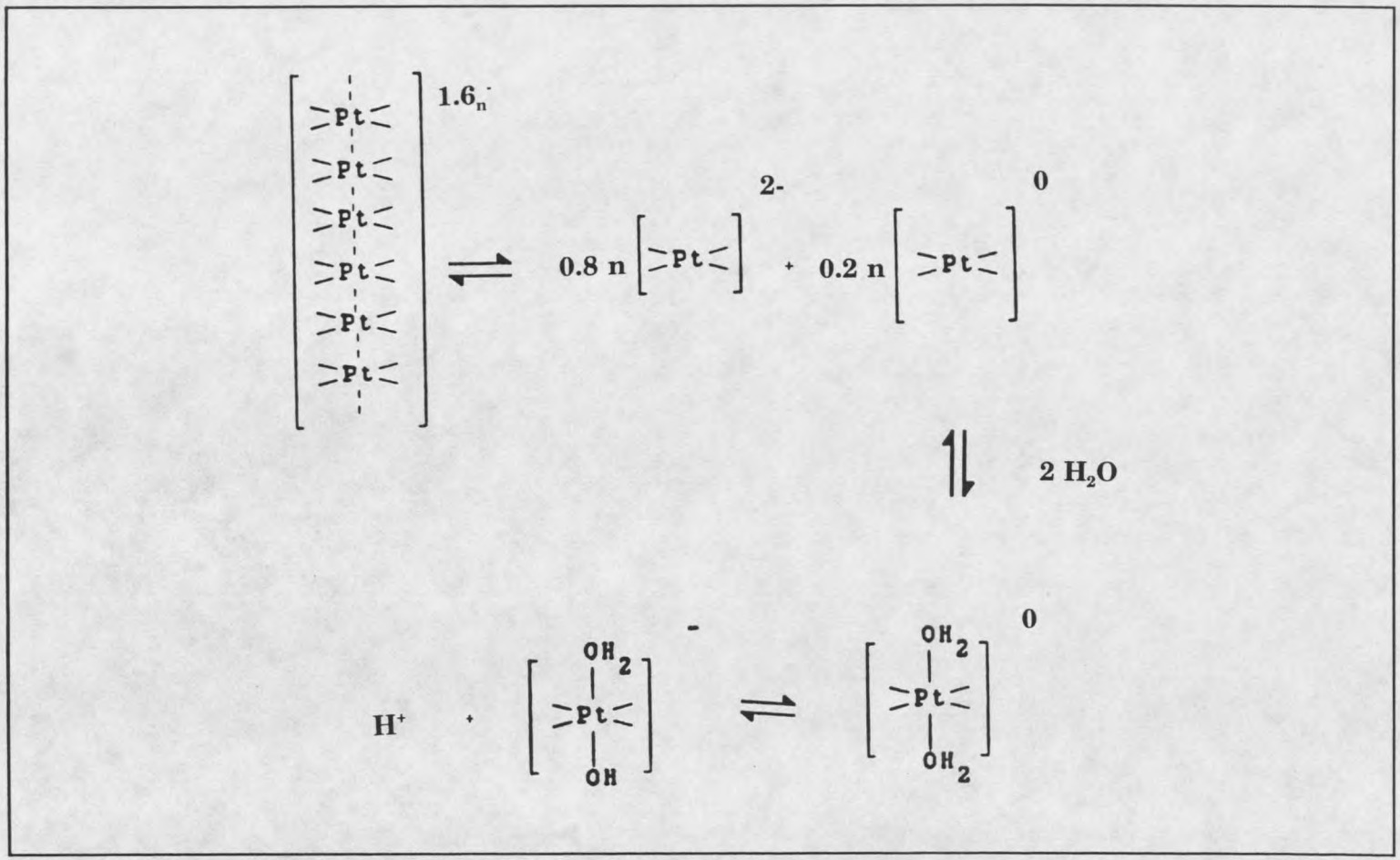

Figure 20 Krogmann Mechanism for Polymerization of One-Dimensional Bis(oxalato)platinates (11).

coordinated water to be the key step in polymerization of bis(oxalato)platinates. Krogmann's osmotic pressure and solution conductivity measurements support that blue/black solutions of 0.4 M $H_{1.64}[Pt(ox)_2(H_2O)]_n$ have an average polymer chain length of 46 monomer units and orange/yellow solutions of 0.01 M contain only monomer. Electronic spectra show that these solutions do not follow Beer's law over the concentration range of 0.01-0.4 M. Papavassilou has studied the absorption spectra of these polymerized complexes (36). His data supports the formation of particles which are close to the wavelength of light used in the experiment. He supports that the polymeric chains are $>=$ 500 nm, which would be a chain of more than 1000 Pt atoms in length.

The conductivity of KCP is 10^6 times greater than that in KPOP which is 10^6 times greater than in WR (7,33,34). All three complexes form linear chains, and are Pt bromides, but the differences in conductivity can be realized by a comparison of the atomic and electron differences of the three complexes (Figure 21). KCP has short metal-metal bonds without bridging halide, and a valence delocalized oxidation state of 2.33. KPOP has bromide bridges between Pt atoms and a valence delocalized oxidation state of 2.5. WR has bromide bridges between Pt atoms, and a valence localized oxidation state of 3.0.

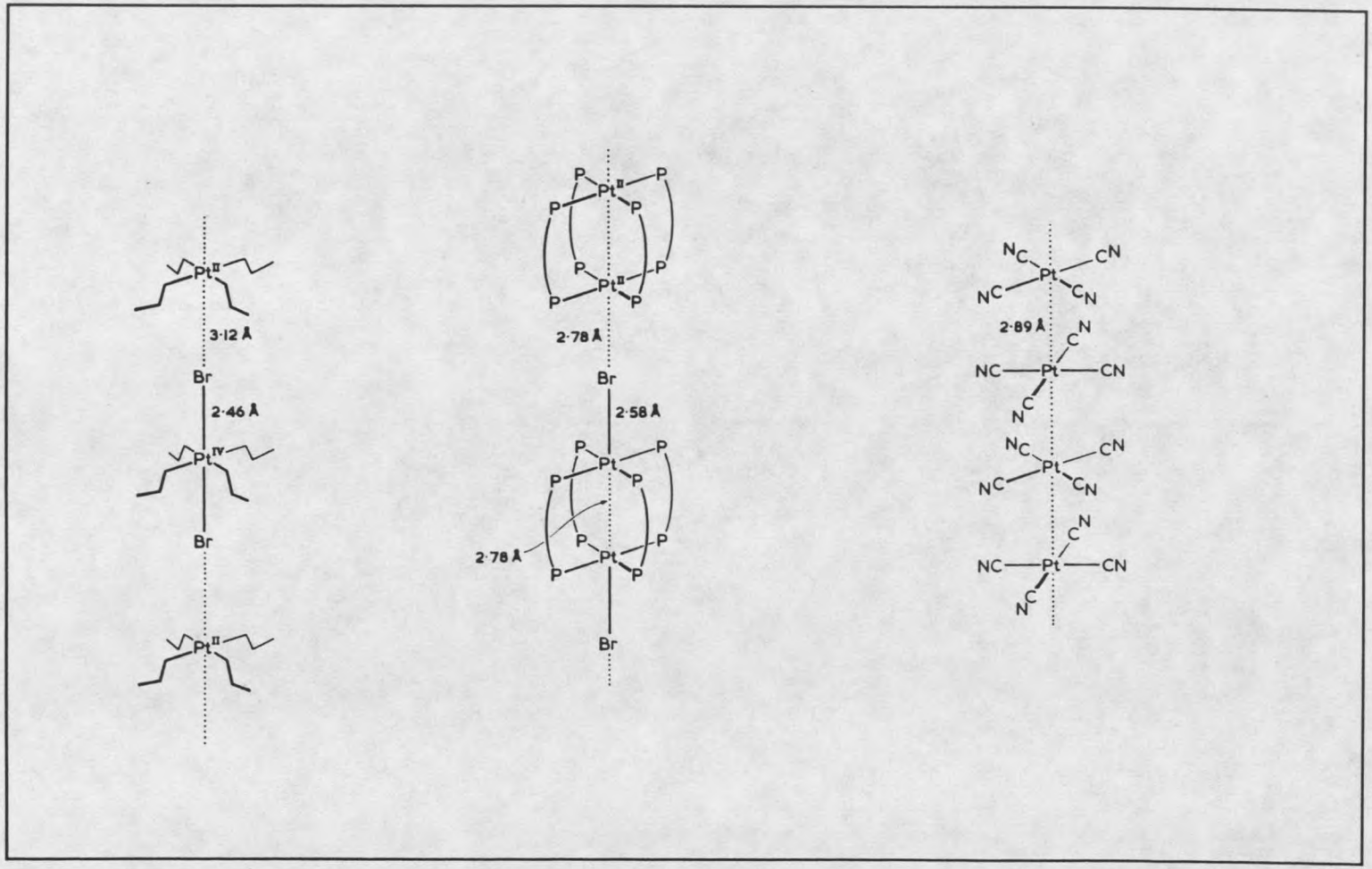

Figure 21 Structure Comparisons of One-Dimensional Platinum Chain Complexes (34).

EXPERIMENTAL METHODS

Preparation of Compounds

Starting Materials

Oxalic (OxH_2), malonic ($MalH_2$), and 2-methyl malonic acids ($MmalH_2$), $(NH_4)_2Ce(SO_4)_3$ (Aldrich); $K^{13}CN$, 50%$H_2{}^{16}O/H_2{}^{18}O$, (Cambridge Isotopes) and $K_2[PtCl_4]$(**1**) (Johnson Matthey) were used as supplied. $[Pt(H_2O)_4]^{2+}$(**6**) was prepared from $K_2[PtCl_4]$(**1**) as previously described (37). $Na_2[PtCl_6]$ was prepared by freeze drying a solution of $K_2[PtCl_6]$ which had been ion exchanged over Dowex-50W-X8 in the sodium form.

Synthesis of Complexes

Potassium Bis(oxalato)platinate(II) Dihydrate(**5**) The complex was prepared by the method of Krogmann and Dodel from $K_2[PtCl_4]$(**1**) and K_2Ox (10,11,38)

Potassium Dichlorooxalatoplatinate(II) Hydrate(**3**) $K_2[Pt(Ox)_2]\cdot 2H_2O$ (**5**) (0.050 g, 0.103 mmol) was dissolved in 3mL H_2O. Ten equivalents of KCl (0.077 g, 1.03 mmol) were added as a solid and the solution heated at 50 C° for 24 hours. ^{195}Pt NMR shows the predominant species to be $[Pt(Ox)Cl_2]^{2-}$ (**3**) with less than 10 % contributions from $[PtCl_4]^{2-}$ (**1**) and $[Pt(Ox)_2]^{2-}$(**5**). The solution was cooled to 5 C° and centrifuged to separate precipitated $K_2[Pt(Ox)_2]\cdot 2H_2O$ (**5**). Vapor diffusion of acetone into the supernate

produced clear and red crystals. The clear crystals were presumed to be KCl and were not investigated. A red crystal was selected and mounted for x-ray diffraction.

Sodium Dichlorooxalatoplatinate(II)(**3**) A modification from the synthesis of potassium dichlooxalatoplatinate(II) was used which proved to be more synthetically useful than for $K_2[Pt(Ox)Cl_2]\cdot H_2O$. K_2PtCl_4 (**1**) was heated at 50 C° with ten equivalents of K_2Ox for 24 hours. The solution was cooled to 5 C° in a refrigerator and $K_2[Pt(Ox)_2]\cdot 2H_2O$ (**5**) was separated by centrifugation as a yellow solid. Two equivalents of tetra-n-butylammonium nitrate ($TBA(NO_3)$) were added as a solid to the supernate containing $[Pt(Ox)Cl_2]^{2-}$ (**3**) and the solution was extracted five times with 5 mL of CH_2Cl_2. Ion exchange of an aqueous/methanol solution of the TBA salt of **3** over Dowex 50W-X8 in the sodium form gave $Na_2[Pt(Ox)Cl_2]$ (**3**) as an orange/red solid.

Tetra-n-butyl ammonium salts These compounds were prepared as previously described (39,40). The solids obtained are soluble in dichloromethane, methanol, ethanol, and chloroform.

Potassium and Sodium Bis(malonato)platinate(II) (**13**) Malonic acid (0.50 g, 4.8 mmol) was dissolved in 25 mL of water. The pH of the solution was adjusted with 3M KOH to 6.0. $K_2[PtCl_4]$ (**1**) (0.200 g, 0.48 mmol) was added as a solid and the solution stirred for 3 days at room temperature during which time ^{195}Pt NMR was used to follow the concentration of species in solution. The yellow solution was rotary evaporated to near dryness and the solid dissolved in a minimum amount of warm water. The solution was left overnight in a refrigerator at 5 C°, and the solid was centrifuged from the

supernate. The solid was washed twice with 1 Ml of cold water. Repeated stirring and concentration of the supernate gives 75 % yield (0.184 grams). The preparation of the sodium salt is the same as for the potassium salt, except the malonic acid solution was neutralized with 3M NaOH. The sodium salt is less soluble than the potassium salt.

Potassium and Sodium *syn-* and *anti*-Bis(2-methylmalonato)platinate(II) (**22**,**23**) The potassium and sodium salts were prepared by the same procedure as for the malonato complex (86 % yield). Sodium salts are less soluble than potassium salts. The syn and anti isomers can be separated from each other by their solubility in H_2O. When the yellow solid obtained from concentrating and cooling to 5 C° is washed with cold water the supernate is enriched in the syn isomer **22**. Dissolving both isomers in a minimum amount of warm water and then storing overnight at 5 C° leaves predominantly the anti isomer **23** as a yellow solid. Vapor diffusion of acetone into an aqueous solution of the yellow solid gave yellow/green needles that were used for x-ray diffraction.

Potassium *trans*-dihydroxobis(oxalato)platinate(IV) Hexahydrate (**28**) The preparation was essentially the same as first reported by Werner and most recently by Preetz (39-41). ^{195}Pt and ^{13}C NMR showed complete oxidation of $[Pt(Ox)_2]^{2-}$ (**5**) to the trans-dihydroxo Pt(IV) complex **28**. Diffusion of acetone into an aqueous solution gave green crystals of $K_2[trans\text{-}Pt(OH)_2(Ox)_2]\cdot x\ H_2O$ (**28**). The sodium salt $Na_2[trans\text{-}Pt(OH)_2(Ox)_2]\cdot 6\ H_2O$ was prepared by ion exchange of an aqueous solution of the potassium salt over Dowex 50W-X8 in the sodium form. Diffusion of acetone into an

aqueous solution of **28** in the sodium form gave yellow crystals of Na_2[*trans*-$Pt(OH)_2(Ox)_2]\cdot 6\ H_2O$ (**28**).

Potassium *cis*-dihydroxobis(oxalato)platinate(IV) Hydrate(**40**) A solution of trans-$Pt(OH)_2(Ox)_2$ (**28**) was heated at 70 C° for 4 days. ^{195}Pt NMR showed the solution to be a 80/20 mixture of cis/trans. Diffusion of acetone into an aqueous solution gave yellow crystalls of two types. Plate shaped crystals were shown to be K_2 cis-$Pt(OH)_2(Ox)_2\cdot xH_2O$ (**40**) by x-ray crystallography.

Sodium *trans*-dihydroxobis(malonato)platinate(IV) Hexahydrate (**31**). The sodium salt was prepared by addition of 2 equivalents of H_2O_2 to an aqueous solution of $Na_2[Pt(Mal)_2]$ (**13**), and heating the solution at 50 C° for 15 minutes. ^{195}Pt and ^{13}C NMR showed complete conversion of **13** to the *trans*-dihydroxo Pt(IV) complex. Sodium [*trans*-$Pt(OH)_2(Mal)_2]^{2-}$ was recrystallized from aqueous solutions as green yellow needles of Na_2[*trans*-$Pt(OH)_2(Mal)_2]\cdot 6\ H_2O$ (**31**).

Spectroscopy

Nuclear Magnetic Resonance (NMR) All NMR spectra were obtained on either Bruker WM250, AC300, or AM500 spectrometers. ^1H NMR spectra were recorded in 5mm single frequency or dual frequency probes operating at 250.132, 300.132, or 500.132 Mhz. ^1H NMR spectra were typically run at 5,000 Hz spectral width, with 16-64 scans, 16K data points, and 1 sec. delay between 5-μs pulses (60° tilt). Gaussian line

shapes were obtained for high resolution spectra by the application of a gaussian weighting of the data before fourier transformation. The gaussian weighting was typically -2 to -4 Hz with gaussian broadening of 0.2 to 0.6. Integratable ^{1}H NMR spectra were run with 30 sec. delay between scans. Solutions in H_2O or D_2O/H_2O mixtures were run with 1 sec. presaturation of the HOD resonance. Chemical shifts were measured relative to internal references of dioxane (3.53 ppm) in water and $CHCl_3$ (7.24 ppm) in chloroform.

^{13}C NMR spectra were recorded in 5mm or 10mm dual frequency probes operating at 62.89, 75.46, or 125.76 Mhz. ^{13}C NMR spectra were typically run at 15,000 Hz spectral width, with 400-4000 scans, 32K data points, and 3 sec. delay between 5-μs pulses (40° tilt). Signal to noise enhancement was achieved by the application of an exponential weighting of the data before fourier transformation. The exponential weighting was typically 2-5 Hz. Integratable ^{13}C NMR spectra were run in the inverse gated mode, with 60 sec. delay between scans. Chemical shifts were measured relative to internal references of dioxane (67.73 ppm) in water and $CDCl_3$ (77.0 ppm) in $CDCl_3$.

^{31}P NMR spectra were recorded in 5mm or 10mm dual frequency probes operating at 101.27 or 202.49 MHz. ^{31}P NMR spectra were typically run at 10,000-30,000 Hz for WM250, and 30,000-100,000 Hz spectral width for the AM500, with 256-4000 scans, 32K data points, and 0.5 sec. delay between 30-μs pulses (50° tilt WM250; 10-μs pulses = 60° tilt AM500). Signal to noise enhancement was achieved by the application of an exponential weighting of the data before fourier transformation. The

exponential weighting was typically 4 to 10 Hz. Chemical shifts were measured relative to an external reference of 1 M $[PO_4]^{3-}$ (0 ppm), except when $[PO_4]^{3-}$ was present in solution.

^{195}Pt NMR spectra were recorded in 5mm or 10mm dual frequency probes operating at 53.52 or 107.47 MHz. ^{195}Pt NMR spectra were typically run at 50,000 Hz for WM250, and 125,000 Hz spectral width for AM500, with 4000-64000 scans, 16K data points, and 0.04 sec. delay between 30-μs pulses (50° tilt WM250; 10-μs pulses = 60° tilt AM500). Signal to noise enhancement was achieved by the application of an exponential weighting of the data before fourier transformation. The exponential weighting was typically 25 to 75 Hz. Gaussian lineshapes were obtained for high resolution spectra by the application of a gaussian weighting of the data before fourier transformation. The gaussian weighting was typically -10 to -20 Hz with gaussian broadening of 0.2 to 0.6. Integratable and high resolution ^{195}Pt NMR spectra were run with 0.5 sec. delay between scans and a spectral width of 10,000 Hz. Chemical shifts were measured relative to an external reference of 0.1 M $Na_2[PtCl_6]$ (0 ppm).

Ultraviolet and Visible (UV-vis).

Ultraviolet-Visible spectra (UV-vis) were collected on a Shimadzu UV-3000 dual wavelength double beam spectrophotometer in 0.2 mm quartz cells. The reference cell contained the solvent system used for dissolving the sample. Spectra were accumulated by a IBM personal computer interfaced with the spectrophotometer and displayed with the program Spectra Calc.

Oxidative Titrations

Oxidative titrations were monitored potentiometrically and by UV-vis spectra. The oxidations were carried out in 0.1 N H_2SO_4 in a thermostated vessel at 23 C° with $(NH_4)_2Ce(NO_3)_6$ (dissolved in 1 N H_2SO_4) as the oxidizing agent. Typically the concentration of $[Pt(Ox)_2]^{2-}$(**1**) was $1x10^{-3}$M and the oxidant was $1x10^{-1}$M. Potentiometric measurements were monitored with a platinum electrode and a Ag/AgCl reference electrode using a multimeter from Radiometer Copenhagen.

X-Ray Crystallography

Suitable crystals for x-ray crystallography were frequently obtained by diffusing a non-solvent (acetone) into an aqueous solution of the purified compound. Suitable crystals were further selected by the extinction of polarized light under a microscope. Crystals were mounted to a glass fiber with epoxy resin. A viscous solution of paratone "N" and mineral oil (3:1) was applied to crystals which were moisture and/or air sensitive. Unit cell dimensions were obtained by least-squares refinement using 25 centered reflections for which $15° < 2\Theta < 30°$. The radiation typically used was graphite-monochromatized Mo Kα (λ=0.71069 Å). Intensity data were taken on a Nicolet R3mE four-circle diffractometer operating in the $\Theta/2\Theta$ or w mode. All crystallographic calculations were performed on a Data General Eclipse computer using a SHELXTL program package by G.M. Sheldrick, Nicolet Instrument Corp., Madison WI. Three check reflections were monitored every 100 reflections to assess any losses of intensity due to crystal degradation. When present, data obtained during degradation

was scaled due to the loss of intensity. Data reduction was carried out for all reflections with $I > 3\sigma(I)$ for structure refinement. The space group was determined from systematic absences in the data collected and the final refinement characteristics of the structure (R_w, R_m). The Pt and other heavy atom positions were determined from Patterson synthesis. The remaining non-hydrogen atoms were determined by difference synthesis, and from independent information obtained by other analytical methods for the presumed composition of the complex. All non-hydrogen atoms were refined anisotropically by block-cascade least-squares minimizing $\Sigma w\Delta^2$. The weighting scheme used was $w=k(\sigma^2(F_o) + 0.001\ F_o^2)^{-1}$. Absorption corrections were calculated by Gaussian integration using crystal dimensions between indexed crystal faces. Atomic scattering factors, including terms for anomalous scattering, were taken from the International Tables for X-ray Crystallography (42). Hydrogen atom refinement included a common refined isotropic thermal parameter, and calculated positions when difference map peaks were ambiguous to the hydrogen location. Hydrogen atom positions were removed from the model if the model's refinement was not improved.

Listings of observed and calculated structure factors for each complex are listed in Appendix A and are available upon request from the Department of Chemistry at Montana State University.

RESULTS AND DISCUSSION

Reactions of Pt(II) with Dicarboxylic Acids

In this chapter, the solution chemistry of Pt(II) with several dicarboxylic acids will be presented. The bis(oxalato)platinate(II) complex is one of the mononomeric components in the synthesis of one-dimensional Pt chain compounds (86,87). An understanding of the chemistry for these mononuclear Pt(II) complexes is a prerequisite to studying the more complex solution properties for one-dimensional Pt chains. The chemistry of several other dicarboxylic acids has been investigated with the hope of providing new monomers for one-dimensional Pt chain polymerizations.

The solution coordination chemistry of multidentate ligands with both nitrogen and oxygen donor atoms to platinum(II) has been well investigated (43-45). Considerably less is known about multidentate ligand complexes with only oxygen donors. The bis(oxalato)platinate(II) complex was identified over a century ago, and has been well characterized (38,39). The extensions to bis malonato, squarato, and acetylacetato complexes have been described only recently (40,46,47). Complexes of platinum(II) with bidentate oxygen donors have generated considerable interest in several areas. A new generation of antitumor drugs is based on mixed ligand complexes involving a cis-diammineplatinum(II) fragment and various bidentate oxygen donor ligands (43,48,49). Partially oxidized polymers of bis(oxalato)platinate(II) are one dimensional conductors (3,7,32). These one-dimensional complexes are the principle interest of this study. An understanding of the chemistry of the monomeric Pt(II) complexes is needed before undertaking the investigation of the one-dimensional complexes.

It is well established that ^{195}Pt NMR is a valuable method for structure elucidation and determination of reaction mechanisms of platinum complexes (6). ^{195}Pt NMR studies of amino acid complexes of cis-$[Pt(NH_3)_2(H_2O)_2]^{2+}$ have shown that unidentate O-bound ligands can have a long lifetime before ring closure to form a N,O chelate ring. However, recent reports of the reaction between cis-$[Pt(NH_3)_2(H_2O)_2]^{2+}$ and 2-aminomalonic acid studied by ^{195}Pt NMR indicate that monodentate O-bound species are not observed enroute to the bidentate metastable O,O' bound 2-aminomalonato complex (43).

In this chapter, multinuclear NMR and X-ray crystallography are used to demonstrate the structure of complexes formed between platinum(II) and multidentate oxygen donor ligands. Chelated complexes are the eventual products, but monodentate complexes are present in high concentrations during ligand substitution reactions, and in low concentrations at equilibrium. Monodentate complexes could have considerable importance in the substitution reactions of platinum(II).

Two principles were used extensively in assigning the observed NMR resonances:

1. For monodentate complexes, ^{195}Pt shifts depend in a additive way on the nature of the donor atom (6).

2. When five and six membered bidentate chelate rings are formed between given donor atoms, large upfield shifts are observed.

Reactions with $[PtCl_4]^{2-}$ (**1**) were studied as follows. Approximately 0.050 g of **1** was dissolved in 1.5 mL of H_2O. The solution was centrifuged and the supernate was placed in a 10 mm NMR tube. Ten mole equivalents of dicarboxylic acid ligand was

dissolved in 1.4 mL of H_2O and added to the solution of **1**. 0.1 mL of D_2O was added for a lock signal. The pH of the solution was adjusted with 3M KOH or NaOH. To follow the reaction of $[Pt(H_2O)_4]^{2+}$ (**6**) with one of the dicarboxylic acid ligands, approximately 20 mL of a stock solution of **6** in 1 M $HClO_4$ (2.5 mg/mL) was precipitated as $[Pt(OH)_2]\cdot nH_2O$ at pH 7.0 by addition of NaOH (37). The solid $[Pt(OH)_2]\cdot nH_2O$ was filtered, washed with 3 mL cold water, and immediately dissolved in 2.9 mL H_2O containing 0.1 mL D_2O and 10 mole equivalents of the acid form of the ligand. ^{195}Pt NMR shows only a single resonance for **6** when $[Pt(OH)_2]\cdot nH_2O$ solid dissolves. The solution/suspension was degassed by freeze thawing and flushing with argon five times in a 10 mm NMR tube fitted with a rubber septum. Undissolved $[Pt(OH)_2]\cdot nH_2O$ slowly dissolves as the reaction progresses. These solutions were stable for at least three weeks after which time dark blue/black colored solutions were observed owing to oxidation of platinum complexes. Solutions that were not degassed turned dark blue/black as complexes are formed.

Reaction of Oxalic acid and $K_2[PtCl_4]$ (**1**).

Nuclear Magnetic Resonance When oxalic acid is added to a solution of $[PtCl_4]^{2-}$ (**1**) (Figure 22), new resonances appear at -1167 ppm and -1005 ppm, downfield from the starting material. The resonance at -1167 ppm is 18 ppm from $[PtCl_3(H_2O)]^-$ and is assigned to $[Pt(OxH\text{-}O)Cl_3]^{2-}$ (**2**) in which the oxalate is monodentate. The small shift is consistent with the substitution of the H_2O ligand with the oxygen ligand from carboxylate. The peak at -1005 ppm is larger and is assigned to $[PtOxCl_2]^{2-}$ (**3**), in which

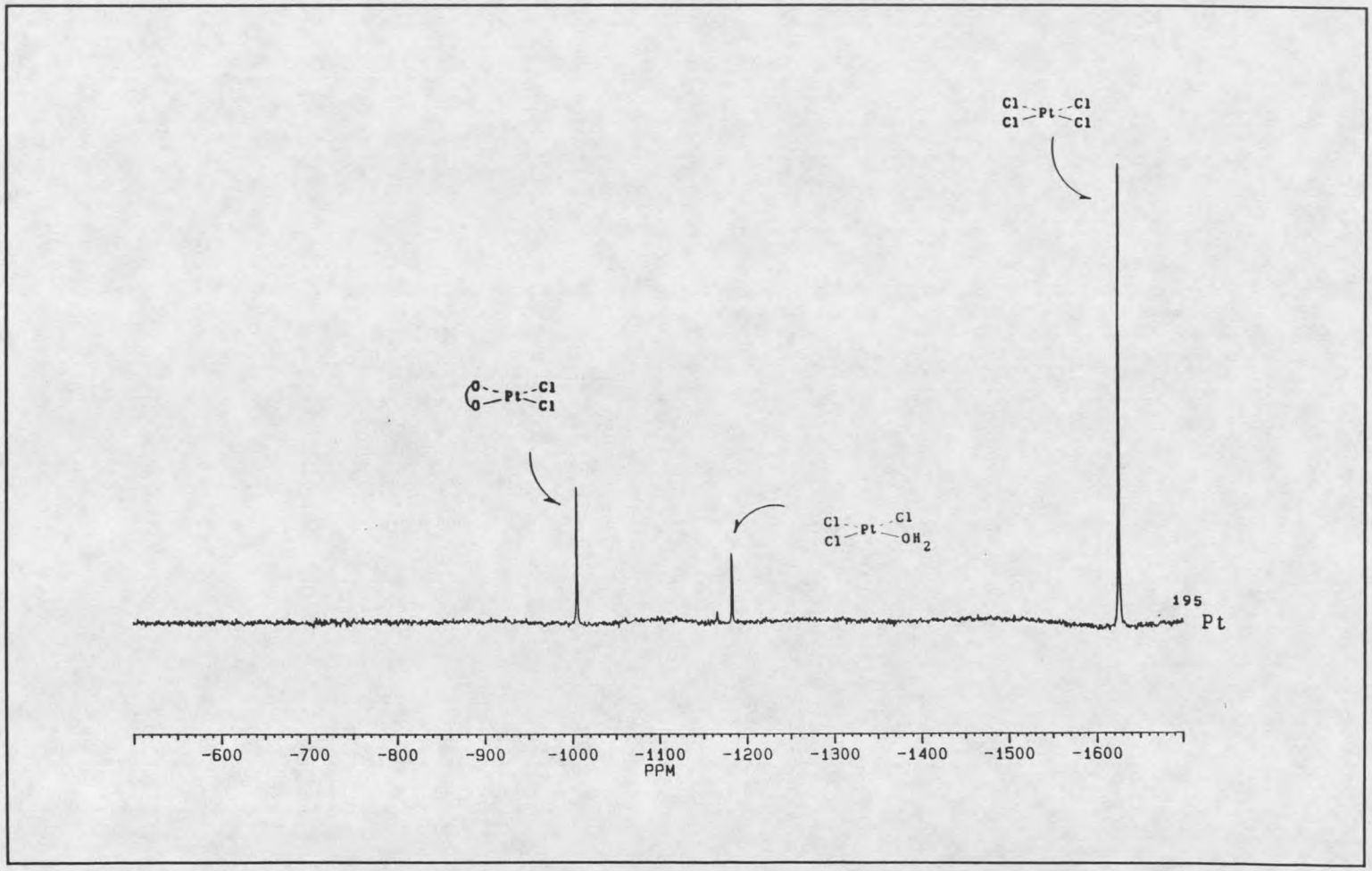

Figure 22 ^{195}Pt NMR of the Reaction of $[PtCl_4]^{2-}$ with Oxalic Acid pH=3.0.

oxalate is bidentate. $[PtOxCl_2]^{2-}$ falls 194 ppm to higher field than cis-$[PtCl_2(H_2O)_2]$, in keeping with the large upfield shift observed upon formation of five and six membered bidentate chelate rings. The carboxylato group for **3** is a single ^{13}C resonance at 170.12 ppm. The structure of **3** was confirmed by x-ray crystallography, (vide infra). At pH 2.0, these are the only resonances observed except for the hydrolysis products of **1**.

When the pH is raised above 3.0, new resonances are observed at -620 ppm and -525 ppm in the ^{195}Pt NMR before a yellow-green solid begins to precipitate. The solid was recrystallized from warm water to yield $K_2[Pt(Ox)_2]\cdot 2H_2O$ (**5**) which is identified from its crystallographic unit cell (38). A single ^{13}C resonance is observed for **5** at 170.2 ppm, and a single ^{195}Pt resonance at -525 ppm. The ^{195}Pt resonance for **5** is 560 ppm upfield from $[Pt(H_2O)_4]^{2+}$ (**6**), again demonstrating the additive large upfield shift observed upon formation of bidentate chelate rings. The resonance at -620 ppm arises from a transitory species formed as **3** is converted to **5**. Its low concentration prevented ^{13}C NMR data collection. The ^{195}Pt resonance is 384 ppm downfield from **3** and could be consistent with either of two complexes. The first is formed by replacement of chloride with an oxygen donor, and the second is the formation of a binuclear bridged μ-chloro or μ-hydroxo chloro species. However, a bridged species should not be favored in this pH range (50). We favor the formulation $[Pt(Ox)(OxH\text{-}O)Cl]^{2-}$ (**4**) where one oxalate is monodentate and the other oxalate is a bidentate ligand. When KCl is added to a solution of **5** at pH 5.0 (Figure 23), ^{195}Pt NMR shows the predominant complexes to be **3** and **1**. The intermediate complexes **2** and **4** are not observed in this pH range because of the fast chelate ring closure of deprotonated oxalate ligand. We find no

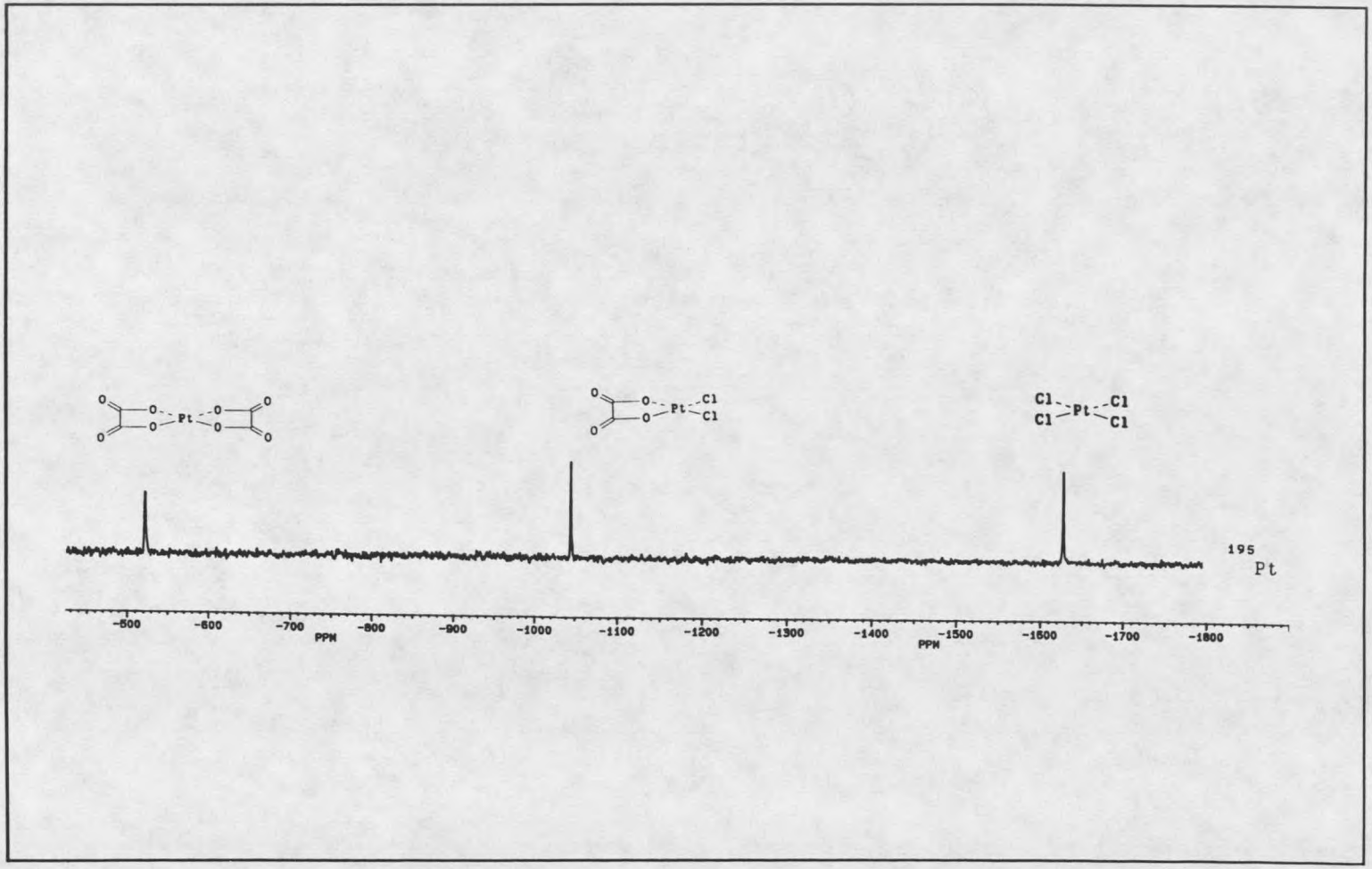

Figure 23 ^{195}Pt NMR of the Reaction of $[Pt(Ox)_2]^{2-}$ with KCl pH=5.0.

evidence for trans-$[Pt(OxH\text{-}O)_2Cl_2]^{2-}$ species proposed by Hoch and Milburn (51). It would appear that the intermediate species they observed was indeed **3**, and that the chelate effect dominates the trans effect of chloride in these Pt(II) complexes at pH=5.0. ^{195}Pt and ^{13}C NMR data for these complexes are summarized in Tables 1 and 2.

TABLE 1. ^{13}C NMR DATA

COMPLEX	STRUCTURE #	δ ^{13}C (ppm)
$[Pt(Ox)Cl_2]^{2-}$	3	170.12
$[Pt(Ox)Cl_2]^{2-}$ [a]	3	168.02
$[Pt(Ox)_2]^{2-}$	5	170.20
$[Pt(Ox)_2]^{2-}$ [a]	5	168.39

Ox = oxalato, [a] Tetra-n-butyl ammonium salts in $CDCl_3$.

TABLE 2. ^{195}Pt NMR DATA

COMPLEX	STRUCTURE #	δ Pt (ppm)
$[PtCl_4]^{2-}$ [a]	1	-1624
$[Pt(OxH\text{-}O)Cl_3]^{2-}$	2	-1167
$[Pt(Ox)Cl_2]^{2-}$	3	-1005
$[Pt(Ox)(OxH\text{-}O)Cl]^{2-}$	4	- 620
$[Pt(Ox)_2]^{2-}$	5	- 525
$[Pt(H_2O)_4]^{2+}$ [a]	6	24
$[Pt(OxH\text{-}O)(H_2O)_3]^{+}$	7	- 24
$[Pt(Ox)(H_2O)_2]$	8	- 338
$[Pt(Ox)(OxH\text{-}O)(H_2O)]^{-}$	9	- 345

Ox = oxalato, [a] chemical shifts reported in ref. 6.

X-Ray Crystallography $K_2[Pt(C_2O_4)Cl_2]\cdot H_2O$ (3). A thin plate-shaped red crystal (approximately 0.04 x 0.13 x 0.30 mm) was mounted on a glass fiber for crystallographic data collection. Unit cell dimensions were obtained by least-squares refinement using 25 centered reflections for which $18° < 2\theta < 26°$. Intensity data ($\pm h, \pm k, l$) were collected, and due to gradual loss of beam intensity from a weak x-ray tube, the three check reflections, monitored every 100 reflections, showed approximately 37% loss of intensity during the course of data collection. Since the loss of intensity for the check reflections followed a smooth curve, intensity data were scaled from that curve. Crystallographic data for this compound appear in Table 3.

TABLE 3. Crystallographic Data

	$K_2[Pt(C_2O_4)Cl_2\cdot H_2O$
a = 7.136 (2) Å	fw = 450.25
b = 7.308 (2) Å	space group $P\bar{1}$
c = 10.130 (4) Å	T = 24 C°
α = 86.75 (3) °	lambda = 0.71069 Å (Mo Kα)
β = 74.58 (3) °	ρ calcd = 3.27 g cm^{-3}
γ = 64.28 (2) °	μ = 169.6 cm^{-1} (Mo Kα)
V = 457.7 (3) $Å^3$	transm factor range = 0.10- 0.49
Z = 2	F (000) = 408
$R_w(F_o)$ = 0.0518	no. of unique rflns = 3994
$R(F_o)$ = 0.0526	no. of obsd. rflns, $I>3\sigma(I)$ = 1985
scan mode = $\Theta/2\Theta$	goodness of fit = 1.06

Data reduction, including corrections for Lorentz and polarization effects, gave 3994 independent reflections in the range $4° < 2\theta < 70°$, of which 1985 with $I > 3\sigma(I)$ were used for structure refinement. The volume of the triclinic unit cell was appropriate for two formula units so the centric space group was assumed and later confirmed by successful structure solution and refinement. The platinum position was determined from a Patterson synthesis, and remaining non hydrogen positions were determined by difference synthesis. Five reflections in the data set showed significant extinction and were excluded during final refinements. The refinement did not converge in the acentric space group. Final difference maps showed only the usual ripple near the platinum positions. Atom coordinates are given in Table 4. The structure of the anionic complex of **3** is shown in Figure 24 and bond distances and angles are in Tables 5 and 6. Bond lengths and angles are comparable to other known Pt-oxalate structures (38,49). An interesting feature of the crystal structure is the zig-zag chain structure of the anionic units. The chloride of one complex is positioned above the oxalate carbonyl carbon of the adjacent complex resulting in an electrostatically favored conformation. The Pt-Pt separation of 3.799(2) Å between Pt's in the same unit cell and 3.815(2) Å between Pt's in adjacent unit cells suggests minimal Pt-Pt interaction. For **3**, the potassium ions K(1) and K(2) are eight and seven coordinated respectively. If there is hydrogen bonding to the lattice water in **3**, it is very weak (nearest O...O contact is 3.00 Å)

TABLE 4. $K_2[Pt(C_2O_4)Cl_2]\cdot H_2O$: Atomic Coordinates and Equivalent Isotropic Temperature Factors ($Å^2$) with Standard Deviations.

Atom	x/a	y/b	z/c	*U*eq[a]
Pt	0.5230 (1)	0.2449 (1)	0.4452 (1)	0.0221 (2)
Cl (1)	0.3486 (6)	0.3917 (6)	0.2790 (4)	0.037 (2)
Cl (2)	0.8435 (5)	0.0581 (6)	0.2870 (4)	0.034 (1)
O (1)	0.251 (2)	0.394 (2)	0.598 (1)	0.030 (4)
O (2)	0.652 (2)	0.129 (2)	0.606 (1)	0.027 (4)
C (1)	0.279 (2)	0.356 (2)	0.718 (1)	0.024 (5)
C (2)	0.511 (2)	0.187 (2)	0.722 (2)	0.025 (5)
O (3)	0.144 (2)	0.436 (2)	0.826 (1)	0.045 (5)
O (4)	0.545 (2)	0.119 (2)	0.831 (1)	0.040 (5)
K (1)[b]	0.9967 (4)	-0.2492 (4)	0.5096 (4)	0.031 (1)
K (2)[b]	0.1612 (6)	0.1860 (6)	0.0451 (4)	0.049 (2)
O (5)[b]	0.229 (2)	-0.251 (3)	0.011 (2)	0.08 (1)

[a]Equivalent isotropic *U* defined as one-third of the trace of the orthogonalized U_{ij} tensor.
[b]The potassium ions and water oxygen atom are not shown in Figure 24.

TABLE 5. Bond Lengths (Å) with Standard Deviations for $K_2[Pt(C_2O_4)Cl_2]\cdot H_2O$

Bond	Length	Bond	Length
Pt-Cl(1)	2.298 (4)	Pt-Cl(2)	2.291 (3)
Pt-O(2)	2.04 (1)	Pt-O(1)	2.03 (1)
O(3)-C(1)	1.23 (2)	O(2)-C(2)	1.28 (2)
C(1)-C(2)	1.59 (2)	O(4)-C(2)	1.22 (2)
O(1)-C(1)	1.28 (2)		

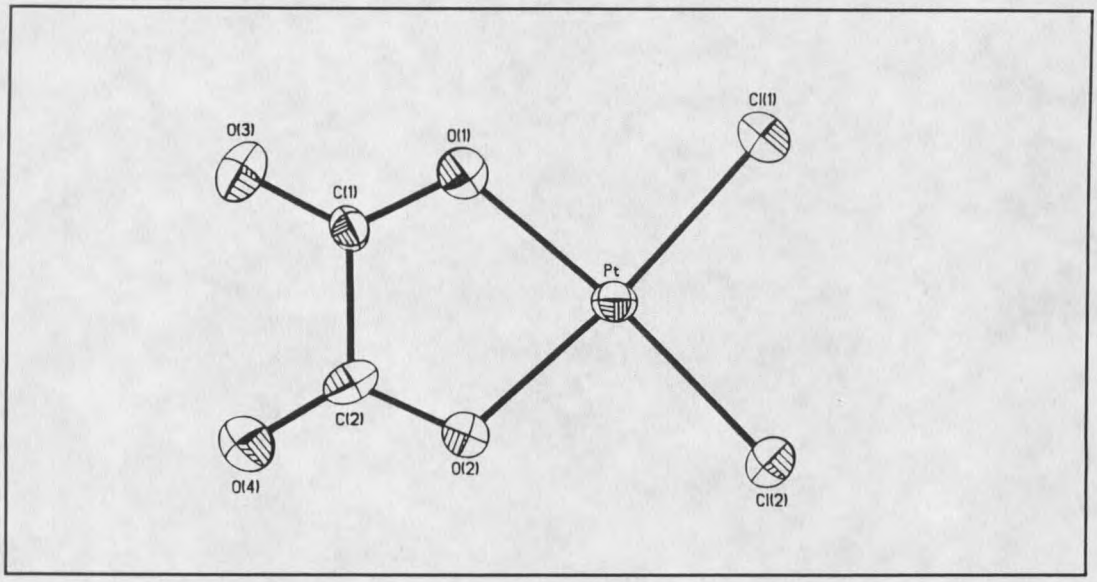

Figure 24 Thermal ellipsoid plot of $[Pt(Ox)Cl_2]^{2-}$ showing 50 % probability ellipsoids and numbering scheme for the structure.

TABLE 6. Bond Angles (deg) with Standard Deviations for $K_2[Pt(C_2O_4)Cl_2]\cdot H_2O$

Bond	Angle	Bond	Angle
Cl(1)-Pt-Cl(2)	93.0 (1)	Cl(1)-Pt-O(2)	174.7 (2)
Cl(2)-Pt-O(2)	92.3 (2)	Cl(1)-Pt-O(1)	91.9 (3)
Cl(2)-Pt-O(1)	174.9 (3)	O(2)-Pt-O(1)	82.8 (4)
Pt-O(2)-C(2)	113 (1)	Pt-O(1)-C(1)	113 (1)
O(3)-C(1)-O(1)	126 (1)	O(3)-C(1)-C(2)	119 (1)
O(1)-C(1)-C(2)	116 (1)	O(2)-C(2)-O(4)	125 (1)
O(2)-C(2)-C(1)	115 (1)	O(4)-C(2)-C(1)	121 (1)

TABLE 7. Anisotropic thermal parameters ($Å^2$ x 10^3) $K_2[Pt(C_2O_4)Cl_2]\cdot H_2O$:

ATOM	U_{11}	U_{22}	U_{33}	U_{23}	U_{13}	U_{12}
Pt	19(1)	23(1)	24(1)	4(1)	- 6(1)	- 8(1)
K(1)	28(1)	24(1)	40(2)	6(1)	-12(1)	-10(1)
K(2)	36(2)	50(2)	37(2)	10(2)	2(1)	- 5(1)
Cl(1)	33(2)	43(2)	30(2)	8(2)	-13(1)	- 9(1)
Cl(2)	26(1)	36(2)	28(2)	2(2)	- 1(1)	- 6(1)
O(1)	30(5)	30(5)	28(6)	2(4)	- 9(4)	-11(4)
O(2)	24(4)	29(5)	24(5)	2(4)	- 8(4)	- 6(4)
O(3)	32(5)	59(7)	29(6)	- 4(6)	2(5)	-11(5)
O(4)	36(5)	44(6)	33(6)	11(5)	-11(5)	-12(5)
C(1)	20(5)	38(7)	16(6)	4(5)	- 7(5)	-13(5)
C(2)	18(5)	20(6)	32(8)	- 3(5)	- 1(5)	- 6(4)
O(5)	55(8)	137(16)	43(9)	-18(9)	- 5(7)	-37(10)

The anisotropic temperature factor exponent takes the form:
$-2\pi^2(H^2a^{*2}U_{11} + \ldots + 2hka^*b^*U_{12})$

$K_2[Pt(C_2O_4)_2]\cdot 2H_2O$ (**5**). The crystal structure for this complex was first determined by Krogmann (38). Crystals obtained from aqueous solutions were determined to have the same unit cell parameters as determined by Krogmann.

Reaction of Oxalic acid and $[Pt(H_2O)_4]^{2+}$ (**6**)

Nuclear Magnetic Resonance When an oxalic acid solution is used to dissolve precipitated $[Pt(OH)_2]\cdot nH_2O$ (Figure 25), new resonances are observed at -24 ppm and -338 ppm at the expense of **6**. The smaller peak, at -24 ppm, is consistent with

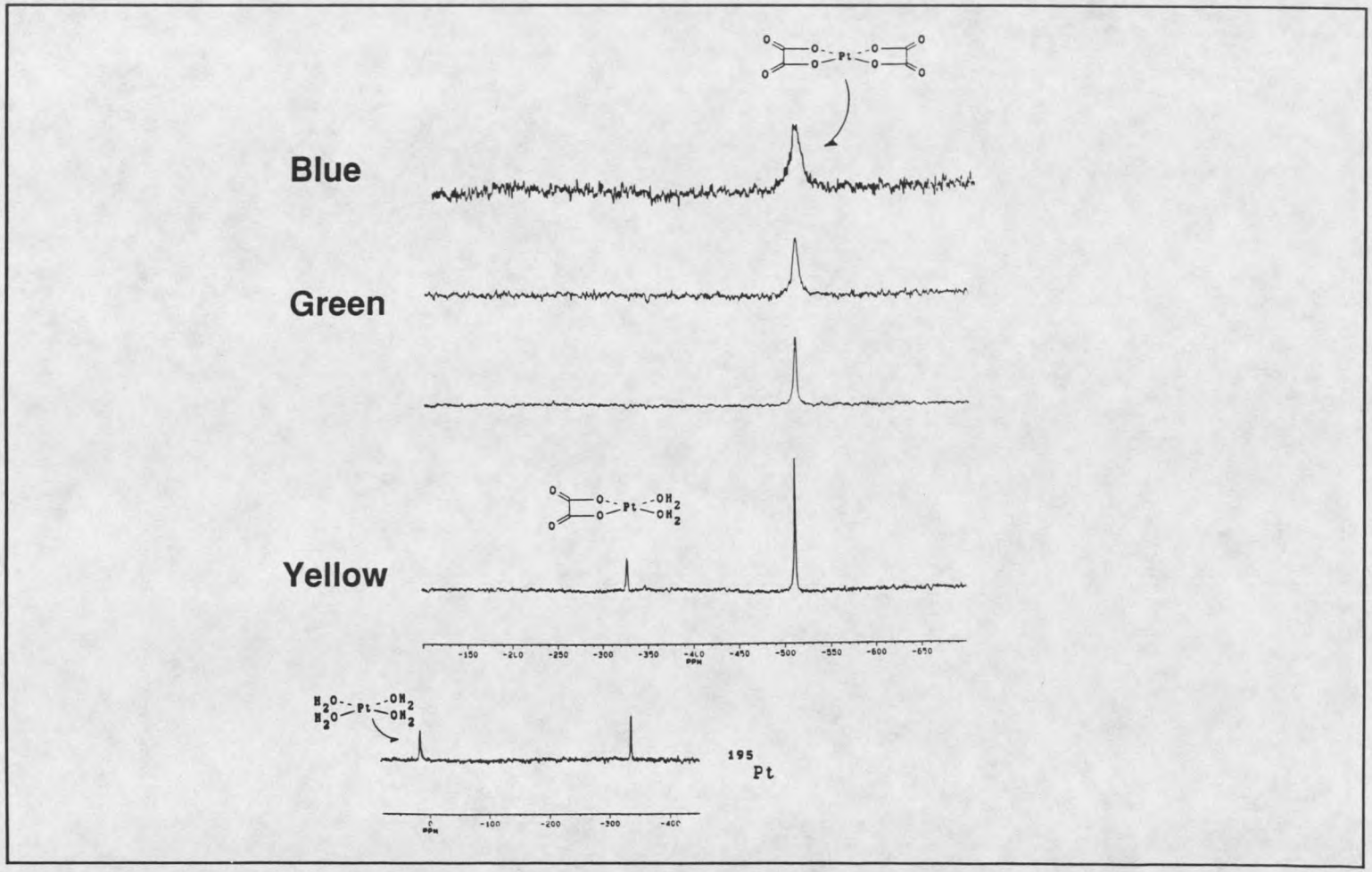

Figure 25 ^{195}NMR of the Reaction of $[Pt(H_2O)_4]^{2+}$ with Oxalic Acid.

monodentate carboxylato substitution for H_2O (52). This resonance is assigned to the monodentate $[Pt(OxH\text{-}O)(H_2O)]_3^+$ (**7**). The dominant peak in the spectrum is at -338 ppm. The large upfield shift of this resonance from **6** and **7** is consistent with the formation of bidentate $[Pt(Ox)(H_2O)_2]$ (**8**). As the reaction progresses, the resonance at -338 ppm is replaced by a peak at -525 ppm consistent with the formation of **5** as discussed previously. A small peak is also observed at -345 ppm. The small shift of this peak from **8** indicates a complex with one oxalate ligand bidentate and the other monodentate. The complex is assigned as $[Pt(Ox)(OxH\text{-}O)(H_2O)^-]$ (**9**).

When equilibrium solutions of **6**, **7**, **8**, and **9** are exposed to oxygen, dark blue colors are observed followed by broadening and disappearance of the resonance for **5**. The broadening is specific for **5** in these solutions as shown in Figure 26. The resonances for **8** and **9** in Figure 26 remain unaffected by the broadening of **5**. The linewidth of **5** could be attributed to several processes. The first could be a paramagnetic interaction. A paramagnetic complex has an unpaired electron associated with the complex. The magnetic field induced by the unpaired electron has ca 1000 times the magnetic field of a nucleus observed in NMR. The magnetic field of the electron is rapidly fluctuating, and this fluctuating magnetic field can efficiently couple with the magnetic field of the nucleus. The coupling between a free electron and nuclear magnetic moment causes the nucleus to relax from excited state to ground state very fast on the NMR time scale. This fast relaxation will result in broadening of NMR transitions. As the relaxation time becomes increasingly shorter, the energy of the NMR transition becomes more uncertain, and the resonance broadens.

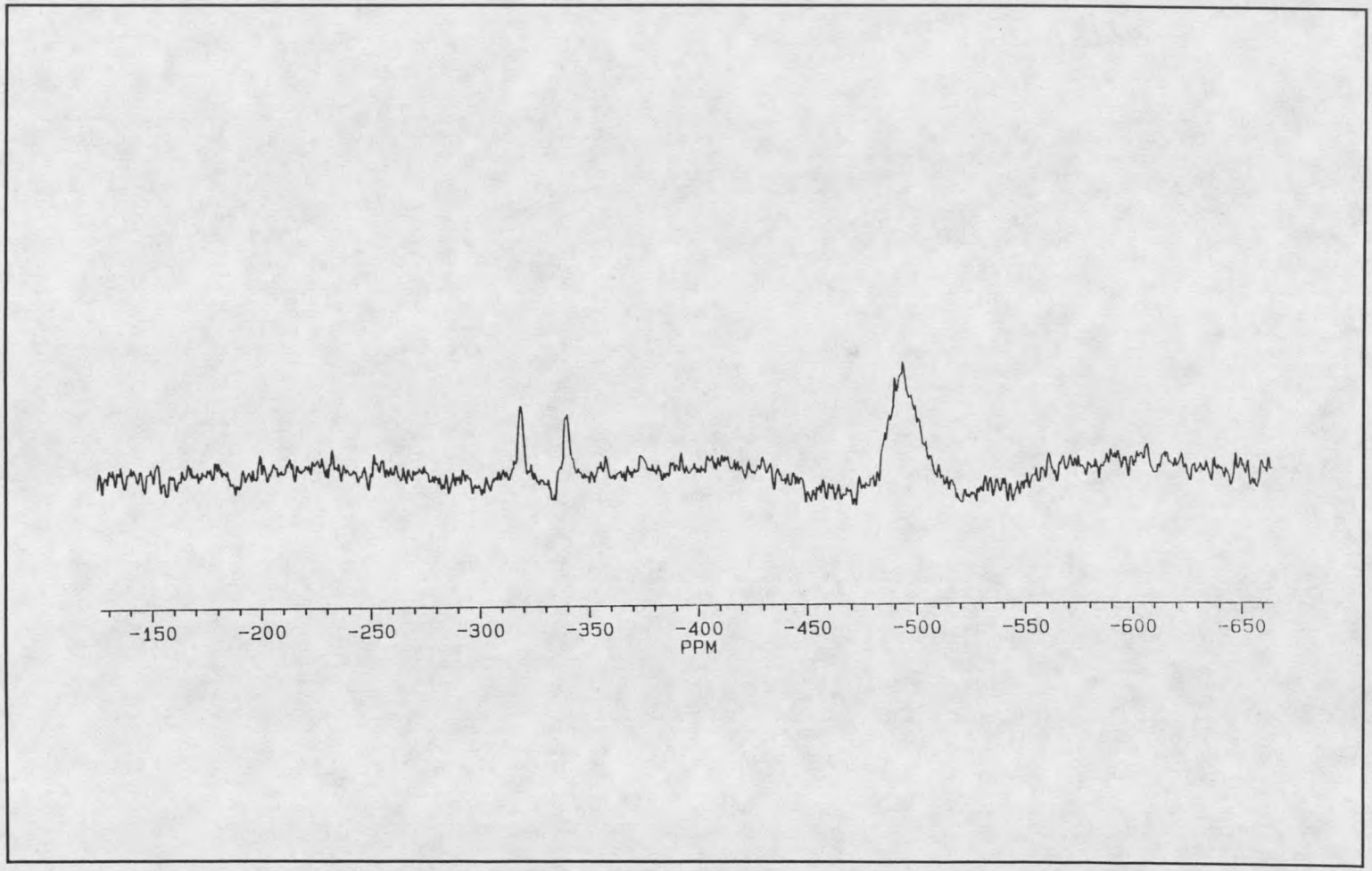

Figure 26 ^{195}Pt NMR Spectrum of Blue $[Pt(Ox)_2]^{2-}$ Solutions.

If the broadening of **5** is the result of a paramagnetic interaction, it is specific only to **5**. This is unusual in cases of bulk paramagnetic species in NMR solutions. A typical use of paramagnetic relaxation is the introduction of $[Cr(acac)_3]$. $[Cr(acac)_3]$ is paramagnetic and it reacts nonspecifically with the entire NMR sample, so all NMR resonances are broadened equally. An example of specific broadening in NMR is the interaction of $[Cr(phen)_3]^{3+}$ with small oligonucleotides (53). The specific binding of $[Cr(phen)_3]^{3+}$ to the oligonucleotide causes only ^1H NMR resonances adjacent to the binding site to be broadened. Any ^1H resonances that are distant from the binding region are not affected by the $[Cr(phen)_3]^{3+}$ binding. If the broadening is paramagnetic broadening, it is a specific interaction with **5** only. A second possible mechanism for broadening of **5** is related to large molecular weight and ordered molecules in solution. An NMR transition is a tensor property which is subject to the magnetic field in all directions of space. For small molecules in solution, the molecule can sample all orientations in space, and the nmr tensors σ_1 σ_2 and σ_3 are averaged by these rapid molecular motions into a single tensor $\sigma_{avg.}=(\sigma_1+\sigma_2+\sigma_3)/3$. If a molecule cannot sample all orientations in space, the tensors will not be averaged. This can happen in two ways. The first is if the molecule has a large molecular weight, it will move slowly through solution in comparison to the NMR frequency for the nucleus. The second is if the molecule orientates itself in the magnetic field. Magnetic field orientation does not allow the molecule to sample all orientations in comparison to the NMR frequency for the nucleus. This would be expected for molecules which possess a large intrinsic electrical or magnetic dipole. When these solutions are heated between 20 - 60 C° (Figure 27), the linewidth at half

height changes from 1000 Hz to 200 Hz at the same time as the color of the solution changes from dark blue to light green. When blue solutions are diluted with H_2O (Figure 28), the linewidth at half height changes from 1000 Hz to 200 Hz as the color of the solutions change from blue, to green, to yellow. When alkali salts are added to acidic blue solutions, copper colored needles rapidly precipitate from solution. These observations are consistent with reports of polymerization of air oxidized concentrated solutions of **5** (8,10,11). The ^{195}Pt and ^{13}C NMR data for these complexes are listed in Tables 1 and 2.

Reaction of Malonic acid and $K_2[PtCl_4]$ (**1**)

Nuclear Magnetic Resonance When malonic acid is added to a solution of **1**, and the pH of the solution is adjusted to 3.0, new resonances are observed in the ^{195}Pt spectrum as shown in Figure 29. A small peak is observed at -1149 ppm, which is 36 ppm to lower field than $[PtCl_3(H_2O)]^-$. This shift is consistent with replacement of coordinated H_2O with monodentate carboxylato and is assigned to the monodentate malonato complex, $[Pt(MalH\text{-}O)Cl_3]^{2-}$(**10**). The dominant peak in the ^{195}Pt spectrum is at -978 ppm, 167 ppm to higher shielding than the cis isomer of $[PtCl_2(H_2O)_2]$. The ^{13}C NMR spectrum of a solution containing 90% of this complex shows a single resonance in the carboxyl region at 179.47 ppm. This is consistent with a bidentate malonato complex, with equivalent carboxylato groups. This peak is assigned to the bidentate malonato species $[PtCl_2(Mal)]^{2-}$ (**11**). Two small peaks are observed at -595

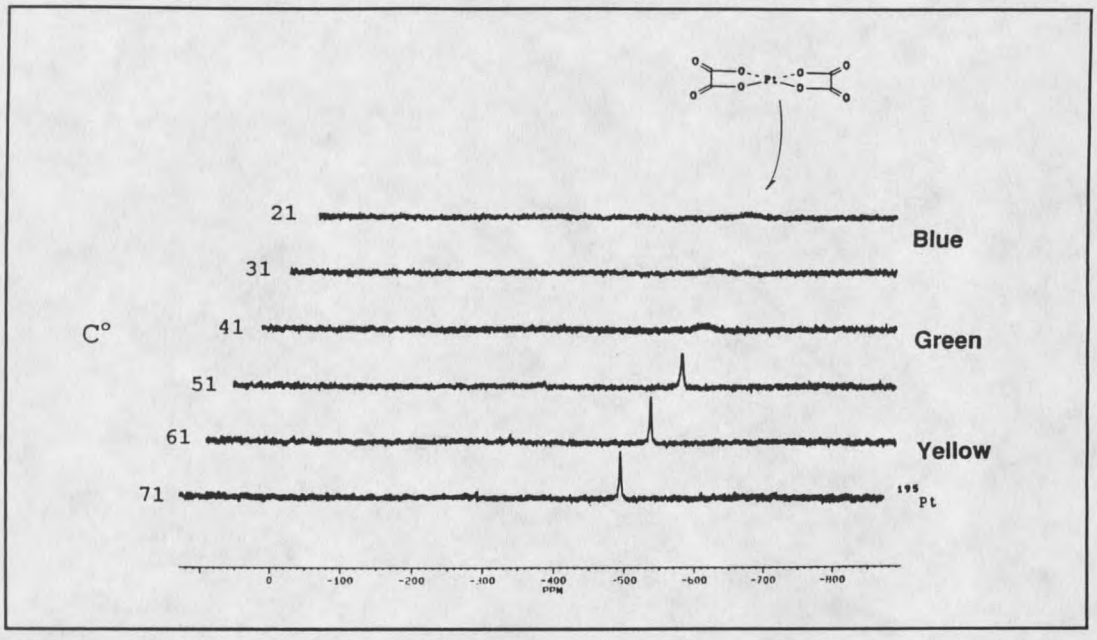

Figure 27 ^{195}Pt NMR of the Temperature Dependence of the Line Width of $[Pt(Ox)_2]^{2-}$ Blue Solutions.

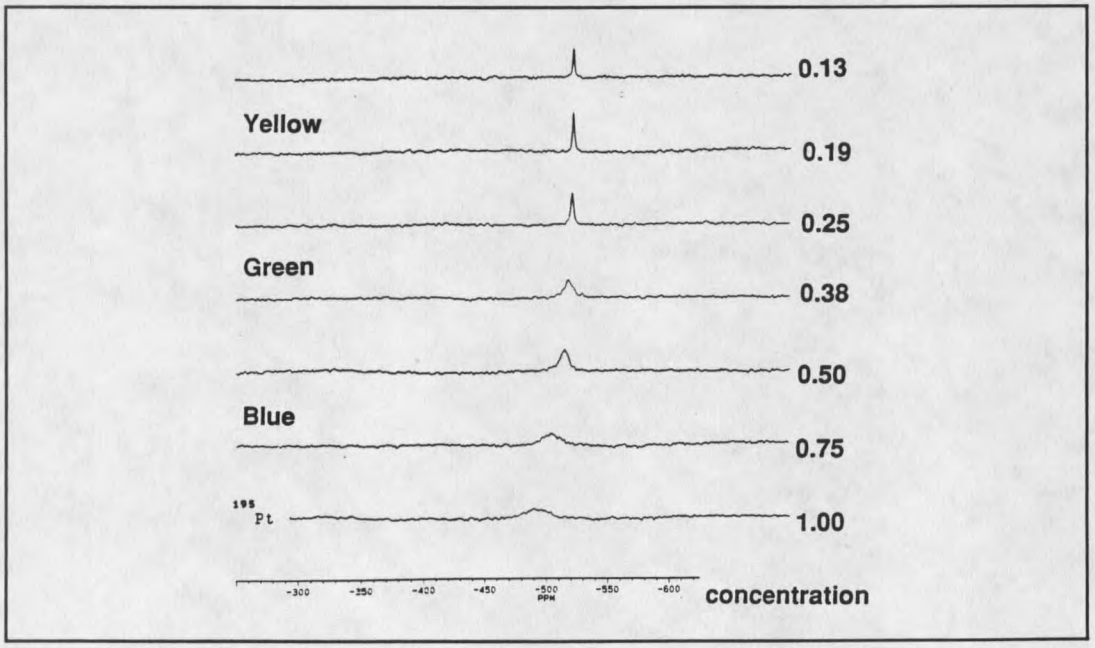

Figure 28 ^{195}Pt NMR of the Concentration Dependence for $[Pt(Ox)_2]^{2-}$ Blue Solutions.

ppm and -562 ppm in the ^{195}Pt NMR spectra. These resonances become dominant species at equilibrium in solutions at pH 6.0. Concentration of these solutions causes precipitation of a yellow solid. When this solid is isolated and dissolved in H_2O, a single resonance is observed at -562 ppm. The ^{13}C NMR spectrum shows a single resonance in the carboxyl region at 180.36 ppm. The resonance at -562 ppm is assigned to the bis malonato complex with both malonates bidentate, $[Pt(Mal)_2]^{2-}$ (**13**). The resonance at -595 loses intensity as the resonance for **13** increases, and the resonance at -595 ppm is the predominant resonance in the supernate after isolating **13**. The resonance at -595 ppm is consistent with the monochloro bis malonato complex $[Pt(Mal)(MalH\text{-}O)Cl]^{2-}$ (**12**) with one malonate bidentate and the other malonate monodentate. An integratable ^{13}C and ^{195}Pt NMR spectrum of the reaction of **13** with KCl is shown in Figure 30. The ^{13}C spectrum reveals four different carboxyl carbons of equal intensity shifted from the overlapping resonances of **11** and **13**, and the free malonic acid resonance. The four resonances are in agreement with four nonequivalent carboxyl groups in **12**. The ^{195}Pt and ^{13}C NMR data for these malonato complexes are listed in Tables 8 and 9.

TABLE 8. ^{195}Pt NMR Data.

COMPLEX	STRUCTURE #	δ Pt (ppm)
$[Pt(MalH\text{-}O)Cl_3]^{2-}$	10	-1149
$[Pt(Mal)Cl_2]^{2-}$	11	- 978
$[Pt(Mal)(MalH\text{-}O)Cl]^{2-}$	12	- 595
$[Pt(Mal)_2]^{2-}$	13	- 562
$[Pt(MalH\text{-}O)(H_2O)_3]^{+}$	14	- 32
$[Pt(MalH\text{-}O)_2(H_2O)_2]$	15	- 74
$[Pt(Mal)(H_2O)_2]$	16	- 314
$[Pt(Mal)(MalH\text{-}O)(H_2O)]^{-}$	17	- 331

Mal=Malonato.

TABLE 9. ^{13}C NMR Data

COMPLEX	STRUCTURE #	δ ^{13}C carboxyl	(ppm) methylene
$[Pt(Mal)Cl_2]^{2-}$	11	179.47	49.24
$[Pt(Mal)(MalH\text{-}O)Cl]^{2-}$	12	180.14	[a]
	12	179.72	[a]
	12	179.42	[a]
	12	177.08	[a]
$[Pt(Mal)_2]^{2-}$	13	180.36	48.31
$[Pt(Mal)_2]^{2-}$ [b]	13	177.19	49.89
$[Pt(MalH\text{-}O)(H_2O)_3]^{+}$	14	178.70	[a]
	14	173.36	[a]
$[Pt(Mal)(H_2O)_2]$	16	180.37	48.84

Mal = malonato, [a] = Overlapping resonances does not allow specific assignment of chemical shift. [b] = Tetra-n-butylammonium salts in $CDCL_3$

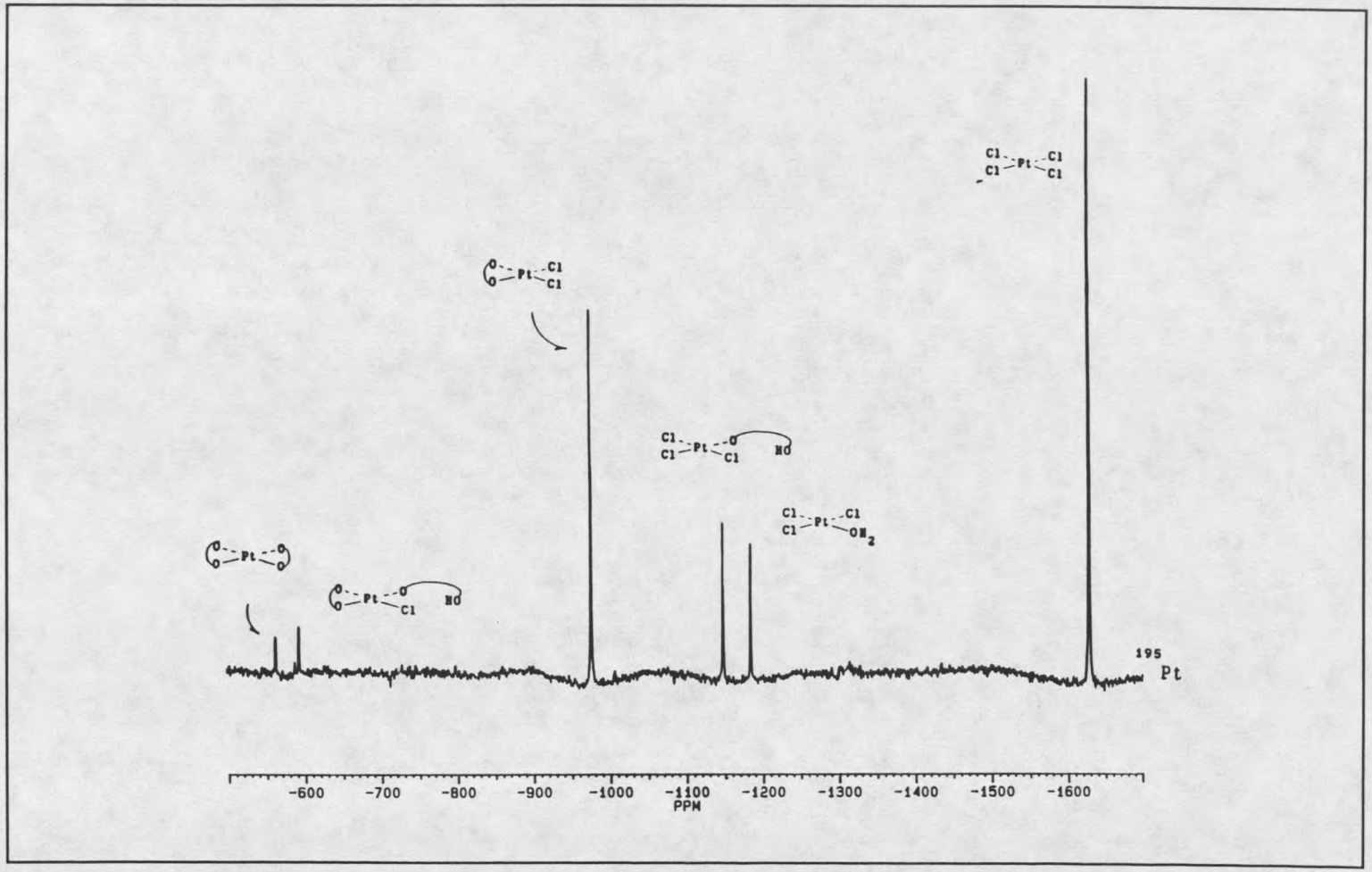

Figure 29 ^{195}Pt NMR of the Reaction of $[PtCl_4]^{2-}$ with Malonic Acid pH=3.0.

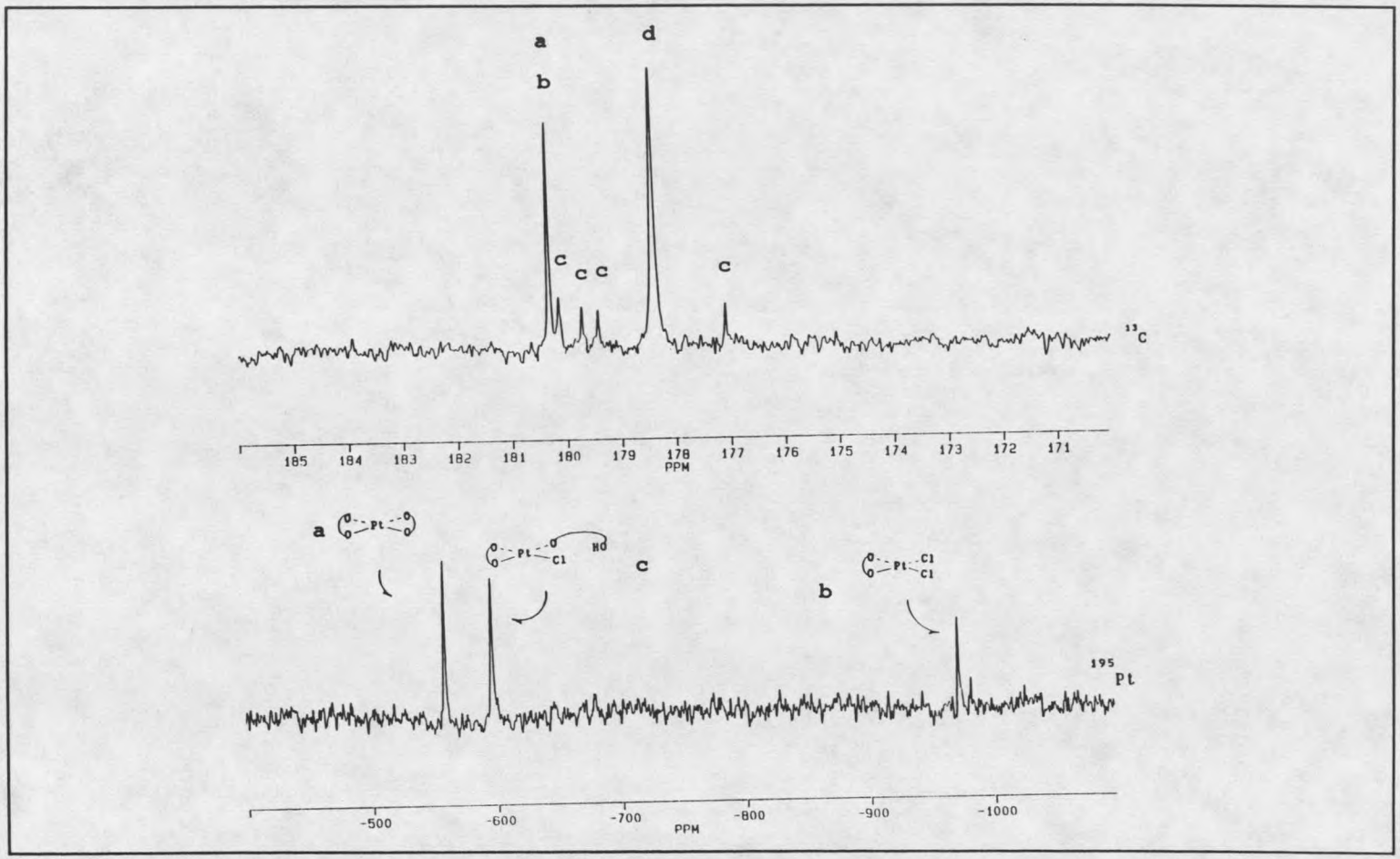

Figure 30 Reaction of $[Pt(Mal)_2]^{2-}$ with KCl pH=5.0. a = $[Pt(Mal)_2]^{2-}$, b = $[Pt(Mal)Cl_2]^{2-}$; c = $[Pt(Mal)(MalH\text{-}O)Cl]^{2-}$; d = $MalH_2$. Mal = malonato.

Reaction of Malonic acid and $[Pt(H_2O)_4]^{2+}$ (**6**)

Nuclear Magnetic Resonance When malonic acid was used to dissolve the neutral solid $[Pt(OH)_2]\cdot nH_2O$ new resonances were observed to form at the expense of **6**, as shown in Figure 31. A new resonance is observed at -32 ppm. The small shift from **5** indicates that the new species is formed by replacement of H_2O with monodentate carboxylate. This resonance is assigned to $[Pt(MalH\text{-}O)(H_2O)_3]^+$ (**14**). Subsequently, a peak is observed at -314 ppm. The large upfield shift of this resonance from **6** and **14** is consistent with the formation of the bidentate complex $Pt(Mal)(H_2O)_2$ (**16**). Two other resonances are observed at -74 ppm and -331 ppm. The small shift of the resonance at -74 ppm from **14** is consistent with the formation of a bis malonato complex with both malonates monodentate. Cis or trans geometry cannot be established from the NMR spectrum; however, the structure of the complex can be rationalized using the trans effect and chelate ring formation. The bis complex with two monodentate carboxylato groups is only observed for reactions of $MalH_2$ and $MmalH_2$ with **6**. A second carboxylato group added to **14** should be directed trans to the first because carboxylato is a better trans director than water. However, cis and trans-bis carboxylato species have been observed for the reaction of glycine and **6**. The pH of the reaction of **6** and glycine was 1.5 so that the amine nitrogen of glycine was protonated. Kinetically, glycine chelate ring closure could be much slower than for the monodentate carboxylato species described here. The absence of cis-bis monodentate species under our reaction conditions can then be accounted for by carboxylate being a better trans director than water and fast

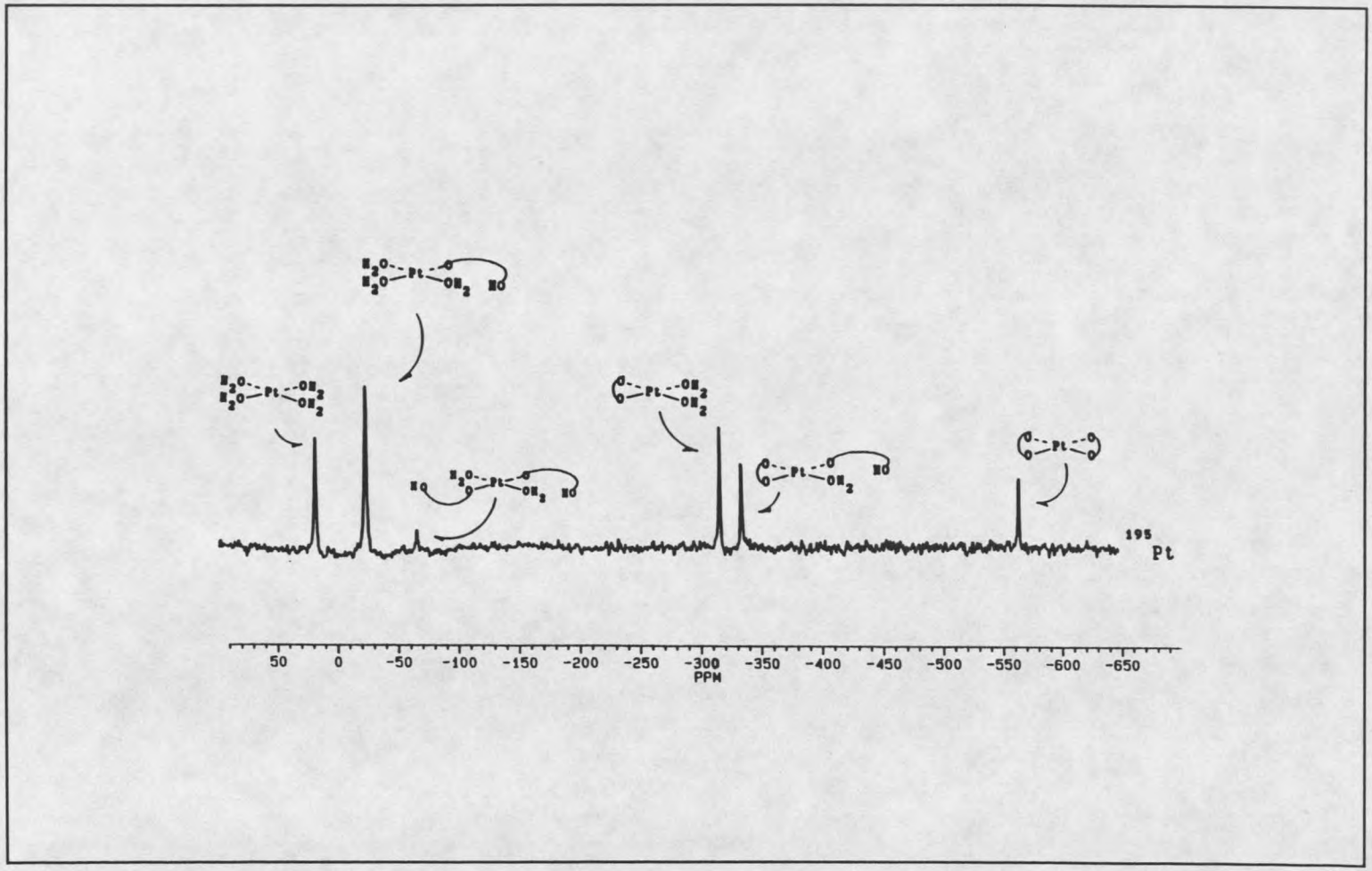

Figure 31 ^{195}Pt NMR of the Reaction of $[Pt(H_2O)_4]^{2+}$ with Malonic Acid.

chelate ring closure of any cis-bis species. In the reactions of $MalH_2$ and $MmalH_2$ with **1**, chelate ring closure of a monodentate species would be favored over formation of cis or trans-bis monodentate complexes because chloride is a better trans director than carboxylato. We assign the peak to trans-$[Pt(MalH\text{-}O)_2(H_2O)_2]$ (**15**) with both malonates monodentate.

Another resonance is observed at -331 ppm in the ^{195}Pt NMR spectrum. The small shift of this resonance from **16** is consistent with the formation of a bis malonato complex with one malonate bidentate and the other malonate monodentate. The resonance is assigned to the complex $[Pt(Mal)(MalH\text{-}O)(H_2O)]^-$ (**17**). The resonance for **13** at -562 ppm is observed to increase in concentration as the reaction progresses. The ^{195}Pt and ^{13}C NMR data for these malonato complexes are listed in Tables 8 and 9.

Reaction of 2-Methylmalonic acid and $K_2[PtCl_4]$ (**1**)

Nuclear Magnetic Resonance Figure 32 is the ^{195}Pt NMR spectra observed when 2-methylmalonic acid is added to a solution of **1** at pH 3.0. A new resonance is observed at -1149 ppm. The proximity of this resonance to that of $[PtCl_3(H_2O)]^-$ is consistent with replacement of coordinated H_2O with a carboxylato group, and this resonance is assigned to the monodentate 2-methyl malonato complex $[Pt(MmalH\text{-}O)Cl_3]^{2-}$ (**18**). The dominant peak in the ^{195}Pt spectrum is at -995 ppm, 184 ppm to higher field than cis-$[PtCl_2(H_2O)_2]$. The ^{13}C spectrum of a solution containing 90% of this complex shows a single dominant resonance in the carboxyl region at 181.43 ppm, consistent with a bidentate 2-methyl malonato species. This resonance is assigned to the bidentate 2-

methyl malonato species, $[Pt(Mmal)Cl_2]^{2-}$ (**19**). At low digital resolution ^{195}Pt NMR spectra, three small peaks are observed at -623, -608, and -600 ppm at pH 3.0 and greater. These peaks become dominant when solutions of pH 6.0 are allowed to reach equilibrium. At higher digital resolution,the resonance at -623 ppm is observed to be two peaks of equal intensity separated by 0.5 ppm. The resonances at -623 ppm arise from two diastereomers of $[Pt(Mmal)(MmalH\text{-}O)Cl]^{2-}$ (**20**,**21**) in which one of the ligands is bidentate and the other monodentate. The two resonances result from an interesting form of diastereoisomerism arising from the fact that both α carbon atoms are chiral in a complex like **20** shown in Figure 33. The two chiral centers result in two diasteromeric pairs of enantiomers for **20** and **21**. Thus, the observation of two ^{195}Pt resonances at -623 ppm affords further evidence for monodentate, bidentate structures. Concentration of these solutions gives a yellow solid. When this solid is isolated and dissolved in H_2O two resonances are observed at -608 and -600 ppm. These peaks are consistent with formation of two different isomers of bidentate bis(2-methylmalonato)platinate(II) as shown in Figure 33. We have drawn the chelate rings in an idealized planer geometry which makes it apparent that one isomer has methyl groups in a syn orientation with respect to the coordination plane of the Pt (**22**), and the other isomer has methyl groups in an anti orientation (**23**). Other workers have shown that Pt(II) complexes with malonato chelate rings prefer a boat conformation in the solid state (48,49). Several conformations of this chelate ring have similar energies and can be observed in solution. The solubilities of the syn and anti isomers are different. When the yellow solid is extracted with cold water, the ^{195}Pt, ^{1}H, and ^{13}C NMR spectra show

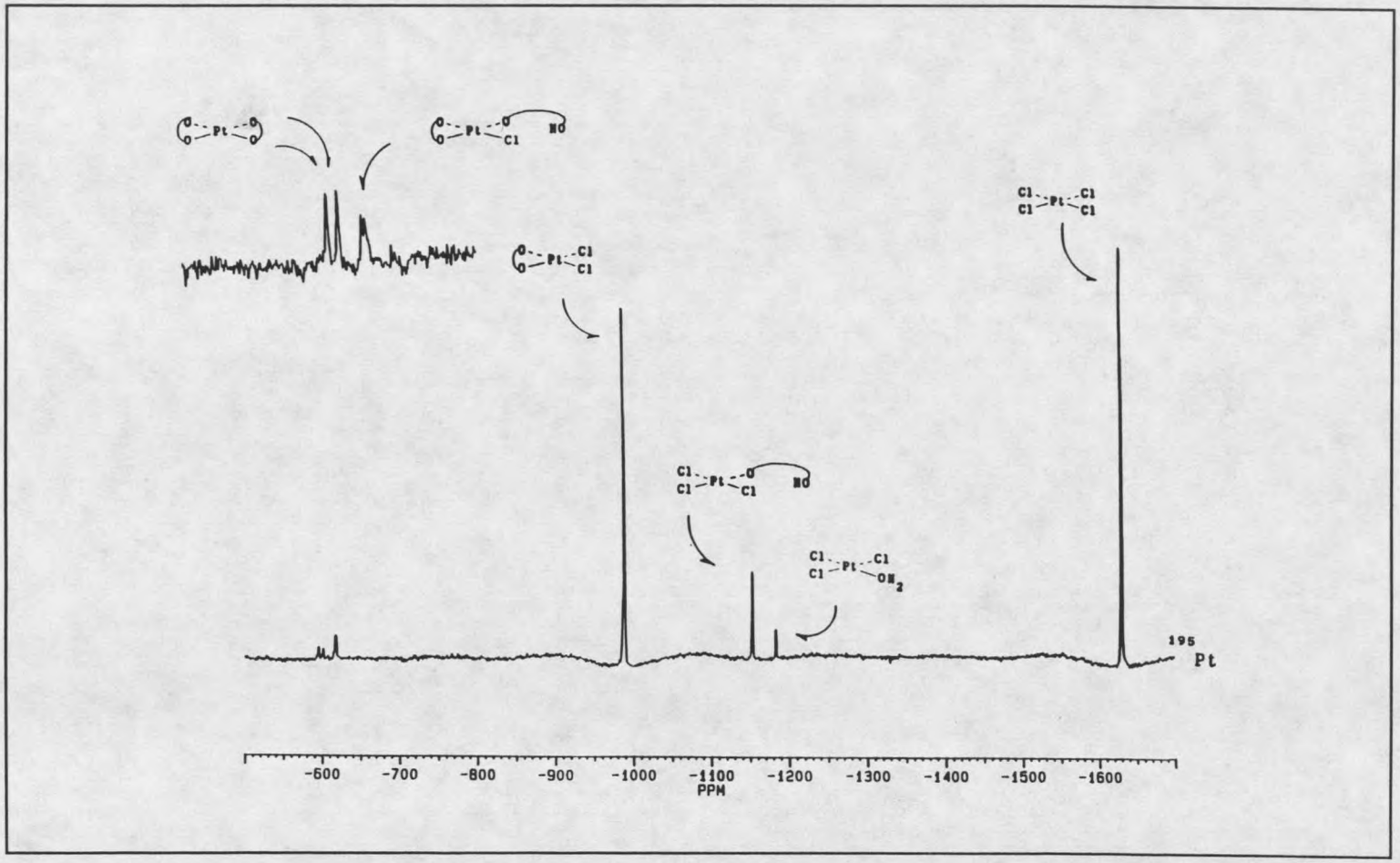

Figure 32 ^{195}Pt NMR of the Reaction of $[PtCl_4]^{2-}$ with 2-Methylmalonic Acid pH=3.0. Upper inset: detail of the bis(2-methylmalonato) region at pH=6.0.

resonances of unequal intensity for the two isomers. When undissolved solid is added to cold water extractions, the resonance for the peak at -600 ppm ^{195}Pt (^{1}H 4.1 ppm q, 1.13 ppm, d) increases in intensity. The structure of the least soluble isomer was shown by x-ray crystallography (vide infra), to be potassium [*anti*-bis(2-methylmalonato)platinate(II)]·$2H_2O$ (**23**). Therefore, the more soluble isomer whose ^{195}Pt resonance is at -608 ppm (^{1}H 4.15 ppm, q, 1.10 ppm, d) is the [*syn*-bis(2-methylmalonato)platinate(II)]$^{2-}$ complex (**22**). The ^{1}H spectra reveal a temperature dependence for the *syn* isomer **22** (Figure 34). Between 0 and 60 C°, the methine resonance for **22** shifts 0.18 ppm downfield; while the proton resonances of the trans isomer **23** are only slightly temperature dependent (0.03 ppm). The methine resonance for **23** is upfield from **22**, while the methyl resonance for **23** is downfield from **22**. This is as expected from the crystal structure in which it is observed that the methine protons of **23** lie in the shielding cone of the carbonyl group; while the methyl protons in the plane of the carbonyl group are deshielded. The equivalence of the protons for **22** shows that ring conformations are in rapid equilibrium on the NMR time scale. The temperature dependence of **22** suggests that ring conformations are differentially populated over the temperature range studied. ^{195}Pt and ^{13}C NMR data for these 2-Methylmalonato complexes are listed in Tables 10 and 11.

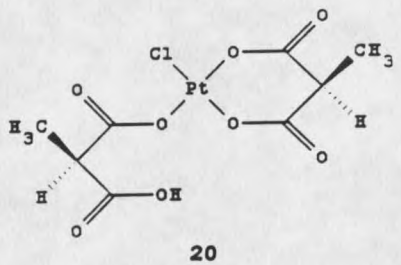

20

$[Pt(Mal)(MmalH\text{-}O)Cl]^{2-}$

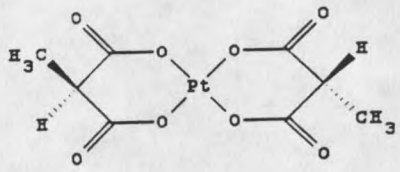

23

anti-$[Pt(Mmal)_2]^{2-}$

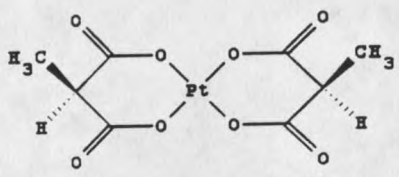

22

syn-$[Pt(Mmal)_2]^{2-}$

Figure 33 Idealized Drawings of 2-Methylmalonato Complexes.

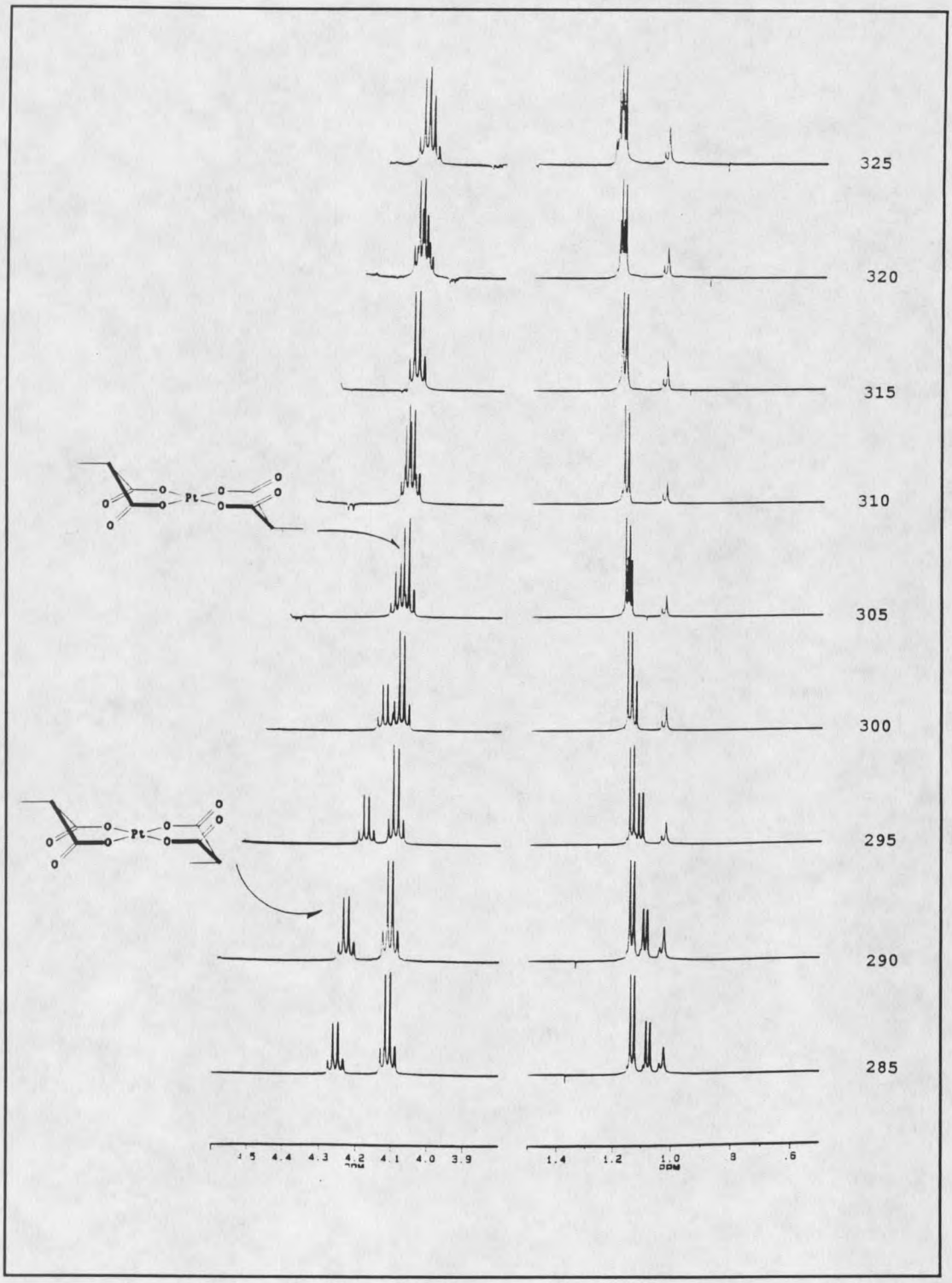

Figure 34 ^{1}H NMR Spectra of the Temperature Dependence for *syn*- and *anti*-$[Pt(Mmal)_2]^{2-}$ in Water.

TABLE 10. ^{195}Pt NMR Data.

COMPLEX	STRUCTURE #	δ Pt (ppm)
$[Pt(MmalH\text{-}O)Cl_3]^{2-}$	18	-1149
$[Pt(Mmal)Cl_2]^{2-}$	19	- 995
$[Pt(Mmal)(MmalH\text{-}O)Cl]^{2-}$	20	- 623
$[Pt(Mmal)(MmalH\text{-}O)Cl]^{2-}$	21	- 623
$[Pt(Mmal)_2]^{2-}$ [a]	22	- 608
$[Pt(Mmal)_2]^{2-}$ [b]	23	- 600
$[Pt(MmalH\text{-}O)(H_2O)_3]^{+}$	24	- 34
$[Pt(MmalH\text{-}O)_2(H_2O)_2]$	25	- 78
$[Pt(Mmal)(H_2O)_2]$	26	- 339
$[Pt(Mmal)(MmalH\text{-}O)(H_2O)]^{-}$	27	- 356

Mmal = 2-methylmalonato, [a] = methyl groups syn, [b] = methyl groups anti.

TABLE 11. ^{13}C NMR Data

COMPLEX	STRUCTURE #	δ ^{13}C (ppm) carboxyl	methine	methyl
$[Pt(Mmal)Cl_2]^{2-}$	19	181.43	52.05	14.49
$[Pt(Mmal)_2]^{2-}$ [a]	22	182.34	51.79	14.57
$[Pt(Mmal)_2]^{2-}$ [b]	23	182.43	51.92	14.69
$[Pt(Mmal)_2]^{2-}$ [a,c]	22	178.98	51.39	14.60
$[Pt(Mmal)_2]^{2-}$ [b,c]	23	179.17	51.21	14.47
$[Pt(MmalH\text{-}O)(H_2O)_3]^{+}$	24	176.65	47.51	14.65
$[Pt(Mmal)(H_2O)_2]$	26	182.18	51.61	14.97

Mmal = 2-methylmalonato, [a] = methyl groups syn, [b] = methyl groups anti. [c] Tetra-n-butyl ammonium salts in $CDCl_3$

X-ray Crystallography $K_2[anti\text{-}Pt(C_4O_4H_4)_2]\cdot 2H_2O$ (23). A yellow/green needle-shaped crystal (approximately 0.08 x 0.11 x 0.28 mm) was mounted on a glass fiber. Unit cell dimensions were obtained by least-squares refinement using 25 centered reflections for which $20° < 2\theta < 30°$. Three check reflections, monitored every 100 reflections, showed approximately 5% loss of intensity during the course of data collection, and intensity data were scaled accordingly. Crystallographic data for this compound appear in Table 12.

Data reduction gave 4806 unique reflections in the range $4° < 2\theta < 83°$, of which 3616 with $I > 3\sigma(I)$ were used for structure refinement. The volume of the triclinic unit cell was appropriate for one formula unit. A Patterson synthesis did not reveal any non-origin peak of sufficient magnitude for a platinum-platinum vector, confirming the indication from the unit cell volume. Placement of the platinum atom on the inversion center in the centric space group led to successful structure solution and refinement. The remaining positions of the chelate ring were located from difference synthesis. Calculated hydrogen positions with a refined isotropic thermal parameter were used, with the orientation of the methyl group in **23** determined from a difference map. Water hydrogens were not included. Five reflections in the data set showed significant extinction and were excluded during final refinements. The refinement did not converge in the acentric space group. Final difference maps showed only the usual ripple near the platinum positions. Atom coordinates are given in Table 13. The structure of the anionic complex of **23** is shown in Figure 35, and bond distances and angles are in Tables 14 and 15. Crystallographic studies on malonato and other substituted malonato

Pt complexes are in agreement with the bond length and bond angle determinations we have made for **23** (48,49,55). The 2-methylmalonato ligand is in a boat conformation as is the case with other Pt(II) malonate derivatives. The boat conformation allows the methyl groups to have the smallest interaction with the Pt. This conformation places the methyl group into a common plane with the carbonyl group. The methine hydrogens are directed toward the Pt in this conformation. The anionic units also stack in a columnar chain along the crystallographic a axis. The long Pt-Pt distance of 4.059(2) Å, suggests little interaction between metal centers. Hydrogen bonding between pairs of lattice waters and the O(4) atoms of neighboring anionic units (each water hydrogen bonded to two O(4) atoms and each O(4) to two waters in a diamond pattern) link neighboring "columns" of anionic units in chains that run along the unit cell a,c diagonal. The potassium ion is coordinated to seven oxygen atoms in **23**.

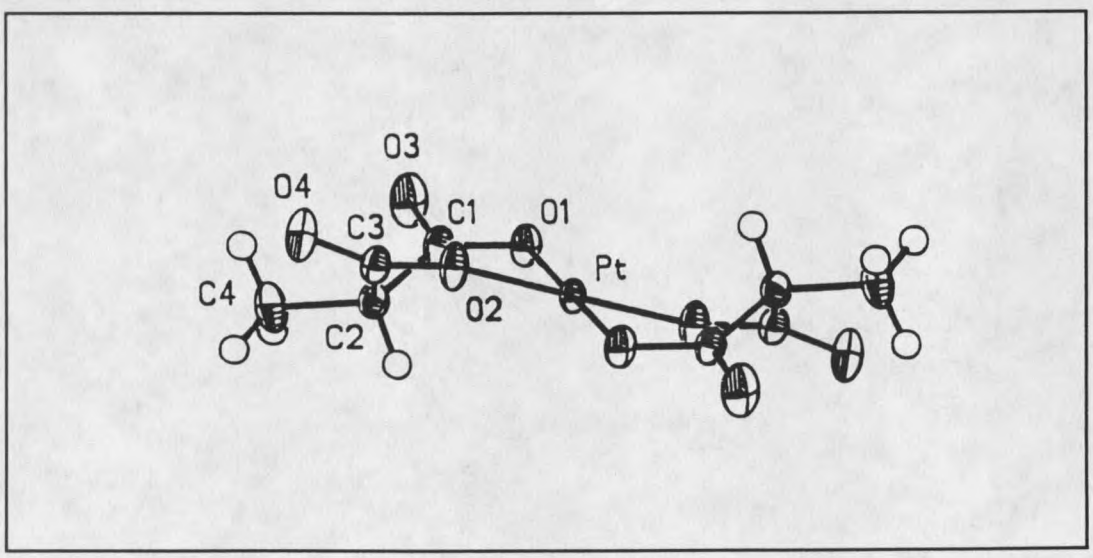

Figure 35 Thermal ellipsoid plot of *anti*-$[Pt(Mmal)_2]^{2-}$ showing 50% probability ellipsoids, and numbering scheme for the structure.

TABLE 12. Crystallographic Data

	$K_2[anti\text{-}Pt(C_4H_4O_4)_2]\cdot 2H_2O$
a = 4.059 (1) Å	fw = 541.5
b = 9.107 (2) Å	space group $P\bar{1}$
c = 10.111 (2) Å	T = 24 C°
α = 98.49 (1) °	lambda = 0.71069 Å (Mo Kα)
β = 101.28 (1) °	ρ calcd = 2.56 g cm^{-3}
γ = 101.84 (1) °	μ = 107.1 cm^{-1} (Mo Kα)
V = 351.8 (1) $Å^3$	transm factor range = 0.14 - 0.43
Z = 1	F (000) = 256
$R_w(F_o)$ = 0.0451	total no. of unique rflns = 4806
$R(F_o)$ = 0.0456	no. of obsd rflns, $I>3\sigma(I)$ = 3616
scan mode = $\Theta/2\Theta$	goodness of fit = 1.02

TABLE 13. $K_2[anti\text{-}Pt(C_4H_4O_4)_2]\cdot 2H_2O$: Bond Lengths (Å) and with Standard Deviations for all non Hydrogen atoms.

Bond	Length Å	Bond	Length Å
Pt-O(1)	2.010 (4)	Pt-O(2)	2.000 (4)
O(1)-C(1)	1.301 (6)	O(2)-C(3)	1.290 (6)
C(1)-C(2)	1.519 (7)	C(1)-O(3)	1.226 (8)
C(2)-C(3)	1.537 (7)	C(2)-C(4)	1.518 (7)
C(3)-O(4)	1.228 (8)		

TABLE 14. K_2[anti-Pt($C_4H_4O_4$)$_2$]·$2H_2O$: Atomic Coordinates for all atoms and Equivalent Anisotropic Temperature Factors (Å^2) with Standard Deviations.

atom	x/a	y/b	z/c	*U*eq[a]
Pt	0.00000	0.00000	0.00000	0.0177 (1)
O (1)	0.096 (1)	-0.2077 (4)	0.0023 (4)	0.026 (1)
O (2)	0.172 (1)	0.0182 (4)	-0.1706 (4)	0.027 (1)
C (1)	0.096 (1)	-0.2969 (5)	-0.1108 (5)	0.023 (1)
C (2)	-0.050 (1)	-0.2562 (5)	-0.2470 (5)	0.023 (1)
C (3)	0.154 (1)	-0.1000 (5)	-0.2619 (5)	0.022 (1)
C (4)	-0.086 (2)	-0.3806 (7)	-0.3702 (6)	0.036 (2)
O (3)	0.211 (2)	-0.4116 (5)	-0.1073 (5)	0.040 (2)
O (4)	0.299 (1)	-0.0897 (5)	-0.3573 (5)	0.036 (1)
K (1)[b]	0.3638 (4)	0.3189 (1)	0.8291 (1)	0.0310 (3)
O (5)[b]	0.302 (1)	-0.2051 (6)	-0.6369 (5)	0.040 (2)
H(2)[c]	-0.3101	-0.2470	-0.2453	0.05 (1)
H(4a)[c]	-0.2317	-0.4879	-0.3556	0.05 (1)
H(4b)[c]	0.1680	-0.3917	-0.3809	0.05 (1)
H(4c)[c]	-0.2194	-0.3508	-0.4620	0.05 (1)

[a]Equivalent isotropic *U* defined as one-third of the trace of the orthogonalized U_{ij} tensor. [b]Potassium ions and water oxygen atoms are not shown in Figure 35. [c]Hydrogen atoms refined with a common isotropic *U* and distance constraints.

TABLE 15. $K_2[anti\text{-}Pt(C_4H_4O_4)_2]\cdot 2H_2O$: Bond Angles (deg) with Standard Deviations for all non Hydrogen atoms.

Bond	Angle	Bond	Angle
O(1)-Pt-O(2)	92.5 (2)	Pt-O(1)-C(1)	121.0 (4)
Pt-O(2)-C(3)	122.1 (3)	O(1)-C(1)-C(2)	118.4 (5)
O(1)-C(1)-O(3)	120.7 (5)	C(2)-C(1)-O(3)	120.9 (5)
C(1)-C(2)-C(3)	111.6 (3)	C(1)-C(2)-C(4)	113.3 (5)
C(3)-C(2)-C(4)	112.0 (5)	O(2)-C(3)-C(2)	117.9 (5)
O(2)-C(3)-O(4)	121.6 (5)	C(2)-C(3)-O(4)	120.4 (4)

TABLE 16. Anisotropic thermal parameters ($Å^2 \times 10^3$) $K_2[anti\text{-}Pt(C_4H_4O_4)_2]\cdot 2H_2O$:

Atom	U_{11}	U_{22}	U_{33}	U_{23}	U_{13}	U_{12}
Pt	24(1)	13(1)	16(1)	0(1)	5(1)	6(1)
K(1)	44(1)	23(1)	30(1)	5(1)	12(1)	14(1)
O(1)	41(2)	17(1)	23(1)	4(1)	9(1)	14(1)
O(2)	46(2)	17(1)	23(1)	3(1)	14(1)	10(1)
O(3)	69(3)	26(2)	33(2)	6(2)	12(2)	27(2)
O(4)	53(3)	29(2)	28(2)	1(1)	22(2)	8(2)
C(1)	29(2)	16(2)	24(2)	0(1)	8(2)	8(1)
C(2)	27(2)	18(2)	21(2)	-1(1)	5(1)	8(1)
C(3)	29(2)	19(2)	20(2)	3(1)	9(1)	9(1)
C(4)	48(3)	25(2)	26(2)	-9(2)	6(2)	3(2)
O(5)	61(3)	31(2)	29(2)	2(2)	15(2)	8(2)

The anisotropic temperature factor exponent takes the form:
$-2\pi^2 (h^2a^{*2}U_{11} + \ldots + 2hka^*b^*U_{12})$

Reaction of 2-Methylmalonic Acid and $[Pt(H_2O)_4]^{2+}$ (6)

Nuclear Magnetic Resonance When 2-methyl malonic acid was added to the neutral solid $[Pt(OH)_2]\cdot nH_2O$ new resonances were observed to form at the expense of $[Pt(H_2O)_4]^{2+}$ (**6**). A peak is observed at -34 ppm. The small shift from **6** indicates that the new species is formed by replacement of H_2O by a carboxylato group. This resonance is assigned to $[Pt(MmalH\text{-}O)(H_2O)_3]^{+}$ (**24**). The next peak that is observed is at -339 ppm. The large shift of this resonance from **6** and **24** is consistent with the formation of the bidentate complex $[Pt(Mmal)(H_2O)_2]$ (**26**). Small single resonances are also observed at -78 ppm and -356 ppm. The small shift of the resonance at -78 ppm from **24** is consistent with the formation of a bis 2-methyl malonato complex with both 2-methyl malonate ligands monodentate. We predict that the carboxylato groups have trans geometry about the Pt, as previously described for the analogous bis malonato complex **15**. The resonance is assigned to trans-$[Pt(MmalH\text{-}O)_2(H_2O)_2]$ (**25**). The small shift of the peak at -356 ppm from **26** is consistent with a complex having one 2-methylmalonato ligand bidentate and the other 2-methylmalonato ligand monodentate. The resonance is assigned to the complex $[Pt(Mmal)(MmalH\text{-}O)(H_2O)]^{-}$ (**27**). The remaining peaks that are observed are at -600 and -608 ppm. These resonances correspond to the bis bidentate complexes **23** and **22** discussed above. ^{195}Pt and ^{13}C NMR data for these 2-Methylmalonato complexes are listed in Tables 10 and 11.

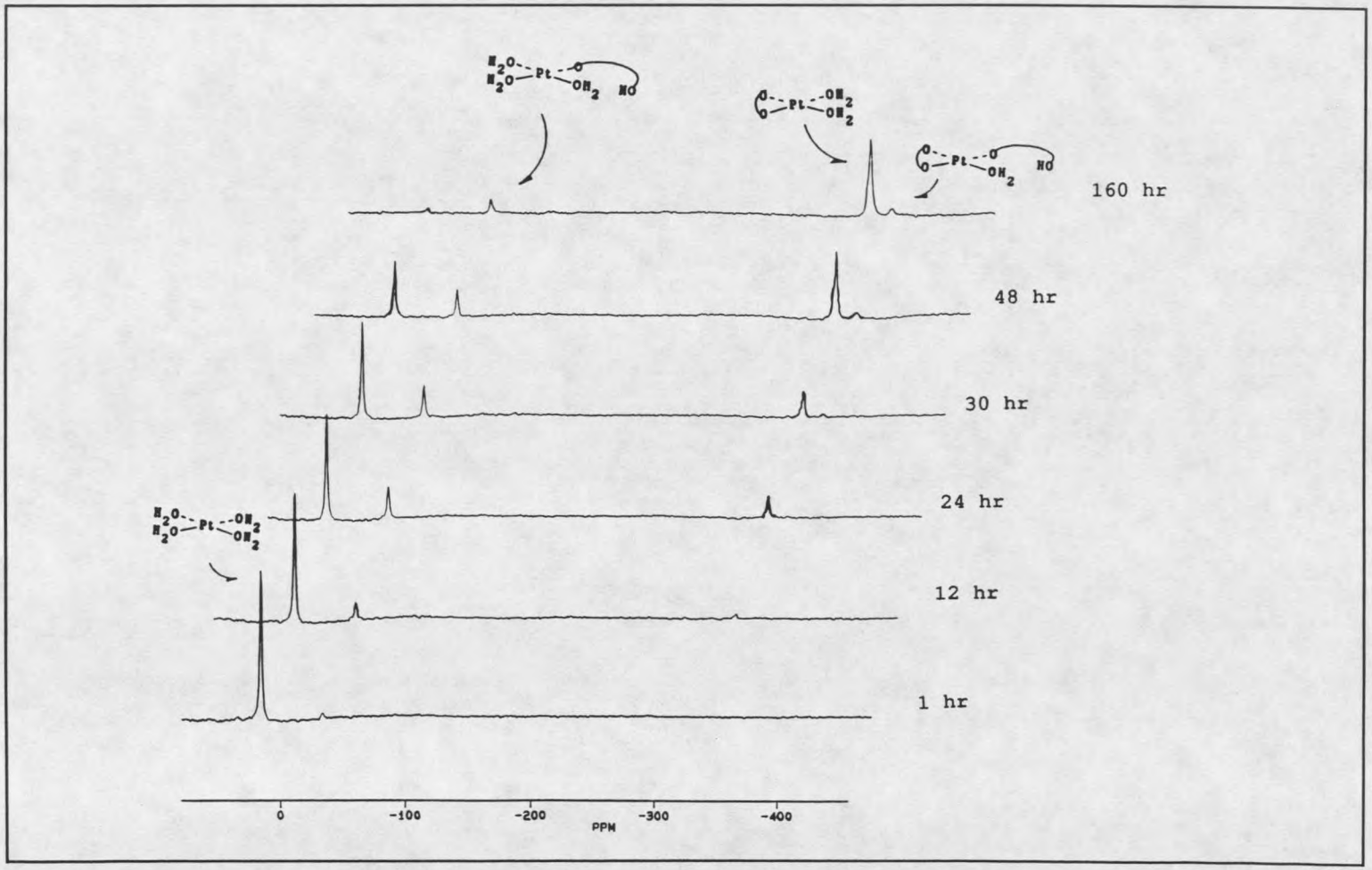

Figure 36 ^{195}Pt NMR of the Reaction of $[Pt(H_2O)_4]^{2+}$ with 2-Methylmalonic Acid.

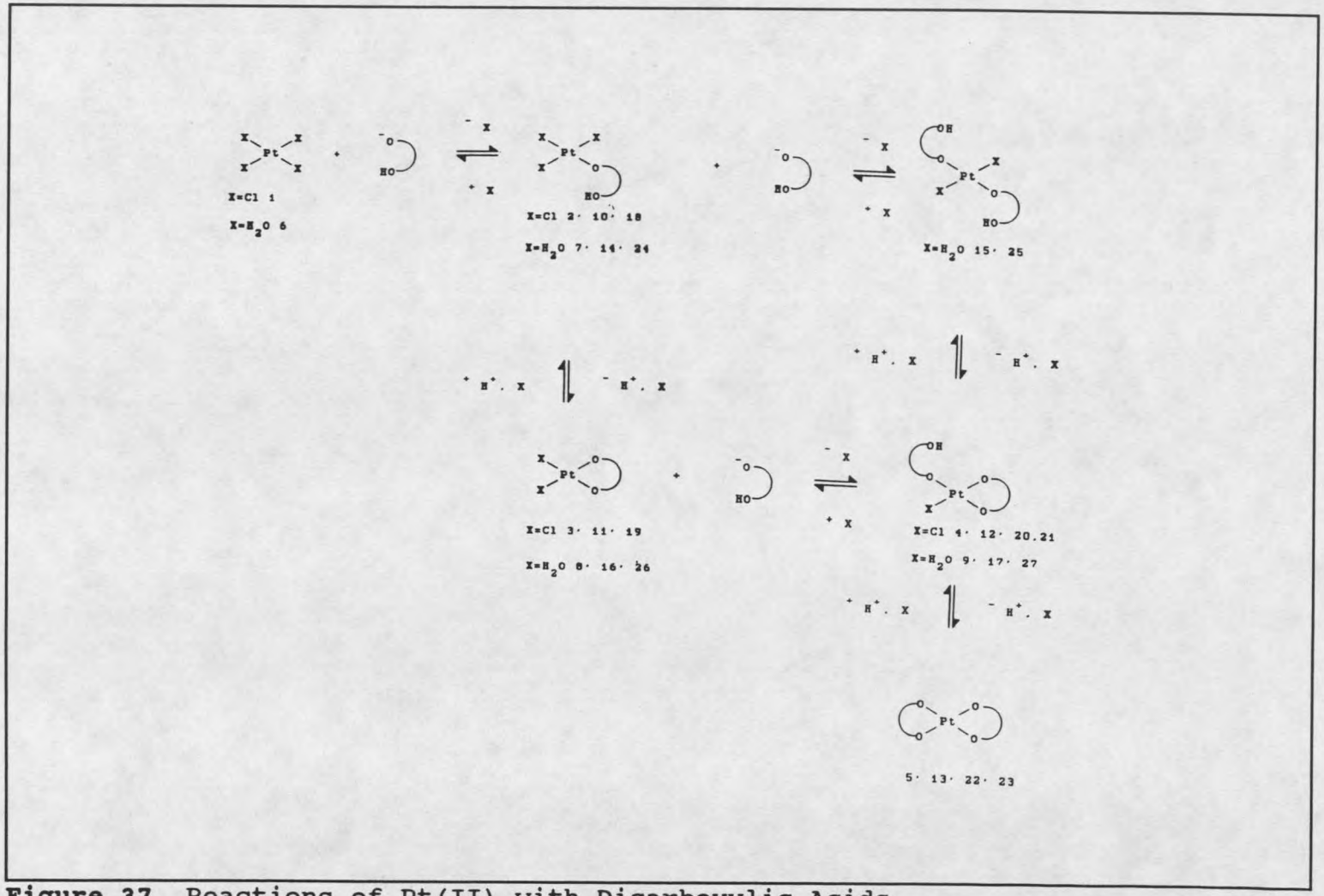

Figure 37 Reactions of Pt(II) with Dicarboxylic Acids.

OXIDATION REACTIONS OF PLATINUM(II) COMPLEXES

In this chapter, several oxidation reactions of Pt(II) complexes will be presented. These reactions are important because they result in the Pt(IV) complexes that are used in the synthesis of the one-dimensional chain complexes.

Hydrogen peroxide is a widely studied oxidizing agent for inorganic complexes. A number of different mechanisms are observed. The hydrogen peroxide oxidation of Pt(II) complexes to Pt(IV) complexes has been utilized in many important aspects of platinum chemistry such as the formation of platinum blues and greens, the synthesis of mixed valence linear chain complexes,(7,8,35,55,56) and the design of Pt(IV) anti-tumor drugs (57,58,59). Several crystal structures as well as ^{15}N and ^{195}Pt nuclear magnetic resonance (NMR) strongly suggest that hydrogen peroxide oxidation of Pt(II) complexes results in *trans*-dihydroxo Pt(IV) complexes (57-60). While one electron oxidation involving hydroxyl radicals occurs with many metals, a one-step two-electron oxidation has been suggested in the oxidation of $[Pt(NH_3)_4]^{2+}$ and $[PtCl_4]$(**1**) (57,61,62).

Pt(II) complexes have also been oxidized with Br_2 and Cl_2. These oxidations have been suggested to result in trans dihalo products when an excess of halogen is used in the oxidation (38,39,64,68-70). When less than one equivalent of halogen is used in the oxidation of the Pt(II), one-dimensional Pt chain complexes can be synthesized (7,8,35,55,56).

^{195}Pt NMR is a sensitive probe for the environment of the Pt nucleus (6). Elding has observed that coordinated $H_2{}^{18}O$ shifts ^{195}Pt NMR resonances ca. one ppm from the

corresponding $H_2{}^{16}O$ resonance. He used this isotopic shift to study the reaction mechanism for Cl_2 oxidation of Pt(II) complexes and to determine water exchange rates for Pt(II) complexes (63,64). Herein, we have extended this approach to study the mechanism and product distribution for the hydrogen peroxide oxidation for a number of Pt(II) complexes.

Hydrogen Peroxide Oxidation

Bis(oxalato)platinate(II) (5)

Nuclear Magnetic Resonance When 30% H_2O_2 is added to an aqueous solution of $[Pt(Ox)_2]^{2-}$(**5**) the ^{195}Pt NMR resonance for **5** at -525 ppm diminishes over 30 minutes at room temperature. It is replaced by a single new resonance at 2873 ppm in the ^{195}Pt NMR spectrum, and a single new resonance is observed in the ^{13}C NMR spectrum at 167.1 ppm. The large shift in the ^{195}Pt NMR spectrum is consistent with the oxidation of **5** to a Pt(IV) complex with six oxygen ligands (6). The new resonance is 400 ppm upfield from the resonance for $[Pt(OH)_6]^{2-}$. Such an upfield shift is in agreement with chemical shifts observed for Pt(II) complexes with oxalato ligands. The resonance at 2873 ppm is assigned to *trans*-$[Pt(OH)_2(Ox_2]^{2-}$ (**28**) since the *cis*-dihydroxobis(oxalato)platinate(IV) complex should have two ^{13}C resonances. Vapor diffusion of acetone into an aqueous solution of the sodium or potassium salt at pH=5.0 gives green/yellow crystals. X-ray crystallography shows the anionic complex to be *trans*-$[Pt(OH)_2(Ox)_2]^{2-}$ (**28**) (vida infra).

When **5** is dissolved in 50% $H_2{}^{16}O$/ 50% $H_2{}^{18}O$ and oxidized by a 30% aqueous solution of $H_2{}^{16}O_2$ the ^{195}Pt NMR resonance for **28** is observed to be two peaks separated by 0.52 ppm, as illustrated in Figure 38. The resonances arise from two of three possible isotopically labeled forms of complex **28**. The lowest field resonance is **28** where both hydroxo ligands are ^{16}OH. For the second resonance, one hydroxo ligand is ^{16}OH and the other is ^{18}OH. Generally, the substitution of a heavier isotope causes an upfield shift of the ^{195}Pt resonance (6,63,64). The ratio of the two isotopomeric resonances observed depends solely upon the ratio of $H_2{}^{16}O$ and $H_2{}^{18}O$ present in the solvent. The ^{13}C NMR spectrum of ^{18}O isotopically labeled **28** is a single resonance at 167.1 ppm. The single resonance observed in the ^{13}C spectrum shows that the isotopic shift in the ^{195}Pt spectrum is not the result of isotopic exchange of oxygen on the oxalato ligand, a process which occurs more slowly (65,66,vida infra). ^{195}Pt spectra taken over several weeks show that the isotopic ratio of the two resonances remains unchanged. Exchange of coordinated OH of **28** is slow in this pH range (vida infra). If significant exchange occurred, the ratio of the two resonances should change and a resonance corresponding to the $^{18}O,^{18}O$ complex should be observed. The absence of a resonance for a species with two ^{18}OH ligands indicates that the mechanism begins with the addition of $H_2{}^{16}O_2$ to an axial position of the Pt(II) square. After formation of a hydrogen peroxide Pt bond, two rapid one-electron transfers reduce the hydrogen peroxide and oxidize the Pt(II) to Pt(IV). After this rate determining step, the trans axial site of the Pt(IV) is coordinated by either an $H_2{}^{16}O$ or an $H_2{}^{18}O$ from the solvent. The retention of the ^{16}OH from hydrogen peroxide shows the two-electron transfer occurs after the

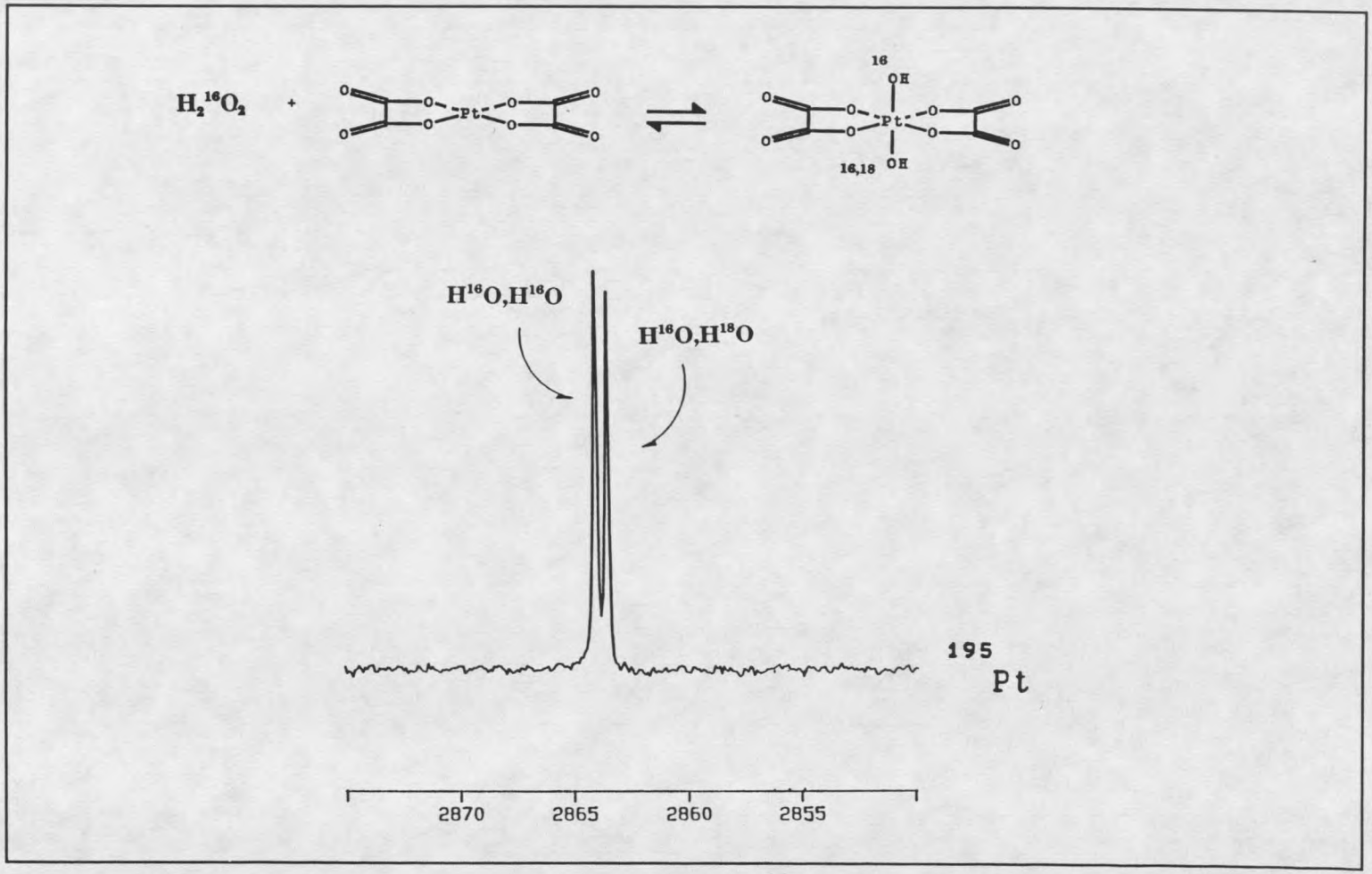

Figure 38 ^{195}Pt NMR of the Reaction of $H_2{}^{16}O_2$ with $[Pt(Ox)_2]^{2-}$ in 50% $H_2{}^{16}O$ / 50% $H_2{}^{18}O$.

hydrogen peroxide oxygen enters the inner coordination sphere of the Pt(II). The trans product shows that the oxidation occurs via a square bottom pyramidal intermediate (Figure 39).

The axial coordination site trans to hydrogen peroxide addition can be occupied by other solvents with oxygen donors. Hydrogen peroxide oxidation of $(TBA)_2[Pt(Ox)_2]$ (**5**) in methanol results in the disappearance of the resonance for **5** and the appearance of a new resonance at 2774 ppm in the ^{195}Pt NMR spectrum. The ^{1}H spectrum shows a new resonance at 2.93 ppm with a spin coupling of 23.6 Hz to ^{195}Pt. The ^{13}C spectrum also shows a new resonance at 56.6 ppm, and a single resonance is observed in the carboxyl region at 165.9 ppm. Positive ion mass spectroscopy by fast atom bombardment (FAB) shows a molecular ion peak at m/z = 903 for $(TBA)_2[Pt(Ox)_2(OH)(OMe)H]^+$. The predominant peak is at m/z = 1145 corresponding to $(TBA)_3[Pt(Ox)_2(OH)(OMe)]^+$. The new complex is assigned to *trans*-$[Pt(OH)(OMe)(Ox)_2]^{2-}$ (**29**). Oxidation in 50 % methanol/ 50 % H_2O results in the formation of an equal mixture of **28** and **29** which supports the idea that hydrogen peroxide Pt bond formation occurs before the trans axial position is coordinated by solvent. If solvent coordination occurred first, we might expect to see a distribution of products that may favor H_2O or methanol coordination. H_2O_2 oxidation of **5** in ethanol results in the appearance of a new resonance in the ^{195}Pt NMR spectrum at 2800 ppm. The ^{1}H spectrum shows two new resonances at 0.98 ppm (CH_3) and 3.30 ppm (CH_2). The ^{13}C spectrum also shows new resonances at 18.56 ppm (CH_3), 63.34 ppm (CH_2), and a single resonance is observed in the carboxyl region at 165.9 ppm. These new

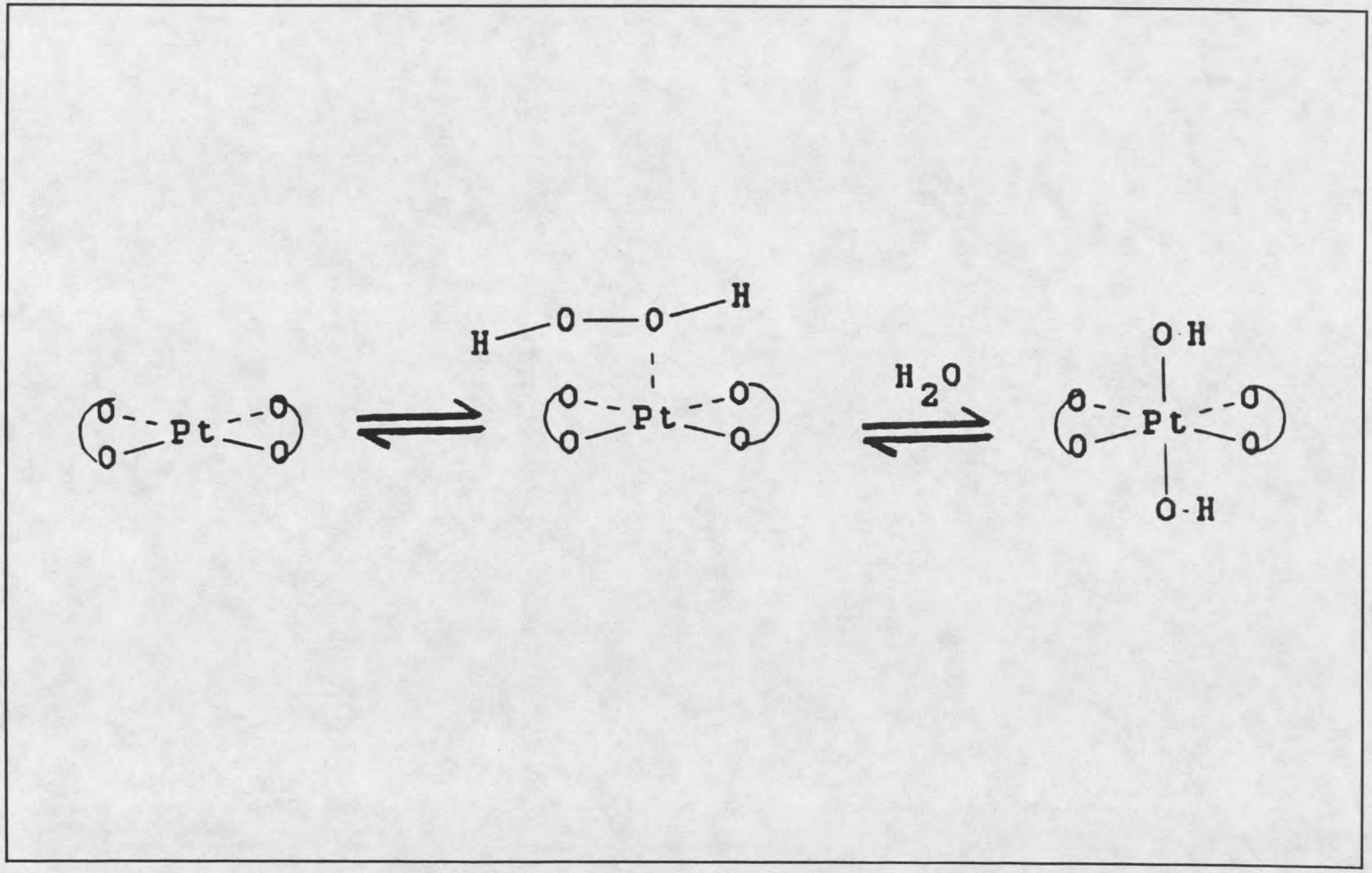

Figure 39 Mechanism for Hydrogen Peroxide Oxidation of Platinum(II) Complexes.

resonances are assigned to the formation of *trans*-$[Pt(OH)(OEt)(Ox)_2]^{2-}$ (**38**). The NMR data for **28**, **29**, and **30** is summarized in Tables 17 and 18.

TABLE 17. ^{195}Pt NMR Data.

COMPLEX	Structure #	δ Pt (ppm)	Isotope Shift
[*trans*-$Pt(OH)_2(Ox)_2]^{2-}$	28	2873	0.52[a]
[*trans*-$Pt(OH)(OMe)(Ox)_2]^{2-}$	29	2774	
[*trans*-$Pt(OH)(OEth)(Ox)_2]^{2-}$	30	2800	

Ox = oxalato, [a] = $^{16}O/^{18}O$ isotopic shift.

TABLE 18. ^{13}C and ^{1}H NMR Data

COMPLEX	Struct #	C=O	CH_3	CH_2
		^{13}C	$^{13}C/^{1}H$	$^{13}C/^{1}H$
[*trans*-$Pt(OH)_2(Ox)_2]^{2-}$	28	167.11		
[*trans*-$Pt(OH)(OMe)(Ox)_2]^{2-}$	29	165.90	56.6 2.93	
[*trans*-$Pt(OH)(OEt)(Ox)_2]^{2-}$	30	166.00	18.56 3.30	63.34 0.98

Ox = Oxalato

X-Ray Crystallography Na_2[*trans*-$Pt(OH)_2(C_2O_4)_2$].6 H_2O (**28**). A yellow plate shaped hexagonal crystal (approximately 0.16 x 0.44 x 0.74 mm) was mounted on a glass fiber for crystallographic data collection. Unit cell dimensions were obtained by least-

squares refinement using 25 centered reflections for which $20° < 2\theta < 30°$. Intensity data for the orthorhombic unit cell (+h, +k, +l) were collected, and three check reflections, monitored every 100 reflections, showed less than 3% loss of intensity for **28** during the course of data collection. Crystallographic data for this compound appear in Table 19. Data reduction gave 1749 unique reflections in the range $3° < 2\theta < 70°$, of which 1078 with $I > 3\sigma(I)$ were used for structure refinement. The volume of the orthorhombic unit cell indicated four formula units. Systematic absences predicted the space group to be Cmca. A Patterson synthesis did not reveal any non-origin peak of sufficient magnitude for a platinum-platinum vector. Placement of the platinum atom on a special position in the Cmca space group led to successful structure solution and refinement. The positions of the chelate ring, lattice water, and sodium were located from difference syntheses. Determination of sodium and water occupation were based upon coordination numbers, hydrogen bonding interactions, and changes in R_w when sodium and water positions were switched in the model. Attempts to locate water and hydroxyl hydrogen atom positions from difference map peaks did not improve the model. Because several hydrogen bonding schemes are possible for the complex, calculated coordinates were not used for hydrogen positions and all hydrogens were excluded in the final refinement. Five reflections in the data set showed significant extinction and were excluded during final refinement. Final difference maps showed only the usual ripple near the platinum positions. Atom coordinates are given in Table 20. The structure of the anionic complex of **2** is shown in Figure 40 and bond distances and angles are in Tables 21 and 22. It is interesting that the Pt(IV) complex bond lengths and bond angles

are not statistically different than for the Pt(II) complex $K_2[Pt(Ox)_2].2\ H_2O$ (**5**) (38). We expected a contraction of the Pt-O bond distances for the Pt(IV) complex. The hydrogen bonding network between complexes in adjacent unit cells is extensive.

TABLE 19. Crystallographic Data

	$Na_2[trans\text{-}Pt(OH)_2(C_2O_4)_2]\cdot 6H_2O$
a = 15.562 (2) Å	fw = 559.25
b = 7.200 (1) Å	space group = Cmca
c = 13.840 (1) Å	T = 24 C°
α = 90.00 (1) °	lambda = 0.71069 Å (Mo Kα)
β = 90.00 (1) °	ρ calcd = 2.39 g cm^{-3}
γ = 90.00 (1) °	μ = 92.7 cm^{-1} (Mo Kα)
V = 1550.9 (3) $Å^3$	transm factor range = 0.044-.224
Z = 4	F (000) =
$R_w(F_o)$ = 0.0492	no. of unique rflns = 1671
$R(F_o)$ = 0.0509	no of obsd. rflns = 1083
scan mode = w	goodness of fit = 1.285

TABLE 20. $Na_2[trans\text{-}Pt(OH)_2(C_2O_4)_2]\cdot 6H_2O$:(**28**) Atomic Coordinates and Equivalent Isotropic Temperature Factors ($Å^2$) with Standard Deviations.

atom	x/a	y/b	z/c	*U*eq[a]
Pt	0.5000 (1)	0.5000 (1)	0.5000 (1)	0.0161 (1)
O (1)	0.5849 (3)	0.5850 (7)	0.5981 (4)	0.025 (2)
C	0.5506 (5)	0.651 (1)	0.6762 (6)	0.025 (2)
O (2)	0.5899 (5)	0.708 (1)	0.7446 (5)	0.040 (2)
O (3)	0.5000 (2)	0.7538 (9)	0.4427 (6)	0.024 (2)
O[b] (4)	0.7481 (4)	0.930 (1)	0.6351 (5)	0.038 (2)
O[b] (5)	0.6228 (8)	0.0000 (2)	0.5000 (2)	0.042 (3)
Na[b]	0.7500 (2)	0.691 (1)	0.7500 (1)	0.036 (2)

[a]Equivalent isotropic *U* defined as one-third of the trace of the orthogonalized U_{ij} tensor.
[b]The sodium ions and water oxygen atom are not shown in Figure 40.

TABLE 21. $Na_2[trans\text{-}Pt(OH)_2(C_2O_4)]\cdot 6H_2O$: Bond Lengths (Å) with Standard Deviations for all non Hydrogen atoms.

Bond	Length Å	Bond	Length Å
Pt-O(1)	1.991 (5)	O(1)-C	1.297 (9)
Pt-O(3)	1.992 (7)	C-C(a)	1.57 (2)
C-O(2)	1.20 (1)		

TABLE 22. $Na_2[trans\text{-}Pt(OH)_2(C_2O_4)]\cdot 6H_2O$: Bond Angles (deg) with Standard Deviations for all non Hydrogen atoms.

Bond Angle	Degrees	Bond Angle	Degrees
O(1)-Pt-O(1b)	93.9 (3)	O(1)-C-O(2)	125.0 (8)
O(2)-C-C(a)	92.3 (2)	O(3)-Pt-O(1)	91.9 (3)
O(1)-C-C(a)	174.9 (3)	O(3)-Pt-O(3a)	180.0 (1)
Pt-O(2)-C(2)	113 (1)	Pt-O(1)-C	114.1 (5)

TABLE 23. Anisotropic thermal parameters ($Å^2 \times 10^3$)
$Na_2[trans\text{-}Pt(OH)_2(C_2O_4)]\cdot 6H_2O$

Atom	U_{11}	U_{22}	U_{33}	U_{23}	U_{13}	U_{12}
Pt	14(1)	21(1)	13(1)	- 1(1)	0(1)	0(1)
O (1)	17(2)	33(3)	18(2)	- 2(2)	- 2(2)	-3(2)
C	24(3)	30(4)	21(3)	- 1(3)	0(3)	-1(3)
O (2)	34(3)	56(4)	31(3)	-16(3)	-11(3)	-5(3)
O (3)	30(4)	18(4)	24(4)	5(3)	0(3)	0(3)
O (4)	31(3)	41(3)	42(4)	2(3)	- 2(3)	-5(3)
O (5)	29(4)	33(5)	64(8)	- 2(4)	0(4)	0(4)
Na	34(2)	33(2)	40(3)	0(2)	- 1(2)	0(3)

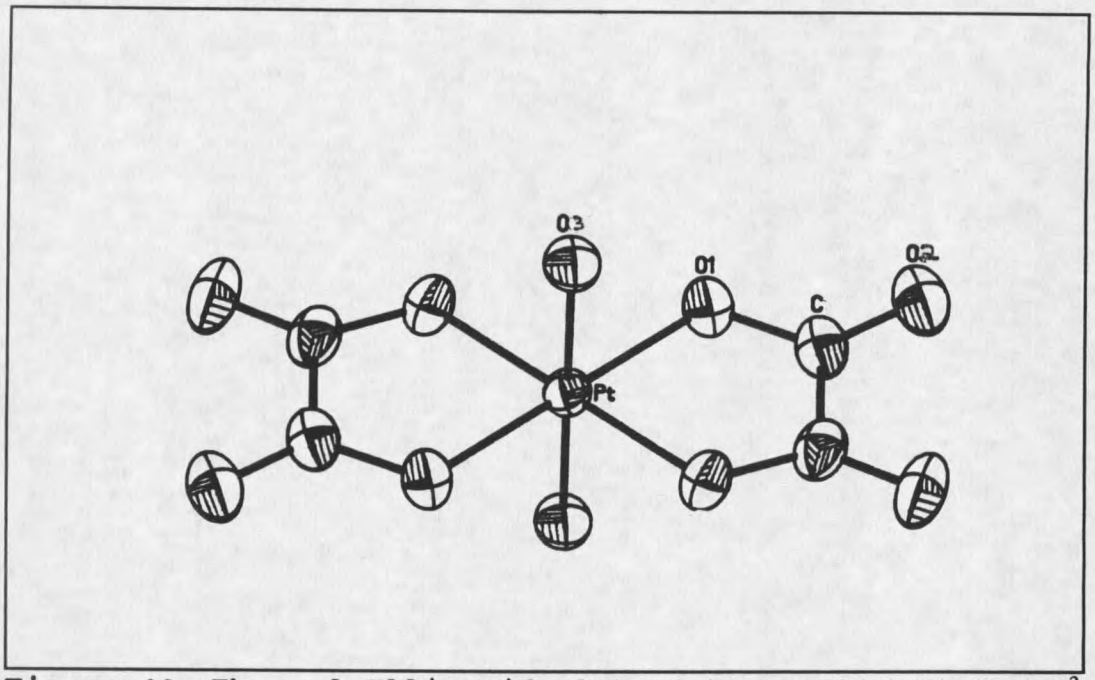

Figure 40 Thermal Ellipsoid plot of *trans*-$[Pt(OH)_2(Ox)_2]^{2-}$ showing 50% probability ellipsoids and numbering scheme for the structure.

K_2[*trans*-$Pt(OH)_2(C_2O_4)_2$].x H_2O **(28)** Single crystals were obtained and crystallographic data accumulated as described above. The trans complex crystalized in a tetragonal unit cell; with a = 12.209(2) Å, b = 12.209(1) Å, c = 13.077(1) Å, α = 90.00(1)°, β = 90.00(1)°, γ = 90.00(1)°, V = 1949.26(1) Å^3. Systematic absences predicted the space group to be *I4/m*. The complex was refined anisotropically and shows disorder between potassium and lattice water sites. The partial occupancy of the potassium and water sites was successfully modeled, and the anionic unit is not statistically different in bond lengths and angles from the well ordered sodium salt. The final refinement was R=0.0579, and R_w=0.0579. Because of the similarity of the two

structures and the disorder problems encountered with the potassium salt, the structure was not further refined.

Bis(malonato)platinate(II)

Nuclear Magnetic Resonance When 30% H_2O_2 is added to an aqueous solution of $[Pt(Mal)_2]^{2-}$(**13**) its ^{195}Pt NMR resonance is replaced by a single peak at 3153 ppm and new resonances are observed in the ^{13}C NMR spectrum at 178.0 ppm (C=O) and 47.0 ppm (CH_2). The chemical shift of the ^{195}Pt NMR resonance is again consistent with oxidation to a Pt(IV) species with six oxygen ligands. The 150 ppm upfield shift of this resonance from $[Pt(OH)_6]^{2-}$ is less than observed in the corresponding oxalato complex, **28**, and is also less than the chelate ring shift observed for the Pt(II) species **13**. Vapor diffusion of acetone into a pH=5.0 aqueous solution of the sodium salt gives green-yellow crystals. X-ray crystallography shows the complex to be Na_2[*trans*-$Pt(OH)_2(Mal)_2]\cdot 6H_2O$ (**31**). Hydrogen peroxide oxidation with $H_2{}^{16}O_2$ in 70% $H_2{}^{16}O$/ 30% $H_2{}^{18}O$ results in two isotopically shifted ^{195}Pt resonances, and the oxidation mechanism is the same as suggested above for **5** (Figure 39). The NMR data for **31** is summarized in Tables 28 and 29.

X-ray Crystallography Na_2*trans*-$[Pt(OH)_2(C_3O_4H_2)_2]\cdot 6H_2O$ (**31**). A yellow-green, needle-shaped crystal (approximately 0.068 x 0.11 x 0.44 mm) was mounted on a glass fiber for crystallographic data collection. Unit cell dimensions were obtained by least-squares refinement using 25 centered reflections for which $20° < 2\theta < 30°$. Intensity

data for the triclinic unit cell ($\pm$h, $\pm$k, +l) were collected and three check reflections, monitored every 100 reflections, showed less than 3% loss of intensity for **31** during the course of data collection. Crystallographic data for **31** are listed in Table 23. Data reduction, including corrections for Lorentz and polarization effects, gave 3670 unique reflections in the range $3° < 2\theta < 70°$, of which 3581 with $I > 3\sigma(I)$ were used for structure refinement. The volume of the triclinic unit cell was appropriate for one formula unit. A Patterson synthesis did not reveal any non-origin peak of sufficient magnitude for a platinum-platinum vector, confirming the indication from the unit cell volume. Placement of the platinum atom on the inversion center in the centric space group led to successful structure solution and refinement. The positions of the chelate ring atoms were located by difference synthesis. Water and hydroxyl hydrogen atom postions were consistent with peaks on difference maps and reasonable hydrogen bonding positions. All hydrogen atoms were refined with the same isotropic thermal parameter and distance constraints. Seven reflections in the data set showed significant extinction and were excluded during final refinement. The refinement did not converge in the acentric space group. Final difference maps showed only the usual ripple near the platinum position. Atom coordinates are given in Table 25. The structure of **31** is shown in Figure 41, and bond distances and angles are in Tables 24 and 26. Bond length and bond angle determinations are in agreement with crystallographic studies on Pt(II) malonato and other subsitituted Pt(II) malonato complexes. The malonato ligand is in a boat conformation as is the case with Pt(II) malonato complexes. An interesting feature of the crystal structure is the extensive hydrogen bonding network. These interactions

facilitated the refinement of hydrogen atom postions in the model.

TABLE 24. Crystallographic Data

	$Na_2[trans\text{-}Pt(OH)_2(C_2O_4)_2]\cdot 6H_2O$
a = 6.648 (1) Å	fw = 587.3
b = 8.234 (1) Å	space group $P\bar{1}$
c = 9.065 (1) Å	T = 24 C°
α = 63.82 (1) °	lambda = 0.71069 Å (Mo Kα)
β = 70.67 (1) °	ρ calcd = 2.37 g cm^{-3}
γ = 71.77 (1) °	μ = 87.3 cm^{-1} (Mo Kα)
V = 457.7 (3) $Å^3$	transm factor range = 0.290- 0.575
Z = 1	F (000) = 282
$R_w(F_o)$ = 0.0300	no. of unique rflns = 3670
$R(F_o)$ = 0.0308	no. of obsd rflns, $I>3\sigma(I)$ = 3588
scan mode = w	goodness of fit = 1.005

TABLE 25. $Na_2[trans\text{-}Pt(OH)_2(C_3H_2O_4)_2]\cdot 6H_2O$: Bond Lengths (Å) with Standard Deviations for all non Hydrogen atoms.

Bond	Length Å	Bond	Length Å
Pt-O(1)	1.983 (3)	Pt-O(2)	1.985 (3)
Pt-O(5)	1.993 (3)	O(1)-C(1)	1.295 (4)
O(2)-C(3)	1.298 (4)	O(3)-C(1)	1.232 (6)
O(4)-C(3)	1.224 (5)	C(1)-C(2)	1.506 (5)
C(2)-C(3)	1.514 (7)		

TABLE 26. $Na_2[trans\text{-}Pt(OH)_2(C_3H_2O_4)_2]\cdot 6H_2O$: Atomic Coordinates and Equivalent Isotropic Temperature Factors ($Å^2$) with Standard Deviations.

atom	x/a	y/b	z/c	*U*eq[a]
Pt	0.5000 (1)	0.5000 (1)	0.5000 (1)	0.017 (2)
O (1)	0.6139 (4)	0.3771 (3)	0.3353 (3)	0.025 (1)
O (2)	0.6201 (4)	0.7256 (3)	0.3458 (3)	0.025 (1)
O (3)	0.7475 (6)	0.3746 (4)	0.0824 (4)	0.039 (1)
O (4)	0.7321 (6)	0.9255 (4)	0.0970 (4)	0.035 (1)
C (1)	0.6714 (6)	0.4642 (5)	0.1738 (4)	0.024 (1)
C (2)	0.6349 (8)	0.6718 (5)	0.0971 (5)	0.032 (1)
C (3)	0.6676 (6)	0.7803 (4)	0.1826 (4)	0.023 (1)
O (5)	0.7804 (4)	0.3818 (4)	0.5728 (3)	0.026 (1)
Na [b]	0.7047 (3)	0.0512 (2)	0.3122 (2)	0.032 (1)
O (6)[b]	0.0905 (5)	-0.0186 (4)	0.2525 (4)	0.034 (1)
O (7)[b]	0.6835 (5)	-0.1021 (4)	0.6116 (4)	0.035 (1)
O (8)[b]	0.1061 (5)	0.4697 (5)	0.2642 (4)	0.036 (1)
H (2a)[c]	0.7431	0.7077	-0.265	0.05 (1)
H (2b)[c]	0.4684	0.7200	0.0840	0.05 (1)
H (5)[c]	0.8892	0.3820	0.4719	0.05 (1)
H (6a)[c]	0.1439	0.8505	0.2969	0.05 (1)
H (6b)[c]	0.1589	1.0017	0.1362	0.05 (1)
H (7a)[c]	0.7630	0.9539	0.6414	0.05 (1)
H (7b)[c]	0.7442	0.7693	0.6348	0.05 (1)
H (8a)[c]	0.1432	0.5448	0.3038	0.05 (1)
H (8b)[c]	0.1481	0.5263	0.1435	0.05 (1)

[a]Equivalent isotropic *U* defined as one-third of the trace of the orthogonalized U_{ij} tensor.
[b]The sodium ions and water oxygen atom are not shown in Figure 41.

TABLE 27. $Na_2[trans\text{-}Pt(OH)_2(C_3H_2O_4)_2]\cdot 6H_2O$: Bond Angles (deg) with Standard Deviations for all non Hydrogen atoms.

Bond Angle	Degrees	Bond Angle	Degrees
O(1)-Pt-O(2)	95.0 (1)	O(1)-Pt-O(5)	87.4 (1)
O(2)-Pt-O(5)	89.2 (1)	Pt-O(1)-C(1)	123.6 (3)
Pt-O(2)-C(3)	123.6 (3)	O(1)-C(1)-O(3)	118.7 (3)
O(1)-C(1)-C(2)	121.1 (4)	O(3)-C(1)-C(2)	120.1 (3)
C(1)-C(2)-C(3)	121.2 (4)	O(2)-C(3)-O(4)	119.2
O(2)-C(3)-C(2)	121.0 (3)	O(4)-C(3)-C(2)	119.7

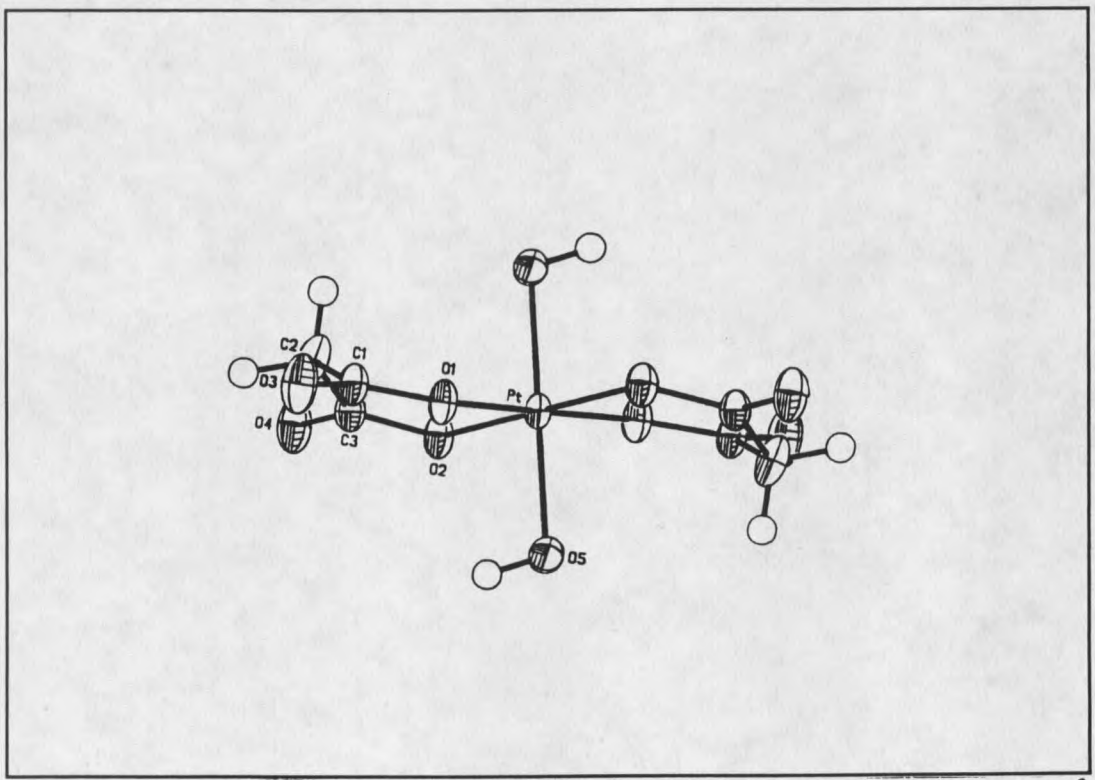

Figure 41 Thermal Ellipsoid Plot of *trans*-$[Pt(OH)_2(Mal)_2]^{2-}$ showing 50% probability ellipsoids, and numbering scheme for the structure.

TABLE 28. Anisotropic thermal parameters ($Å^2$ x 10^3) $Na_2[Pt(C_3H_2O_4)_2(OH)_2]\cdot 6H_2O$:

ATOM	U_{11}	U_{22}	U_{33}	U_{23}	U_{13}	U_{12}
Pt	23(1)	15(1)	13(1)	- 6(1)	- 1(1)	- 6(1)
O(1)	36(1)	20(1)	17(2)	- 8(1)	0(1)	- 7(1)
O(2)	37(1)	21(1)	19(1)	- 7(1)	-1(1)	-14(1)
O(3)	64(2)	29(1)	24(1)	-15(1)	0(1)	-11(1)
O(4)	56(2)	26(1)	23(1)	- 5(1)	0(1)	-22(1)
C(1)	32(2)	24(1)	18(1)	-10(1)	- 2(1)	- 9(1)
C(2)	57(2)	23(1)	19(1)	- 6(1)	-10(1)	-11(1)
C(3)	30(1)	19(1)	20(1)	- 6(1)	- 2(1)	- 7(1)
O(5)	25(1)	29(1)	22(1)	- 8(1)	- 5(10	- 2(1)
Na	33(1)	32(1)	32(1)	-13(1)	- 6(1)	- 6(1)
O(6)	28(1)	30(1)	30(1)	- 9(1)	- 7(1)	- 6(1)
O(7)	38(1)	31(1)	39(1)	-14(1)	-13(1)	- 6(1)
O(8)	42(2)	39(2)	31(1)	-17(1)	- 2(1)	-15(1)

The anisotropic temperature factor exponent takes the form:
$-2\pi^2 (h^2a^{*2}U_{11} + \ldots + 2hka^*b^*U_{12})$

Syn- and *Anti*-Bis(2-methylmalonatoplatinate(II)$_2$] (**22**,**23**).

Nuclear Magnetic Resonance When 30% H_2O_2 is added to an aqueous solution of *anti*-(**23**) and *syn*-$[Pt(Mmal)_2]^{2-}$ (**22**), where (**23**) is the predominant species, the ^{195}Pt NMR resonances are replaced by peaks at 3120 (dominant) and 3140 ppm. The ca. 150 ppm upfield shift of these resonances from $[Pt(OH)_6]^{2-}$ is less than would be predicted from analogous comparisons among Pt(II) complexes, but it is consistent with the upfield

shift for **31**. It appears that the malonato six membered chelate ring system causes less of a shift in the Pt(IV) complexes than in the malonato chelated Pt(II) complexes. Two sets of resonances of different intensity are observed for the methyl, methylene, and carboxyl carbons in the ^{13}C NMR spectrum, consistent with the formation of the two different *trans*-dihydroxo Pt(IV) isomers. These resonances are assigned by their relative intensities to *anti-trans*-$[Pt(OH)_2(Mmal)_2]^{2-}$ (**32**) (dominant), and *syn-trans*-$[Pt(OH)_2(Mmal)_2]^{2-}$ (**33**). Isotopic labeling experiments with $H_2{}^{18}O$ are shown in Figure 42. Oxidation of **22** and **23** with $H_2{}^{16}O_2$ in 60% $H_2{}^{16}O$/ 40% $H_2{}^{18}O$ gives two isotopically shifted resonances for both **32** and **33** in the ratio of 60% / 40%. These results are analogous to those observed for the formation of **28** and **31** and so the hydrogen peroxide oxidation mechanism remains unchanged (Figure 39). NMR data for **32** and **33** are listed in Tables 28 and 29.

TABLE 29. ^{195}Pt NMR Data.

COMPLEX	Structure #	δ Pt (ppm)	Isotope Shift
trans-$[Pt(OH)_2(Mal)_2]^{2-}$	31	3153	0.55[a]
anti,trans-$[Pt(OH)_2(Mmal)_2]^{2-}$	32	3120	0.56[a]
syn,trans-$[Pt(OH)_2(Mmal)_2]^{2-}$	33	3141	0.57[a]

Mal = malonato, Mmal = 2-methylmalonato, [a] = $^{16}O/^{18}O$ isotopic shift.

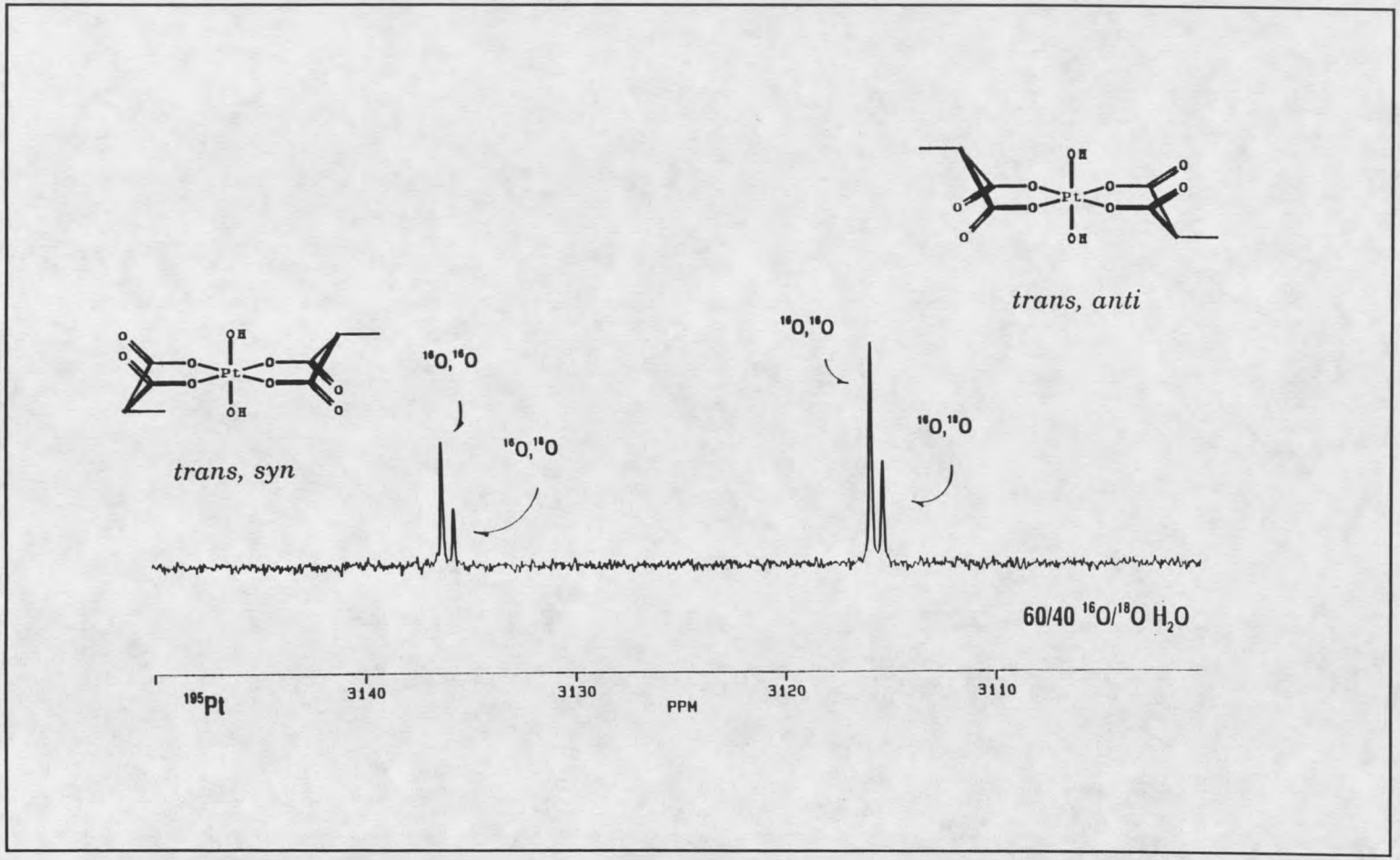

Figure 42 ^{195} NMR Spectrum of the Reaction of *syn*- and *anti*-$[Pt(Mmal)_2]^{2-}$ with $H_2{}^{16}O_2$ in 60% $H_2{}^{16}O$ / 40% $H_2{}^{18}O$.

TABLE 30. ^{13}C NMR Data

COMPLEX	#	C=O	CH/CH_2	CH_3
[*trans*-$Pt(OH)_2(Mal)_2]^{2-}$	31	177.95	46.96	
[*anti,trans*-$Pt(OH)_2(Mmal)_2]^{2-}$	32	179.36	48.63	13.71
[*syn,trans*-$Pt(OH)_2(Mmal)_2]^{2-}$	33	179.89	49.08	14.11

Mal = malonato, Mmal = 2-methylmalonato.

Dichlorooxaltoplatinate(II) (**3**)

Nuclear Magnetic Resonance When 30% H_2O_2 is added to an aqueous solution of $[PtCl_2(Ox)]^{2-}$(**3**) the ^{195}Pt NMR resonance for **3** at -1005 ppm is replaced by a single resonance at 2050 ppm in the ^{195}Pt NMR spectrum, and a single new resonance is observed in the ^{13}C NMR spectrum at 167.7 ppm. These resonances are assigned to trans-$[Pt(OH)_2Cl_2(Ox)]^{2-}$ (**34**). The large shift in the ^{195}Pt spectrum is consistent with oxidation to Pt(IV). The resonance for **34** is 310 ppm to higher shielding than *cis*-$[PtCl_2(OH)_4]^{2-}$ which agrees with the shift for bidentate chelates with 5 membered rings for Pt(II) (6). The high resolution ^{195}Pt NMR spectrum in Figure 43 shows three peaks due to different isotopic contributions from ^{35}Cl and ^{37}Cl in the ratio 1 : 0.64 : 0.10 (6,67). This isotopic abundance confirms that only two chloro ligands are bound to the Pt. Isotopic labeling experiments with 50% $H_2{}^{16}O$/ 50% $H_2{}^{18}O$ shows the oxidation to follow the same mechanism as described above for the bis-oxalato complex. The high resolution ^{195}Pt NMR spectrum of ^{18}O isotopically labeled **34** is also shown in

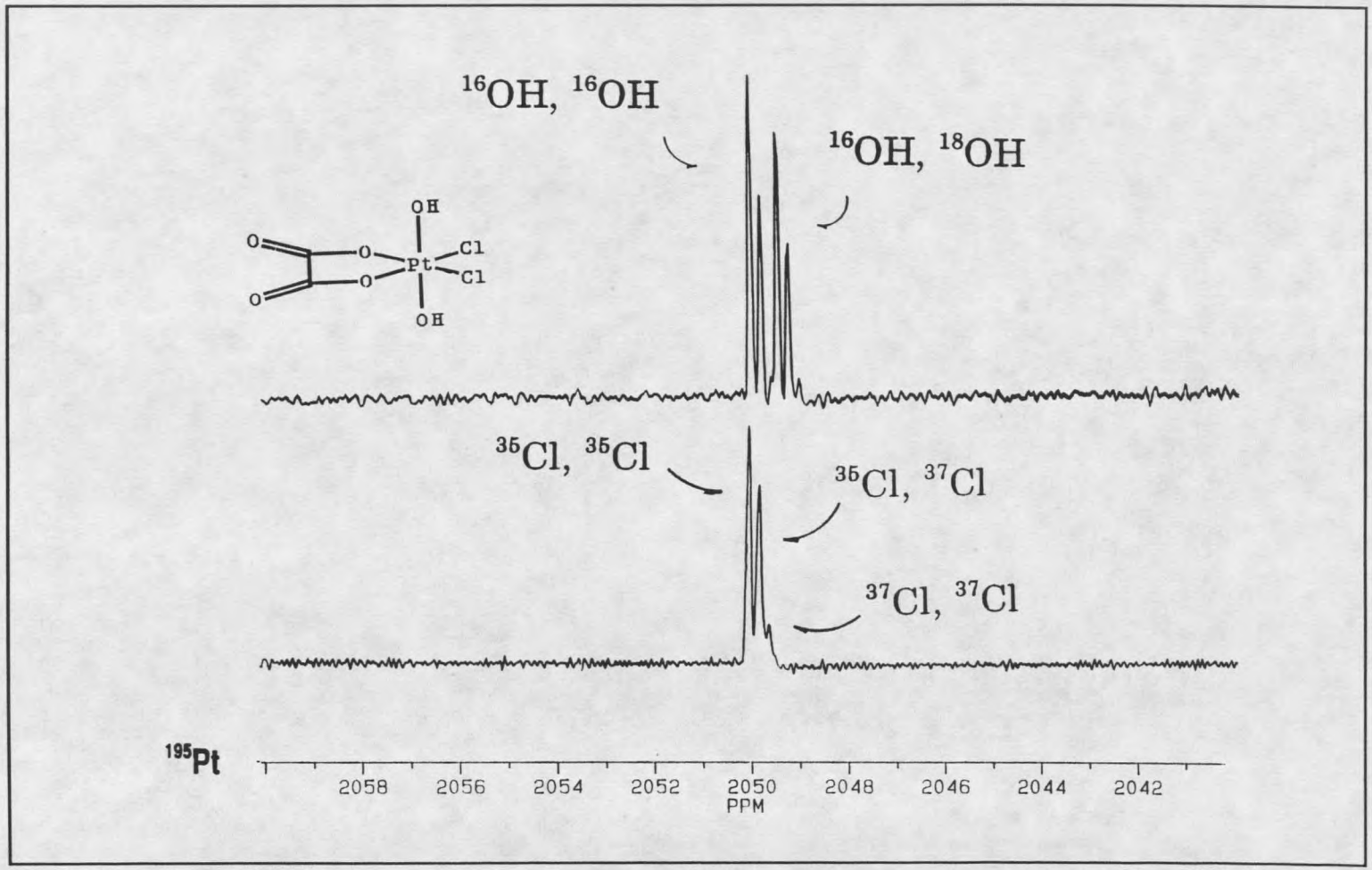

Figure 43 ^{195}Pt NMR Spectra of *trans-cis*-$[Pt(OH)_2Cl_2(Ox)]^{2-}$.

Figure 43. As before, two separate ^{195}Pt resonances are observed, one for the ^{16}O complex and one for the $^{16}O,^{18}O$ species. Each of these resonances is divided into three additional peaks by the chlorine isotopes present, as described above. Each set of chlorine isotopomeric peaks is shifted from one to another by the incorporation of ^{18}OH into 50 % of the trans dihydroxo complex. The NMR data for **34** is listed in Table 30.

Tetrachloroplatinate(II)

Nuclear Magnetic Resonance Studies When 30% H_2O_2 is added to an aqueous solution of $[PtCl_4]^{2-}$(**1**) the ^{195}Pt NMR resonance for **1** at -1624 ppm is replaced by a single resonance at 1247 ppm in the ^{195}Pt NMR spectrum. This resonance has been previously assigned to trans-$[Pt(OH)_2Cl_4]^{2-}$ (**35**) (6). The large shift in the ^{195}Pt spectrum is consistent with oxidation to Pt(IV). The high resolution ^{195}Pt spectrum for **35** shows the ^{35}Cl and ^{37}Cl isotopic contributions in the ratio of 0.78 : 1.0 : 0.48 for each group of resonances (Figure 44) (6,67). Further chlorine isotopomers were not observed due to their low natural abundance, but the ratio of the resonances observed is consistent with the presence of four chloro ligands bound to ^{195}Pt. Isotopic labeling experiments with 60% $H_2{}^{16}O$/ 40% $H_2{}^{18}O$ yields two ^{195}Pt resonances in proportion to the ^{18}O content of the solvent. This shows the mechanism for H_2O_2 oxidation to be the same as described previously for all Pt(II) complexes discussed. The high resolution ^{195}Pt NMR spectrum in Figure 43 shows two sets of three peaks due to $H_2{}^{18}O$ incorporation and ^{35}Cl and ^{37}Cl isotopic contributions in the ratio of 0.78 : 1.0 : 0.48 for each group of resonances (6,67). The NMR data for **35** is listed in Table 30.

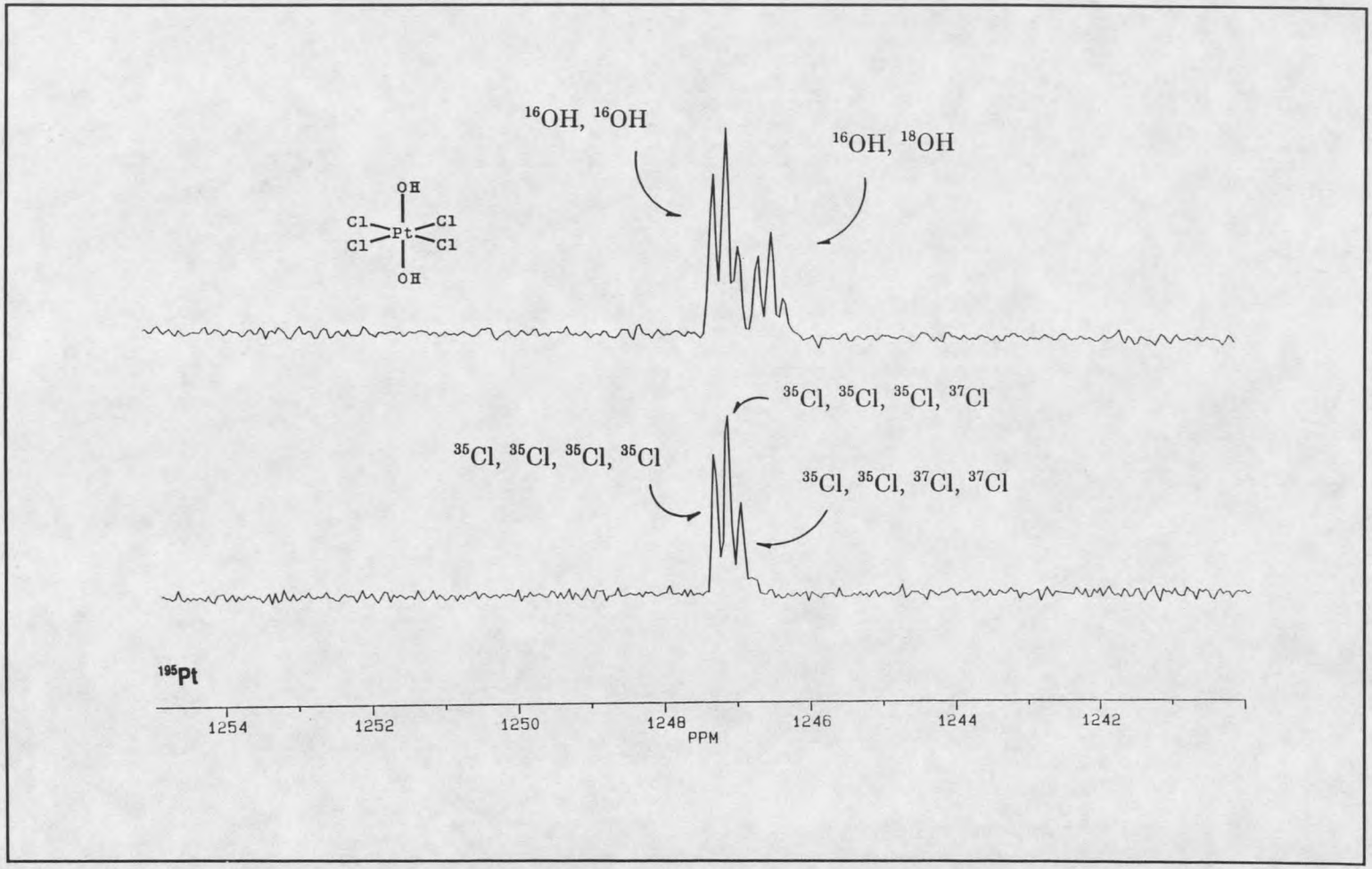

Figure 44 ^{195}Pt NMR Spectra for *trans*-$[Pt(OH)_2Cl_4]^{2-}$.

TABLE 31. ^{195}Pt and ^{13}C NMR Data.

COMPLEX	Structure #	δ Pt δ C ppm	Isotope Shift
trans-cis-$[Pt(OH)_2Cl_2(Ox)]^{2-}$	34	2050	0.69[a]
		167.68	0.20[b]
trans-$[Pt(OH)_2Cl_4]^{2-}$	35	1247	0.68[a]
			0.19[b]

Ox = oxalato, [a] = $^{16}O/^{18}O$ isotopic shift, [b] = $^{35}Cl/^{37}Cl$ isotopic shift.

Chlorine Oxidation of Bis(oxalato)platinate(II)

Nuclear Magnetic Resonance

When Cl_2 gas is bubbled through an aqueous solution of $[Pt(Ox)_2]^{2-}$ (**5**), the ^{195}Pt NMR resonance for **5** at -525 ppm is replaced by a single resonance at 1885 ppm in the ^{195}Pt NMR spectrum. The large shift in the ^{195}Pt spectrum is consistant with oxidation to Pt(IV) (6). The resonance at 1885 ppm is 452 ppm to higher shielding than *trans*-$[PtCl_2(OH)_4]^{2-}$ which agrees with the shift for bidentate chelates with 5 membered rings for Pt(II) and Pt(IV) complexes (6). The high resolution ^{195}Pt NMR spectrum of **36** shows three shifted resonances due to different isotopic contributions from ^{35}Cl and ^{37}Cl in the ratio 1 : 0.64 : 0.10 (6,67). This isotopic abundance confirms the presence of two chloro ligands bound to the Pt. The new resonance is assigned to *trans*-$[PtCl_2(Ox)_2]^{2-}$

(36). For several of the oxidation reactions of **5** with Cl_2 a second minor resonance is observed at 2410 ppm in the ^{195}Pt NMR spectra. The resonance at 2410 falls between the chemical shifts for **28** and **36**. The chemical shift of this resonance is appropriate for the substitution of H_2O for of one Cl^- of **36**. The new resonance is assigned to *trans*-$[Pt(OH)Cl(Ox)_2]^{2-}$ **(37)**. The NMR data for **36** and **37** is listed in Table 31.

Bromine Oxidation of Bis(oxalato)platinate(II)

Nuclear Magnetic Resonance

When an excess of liquid Br_2 is added to an aqueous solution of $[Pt(Ox)_2]^{2-}$ **(5)** the ^{195}Pt NMR resonance for **5** at -525 ppm is replaced by two new resonances at 2208 (minor) and 1420 ppm (dominant) in the ^{195}Pt NMR spectrum. The large shift for these resonances in the ^{195}Pt spectrum is consistent with oxidation to Pt(IV) (6). The resonance at 1420 ppm is consistant with the presence of two bromide ligands bound to Pt(IV) (6). The resonance is assigned to *trans*-$[PtBr_2(Ox)_2]^{2-}$ **(38)**. The resonance at 2208 falls between the chemical shifts for **28** and **38**. The chemical shift is consistent with the substitution of H_2O for Br^- on **38**. The new resonance is assigned to *trans*-$[Pt(H_2O)Br(Ox)_2]^{2-}$ **(39)**. The NMR data for **38** and **39** is listed in Table 31.

TABLE 32. ^{195}Pt NMR Data.

COMPLEX	Structure #	δ Pt (ppm)
trans-$[PtCl_2(Ox)_2]^{2-}$	36	1886
trans-$[PtCl(H_2O)(Ox)_2]^{2-}$	37	3120
trans-$[PtBr_2(Ox)_2]^{2-}$	38	1420
trans-$[PtCl(H_2O)(Ox)_2]^{2-}$	39	2208

Ox = Oxalato

ISOMERIZATION OF DIHYDROXO PLATINUM(IV) COMPLEXES

In this chapter, the isomerization reactions for several *trans*-dihydroxoplatinate(IV) complexes will be presented. Isomerization mechanisms for octahedral metal complexes have been classified into dissociative and intramolecular process (71-74). Dissociative processes require the formation of five coordinate trigonal-bipyramidal intermediates. Intramolecular processes are exemplified by the trigonal or Bailar twist and the rhombohedral, or Ray-Dutt twist. Isomerization of inert chromium(III) and cobalt(III) oxalato and malanato metal complexes $[M(H_2O)_2(O,O)_2]^-$ (M=Cr,Co) have established a dissociative mechanism for isomerization that is consistant with the formation of a monodentate oxalato or malanato complex (71,73).

Trans-dihydroxobis(oxalato)platinate(IV)

Nuclear Magnetic Resonance Studies

When solutions of *trans*-dihyroxobis(oxalato)platinate(IV) (**28**) are heated at 70 C° for 24 hours or kept at room temperature for several weeks, new resonances are observed in the ^{195}Pt and ^{13}C NMR spectra. A single new resonance is observed at 2847 ppm in the ^{195}Pt spectra. The proximity of this resonance to that of **28** suggests a species with six oxygen ligands and one or more bidentate ligands (6). The ^{13}C spectrum shows the appearance of new resonances of equal intensity at 167.33 and 168.11 ppm. These resonances are consistant with carboxylato carbon atoms in different symmetry

environments, as expected for a *cis*-dihydroxobis(oxalato)platinate(IV) complex. Vapor diffusion of acetone into a solution of this species produced crystals for x-ray diffraction. Crystallography shows the anionic unit to be *cis*-dihyroxobis(oxalato)platinate(IV) (**40**). The new ^{195}Pt and ^{13}C NMR resonances are assigned to *cis*-$[Pt(Ox)_2(OH)_2]^{2-}$ (**40**). When the oxidation of $[Pt(Ox)_2]^{2-}$ (**5**) is carried out using $H_2{}^{16}O_2$ in 50% $H_2{}^{16}O$/ 50% $H_2{}^{18}O$, ^{195}Pt NMR shows that two isotopomers of *trans*-$[Pt(Ox)_2(OH)_2]^{2-}$ (**28**) are formed in equal abundance. This is revealed in the observation of two separate isotopic resonances for **28** (Figure 38). The first is a complex with two ^{16}OH and the second resonance to higher field is a complex with one ^{16}OH and one ^{18}OH. When such a solution is heated at 70 C° for 24 hours or left at room temperature for several weeks, new resonances appear at 2847 ppm in the ^{195}Pt NMR spectrum (Figure 45). The new resonances are assigned to the corresponding isotopomers of *cis*-$Pt(OH)_2(Ox)_2]^{2-}$ (**40**). Their isotopic ratio is the same as was present in the original solutions of **28**. The absence of a third isotopomeric resonance, and the constant ratio of $^{16}OH/^{16}OH$ to $^{16}OH/^{18}OH$ shows the isomerization mechanism is an intramolecular process which does not incorprorate further ^{18}O from the 50% $H_2{}^{16}O$ and 50% $H_2{}^{18}O$ solvent. Figure 45 shows the changes observed in the ^{195}Pt NMR spectrum as trans-cis isomerization progresses. The ^{13}C NMR spectrum of the reaction mixture shows a single resonance at 167.11 (**28**) and resonances at 167.33, and 168.11 (**40**). The absence of ^{18}O isotopomeric resonances in the ^{13}C NMR spectra indicates that the isotopic shift in the ^{195}Pt spectrum arises from isotopic substitution at the hydroxide and is not related to isotopic exchange on the oxalate ligand (65,66). The NMR data for **40** is listed in Tables 34 and 35.

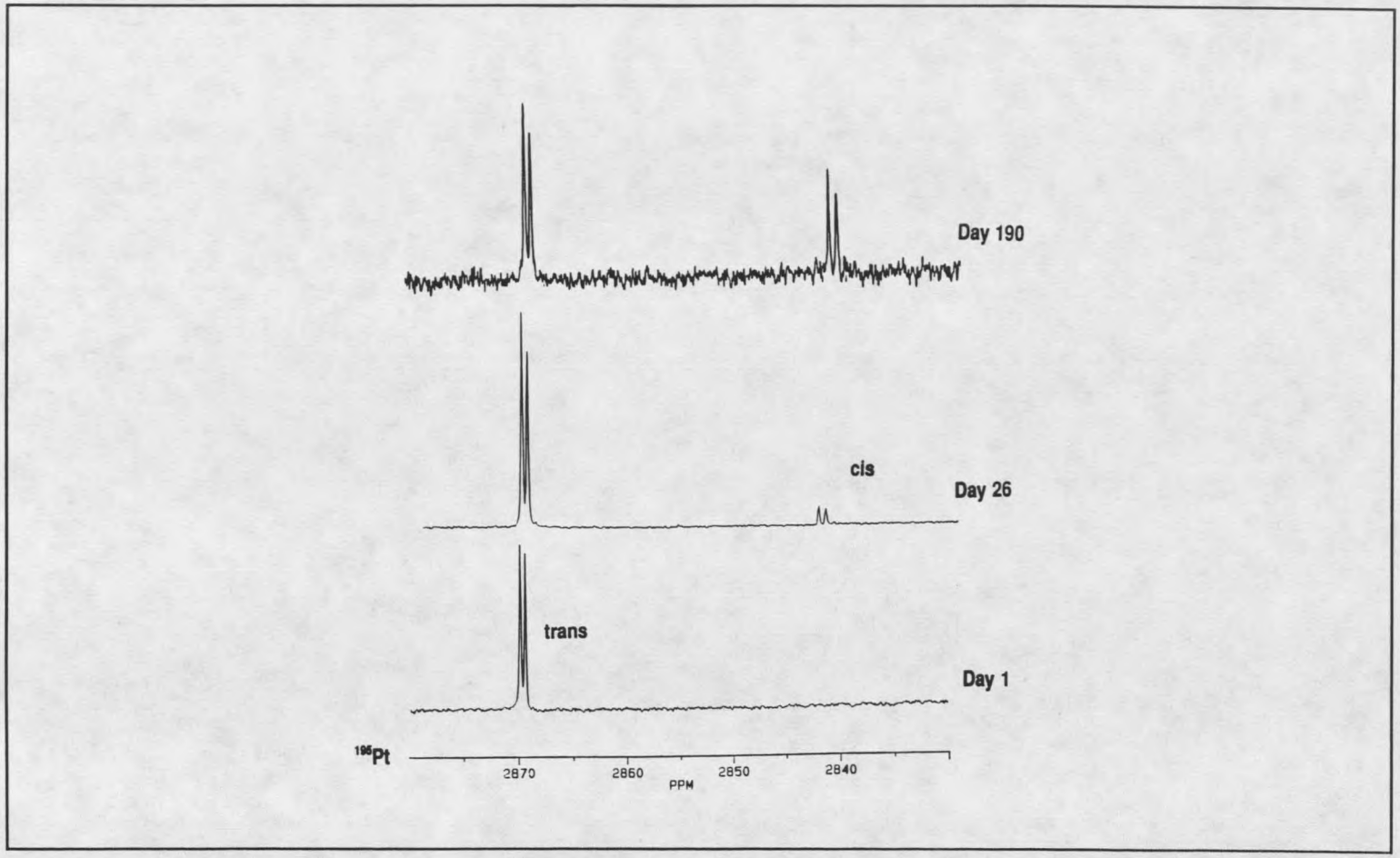

Figure 45 ^{195}Pt NMR Spectra for the Trans-Cis Isomerization of *trans*-$[Pt(OH_2)(Ox)_2]^{2-}$ in 50% $H_2{}^{16}O$ / 50% $H_2{}^{18}O$.

X-Ray Crystallography $K_2[cis\text{-}Pt(OH)_2(C_2O_4)_2].x\ H_2O$ (**40**). The cis complex (Figure 46) crystallized in the monoclinic p unit cell with a = 17.582 (2) Å, b = 17.582 (2) Å, c = 47.414 (2) Å, α = 90.00 (1) °, β = 90.00 (1) °, γ = 120.00 (1) °, V = 1577.7(1) $Å^3$, Z = 4, R = 0.0705, R_w = 0.0691. The complex showed disorder in the potassium and water positions and occupancy numbers. The anionic Pt unit was determined to have cis stereochemistry, and the disorder of the potassium and water sites was modeled. While we are confident of the assignment of the stereochemistry of this complex, a full structure solution was not attempted because of several possible models for the disorder of the potassium and water sites. The primary interest to this investigation is the stereochemistry of the oxalato ligands on the Pt as a confirmation in the assignment of NMR resonances. The bond distances and angles for **40** are listed in Tables 32 and 33.

TABLE 33. Bond Lengths (Å) with Standard Deviations for $K_2cis\text{-}[Pt(OH)_2(Ox)_2]\cdot xH_2O$.

Bond	Length	Bond	Length
Pt-O(1)	1.99 (2)	Pt-O(2)	1.95 (2)
Pt-O(5)	2.04 (2)	Pt-O(6)	1.99 (1)
Pt-O(10)	1.96 (2)	Pt-O(9)	2.02 (2)
C(3)-O(7)	1.19 (3)	C(1)-C(2)	1.55 (3)
C(1)-O(3)	1.19 (3)	C(3)-C(4)	1.56 (3)
C(2)-O(4)	1.26 (3)	O(1)-C(1)	1.28 (3)
C(4)-O(8)	1.25 (3)	O(2)-C(2)	1.30 (4)
O(6)-C(4)	1.21 (3)	O(5)-C(3)	1.26 (2)

TABLE 34. Bond Angles (deg) with Standard Deviations for K_2*cis*-$[Pt(OH)_2(Ox)_2]\cdot xH_2O$.

Bonds	Angle	Bonds	Angle
Pt-O(1)-C(1)	113 (1)	Pt-O(2)-C(2)	112 (1)
Pt-O(5)-C(3)	112 (1)	Pt-O(6)-C(4)	110 (1)
O(1)-Pt-O(2)	84.7 (6)	O(1)-C(1)-C(2)	114 (2)
O(9)-Pt-O(10)	89.8 (7)	O(2)-C(2)-C(1)	117 (2)
O(9)-Pt-O(2)	89.9 (6)	O(5)-C(3)-C(4)	112 (2)
O(9)-Pt-O(6)	91.2 (6)	O(6)-C(4)-C(3)	122 (2)
O(9)-Pt-O(5)	174.8 (6)	O(1)-C(1)-O(3)	126 (2)
O(10)-Pt-O(6)	88.5 (7)	O(2)-C(2)-O(4)	125 (2)
O(10)-Pt-O(5)	89.0 (7)	O(5)-C(3)-O(7)	121 (2)
O(10)-Pt-O(1)	176.5 (5)	O(6)-C(4)-O(8)	125 (2)
O(10)-Pt-O(2)	92.4 (7)	O(3)-C(1)-C(2)	120 (2)
O(6)-Pt-O(5)	83.7 (6)	O(4)-C(2)-C(1)	119 (3)
O(6)-Pt-O(2)	178.6 (5)	O(7)-C(3)-C(4)	127 (2)
O(6)-Pt-O(1)	94.4 (7)	O(8)-C(4)-C(3)	113 (2)
O(5)-Pt-O(1)	89.5 (7)		

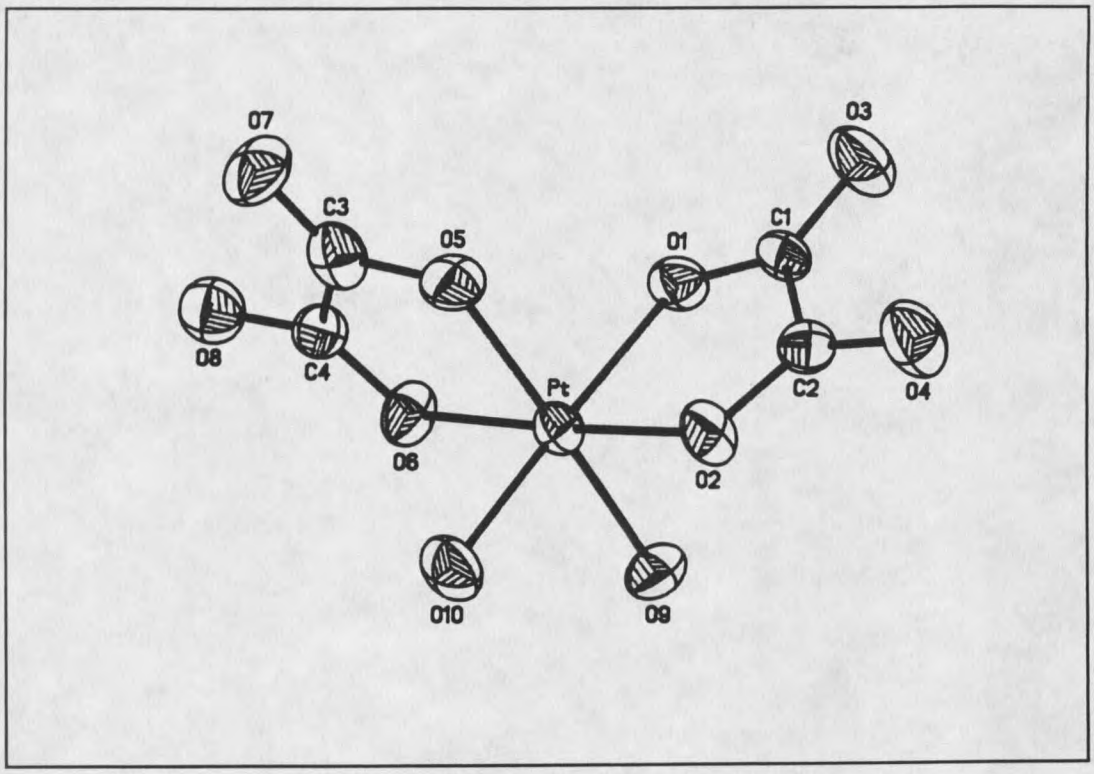

Figure 46 Thermal ellipsoid plot of *cis*-$[Pt(OH)_2(Ox)_2]^{2-}$ showing 50% probability ellipsoids, and numbering scheme for the structure.

Trans-dihydroxobis(malonato)platinate(IV) (**31**)

Nuclear Magnetic Resonance

When solutions of *trans*-dihyroxobis(malonato) platinate(IV) (**31**) are heated at 70 C° for 24 hours or kept at room temperature for several weeks, new resonances are observed in the ^{195}Pt and ^{13}C NMR spectra. A single new resonance is observed at 3158

ppm in the ^{195}Pt spectra. The proximity of this resonance to **31** suggests a species with six oxygen ligands and one or more bidentate ligands. The ^{13}C spectrum shows the appearance of new resonances of equal intensity in both the carboxyl region, and in the methylene region. These resonances are consistent with isomerization of **31** to form *cis*-dihyroxobis(malonato)platinate(IV) complex (**41**). Oxidation of $[Pt(Mal)_2]^{2-}$ (**13**) by $H_2{}^{16}O_2$ in 50% $H_2{}^{16}O$/ 50% $H_2{}^{18}O$ results in the formation of exclusively *trans*-$[Pt(OH)_2(Mal)_2]^{2-}$ (**31**) as the kinetic product isotopically labeled with 50% ^{18}OH at one axial position. The ^{195}Pt NMR resonance for **31** shows only two isotopomeric species as previously described for **28**. When isotopically labled solutions of **31** are heated at 70 C° for 24 hours or left at room temperature for several weeks, new resonances for *cis*-$[Pt(OH)_2(Mal)_2]^{2-}$ (**41**) are observed at 3158 ppm in the ^{195}Pt NMR spectrum. Two $^{16}O/^{18}O$ isotopomers are observed for **41** at 3158 ppm in the same isotopic ratio as were present in the origional solutions of **31**. The absence of a third isotopomeric resonance shows the isomerization process is an intramolecular process which cannot incorprorate further ^{18}O from solvent. The NMR data for **41** is listed in Tables 34 and 35.

Syn- and *anti*-trans-dihydroxobis(2-methylmalonato)platinate(IV) (**32**,**33**)

Nuclear Magnetic Resonance

When solutions of *syn*- and *anti-trans* dihyroxobis(2-methylmalonato)platinate(IV)

(**32**,**33**) are heated at 70 C° for 24 hours or kept at room temperature for several weeks, new resonances are observed in the ^{195}Pt and ^{13}C NMR spectra. The new resonances are observed at 3104, 3100 and 3071 ppm in the ^{195}Pt spectra. The proximity of these resonances to **32** and **33** suggests complexes with six oxygen ligands and one or more bidentate ligands. The ^{13}C spectrum shows the appearance of four new resonances in both the methyl and methylene regions, and the appearance of eight new resonances in the carboxyl region. These resonances are consistent with isomerization to form three isomers of *cis*-dihyroxobis(2-methylmalonato)platinate(IV) (**42**,**43**,**44**). The differences among the cis isomers are most simply visualized if the 2-methylmalonato ligands are constrained to a planar chelate ring conformation as shown in Figure 47. Because there is not a common plane for the cis complexes, the terms syn and anti lose their meaning in describing the location of the methyl groups, and a different nomenclature must be introduced. The Pt is the common fusion point for the two chelate rings in the cis isomers, and the nomenclature for the cis complexes is taken from the commonly used organic terms of exo and endo faces. The endo face is less than 180° between chelate rings, and the exo face is greater than 180° between chelate rings. Depending on how the methyl groups are placed on each of the 2-carbon atoms, cis complexes can form three isomers. The first is when methyl groups are as close as possible to one another and is called endo, endo. The second is when methyl groups are as far away from one another as possible and is called exo, exo. The third is when methyl groups are at an intermediate distance from one another and is called endo, exo. We do not have sufficient spectroscopic evidence to assign the resonances for **42**, **43**, and **44** to the three

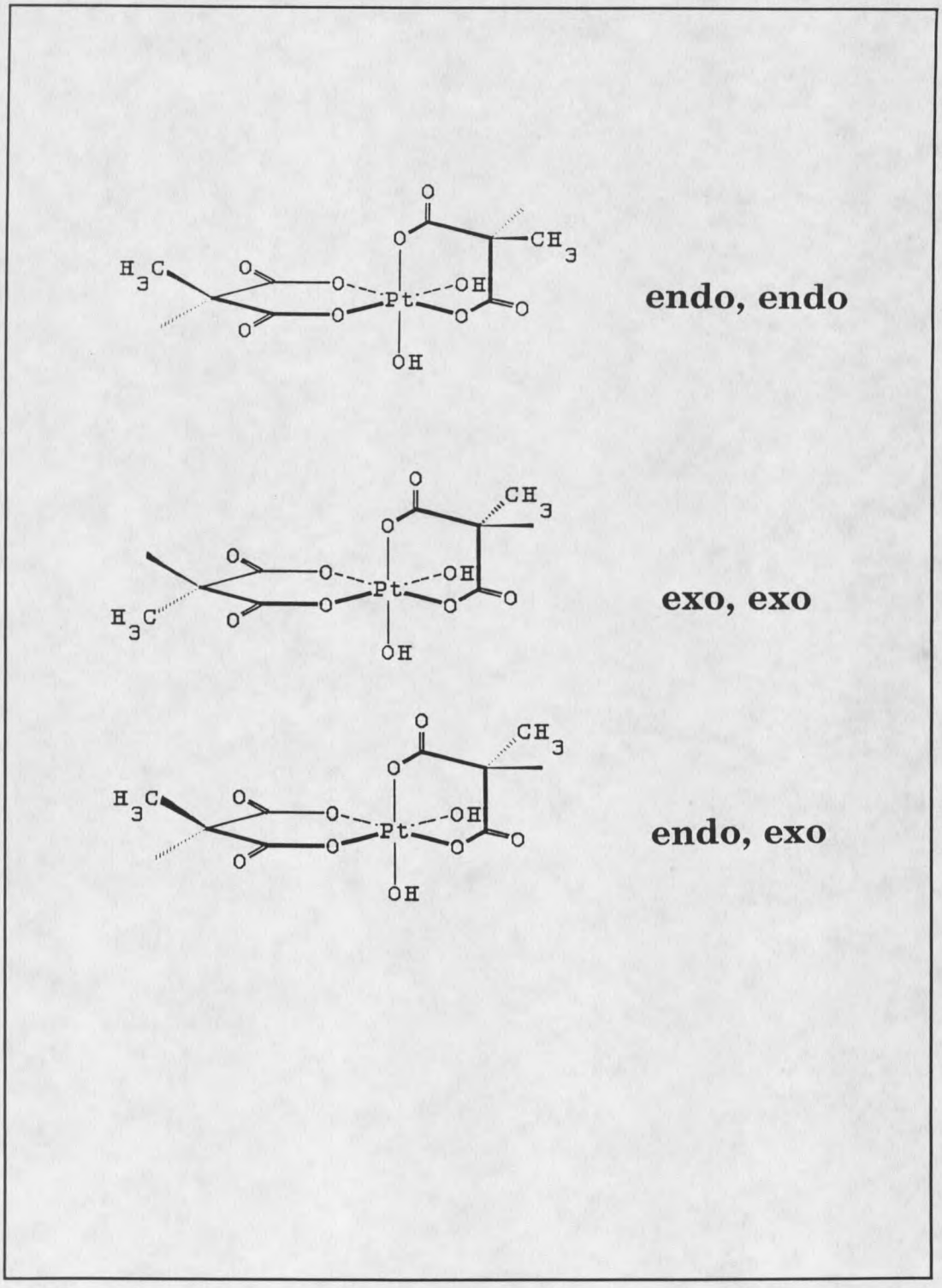

Figure 47 Idealized Stuctures of 2-Methylmalonato Complexes.

cis isomers, but the rationale for their assignment will be presented in the following section which discusses the mechanism for isomerization. Oxidation of *anti-* and *syn-*$[Pt(Mmal)_2]^{2-}$ (**22**) and (**23**) by $H_2{}^{16}O_2$ in 50% $H_2{}^{16}O$/ 50% $H_2{}^{18}O$ results in the formation of exclusively *anti-* and *syn-trans-*$[Pt(OH)_2(Mmal)_2]^{2-}$ (**32, 33**) as the kinetic products isotopically labled with 50% ^{18}OH. The ^{195}Pt NMR spectrum shows only two $^{16}O/^{18}O$ isotopomeric species for **32** and **33** as previously described for **28** and **31.** When isotopically labeled solutions of **32** and **33** are heated at 70 C° for 24 hours or left at room temperature for several weeks, new resonances for *cis-*$[Pt(OH)_2(Mmal)_2]^{2-}$ (**42, 43, 44**) are observed at 3104, 3100, and 3071 ppm in the ^{195}Pt NMR spectrum (Figure 48). Two $^{16}O/^{18}O$ isotopomeric resonances are observed for **42, 43,** and **44** in the same isotopic ratio as were present in the origional solutions of **32** and **33.** The absence of a third isotopomeric resonance shows the isomerization process is an intramolecular process which cannot incorprorate further ^{18}O from solvent. The ^{195} NMR of these solutions is shown in Figure 48. The NMR Data for **42, 43, 44** is listed in Tables 34 and 35.

TABLE 35. ^{13}C NMR Data

COMPLEX	Structure #	C=O	CH_2
[*cis*-$Pt(OH)_2(Ox)_2]^{2-}$	40	167.33 168.11	
[*cis*-$Pt(OH)_2(Mal)_2]^{2-}$	41	168.11 167.33	48.34

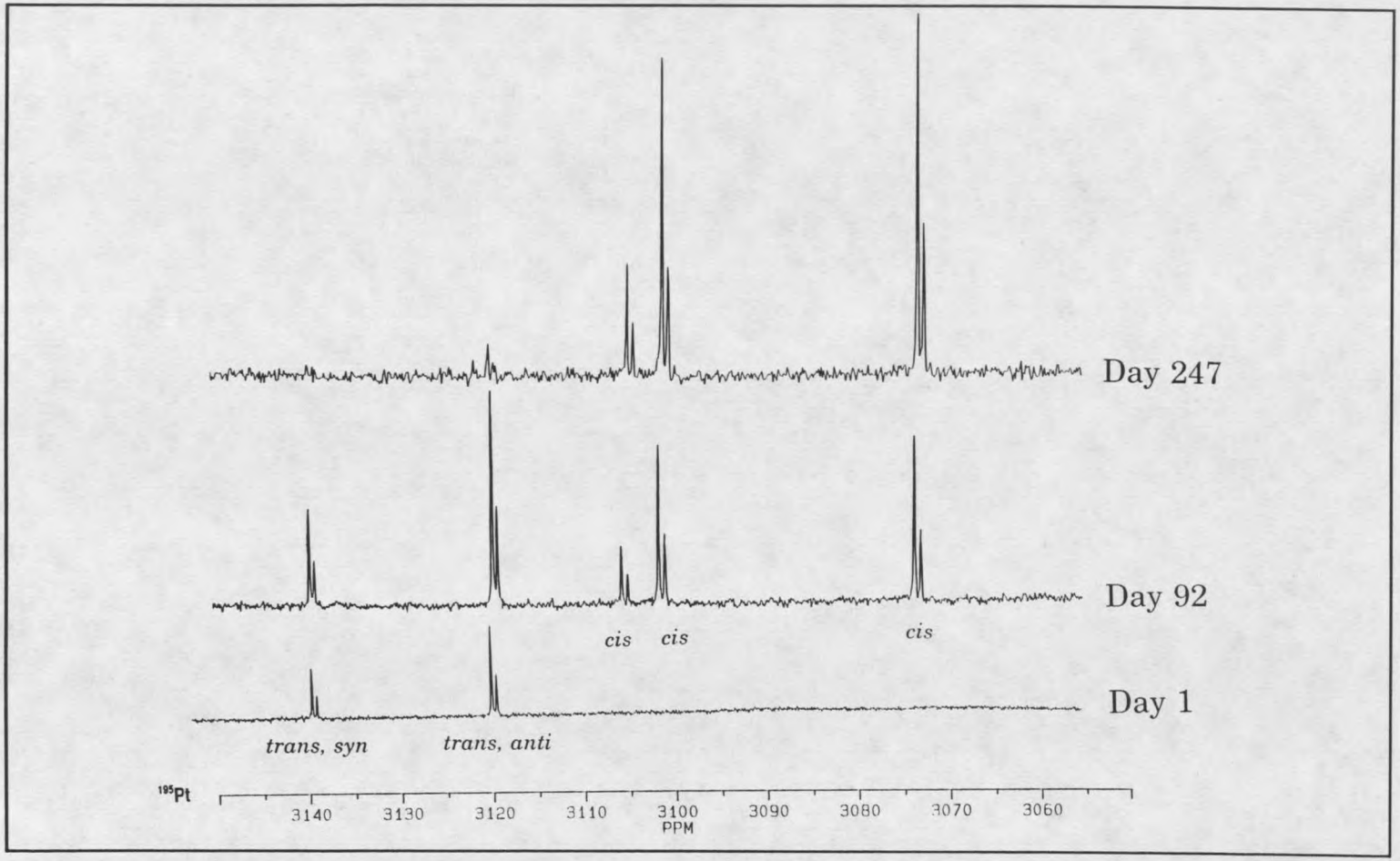

Figure 48 ^{195}Pt NMR Spectra of the trans-cis isomerization for *syn*- and *anti-trans*-$[Pt(OH)_2(Mmal)_2]^{2-}$ in 60% $H_2{}^{16}O$ / 40% $H_2{}^{18}O$.

TABLE 36. ^{195}Pt NMR Data.

COMPLEX	Structure #	δ Pt (ppm)	Isotope Shift
[*cis*-$Pt(OH)_2(Ox)_2$]$^{2-}$	40	2847	0.52[b]
[*cis*-$Pt(OH)_2(Mal)_2$]$^{2-}$	41	3158	0.55[b]
[*cis*-$Pt(OH)_2(Mmal)_2$]$^{2-}$ [a]	42	3104	0.72[b]
[*cis*-$Pt(OH)_2(Mmal)_2$]$^{2-}$ [a]	43	3100	0.73[b]
[*cis*-$Pt(OH)_2(Mmal)_2$]$^{2-}$ [a]	44	3071	0.73[b]

Ox = oxalato, Mal = malonato, Mmal = 2-methylmalonato, [a] = absolute conformation of methyl oreigntation is not established, [b] = $^{16}O/^{18}O$ isotopic shift.

Rate for Trans-Cis Isomerization

Integration of the ^{195}Pt NMR spectra over time was used to calculate the rate constants for trans-cis isomerization of **28**, **32**, and **33**. Regression plots for the dissappearance of trans isomer by a first order process were linear. The first order rate constant for isomerization of **28** was determined to be 2.94×10^{-8} sec^{-1}. The first order rate constants for isomerization of **32** and **33** were determined to be 1.04×10^{-7} sec^{-1} and 1.39×10^{-7} sec^{-1}.

Mechanism for Trans-Cis Isomerization.

A mechanism for isomerization from trans to cis must follow two clear experimental results. The first is when isomerization occurs in solutions of $H_2{}^{16}O$ and

$H_2{}^{18}O$, there is no change in the isotopic ratio of $H^{16}O$ and $H^{18}O$ in the newly formed cis complexes. This result is consistent with an intramolecular process. The second experimental result is more subtle, and is the unequal ratio of *cis*-dihydroxobis(2-methylmalanato)platinate(IV) complexes formed upon isomerization. The difference in intensity for the cis complexes originates from the Pt(II) complexes **22** and **23**, which are not present in equal concentrations before oxidation to the Pt(IV) complexes **32** and **33**. *Anti*-$[Pt(Mmal)_2]^{2-}$ (**22**) is the dominant isomer, and *syn*-$[Pt(Mmal)_2]^{2-}$ (**23**) is the minor isomer. After oxidiation with H_2O_2 it follows that, *anti-trans*-$[Pt(OH)_2(MMal)_2]^{2-}$ (**32**) is the major isomer, and *syn-trans*-$[Pt(OH)_2(MMal)_2]^{2-}$ (**33**) is the minor isomer. Isomerization of **32** and **33** leads to three new cis isomers with **44** the major isomer, **43** in moderately lower concentration, and **42** the minor isomer. Any isomerization mechanism should fit this ratio of cis species being formed from the major **32** and minor **33** *trans*-dihyroxo Pt(IV) complexes. Three classical mechanisms have been proposed to explain isomerization processes for octahedral complexes. The first is the formation of a five coordinate trigonal bipyramidal intermediate. This five coordinate intermediate could be formed by the loss of a hydroxo ligand, or the breaking of a Pt oxygen bond from one end of the chelated 2-Methylmalonato ligand. Addition of a hydroxyl ligand, or the reformation of a chelate ring could lead to the isomerization of the complex. It is clear that the isomerization is not a result of hydroxyl exchange. If hydroxyl exchange were happening, there should be an increase in the ^{18}O content of the cis complex with respect to the trans, and hydroxyl exchange would also result in some cis complex with two ^{18}O ligands. A change in the isotopic ratio of the cis complexes is not observed.

The dissociation of a 2-methylmalonato ligand to form a complex with two hydroxyl ligands, a monodentate and a bidentate 2-methylmalonato ligand can also be excluded. We have shown that monodentate O-bound ligands are stable intermediates for substitution reactions of the corresponding bis-(O,O) Pt(II) complexes, and these monodentate, bidentate complexes would be resonable intermediates for Pt(IV) as well. However, the formation of monodentate complex is disfavored by the isomerization of *anti-trans*-$[Pt(OH)_2(Mmal)_2]^{2-}$ (**32**), and *syn-trans*-$[Pt(OH)_2(Mmal)_2]^{2-}$ (**33**), to the cis complexes **42**, **43**, and **44**. Trigonal-bipyramidal intermediates for **32** and **33** are shown in Figures 49 and 50. If *anti-trans*-$[Pt(OH)_2(Mmal)_2]^{2-}$ (**32**) isomerized via a monodentate mechanism, only a single major complex would be generated with one methyl group endo, and the other methyl group exo as shown in Figure 49. If *syn-trans*-$[Pt(OH)_2(Mmal)_2]^{2-}$ (**33**) isomerized via a monodentate mechanism, two minor complexes would be generated with methyl groups in a endo, endo arrangement, and methyl groups in an exo, exo arrangement as shown in Figure 50. Upon isomerization to *cis* complexes, there is not a single predominant resonance. Rather, solutions after isomerization consist of differing amounts of **42**, **43**, and **44**. If these observations can be extended to both oxalato and malanato complexes, a monodenate mechanism is not occurring. Also, it would seem unlikely for the monodentate mechanism to be favored over loss of hydroxyl. A dissociative mechanism would predict that hydoxyl attack of the five coordinate complex, resulting in ^{18}OH exchange, should be competing with reformation of the chelate ring to the bis bidentate complex.

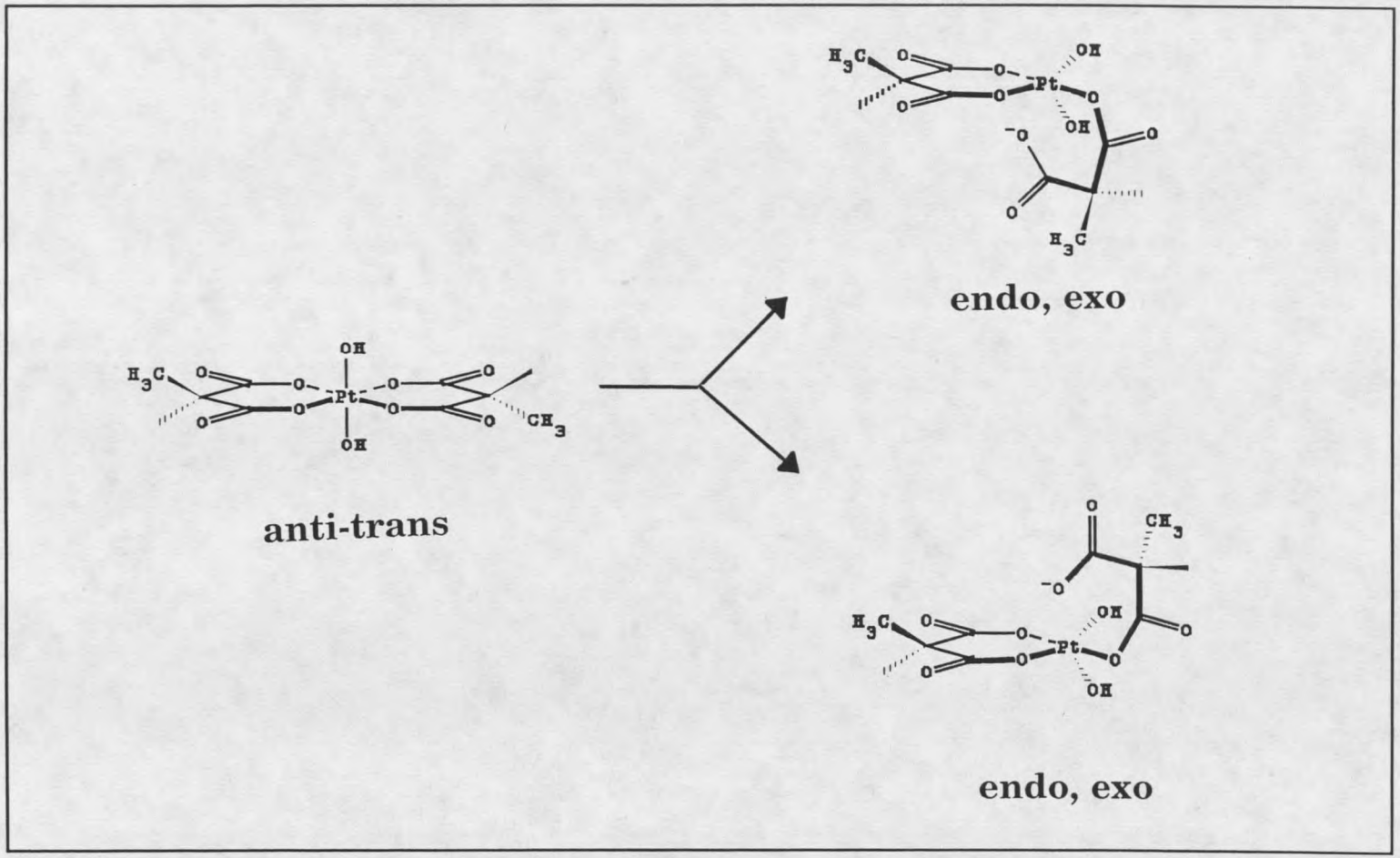

Figure 49 Trans-cis isomerization of *anti-trans*-$[Pt(OH)_2(Mmal)_2]^{2-}$ by a trigonal-bipyramidal mechanism.

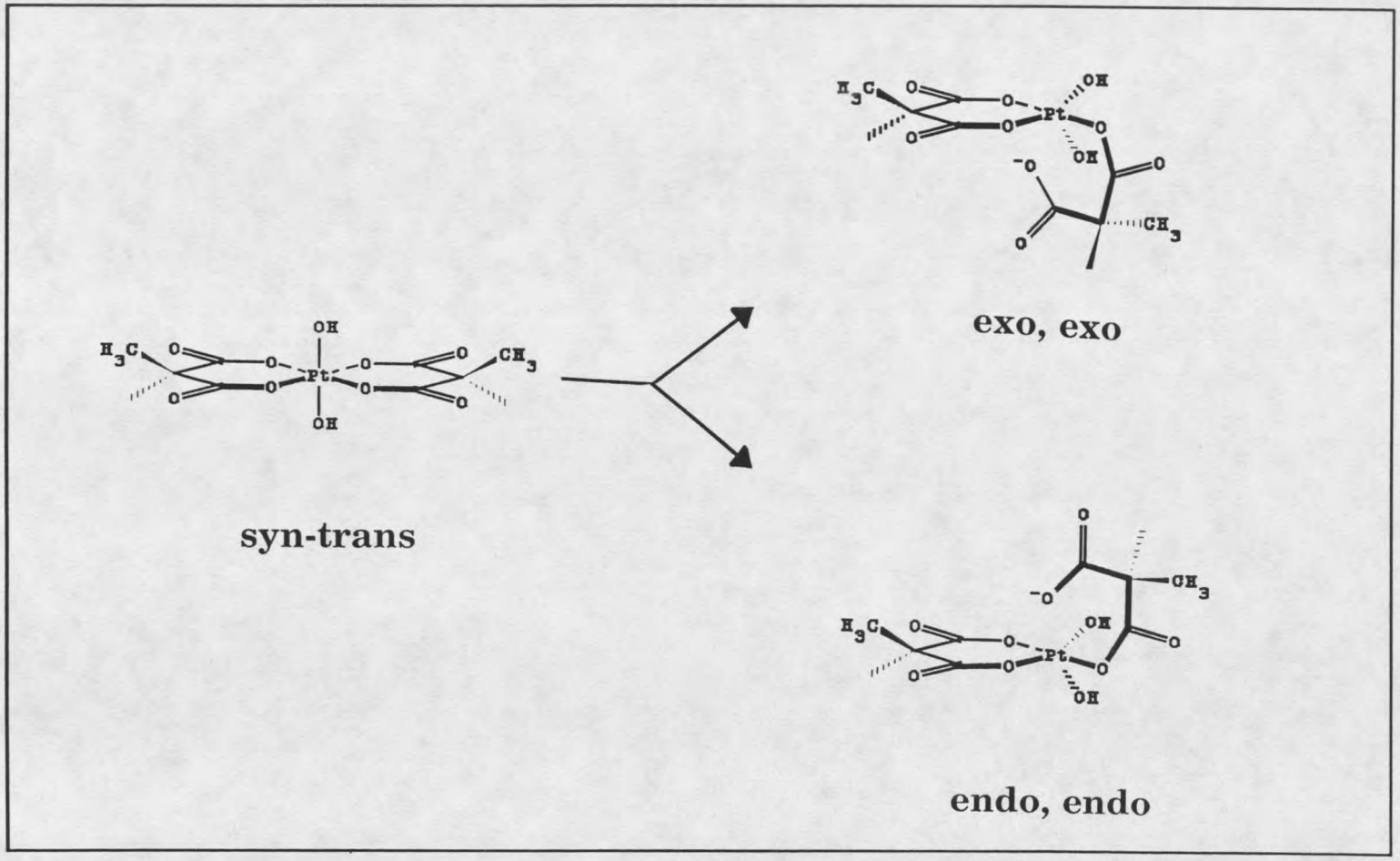

Figure 50 Trans-cis isomerization of *syn-trans*-$[Pt(OH)_2(Mmal)_2]^{2-}$ by a trigonal-bipyramidal mechanism.

A second class of mechanism that has been proposed for isomerization involves concerted rearrangements which do not involve bond breaking such as the Bailar and Ray-Dutt twists. These rearrangements would occur without a change in ^{18}OH content because the twist is an intramolecular process. Both the Bailar and Ray-Dutt twists can give the correct ratios for the formation of the three isomers **42**, **43**, and **44**.

The Bailar twist is a 60° rotation of one of the eight faces of the octahedron as shown in Figures 51 and 52. Steric restraints of the bidentate ligands limit the number of rotatable faces to four, or two faces for each ligand. The two faces of the octahedron for the trans isomers share a common edge which are the oxygen coordination sites for the 2-methylmalonato ligand. A twist of the upper face, which is closest to the methyl group, of *anti-trans*-$[Pt(OH)_2(Mmal)_2]^{2-}$ (**32**) gives the exo, exo isomer; and a twist of the lower face of **32** gives the endo, endo isomer. This would predict two new species would be formed from the dominant isomer **32**, and each of equal concentration if the upper and lower face rotations are equivalent. The upper and lower faces of **32** are not equivalent. Experimentally, **32** isomerizes to give the dominant resonance **44** and the minor resonance **42**. The upper face that would lead to exo, exo isomer has the methyl group closest to the face, and the face that would lead to the endo, endo isomer has the methyne hydrogen closest to the face. Also, the x-ray crystal structure of *anti*-$[Pt(Mmal)_2]^{2-}$ (**23**) shows that the 2-methylmalanato chelate rings are not planer, but they are in a boat conformation in the solid state. This conformation is retained in the solution spectra of **23**. The boat conformation should be quite favorable for the *trans*-dihydroxo species **32** because of the added steric restrictions between axial hydroxyl and

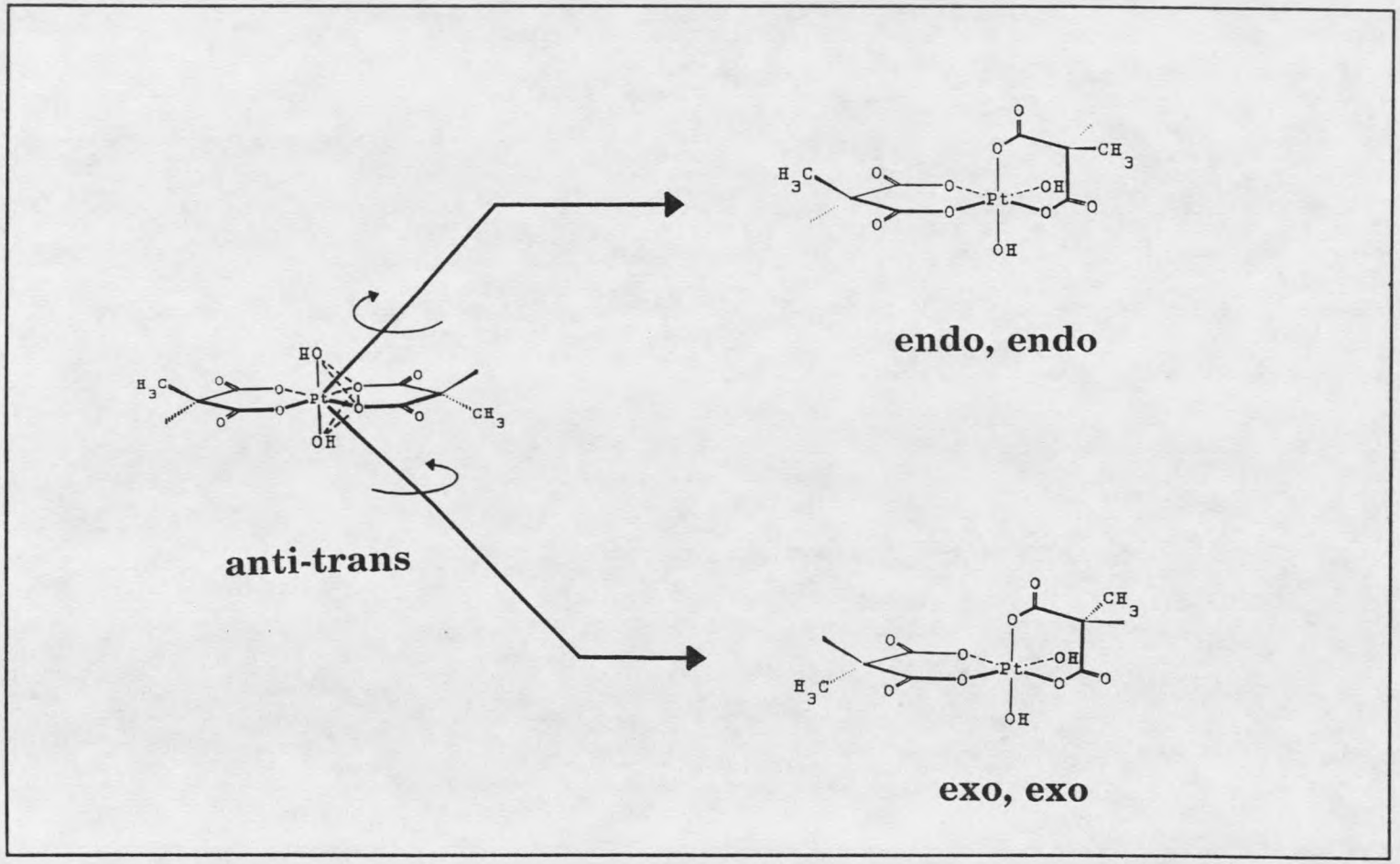

Figure 51 Trans-cis isomerization of *anti-trans*-$[Pt(OH)_2(Mmal)_2]^{2-}$ by a Bailar twist mechanism.

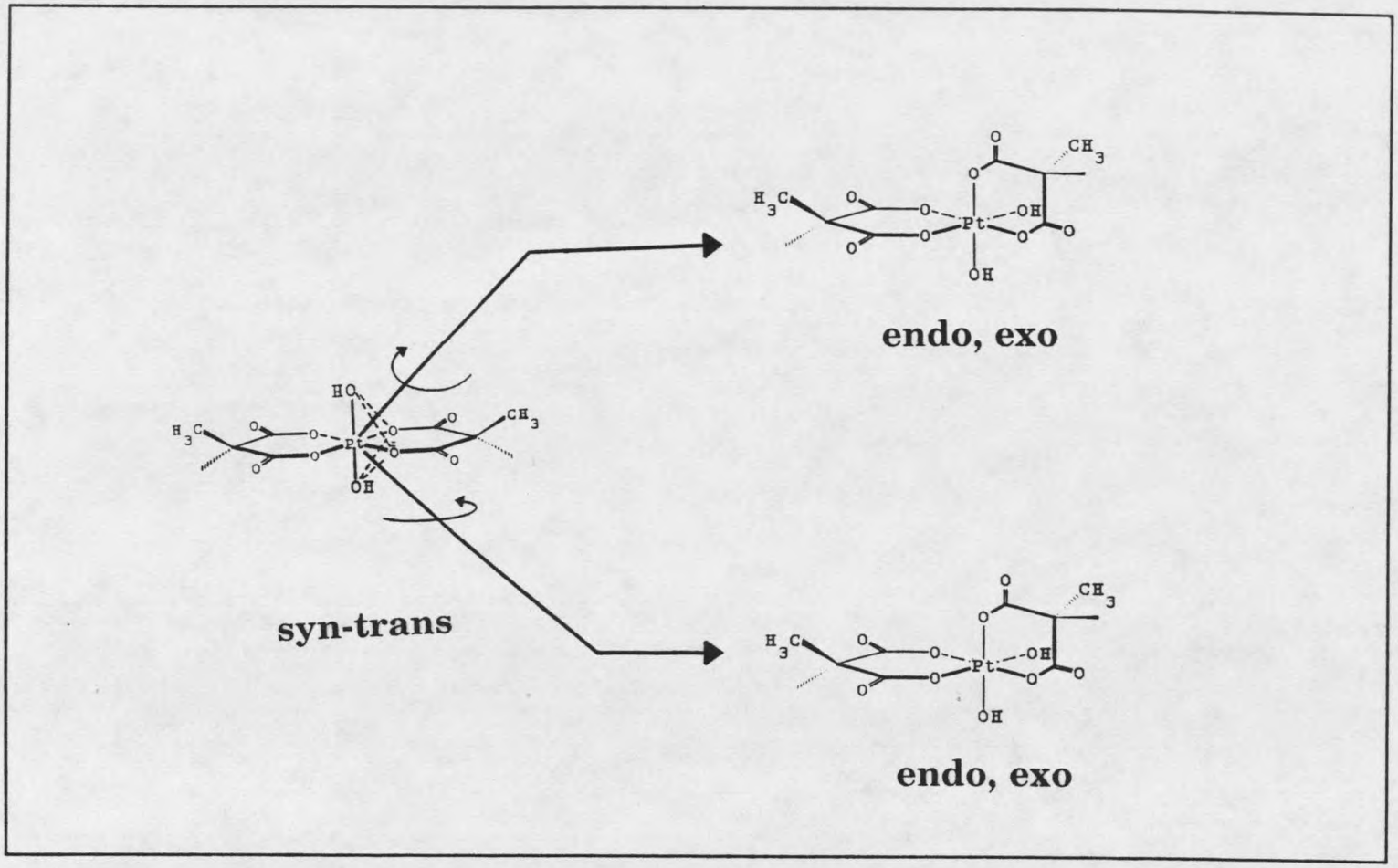

Figure 52 Trans-cis isomerization for *syn-trans*-$[Pt(OH)_2(Mmal)z2]^{2-}$ by a Bailar twist mechanism.

the methyl group of the ligand. The third cis isomer can result from a twist of the upper face of *syn-trans*-$[Pt(OH)_2(Mmal)_2]^{2-}$ (**33**) to give the endo, exo isomer **43** (Figure 52). A twist of the lower face of **33** also gives the endo, exo isomer **43**. This would predict a single minor cis complex arrising from the minor isomer **33**. Integration of ^{195}Pt NMR spectra over time shows that the ratio of **32** to **33** is maintained as the ratio of the sum of **42** and **44** to **43**. From this data, we have made the assignments of **42** to the exo, exo; **43** to the exo,endo; and **44** to the endo,endo isomers. The assignment of **42** and **44** could be switched, but we assign them from the most sterically crowded rotation for **32** having the highest energy barrier and thus the smallest resonance **42**. The Bailar twist mechanism is in complete agreement with the experimental data.

The Ray-Dutt or rhomboid twist is a 120° rotation about a C_3 axis of the octahedron which is different from the C_3 axis of the Bailar twist. The results of the Ray-Dutt twist are the same as the Bailar twist, and these two mechanisms cannot be distinguished from each other for this system. A Ray-Dutt twist can only be distinguished from a Bailar twist if the chelate ligand is asymmetric.

HYDROXYL, AQUO, AND OXALATO OXYGEN EXCHANGE FOR BIS(OXALATO)PLATINUM(IV) COMPLEXES

Coordinated water and hydroxyl exchange reactions for Pt complexes is of interest in the substitution chemistry of Pt(II) and Pt(IV) complexes. These reactions are important in establishing mechanistic insight for ligand substitution and solvent dependent pathways for Pt(II) complexes, and they provide limiting rate constants for the dissociative substitution pathways for Pt(IV) reactions (4). We are particularly interested in the relationship between water exchange and the mechanism of metal-metal bond formation in mixed valence linear chain complexes of cyanato and oxalato platinates. Krogmann has proposed a mechanism for mixed valence linear chain formation of bis(oxalato)platinate complexes which has been invoked by several others in explaining the solution behavior of linear chain Pt complexes (9,11,46). Krogmann's polymerization mechanism relies on the substitution of axial water ligands of *trans*-diaquobis(oxalato)platinum(IV) by the electrons in the dz^2 orbital of bis(oxalato)platinate(II) complex (11). Krogmann proposed this facile reaction as the initiation reaction for metal-metal bond polymerization. It was of great interest to measure the H_2O exchange rate for *trans*-diaquobis(oxalato)platinum(IV) to compare with polymerzation rates for the mixed valence platinum-oxalato polymers. The kinetic stability of Pt(IV) would predict Pt(IV) complexes to exchange H_2O by a slow dissociative process (4). However, we have found no information about H_2O exchange reactions for Pt(IV) complexes, although $H_2{}^{18}O$ has been used to study the exchange rate

for several other metal complexes (71). H_2O exchange for Pt(II) has been established for several compounds. Elding has shown that H_2O exchange for Pt(II) complexes can be studied by the effects of oxygen isotopic labeling in ^{195}Pt NMR (63,64). ^{195}Pt NMR shows large chemical shifts (ca 1.0 ppm) for substitution of ^{18}O for ^{16}O. This work makes use of ^{18}O isotopically shifted resonances in ^{195}Pt NMR to investigate the H_2O exchange reactions of Pt(IV) oxalato complexes. ^{18}O exchange for $[Pt(Ox)_2]^{2-}$ has shown that all eight oxygen atoms for the oxalato ligand exchange at the same rate (65,66). The acid dependent oxalto oxygen exchange reaction has been generalized for several transition metal oxalato complexes (66,71).

pKa Measurements for *trans*-$Pt(OH)_2(Ox)_2$.

Changing the pH of solutions of dihydroxo complexes results in chemical shift changes of ^{195}Pt NMR resonances as coordinated hydroxide ion is protonated or deprotonated (72). Titration of solutions of *trans*- and *cis*-$[Pt(OH)_2(Ox)_2]^{2-}$ (**28**) and (**40**) with NaOH or $HClO_4$ at 25 C° results in two changes in chemical shift for **28** and a single change in chemical shift for **40** (Figure 53). A 25 ppm change in chemical shift for **28** between pH 1.5 and 4.0 is attributed to the deprotonation of coordinated water. This is in agreement with the previously assigned pKa's for **28** of $pKa_1 = 2.3$ and $pKa_2 = 2.83$ (73). The chemical shift for the cis complex **40** does not change between pH 1.0 and 10.0. A 300 ppm change in chemical shift occurs for both **28** and **40** at pH = 10.0 and could be assigned to the formation of hydroxo, oxo, or dioxo complexes. This high pH region has not been studied before except as mentioned by Krogmann for $[Pt(Ox)_2]_n$

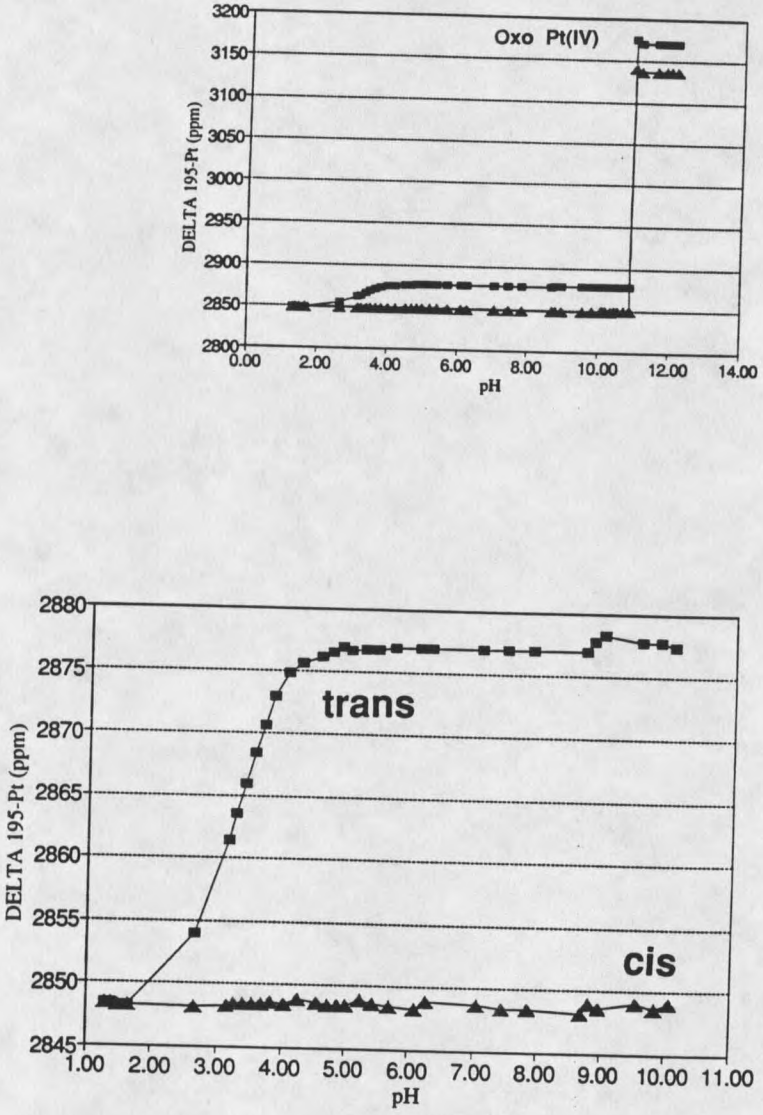

Figure 53 Titration of ^{195}Pt chemical shift for *cis*- and *trans*-$[Pt(OH)_2(Ox)_2]^{2-}$ vs. pH.

in the dissociated form (11). The ^{195}Pt NMR of solutions above pH=10 shows two resonances with the same ratio as in previously observed solutions with pH < 10. This is consistent with retention of the cis and trans nature of the oxalato complexes. Solutions adjusted to pH = 12 in $^{16}OH/^{18}OH$ do not show addition of ^{18}O isotopomeric resonances. This supports the retention of the chelate ring and contradicts addition of OH ligands to form higher coordination isomers, or facial and meridonal monodentate isomers. When solutions of **28** and **40** are returned to acidic pH, their original chemical shifts are slow to return.

Hydroxyl Oxygen Exchange Rate for *cis*- and *trans*-dihydroxobis-(oxalto)platinate(IV)

The ^{195}Pt NMR spectra for the trans-cis isomerization of 50 % ^{18}OH labeled *trans*-dihydroxobis(oxalato)platinate(IV) shows that no hydroxyl exchange takes place during the isomerization process (Figure 45). The lack of hydroxyl exchange over the period of time that the spectra were accumulated (190 days) allows the calculation of a limiting rate constant for this process. The concentration change from the initial spectrum to final times was assumed to be 5 % of the initial intensity. This value was chosen as a limit on the accuracy of integrating the ^{195}Pt NMR spectra. A regression plot for the spectra in Figure 45 gives a first order rate constant of 1×10^{-10} sec^{-1} for hydroxyl exchange.

Hydroxyl Exchange for *syn*-and *anti*-*trans*-dihydroxobis-(2-methylmalonato)platinate(IV)

The ^{195}Pt NMR spectra of the trans-cis isomerization for 50 % ^{18}OH labeled *trans*-dihydroxobis(2-methylmalonato) platinate(IV) shows that no hydroxyl oxygen exchange takes place during the isomerization (Figure 48). The lack of hydroxyl exchange over the period of time that the spectra were accumulated (247 days) allows the calculation of a limiting rate constant for this process. The concentration change from the initial spectrum to final times was assumed to be 5 % of the initial intensity. This value was chosen as a limit on the accuracy of integrating the ^{195}Pt NMR spectra. A linear regression plot for the spectra in Figure 48 gives a first order rate constant of 1 x 10^{-10} sec^{-1} for hydroxyl exchange.

Aquo Oxygen Exchange Rate for diaquobis-oxalatoplatinum(IV)

The pH titration of **28** (Figure 53) indicates that **28** should be the diaquo complex in acidic solutions of pH < 2.5. The exchange of coordinated H_2O for **28** was followed for 24-48 hours by ^{195}Pt NMR in 1M $HClO_4$ solutions (pH=1.0). Integrated ^{195}Pt NMR spectra were used for the measurement of the H_2O exchange rate. To simplify the ^{195}Pt NMR spectra, and the analysis of the rate data, **28** was prepared in 50% $H_2{}^{16}O$ / 50% $H_2{}^{18}O$ by H_2O_2 oxidation of **5**. The solution of **28** labeled with 50 % ^{18}OH at one axial position was rotoevaporated to dryness several times with $H_2{}^{16}O$ water to remove any

$H_2{}^{18}O$ remaining after oxidation. These solutions always showed the appearance of small amounts of labeled **40**. The water exchange rate was followed by the disappearance of the $H_2{}^{16}O/H_2{}^{18}O$ resonance in the ^{195}Pt NMR spectrum after dissolving the dry solid in 1 M $HClO_4$ (Figure 54). The change in the $H_2{}^{16}O/H_2{}^{18}O$ resonance over time is the sum of two rates. The first is the H_2O exchange rate, and the second is the isomerization rate to **40**. The change in the disappearance of the $H_2{}^{16}O/H_2{}^{18}O$ resonance was corrected for isomerization to **40**. The correction does not greatly affect the data in that a rapid equilibrium between **28** and **40** is established in this pH region. The isomerization rate does affect the identification of the exchanging complex, in that the rapid isomerization does not preclude the measured H_2O exchange from occurring on **40**, and a rapid isomerization of the exchanged complex to form **28**. Rate data were linear when plotted for a first order reaction (Figure 55), and the rate constants determined at four temperatures (294-310 K) are listed in Table 36.

The variable temperature rate data were fitted to an Eyring plot and slope and intercept were calculated by best least squares fit (Figure 56). The activation enthalpy from the Eyring plot gave $\Delta H\# = 94.1\ (\pm 13.4)$ kJ $mole^{-1}$. The activation entropy from the Eyring plot gave $\Delta S\# = -28.6\ (\pm 1.8)$ J $mole^{-1}K^{-1}$. These values can be compared to H_2O exchange for other inert metal ions (Table 37). The enthalpy and entropy of activation are reasonable when compared to other dissociative H_2O exchange reactions for inert metal ions. The activation entropy is not large, but a negative value for $\Delta S\#$ for **28** could be indicative of a contraction of the solvent in the cybotactic region of the dissociative reaction (72). A contraction of the solvent would be expected for H_2O

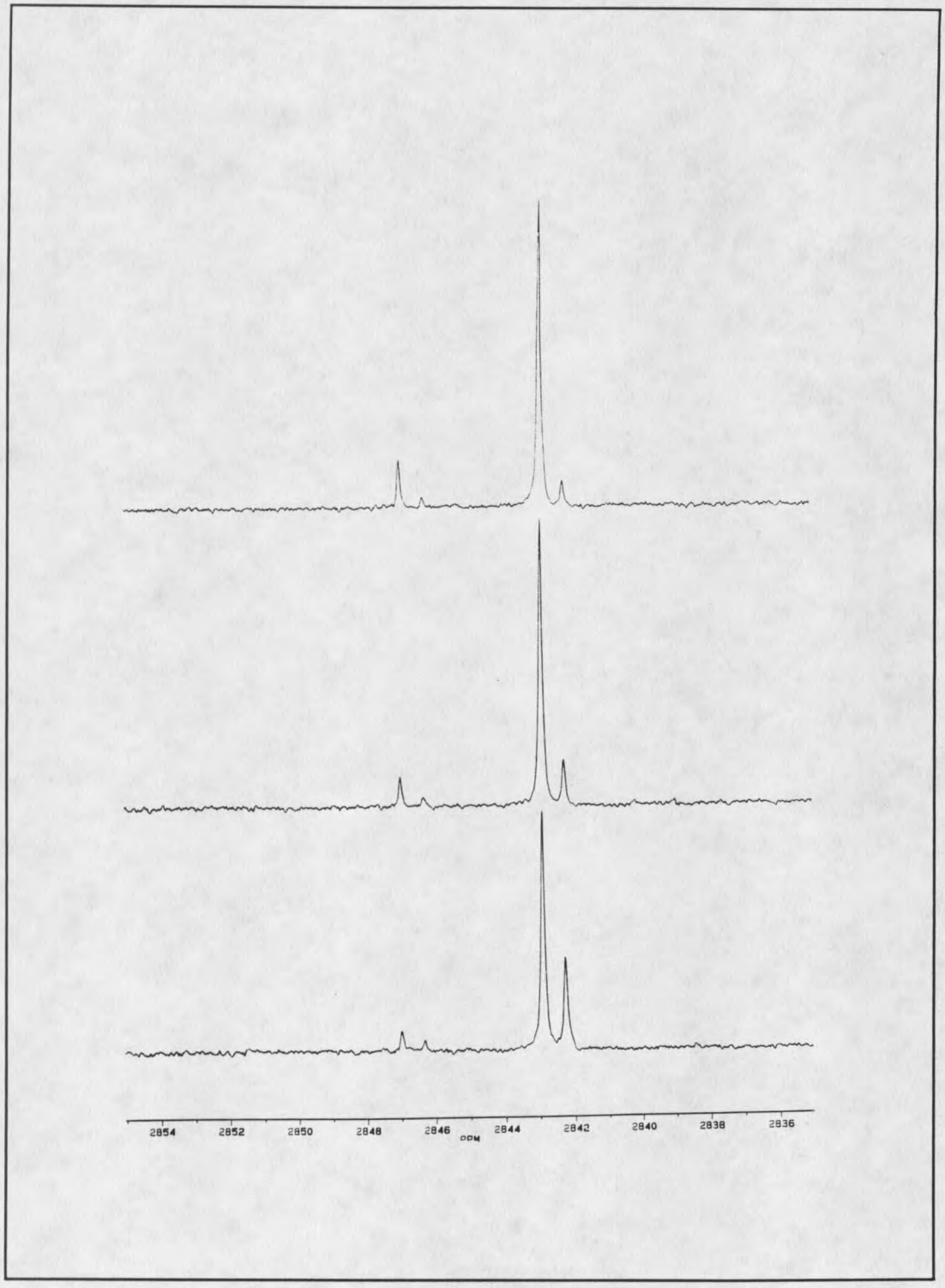

Figure 54 ^{195}Pt NMR for the H_2O exchange reaction of *trans*-$[Pt(H_2O)_2(Ox)_2]$ in 1 M $HClO_4$.

exchange of the neutral complex **28**. The symmetry of **28** is broken as the coordinated H_2O is dissociated. The asymmetric intermediate would have an increased solvation because of the dipolar nature of the five coordinate intermediate. A change in the hydrogen bonding character of the cybotactic region would also be expected as the coordinated water is introduced for several new hydrogen bonding interactions.

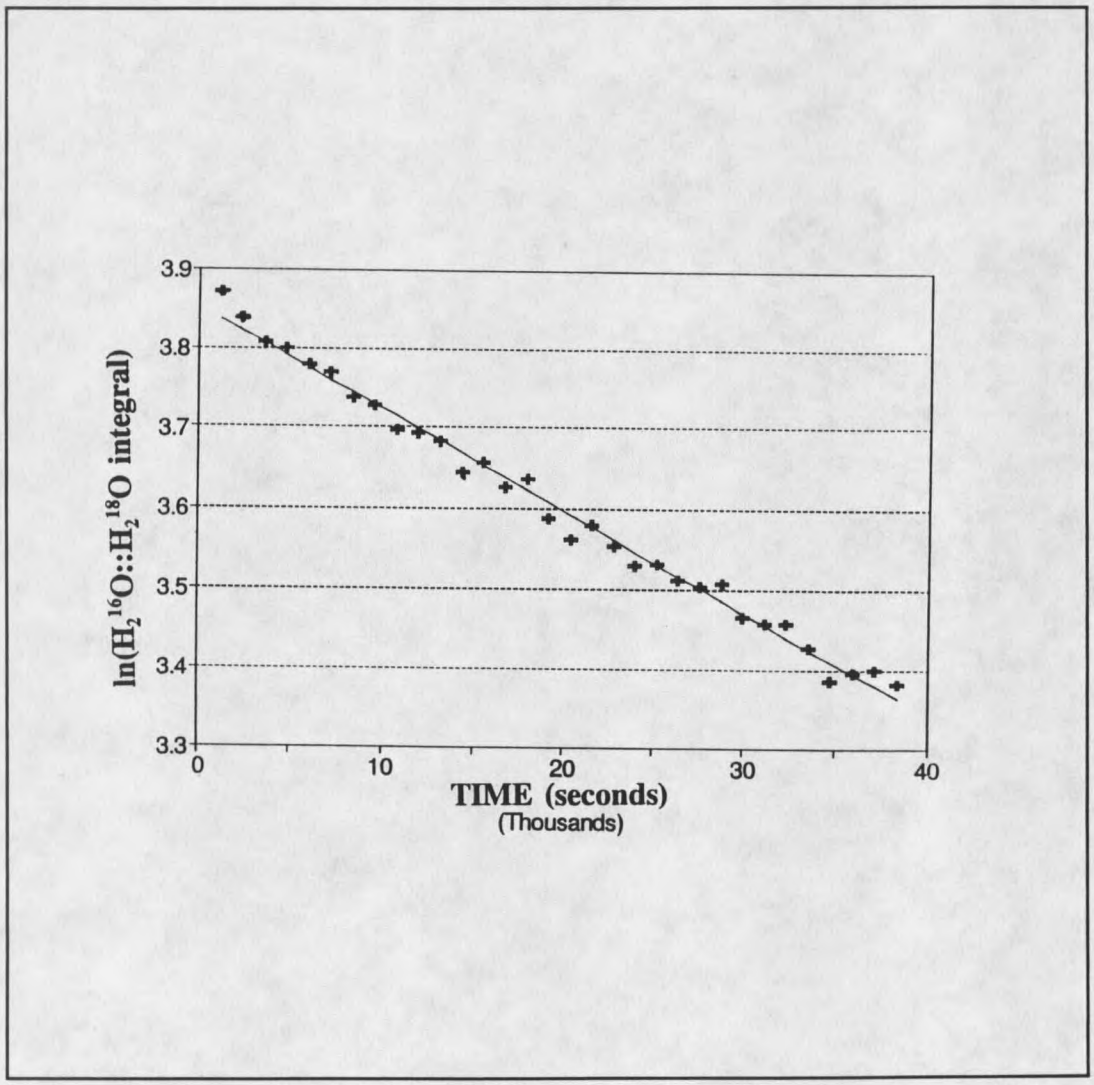

Figure 55 Linear regression plot of the H_2O exchange reaction for *trans*-$[Pt(H_2O)_2(Ox)_2]$ at 300 K.

TABLE 37. Temperature Dependence for the Water Exchange Rate of *trans*-$[Pt(H_2O)_2(Ox)_2$ **(28)**

H_2O Exchange Rate (sec^{-1})	Temperature (K)
3.7 ($\pm$0.4) x 10^{-6}	294
9.4 ($\pm$1.0) x 10^{-6}	300
2.1 ($\pm$0.1) x 10^{-5}	300
2.1 ($\pm$0.1) x 10^{-5}	305
2.5 ($\pm$0.1) x 10^{-5}	310

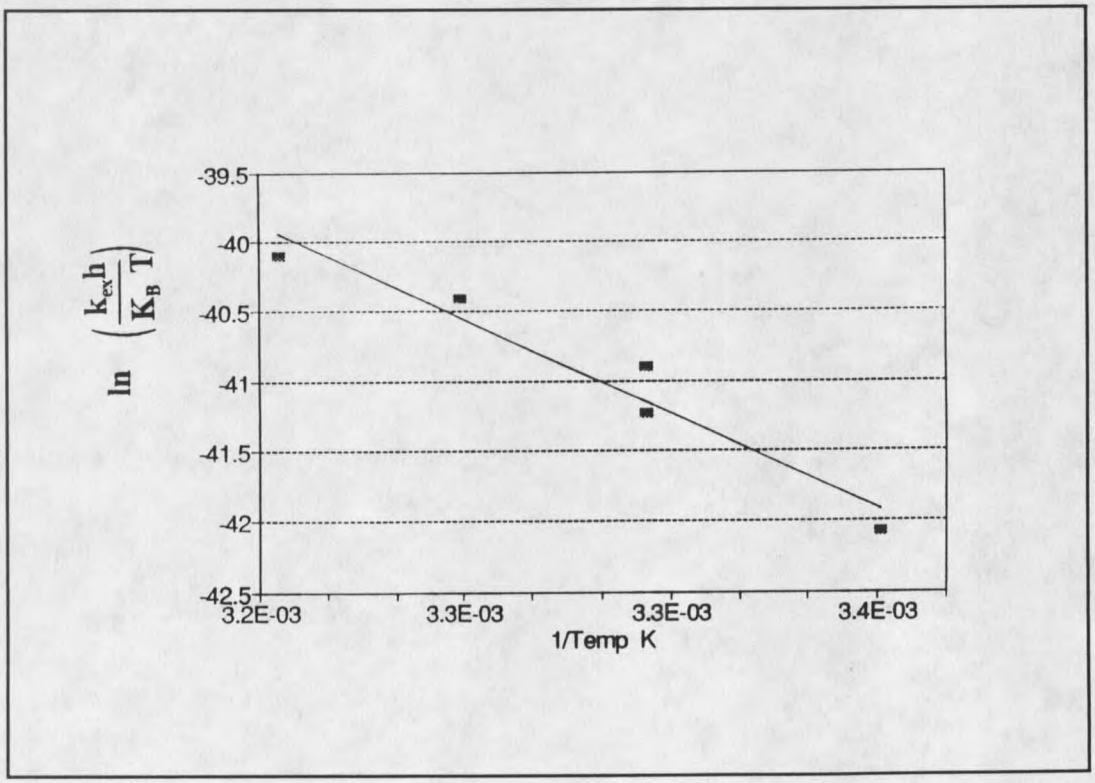

Figure 56 Eyring Plot for the H_2O exchange reaction of *trans*-$[Pt(H_2O)_2(Ox)_2]$.

TABLE 38. H_2O Exchange Rates for Several Inert Transition Metal Complexes

Complex	k_{ex}^{298}/sec^{-1}	$\Delta H\dagger/kJ\ mol^{-1}$	$\Delta S\dagger/JK^{-1}mol^{-1}$
d^6-*trans*-$[Pt(H_2O)_2(Ox)_2]$	4.4×10^{-6}	94.1	-28.6
d^6-$[Co(NH_3)_5(H_2O)]^{3+}$	5.7×10^{-6} [a]	111.3	28.0
d^6-$[Rh(NH_3)_5(H_2O)]^{3+}$	8.7×10^{-6} [a]	102.9	3.3
d^6-$[Ir(NH_3)_5(H_2O)]^{3+}$	6.1×10^{-8} [a]	117.6	11.3
d^6-$[Rh(H_2O)_6]^{3+}$	5.6×10^{-9} [a]	134.1	46.8
d^3-$[Cr(H_2O)_6]^{3+}$	4.5×10^{-7} [a]	109.6	-9.3
d^3-$[Cr(NH_3)_5(H_2O)]^{3+}$	6.1×10^{-5} [a]	97.1	0.0

[a] = Data from reference 71.

Oxalato Oxygen Exchange Rate for diaquobis(oxalato)platinum(IV)

When solutions of **28** in 1 M $HClO_4$ 50% $H_2{}^{16}O/H_2{}^{18}O$ were used to study the H_2O exchange by isotopic dilution with $H_2{}^{18}O$, the ^{195}Pt NMR spectra showed the oxalate ligand was also incorporating $H_2{}^{18}O$. The incorporation was evident by the appearance of a fourth isotopically shifted peak for **28** (Figure 56). H_2O exchange should result in only the three isotopically shifted resonances $^{16}O/^{16}O$, $^{16}O/^{18}O$, and $^{18}O/^{18}O$. Solutions that reached equilibrium showed seven $^{16}O/^{18}O$ isotopomeric resonances (Figure 57). These seven resonances result from substituting all six oxygen Pt bonds with differing amounts of ^{18}O. This observation is consistent with previous results for oxygen exchange of the Pt(II) complex $[Pt(Ox)_2]^{2-}$ (**5**) (34,35). The rate constant for ^{18}O incorporation into

the oxalate ligand was determined by integration of the isotopically shifted resonances in the ^{195}Pt NMR spectra. The oxalato oxygen exchange rate at 300 K is $1x10^{-5}$ sec^{-1}.

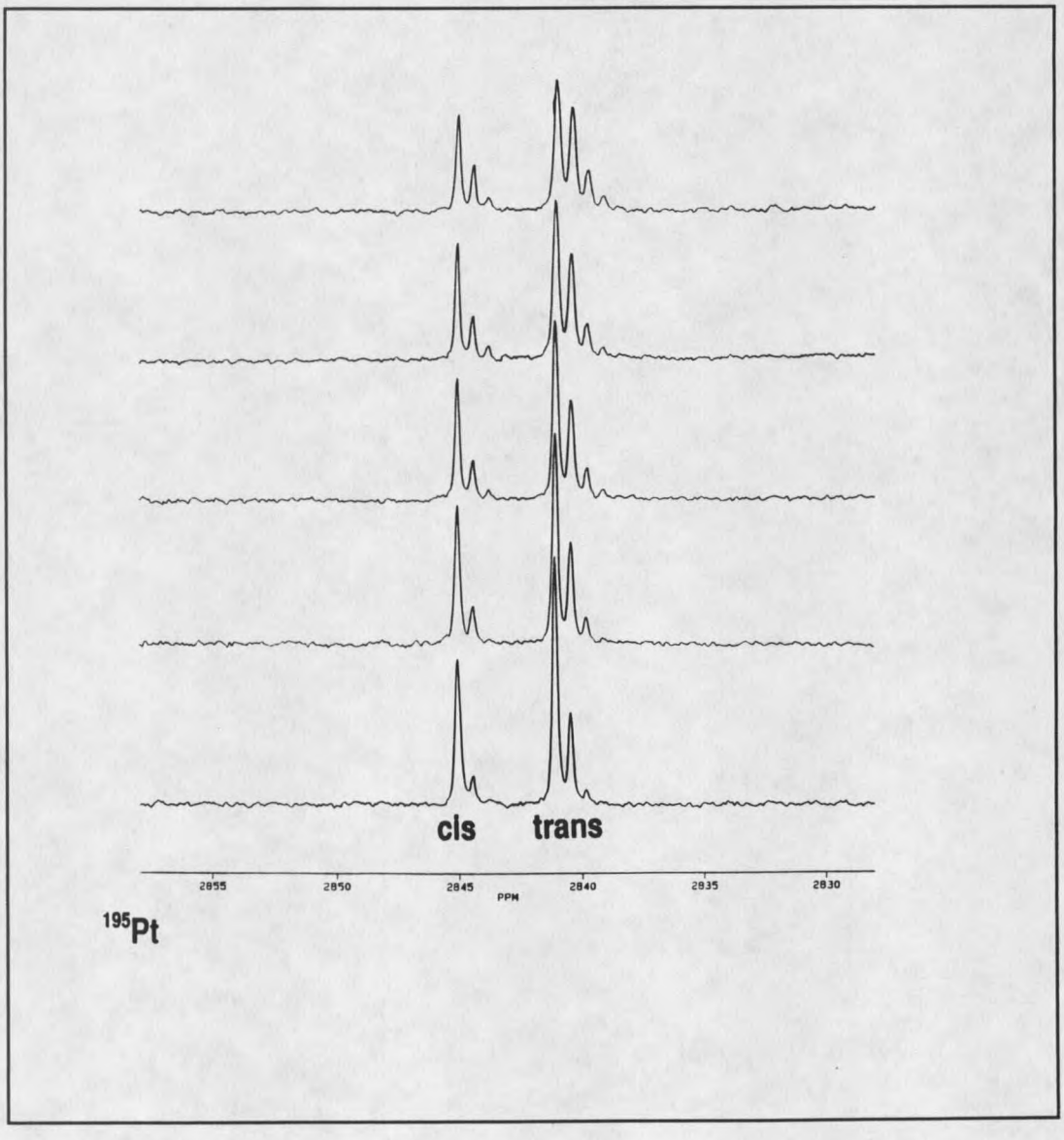

Figure 57 ^{195}Pt NMR spectra of the oxalato oxygen exchange for *trans*-$[Pt(H_2O)_2(Ox)_2]$ in 1 M $HClO_4$.

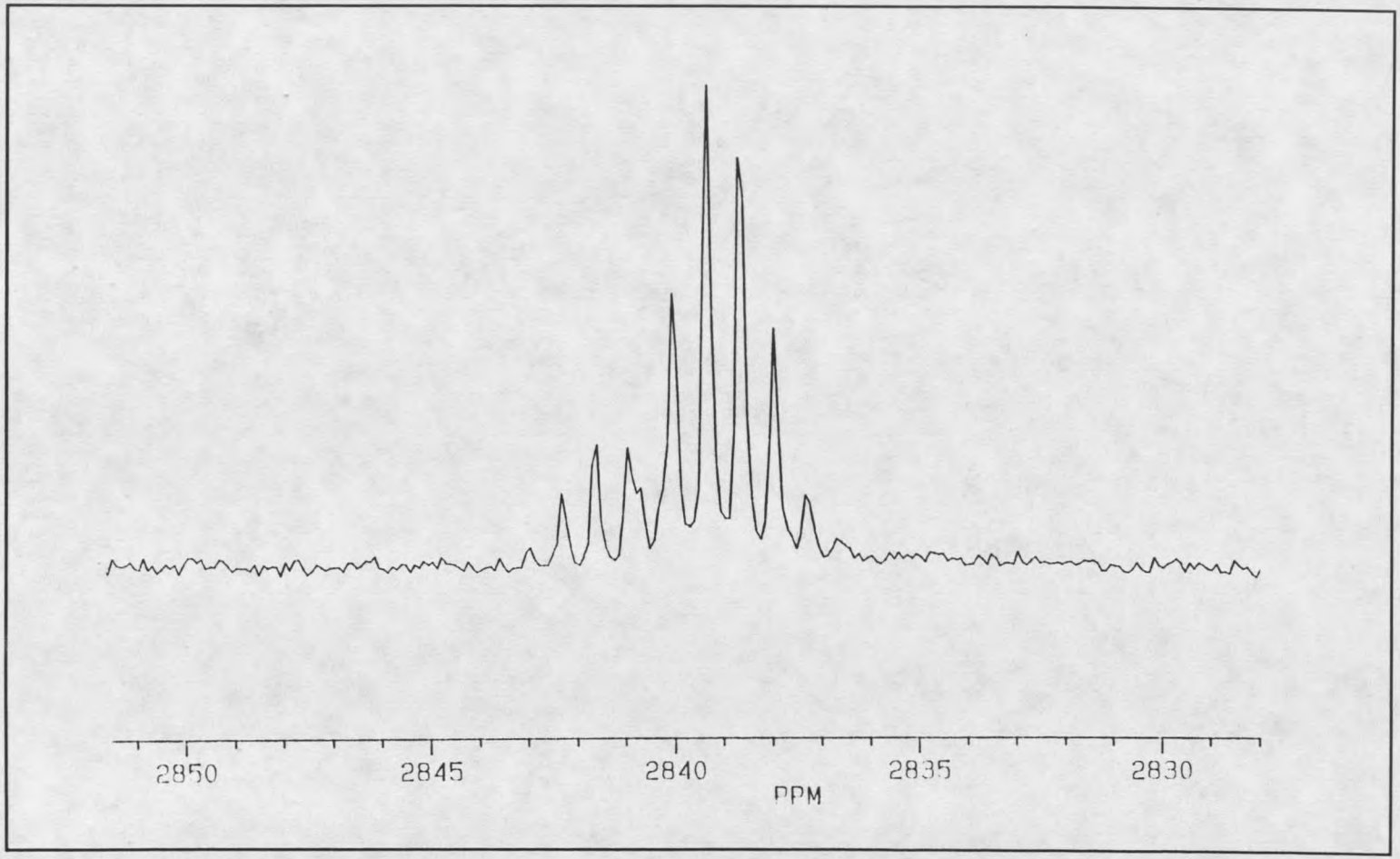

Figure 58 ^{195}Pt NMR spectrum of oxalato oxygen exchange for *cis*- and *trans*-$[Pt(H_2O)_2(Ox)_2]$ in 1 M $HClO_4$.

OXIDATION REACTIONS OF PLATINUM(II)

It is well known that Pt(II) complexes can catalyze the substitution reactions of Pt(IV) (4,14). There has been a general acceptance of two possible reaction mechanisms for this process. Both mechanisms involve the formation of a ligand bridged complex Pt(II)-X-Pt(IV). The difference in the mechanisms is whether the electron transfer between the Pt atoms occurs as rapid two one electron transfers, or by two slower one electron pathways. If the electron transfer occurs via two slow one electron transfers, the formation of a transient Pt(III) complex should be observed. It has been proposed that the formation of metal-metal bonds in the solution chemistry of one-dimensional complexes could be formed by a complimentary redox process (5,35). This reaction would have the same intermediates as the Pt(II) catalyzed reactions of Pt(IV) complexes, only the Pt(II) and Pt(IV) complexes would form a metal-metal bonded product.

Bis(oxalato)platinate(II) (**5**)

Oxidation by Cerium (IV)

Potentiometric Studies The potentiometric oxidative titration of $[Pt(Ox)_2]^{2-}$ (**5**) was carried out with Ce(IV) in 1N H_2SO_4. The titration of **5** shows one distinct endpoint for the one electron oxidation of **5** to a complex with a formal oxidation state of Pt(III). A second endpoint for the formation of Pt(IV) was not observed in these solutions.

solutions. The solutions were observed to undergo distinct changes in color during the potentiometric titration.

Ultraviolet and Visible When the oxidative titration was followed by UV-vis spectroscopy, several distinct absorptions were observed. Figures 59 and 60 show the changes in the UV-vis spectra from 350-900 nm during the oxidative titration of **5** with Ce(IV). Both **5** and Ce(IV) do not have absorption maxima with large ϵ values in the 350-900 nm region. Upon addition of Ce(IV) to a yellow solution of **5**, the solution takes on a deep blue color. The UV-vis spectra of these blue solutions show the presence of four distinct absorbance maxima. The predominant absorbance early in the titration is observed at λ_{max}=680 nm. This species was previously observed by Krogmann and Pappavasilou, and each assigned the absorbance at 680 nm to an oligomeric bis(oxalato)platinate species (11,36). The absorbance at 680 nm reaches a maximum at 0.25 equivalents of Ce(IV). This would indicate an average oxidation state of 2.25 for the Pt species. In order for a Pt complex to be oxidized by 0.25 electrons, the molecule must have at least four Pt atoms in the same molecule. The complex is consistent with the molecular formula $[Pt(Ox)_2]_n^{1.75-}$(**45**) where n $\geq$ 4. Polynuclear Pt complexes with nonintegral oxidation states are known for Pt-blues in solution, and **45** has the same average oxidation state as the α-pyridone blue (PPB) complex $[Pt_4(NH_3)_8(C_5H_4NO)_4]^{5+}$ (28). Formally, **45** corresponds to a platinum complex with one Pt(III) and three Pt(II) subunits. The degree of polymerization is unknown, but the formulation of a polymer with a multiple of four Pt atoms would be consistent with a

delocalized electronic structure. A formulation with Pt(IV) would simply be a doubling of the tetrameric unit with one Pt(IV) and seven Pt(II) subunits. Osmotic pressure measurements by Krogmann have assigned the blue solutions to species with an average chain length of 3.1 - 46.0 bis(oxalato)platinate units. A second absorbance is observed at λ_{max}=600 nm. This species has a optimum stability after the addition of 0.5 equivalents of Ce(IV). This would indicate an average oxidation state of 2.5 for the Pt complex. This complex is consistent with the molecular formula $[Pt(Ox)_2]_n^{1.5-}$(**46**) where $n \geq 2$. Formally, **46** corresponds to a Pt complex with one Pt(III) and one Pt(II) subunit. Again the extent of polymerization of these subunits is unknown, but Krogmann's osmotic pressure assignments would predict a chain length of 1.9-3.1 bis(oxalato)platinate units. This complex has the same oxidation state as the tetranuclear α-pyrrolidone tan (PPT) $[Pt_4(NH_3)_8(C_4H_6NO)_4]^{6+}$ (30). A third absorbance is observed at λ_{max}=510 nm. This Pt complex has a optimum stability at 0.75 equivalents of Ce(IV). This would indicate an average oxidation state of 2.75 for the Pt complex. This complex is consistent with the molecular formula $[Pt(Ox)_2]_n^{1.25-}$(**47**) where $n \geq 4$. Formally, **47** corresponds to a Pt complex with three Pt(III) complexes and one Pt(II). The extent of polymerization is unknown, but Krogmann's osmotic pressure measurements have assigned an average chain length of 1.1-1.9 bis(oxalato)platinate units to these solutions. This complex has the same oxidation state as the chloride bridged tetranuclear complex $\{[Pt(NH_3)_2(MeT)_2PtCl_2]_2Cl\}^+$ (27). When the titration reaches one equivalent of Ce(IV), the maximum stability of a fourth species is observed at λ_{max}=420 nm. This would indicate an average oxidation state of 3.0 for the Pt complex. This complex is consistent

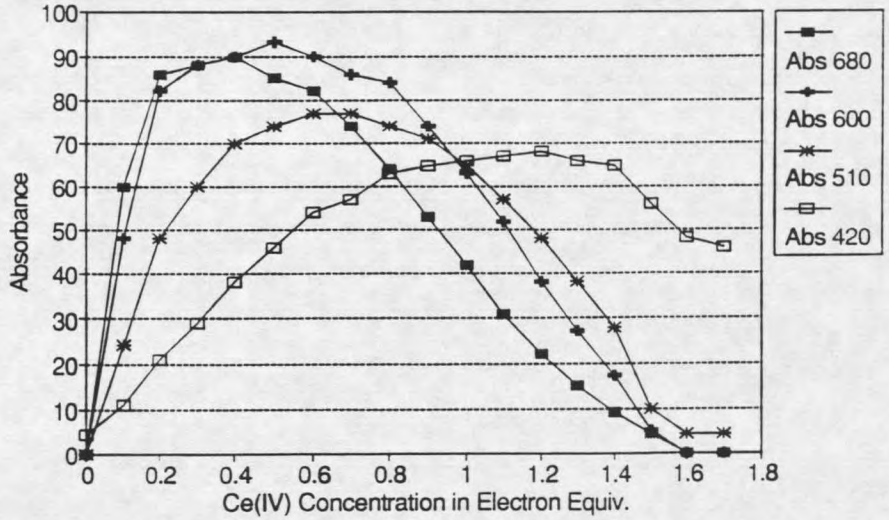

Figure 59 UV-vis data for the oxidation of $[Pt(Ox)_2]^{2-}$ by Ce(IV) in 1N H_2SO_4.

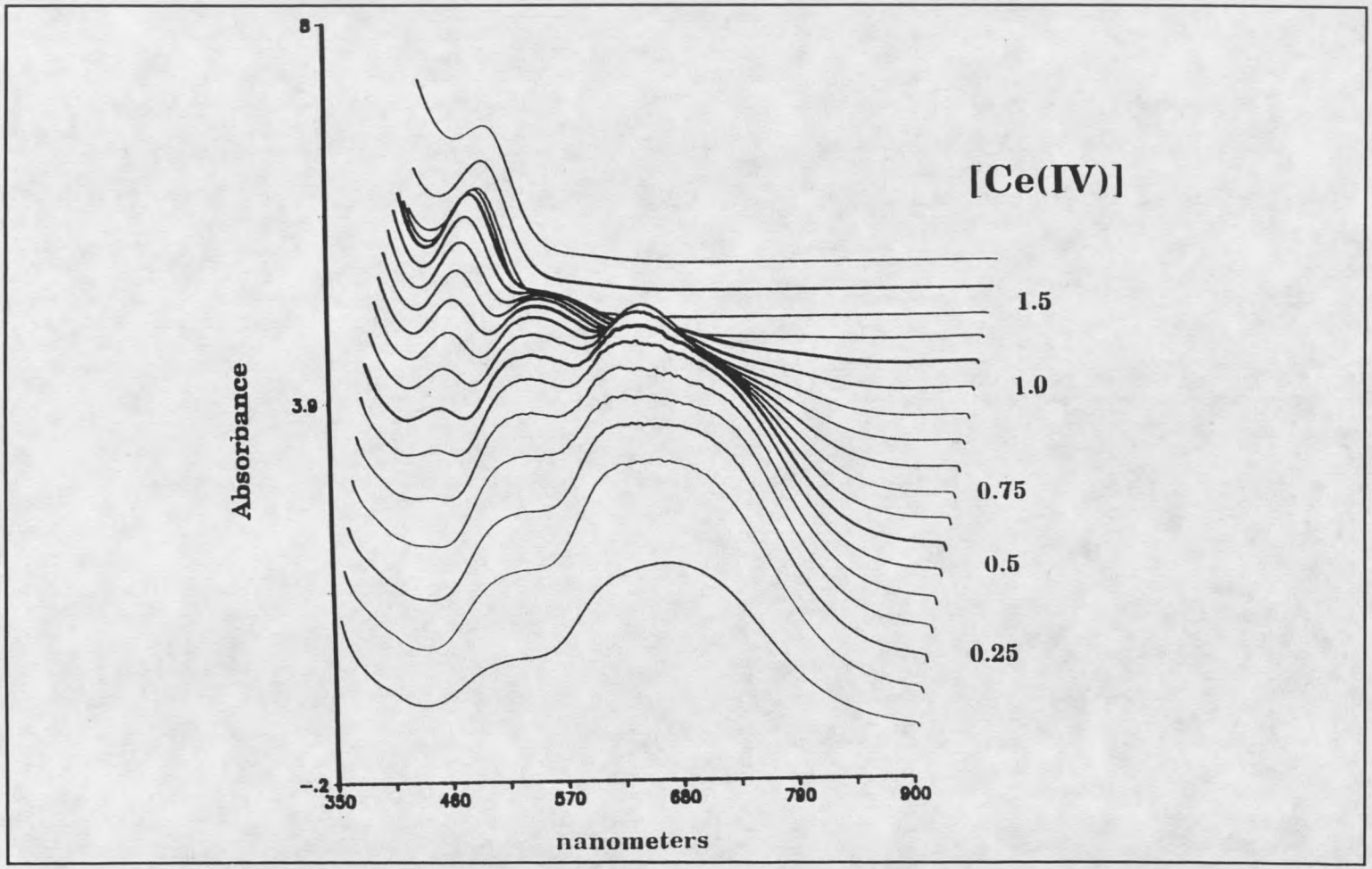

Figure 60 UV-vis Spectra for the oxidation of $[Pt(Ox)_2]^{2-}$ by Ce(IV) in 1N H_2SO_4.

with the molecular formula $[Pt(Ox)_2]_n^-$ (**48**) where n 1. The new Pt(III) species agrees with the absorption spectra of dinuclear sulfato and phosphato Pt(III) complexes (18). The absorbance spectra show that **45**, **46**, **47**, and **48** are all present throughout the early part of the Ce(IV) titration, and only the relative concentrations of each complex are effected by the amount of oxidant that has been added. An endpoint in the potentiometric titration can only be observed if the complex formed is stable to the further addition of Ce(IV). The equilibrium of species was not observed in the potentiometric titration, because of the instability of **45**, **46**, and **47** to be further oxidized to **48**.

The Pt complexes **45-48** are also observed when the polymeric complex $K_{1.66}[Pt(C_2O_4)_2]_n \cdot H_2O$ is dissolved in acidic solutions (11,36) It would appear that the bis(oxalato)platinate polymer is composed of these Pt complexes, and/or the Pt complexes are stable products from disproportionation of the polymeric Pt chain. The UV-vis data for these complexes is listed in Table 38.

TABLE 39. UV-vis Data for bis(oxalato)platinate polymers

COMPLEX	λ_{max} (nm)
$[Pt(Ox)_2]_n^{1.75-}$ (**45**)	680
$[Pt(Ox)_2]_n^{1.5-}$ (**46**)	600
$[Pt(Ox)_2]_n^{1.25-}$ (**47**)	510
$[Pt(Ox)_2]_n^-$ (**48**)	420

Oxidation by Diaquobis(oxalato)platinum(IV)

Ultraviolet and Visible Studies The oxidation of a 1 x 10^{-3}M solution of **5** in 1N H_2SO_4 by *trans*-$[Pt(H_2O)_2(Ox)_2]$ (**28**) was followed by UV-vis spectroscopy. Figure 62 shows the changes in the UV-vis spectra from 350-900 nm during the oxidative titration of **5** by **28**. Both **5** and **28** do not have absorption bands in the 350-900 nm region. Upon addition of **28** to the yellow solution of **5**, the solution takes on a deep blue color. The UV-vis spectra of these blue solutions shows the presence of four distinct absorbance maxima. These absorptions correspond to **45**, **46**, **47**, and **48** as previously characterized for the Ce(IV) oxidations.

Temperature effects on the new complexes **45-48** were assessed by using variable temperature UV-vis spectra (Figure 62). A solution of 1x10^{-3} M **5** in 1N H_2SO_4 was partially oxidized with 0.75 equivalents of **28**. Lowering the temperature from 23 C° to 0 C° shifts the equilibrium of the four Pt complexes to favor the formation of **45** with a lower average oxidation state.

Nuclear Magnetic Resonance When small amounts of **28** are added to a 0.1-0.01 M solution of **5** in 1N H_2SO_4, the yellow solution turns deep blue in color. Within several minutes, the solution precipitates the slightly soluble one-dimensional polymer $K_{1.66}[Pt(C_2O_4)_2]_n \cdot H_2O$. ^{195}Pt NMR of these solutions does not show any resonances for **5** or **28**. After 24-48 hours, the only resonance that is observed is at -353 ppm in the ^{195}Pt NMR spectrum. The resonance at -353 ppm corresponds to the Pt(II) complex *cis*-

$[Pt(H_2O)_2(Ox)]$(**8**). To prevent the rapid precipitation, the reaction of **28** and **5** was diluted to 0.001 M. After addition of **28**, the solution was concentrated for NMR data collection. The solutions deposited brown or copper colored solids for all oxidations where less than one electron equivalent of **28** was added. These solids were assumed to be $K_{1.66}[Pt(C_2O_4)_2]_n \cdot H_2O$ polymer. When a slight excess of **28** was added to a solution of **5**, the solution changes from blue to yellow/orange. The UV-vis of this reaction shows only an absorbance for the Pt(III) complex **48** at 420 nm. ^{195}Pt NMR spectra for this reaction show the appearance of three predominant resonances at 2840, 1150, and -353 ppm (Figure 63). The resonance at 2840 ppm corresponds to the Pt(IV) complex **28**, and the resonance at -353 ppm corresponds to the Pt(II) complex **8**. The chemical shift of 1150 ppm resonance is consistent with two types of complexes. The first is a Pt(IV) complex with two halide donor atoms and four oxygen donor atoms (6). The only halide ligands available in solution would have to arise from the unlikely reduction of $HClO_4$. High resolution spectra of the resonance at 1150 ppm does not show any isotopomeric resonances from ^{35}Cl and ^{37}Cl (6,67). This would indicate that the complex at 1150 ppm must have only oxygen donors as ligands. The second type of complex that is consistent with the 1150 ppm resonance is a binuclear Pt(III) species. The resonance at 1150 ppm is approximately half way between the resonances for Pt(IV) and the Pt(II) complexes with oxygen donors as ligands which is consistent with a Pt(III) oxidation state. The chemical shift is ca 600 ppm upfield from known binuclear Pt(III) complexes with oxygen donating sulphato (1756 ppm) and phosphato (1796 ppm) ligands (21). This difference in chemical shift could result from the ability of oxalato to bridge the two

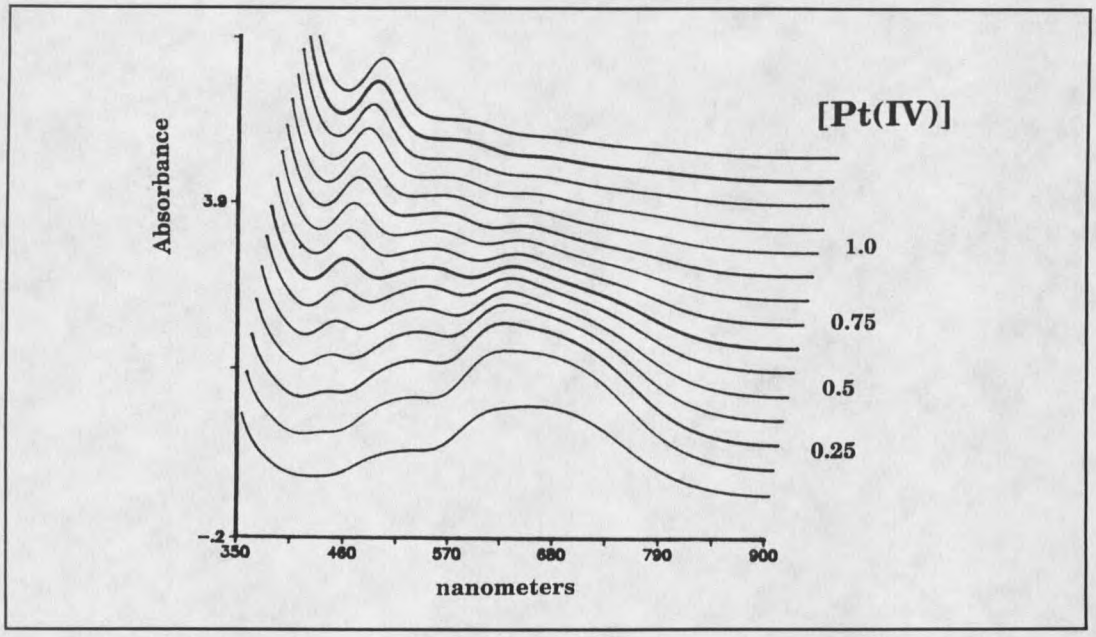

Figure 61 UV-vis spectra of the oxidative titration of $[Pt(Ox)_2]^{2-}$ by *trans*-$[Pt(H_2O)_2(Ox)_2]$ in 1 N H_2SO_4.

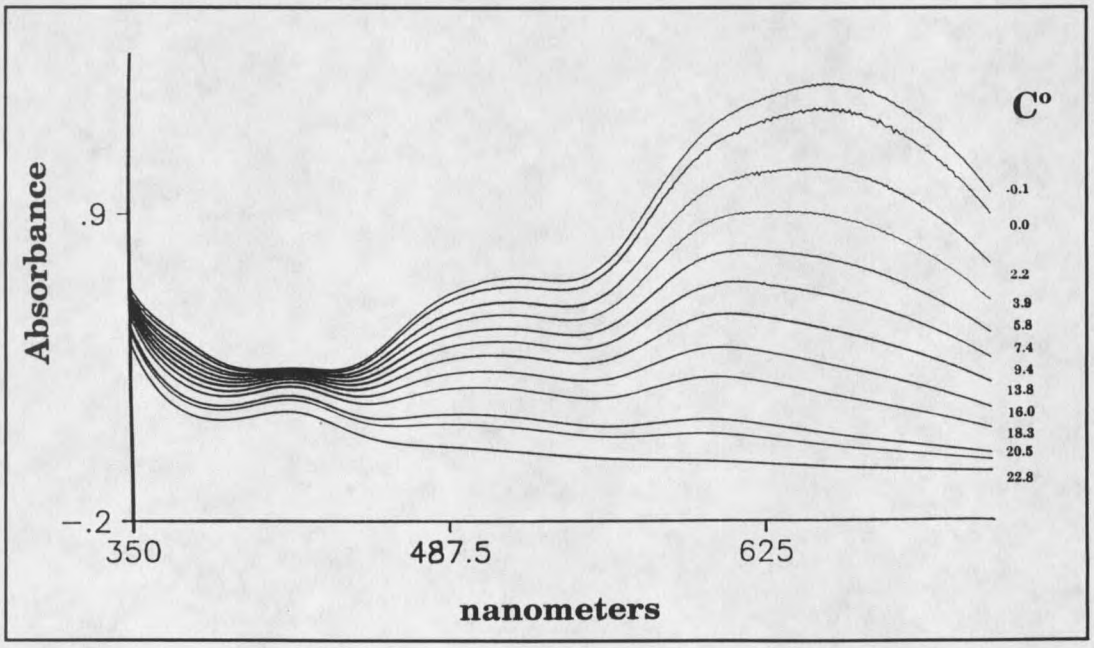

Figure 62 UV-vis spectra of the temperature dependence of bis(oxalato)platinate polymers in 1 N H_2SO_4.

metal centers. We have observed ca 200 ppm upfield shift for the chelation of oxalato ligands to Pt(II) and Pt(IV) complexes. The complex which gives the resonance at 1150 ppm appears to be dinuclear because of the lack of Pt-Pt coupling constants and further resonances for higher nuclearity complexes. A mononuclear Pt(III) would be paramagnetic, and this would not be observed in the ^{195}Pt NMR spectrum. Oxidation of **5** in 1M H_2SO_4 or HNO_3 results in the same new resonance at 1150 ppm.

The oxalato ligands could have two binding modes (Figure 64). The first would be the formation of a bridge between the two metal centers. This would be consistent with the lantern structures for other known Pt(III) sulphato and phosphato dimers. The oxalato ligand should be able to bridge the two metal centers much like the squarato ligands for the binuclear Pt(II) complex (47). The second binding mode for the oxalato ligands would be bidentate and not bridging. If the oxalato ligand is not bridging, this would be the first example of a non bridged binuclear Pt(III) complex. Another possible structure would be a hydroxo or oxo bridged binuclear Pt(III) complex. This structure could give rise to the resonance at 1150 ppm, but there is no precedence for this type of a oxygen bridged complex in Pt chemistry.

The axial positions of a dimeric Pt(III) complex should be made labile by the large trans influence of the Pt-Pt bond (21). These axial positions would be expected to be substituted with H_2O in these acidic solutions. When the solution of **48** is dissolved in 60 % $H_2{}^{16}O$ / 40 % $H_2{}^{18}O$, the ^{195}Pt NMR spectra do not show incorporation of $H_2{}^{18}O$ over several hours. After 12-24 hours, the ^{195}Pt NMR spectra show the incorporation of ^{18}O into **48**. This incorporation rate is similar to the incorporation rate for ^{18}O into

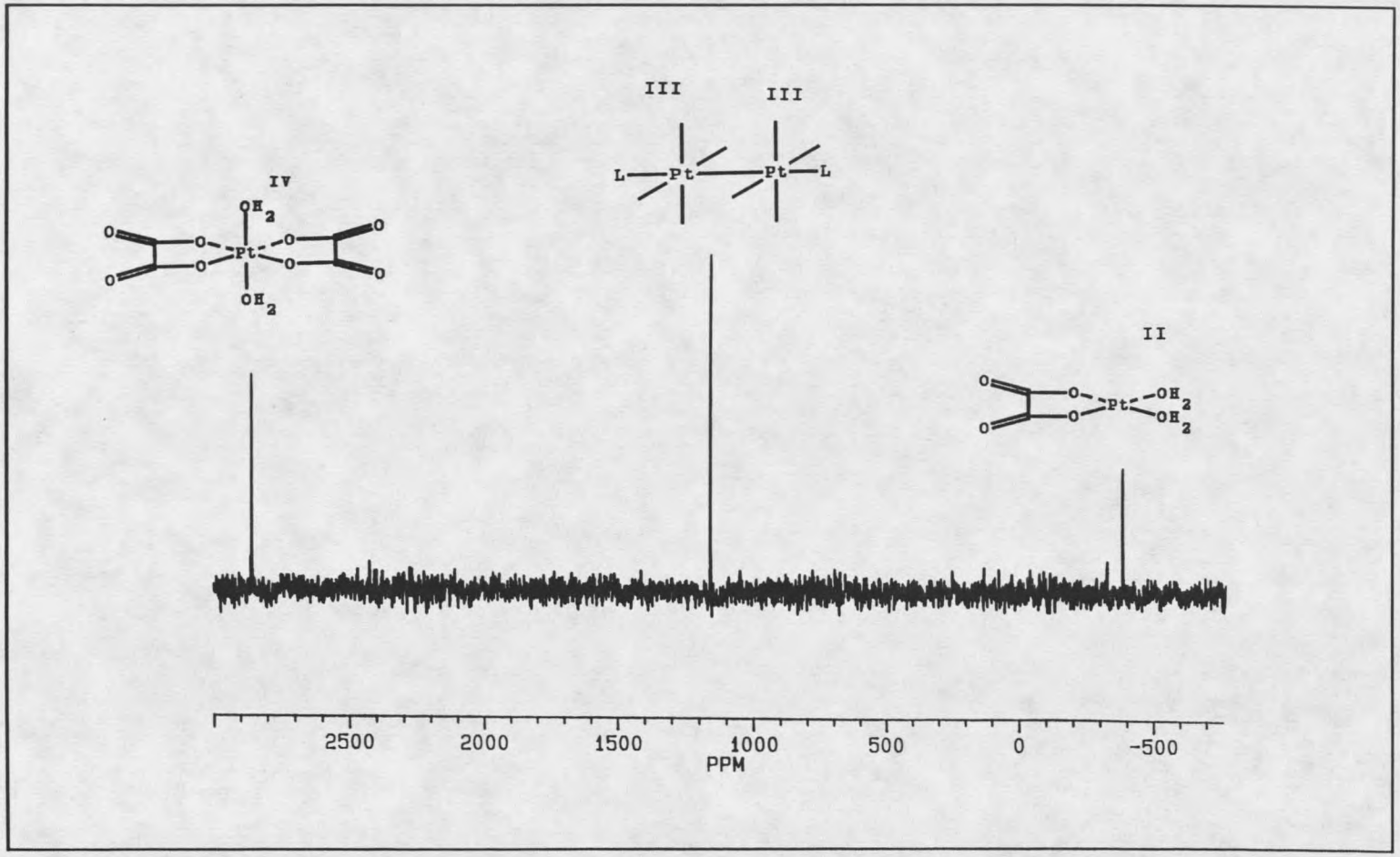

Figure 63 ^{195}Pt NMR spectra for the oxidation of $[Pt(Ox)_2]^{2-}$ by *trans*-$[Pt(H_2O)_2(Ox)_2$ in 1M $HClO_4$.

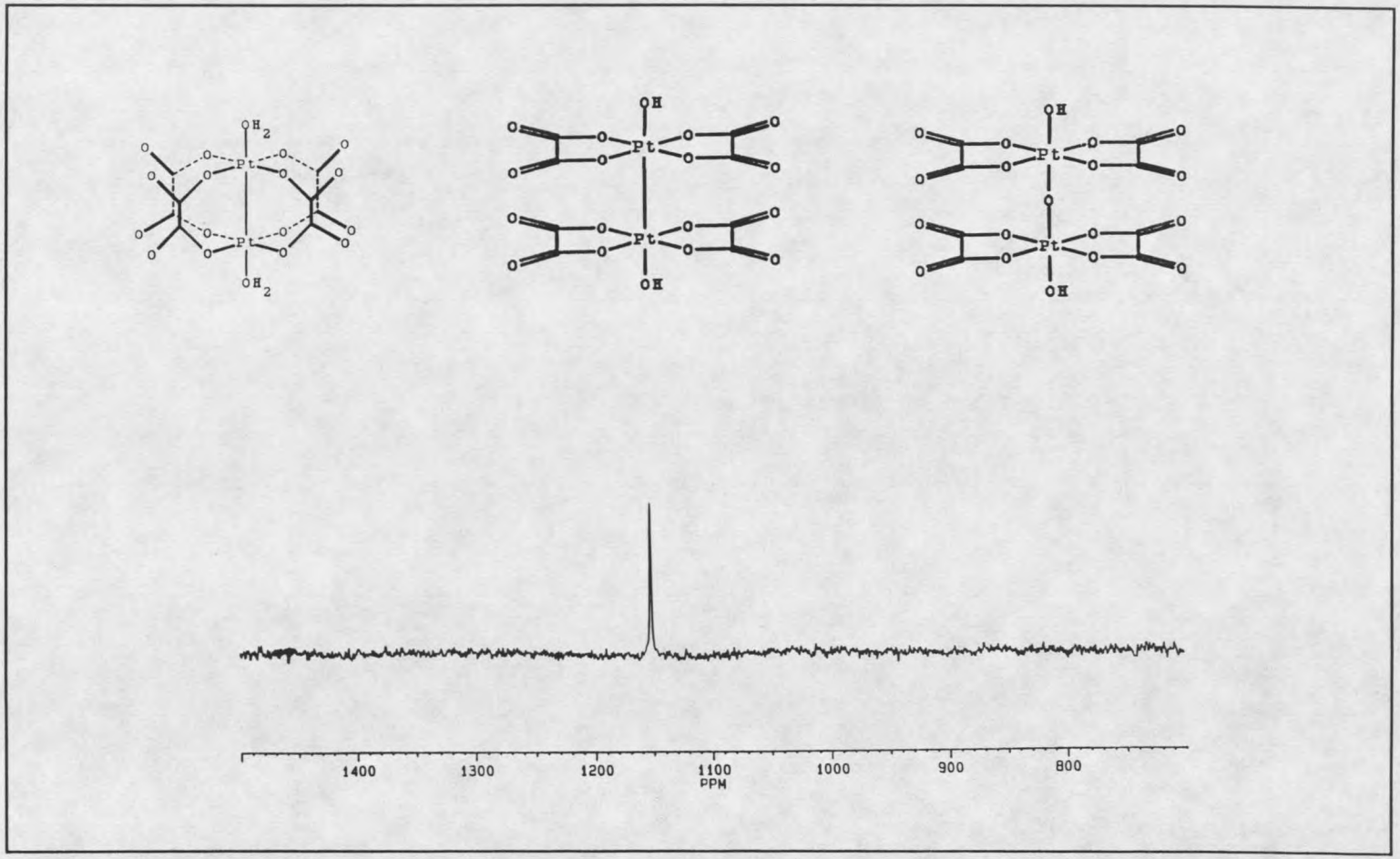

Figure 64 ^{195}Pt NMR spectrum of $[Pt_2(Ox)_2(H_2O)_2]^{2-}$ showing the possible structures for the Pt(III) complex.

the H_2O and oxalato oxygens for **28**. After several weeks, the solutions reach equilibrium, and the ^{195}Pt NMR spectrum shows the presence of only four isotopically shifted resonances for **48** (Figure 65). This is consistent with the presence of only four oxygen atoms bound to the Pt. A fifth isotopically shifted resonance would not be easily observed with the 60% $H_2{}^{16}O$ / 40% $H_2{}^{18}O$. The absence of isotopomers for the axial oxygen atoms of H_2O (seven resonances) can be explained by the rapid exchange of H_2O. Under conditions of rapid exchange, the ^{195}Pt NMR spectrum will not show separate resonances for the $H_2{}^{18}O$ incorporation. Rather, the ^{195}Pt resonance will only be shifted slightly as the average chemical shift for the Pt changes with the amount of $H_2{}^{18}O$ in

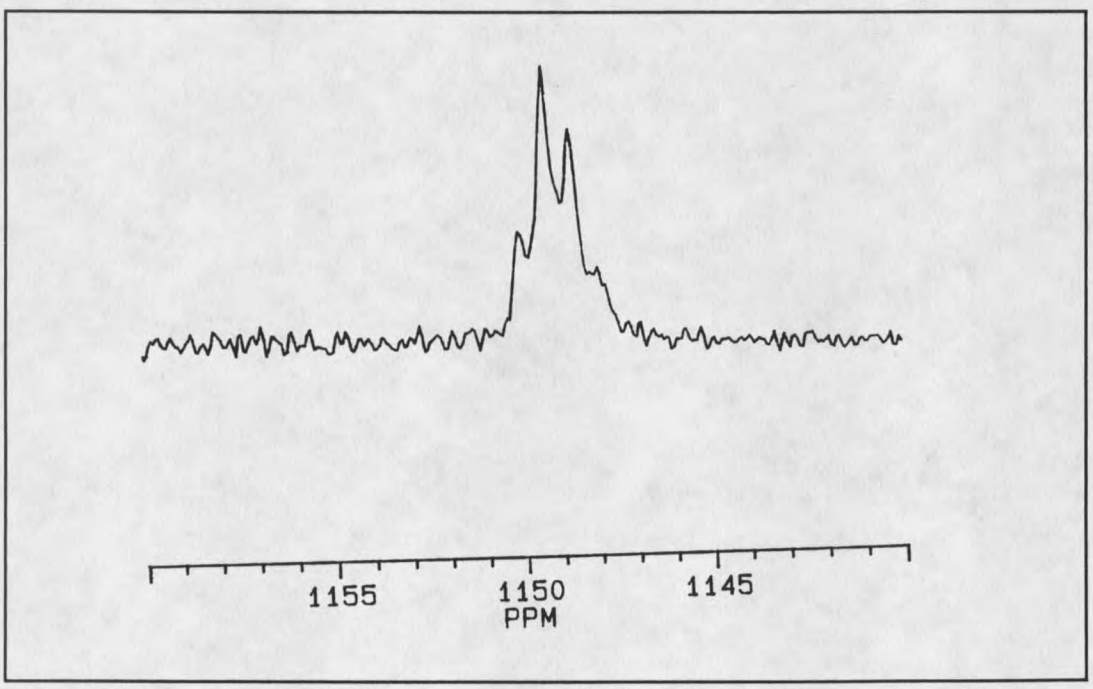

Figure 65 ^{195}Pt NMR spectra for the H_2O exchange reaction for $[Pt_2(Ox)_4(H_2O)_2]^{2-}$ in 60% $H_2{}^{16}O$ / 40% $H_2{}^{18}O$ in 1 M $HClO_4$.

solution. If the kinetics for H_2O exchange on **48** are consistent with this interpretation of the ^{18}O isotopic labeling study, the H_2O exchange rate for **48** $k_{ex} \sim 10^4 sec^{-1}$. The H_2O exchange rate for **48** is ~ rate of polymerization for the one dimensional bis(oxalato)platinates complexes.

When a saturated solution of $NaClO_4$ is added to solutions of **48** a purple/brown solid is precipitated. Dissolution of this solid gives ^{195}Pt NMR resonances for **48** at 1150 and for **5** at -520 ppm in a ratio of 1:4. This ratio would predict the solid to be composed of four moles of Pt(II) and one mole of Pt(III). The solid would correspond to the polymer with the formula $[Pt(Ox)_2]^{-1.88}$ with the average oxidation state of 2.22.

When solutions of **48** are left at room temperature for several weeks, new resonances appear in the ^{195}Pt NMR spectra at 1267 (**49**), 1292 (**50**), and 1358 (**51**) ppm (figure 66). The new resonances are shifted 100-200 ppm down field from **48**. This downfield shift is consistent with the substitution of an oxalato chelate with H_2O. The new resonances show 70-90 Hz coupling to ^1H which is consistent with the ^2J ^{195}Pt-^1H coupling constant for H_2O on the sulphato dimer $[Pt_2(SO_4)_4]^{2-}$. The NMR data for these complexes is listed in Table 39.

Effect of pH on Oxidation When a solution of **5** is added to a solution of both *trans*-$[Pt(OH)_2(Ox)_2$ (**28**) and *cis*-$[Pt(OH)_2(Ox)_2]^{2-}$ (**40**) at pH≥4.0 there is no change in the ^{195}Pt NMR spectra for **5**, **28**, and **40**. When the solution is made acidic (pH=1.0) with 1 M $HClO_4$, a dark blue color rapidly appears, and the polymeric solid $K_{1.66}[Pt(C_2O_4)_2]_n \cdot H_2O$ precipitates. ^{195}Pt NMR of the supernate for this reaction shows no resonance for **5**, and an equal decrease in the resonances for **28** and **40**.

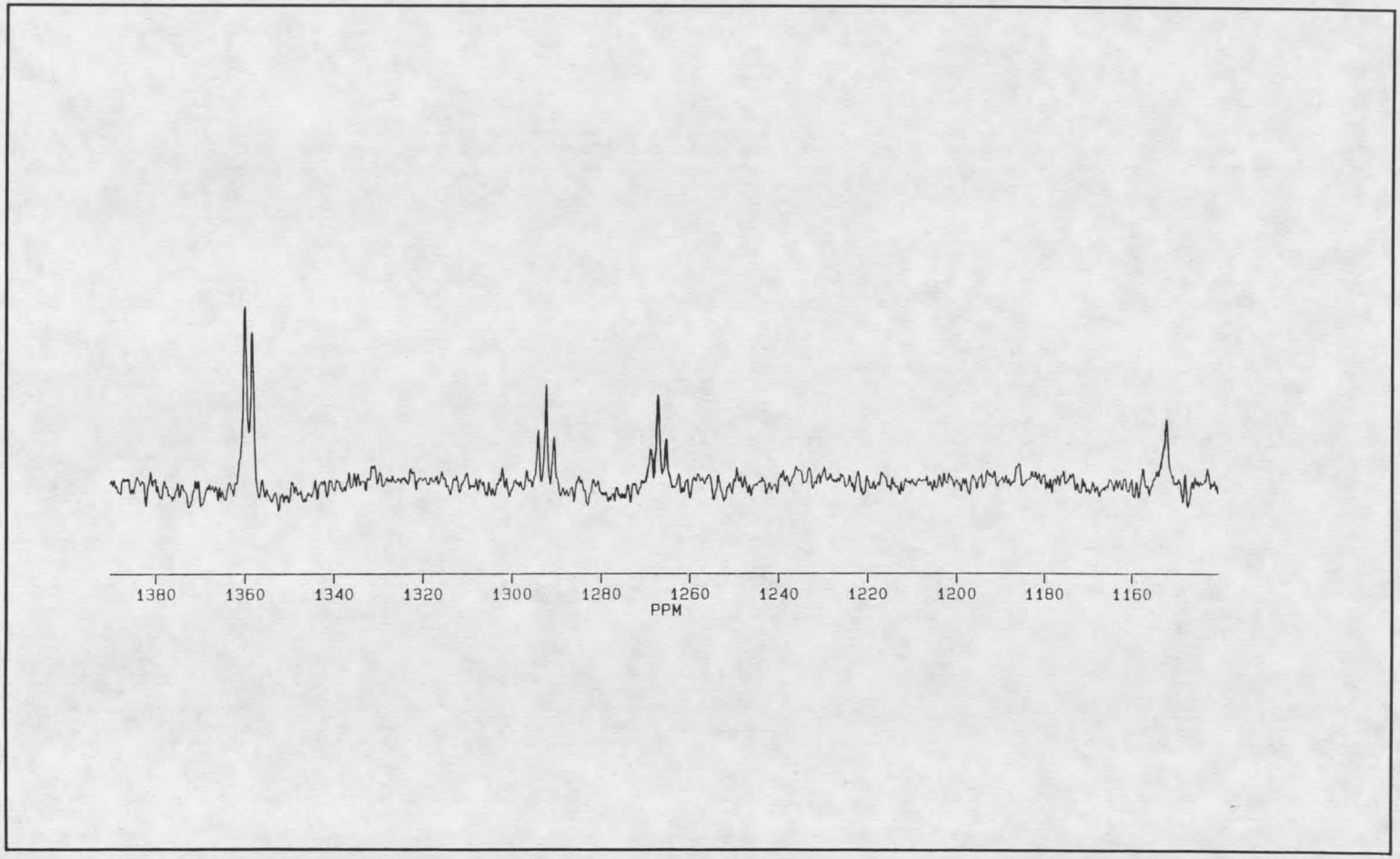

Figure 66 ^{195}Pt NMR of the reaction of *trans*-$[Pt(H_2O)_2(Ox)_2]$ with $[Pt(Ox)_2]^{2-}$ in 1M $HClO_4$.

TABLE 40. ^{195}Pt NMR Data

COMPLEX	δ Pt (ppm)	$J^{195}Pt$-^{1}H	Isotope Shift
$[Pt_2(Ox)_4(H_2O)_2]^{2-}$ **(48)**	1150	[a]	0.72[b] 0.67[b] 0.70[b]
$[Pt_2(Ox)_x(H_2O)_x]^y$ **(49)**	1267	93	
$[Pt_2(Ox)_x(H_2O)_x]^y$ **(49)**	1292	94	
$[Pt_2(Ox)_x(H_2O)_x]^y$ **(49)**	1358	86	
$[Pt_2(Ox/Mal)_x(H_2O)_x]^y$ **(52)**	1428	120	

[a] = coupling constant not observed, [b] $^{16}O/^{18}O$ isotope shift, x,y = unknown number.

This data strongly suggests that there is no preference between **28** and **40** in forming the polymer $K_{1.66}[Pt(C_2O_4)_2]_n \cdot H_2O$ in acidic solutions. This would be consistent with a pH dependent oxidation reaction between the Pt(IV) complexes and the Pt(II) complex to form the one-dimensional chain bis(oxalato)platinate polymers.

Oxidation Reactions with *trans*-diaquobis(malonato)platinate(IV)

Nuclear Magnetic Resonance When an acidic solution of **5** was oxidized with one electron equivalent of *trans*-$[Pt(H_2O)_2(Mal)_2]$ (**31**) the solution turned a dark red/orange color. ^{195}Pt NMR of these solutions show new resonances at 1430 (**51**) and 1290 (**49**) ppm in the Pt(III) region. There are no observed resonances in the Pt(IV) region, and

resonances in the Pt(II) region correspond to $[Pt(Mal)(MalH\text{-}O)(H_2O)]^-$ (**17**) at -331 ppm, $[Pt(Ox)(OxH\text{-}O)(H_2O)]^-$ (**9**) at -345 ppm, $[Pt(Mal)(H_2O)_2]$ (**16**) at -314 ppm, and $[Pt(Ox)(H_2O)_2]$ (**8**) at -338 ppm. The presence of **49** in this reaction and in the oxidation with **28** would suggest that **49** does not have a malonato ligand. This supports the assignment of the complex to a hydrolysis of one or more ligands on the Pt(III) dimer. NMR data for these complexes is listed in Table 39.

Oxidation Reactions with Hexachloroplatinate(IV).

Ultraviolet and Visible Studies The oxidation of a 1 x 10^{-3}M solution of **5** in 1N H_2SO_4 with $[PtCl_6]^{2-}$ was followed by UV-vis spectroscopy. Figure 67 shows the changes in the UV-vis spectra from 350-900 nm during the oxidative titration of **5**. Both **5** and $[PtCl_6]^{2-}$ do not have absorption bands in the 350-900 nm region. Upon addition of $[PtCl_6]^{2-}$ to the yellow solution of **5**, the solution takes on a deep blue color. The UV-vis spectra of these blue solutions show the presence of four distinct absorbance maxima. These absorptions correspond to **45**, **46**, **47**, and **48** as previously characterized for the Ce(IV) oxidations.

Nuclear Magnetic Resonance When $[PtCl_6]^{2-}$ is added to a 0.1-0.01 M solution of **5** in 1N H_2SO_4, the yellow solution turns deep blue in color. Within several minutes, the solution precipitates the slightly soluble $K_{1.66}[Pt(C_2O_4)_2]_n \cdot H_2O$. ^{195}Pt NMR of these solutions do not show any resonances for **5** or $[PtCl_6]^{2-}$. The only resonances that are

observed are for $[PtCl_4]^{2-}$ (**1**) at -1624 ppm and its hydrolysis product $[Pt(H_2O)Cl_3]^-$ at -1185 ppm. After 24-48 hours, the only new resonance that is observed is at -353 ppm in the ^{195}Pt NMR spectrum. The resonance at -353 ppm corresponds to the Pt(II) complex *cis*-$[Pt(H_2O)_2(Ox)]$(**8**). To prevent rapid precipitation, the reaction of $[PtCl_6]^{2-}$ and **5** was diluted to 0.001 M. After addition of $[PtCl_6]^{2-}$, the solution was concentrated for NMR data collection. When a slight excess of $[PtCl_6]^{2-}$ is added to a solution of **5**, the solution changes from blue to yellow/orange. ^{195}Pt NMR of these solutions show resonances at -1185 for $[Pt(H_2O)Cl_3]^-$, and -1624 for **1**. No resonance for **48** was observed. When an excess of $[PtCl_6]^{2-}$ (2 electron equivalents) was added to a solution of **5**, the solution changes from blue to yellow. ^{195}Pt NMR of these solutions show resonances at 1865 for *trans*-$[PtCl_2(Ox)_2]^{2-}$, -1185 for $[Pt(H_2O)Cl_3]^-$, and -1624 for **1**.

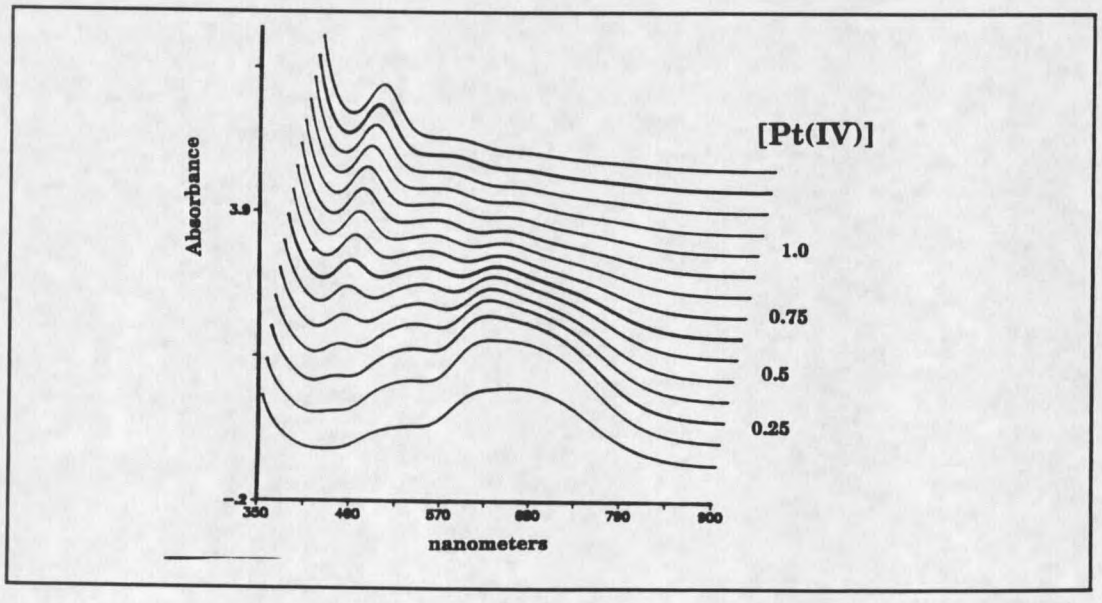

Figure 67 UV-vis spectra of the oxidative titration of $[Pt(Ox)_2]^{2-}$ with $[PtCl_6]^{2-}$ in 1 N H_2SO_4.

Tetra(cyanato)platinate(II).

Oxidation by *trans*-dibromotetra(cyanato)platinate(IV).

Nuclear Magnetic Resonance Figure 68 shows the ^{13}C NMR spectrum of the addition of ^{13}C labeled $[Pt(^{13}CN)_4]^{2-}$ to a solution of non labeled *trans*-$[PtBr_2(CN)_4]^{2-}$ and *trans*-$[Pt(H_2O)Br(CN)_4]^-$. Within the mixing time of the experiment, the Pt(II) and Pt(IV) complexes have come to equilibrium for the distribution of ^{13}C labeled cyanato ligand. This exchange is much too fast to be the result of substituting free $^{13}CN^-$ between the three complexes. The reverse experiment of the addition of ^{13}C labeled *trans*-$[PtBr_2(^{13}CN)_4]^{2-}$ and *trans*-$[Pt(H_2O)Br(^{13}CN)_4]^-$ to non labeled $[Pt(CN)_4]^{2-}$ gives the same rapid exchange reaction of the $^{13}CN^-$ (Figure 68). These NMR data suggest that the exchange of ^{13}C label between the Pt(II) and Pt(IV) is the result of a rapid redox exchange reaction.

When a solution of *trans*-$[PtBr_2(CN)_4]^{2-}$ and $[Pt(CN)_4]^{2-}$ was concentrated, the one dimensional chain complex $[Pt(CN)_4]_n^{2-}$ precipitated. When the polymer was dissolved, the ^{195}Pt NMR spectra showed only resonances for *trans*-$[PtBr(H_2O)(CN)_4]^-$ at -2600 ppm and $[Pt(CN)_4]^{2-}$ at -4746 ppm (Figure 69). The ratio for the Pt(II) and Pt(IV) complexes is not 1:5 in the solutions of the dissolved polymer. This would suggest that oligomeric Pt complexes are not observed in the solutions for the polymer either because of their size or possible paramagnetic properties.

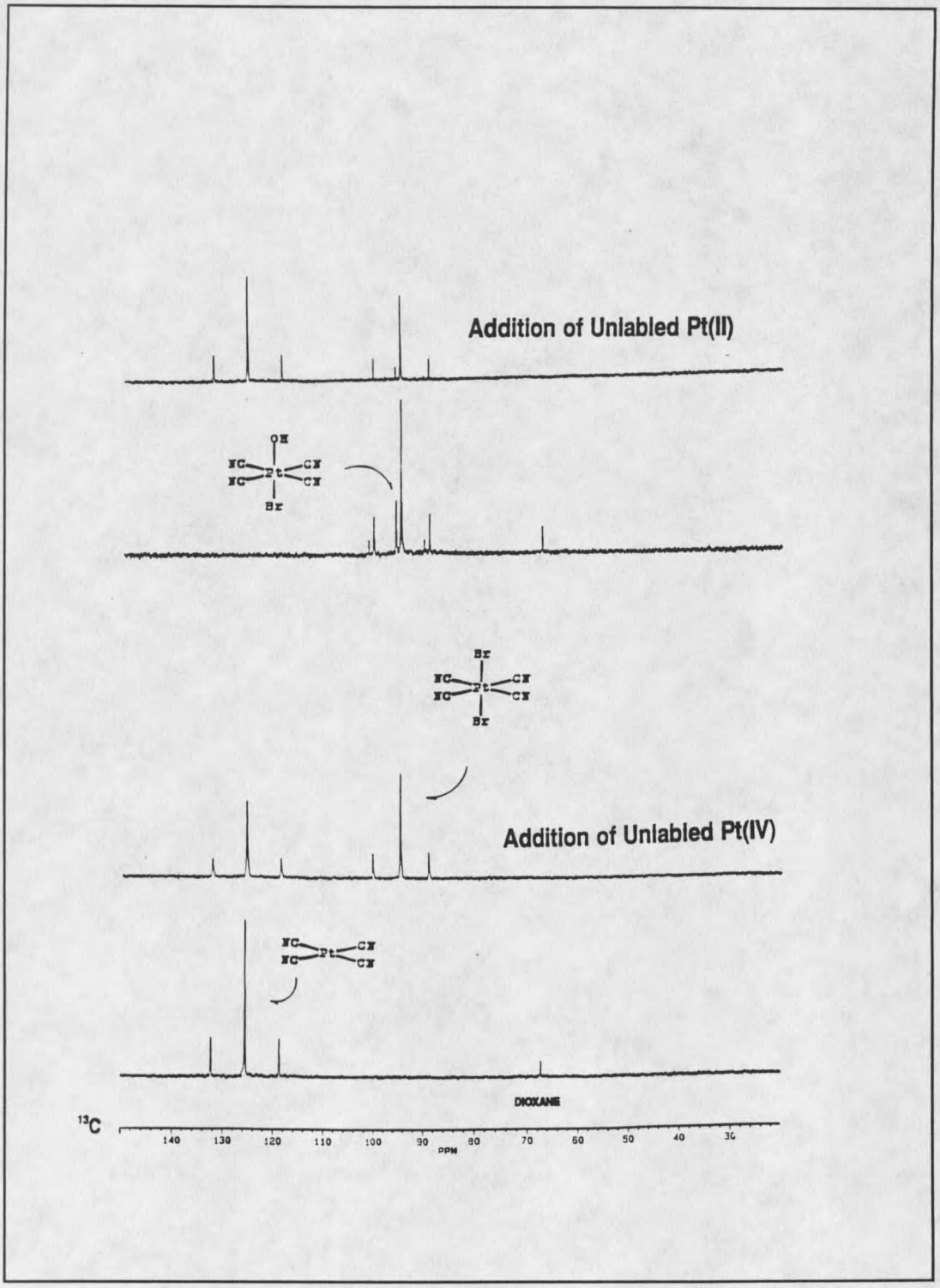

Figure 68 ^{13}C NMR spectra of the redox reactions of ^{13}C labeled $[Pt(CN)_4]^{2-}$ and *trans*-$[PtBr_2(CN)_4]^{2-}$.

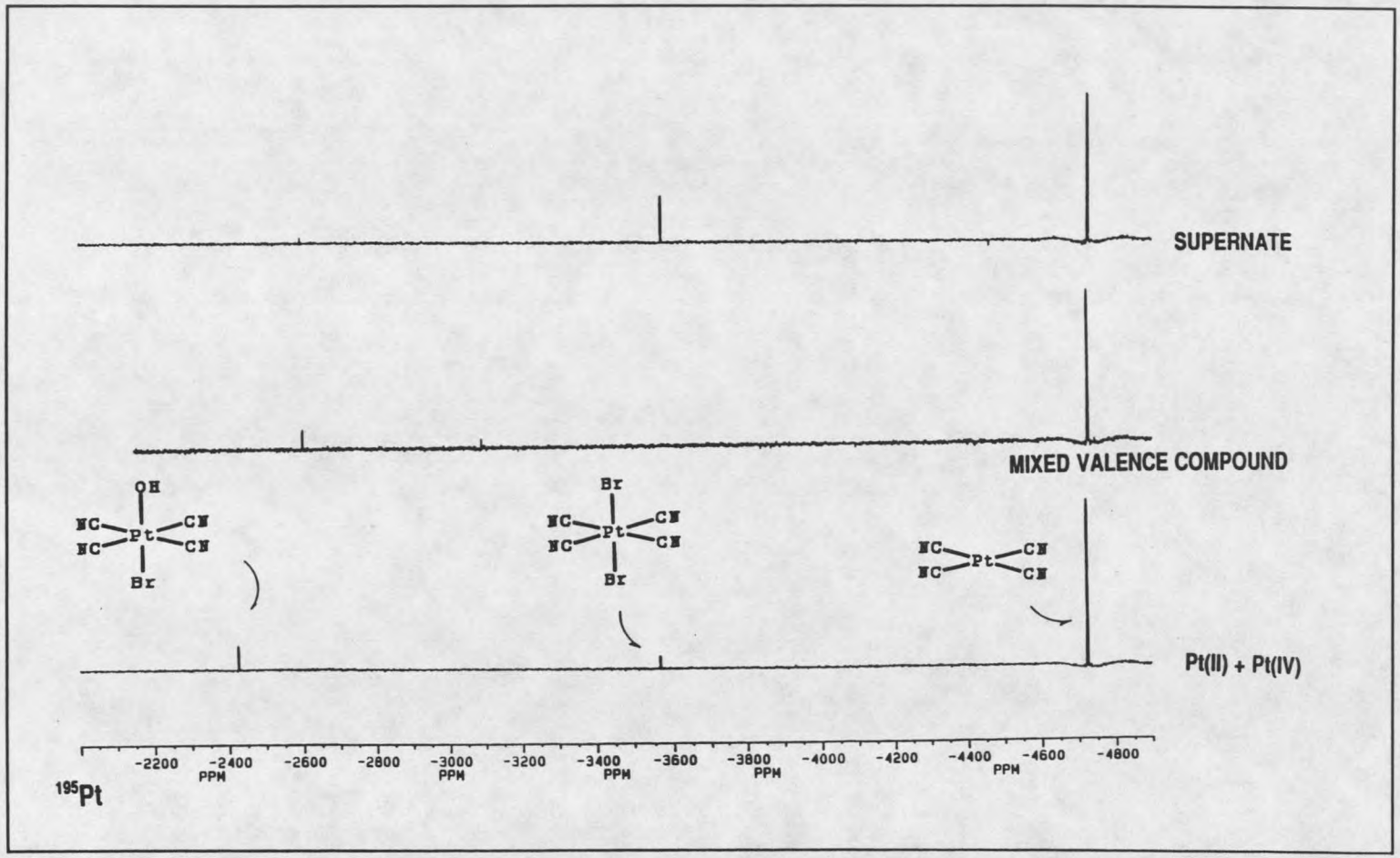

Figure 69 ^{195}Pt NMR spectra for the formation of one-dimensional tetra(cyanato)platinate polymers.

Diphosphitoplatinate (II)

Oxidation by Hexachloroplatinate(IV)

Nuclear Magnetic Resonance Studies Figure 70 shows the ^{31}P NMR spectra for the reaction of $[PtCl_6]^{2-}$ with binuclear phosphitobridged Pt(II) complex $[Pt_2(H_2P_2O_5)_4]^{4-}$ (67 ppm). The ^{31}P NMR spectrum shows the quantitative two electron oxidation of $[Pt_2(H_2P_2O_5)_4]^{4-}$ to the binuclear Pt(III) complex $[Pt_2(H_2P_2O_5)_4Cl_2]^{4-}$ (28 ppm). ^{31}P resonances of intermediate complexes were not observed for these reactions. ^{195}Pt NMR spectra showed the two electron reduction of $[PtCl_6]^{2-}$ to $[PtCl_4]^{2-}$ (**1**).

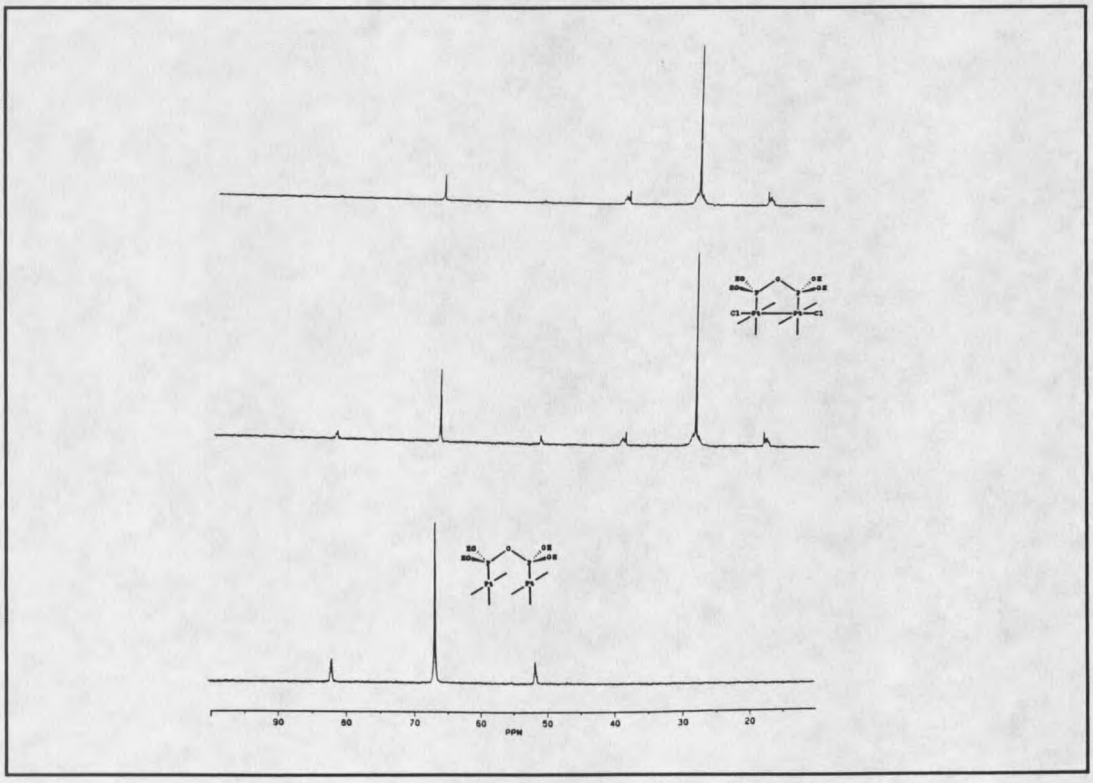

Figure 70 ^{31}P NMR spectra for the reaction of $[Pt_2(H_2P_2O_5)_4]^{4-}$ with $[PtCl_6]^{2-}$.

SUMMARY

The characterization of the solution chemistry for Pt(II) and Pt(IV) complexes used in the synthesis of one-dimensional platinum complexes has been determined by multinuclear ^{195}Pt, ^{13}C and ^{31}P NMR, and x-ray crystallography. Kinetic intermediates in the formation of bis(oxalato) and bis(malonato) Pt(II) complexes include monodentate complexes. The reactions of Pt(II) are dependent upon pH and the ligand, X ($X=Cl^-$, H_2O). NMR spectra provide direct evidence for monodentate complexes in high concentrations during formation reactions, and in low concentrations at equilibrium. New Pt(II) complexes have been characterized by x-ray diffraction, and intermediate species have been identified by their solution NMR spectra. The monodentate complexes are not incorporated into the one-dimensional polymerization reactions. The monodenate complexes are in equilibrium with the polymers, and they are products in the disruption of one-dimensional chain complexes in solution.

Isotopic labeling studies with $H_2{}^{18}O$ have shown that the hydrogen peroxide oxidation mechanism for Pt(II) complexes is a rapid two electron transfer which forms only trans Pt(IV) complexes. For the *trans*-dihydroxoplatinate(IV) complex, one hydroxo ligand originates from hydrogen peroxide, and the trans hydroxo ligand originates from solvent. ^{18}O labeling studies have shown that the *trans*-dihydroxo Pt(IV) complexes isomerize to *cis*-dihydroxo Pt(IV) by an intramolecular twist consistent with a Bailar or Ray-Dutt mechanism. X-ray crystallography has confirmed the structures of the *cis*- and *trans*-dihydroxobis(oxalato)platinate(IV) complexes.

H_2O exchange rates have been measured for trans-diaquobis(oxalato)platinum(IV) by isotopic dilution with $H_2{}^{18}O$. $K_{ex}{}^{298} = 4.4 \times 10^{-6}$ sec^{-1}. This exchange rate is much slower than the polymerization rate for bis(oxalato)platinate one-dimensional complexes. The activation enthalpy for the H_2O exchange process is 94.1 kJ $mole^{-1}$, and the activation entropy is -28.6 J $mole^{-1}K^{-1}$. The Pt(IV) complex is not initiating polymerization by H_2O exchange for a Pt(II) complex as has been proposed by Krogmann and others. The polymerization of bis(oxalato)platinates is consistent with a pH dependent redox process.

Oxidative titration of bis(oxalato)platinate(II) reveals four stable polynuclear complexes in acidic solution. The complexes have the average oxidation states of +2.25, +2.5, +2.75, and +3.0. The +3.0 species has been identified as a binuclear Pt(III) complex from multinuclear NMR. H_2O exchange rates for the Pt(III) complex are $> 1 \times 10^4$ sec^{-1}. The exchange rate is consistent with the rates for polymerization of one-dimensional bis(oxalto)platinate complexes. A facile electron transfer reaction between Pt(II) and Pt(IV) could form the Pt(III) complex. The Pt(III) complex could be the key step in initiation of polymerization for one-dimensional Pt oxalato complexes (Figure 71).

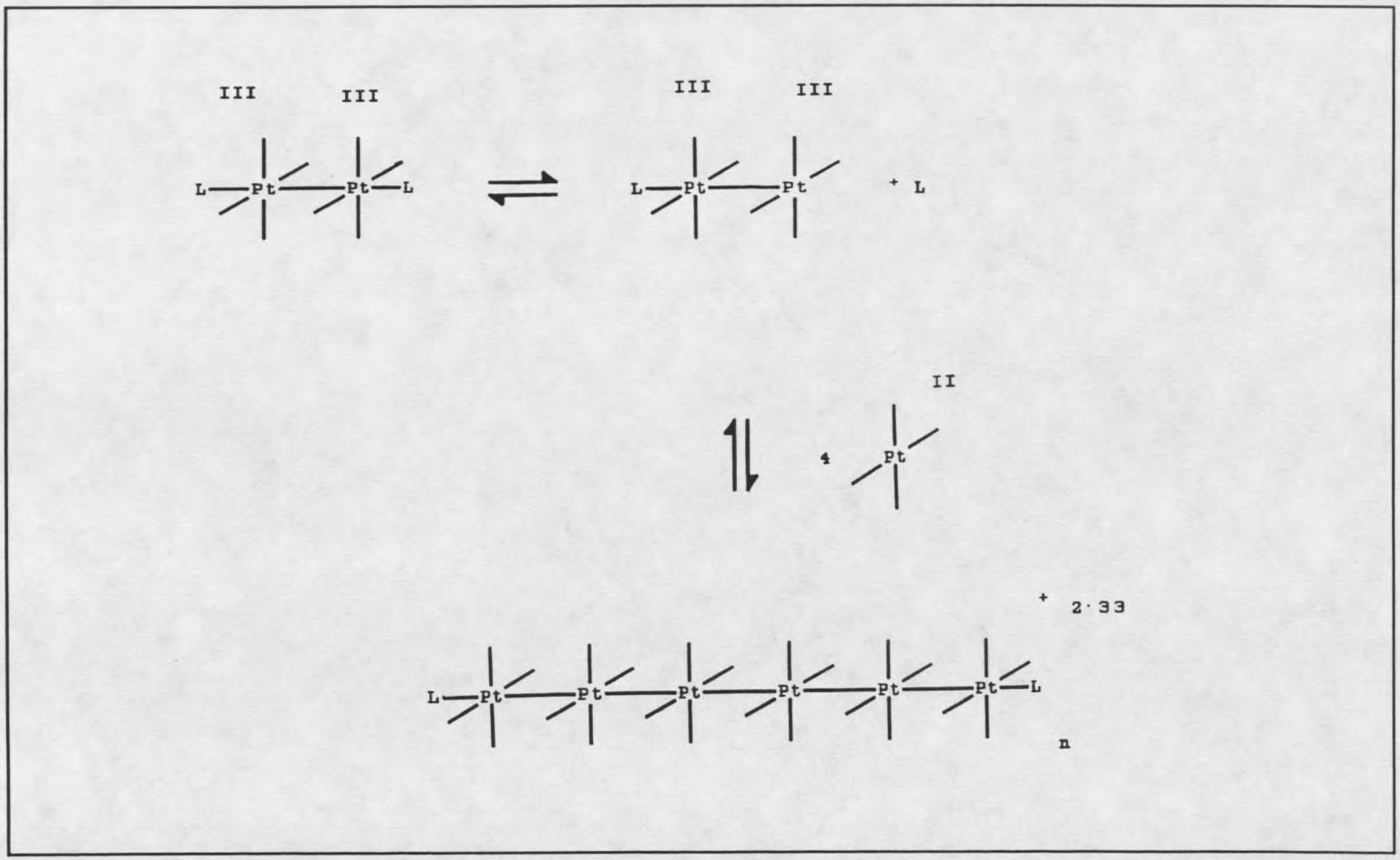

Figure 71 Pt(III) Initiated Polymerization of One-Dimensional Bis(oxalato)platinate Complexes.

REFERENCES CITED

1. Springborg, *J. Adv. Inorg. Chem.* 32, 55 (1988), and references therein.

2. Jameson,C.J. in Multinuclear NMR, J. Mason, Ed. (Plenum Press, New York, 1987) pp. 89-123.

3. Epstein,J.S.; Miller,A.J. *Prog. Inorg. Chem.* 20, 1 (1976), and references therein.

4. Peloso,A. *Coord. Chem. Rev.* 10, 123 (1973), and references therein.

5. Balch,A.L. in Extended Linear Chain Compounds, J.S. Miller, Ed. (Plenum Press, New York, 1982), pp. 1-30, and references therein.

6. Pregosin,P.S. *Coord. Chem. Rev.* 44, 247 (1982).

7. Williams,J.M.; Schultz,A.J.; Underhill,A.E.; Carneiro,K. in Extended Linear Chain Compounds, J.S. Miller, Ed. (Plenum Press, New York, 1982), pp. 73-115, and references therein.

8. Underhill,A.E.; Watkins,D.M.; Williams,J.M.; Carneiro,K. in, Extended Linear Chain Compounds, J.S. Miller, Ed. (Plenum Press, New York, 1982), pp. 119-154, and references therein.

9. Carneiro,K. Electronic Properties of Inorganic Quasi-One-Dimensional Compounds (D. Reidel, Dordrecht, 1985), and references therein.

10. Dodel,P.; Krogmann,K. *Chem. Ber.* 99, 3402 (1966).

11. Dodel,P.; Krogmann,K. *Chem. Ber.* 99, 3408 (1966).

12. Trotscher,G.; Micklitz,W.; Schloohorn,H.; Thewalt,U.; Lippert,B. *Inorg. Chem.* 29, 2541 (1990).

13. Sakai,K.; Matsumoto,K. *J. Am. Chem. Soc.* 111, 3074 (1989).

14. Mason,W.R. *Coord. Chem. Rev.* 7, 241 (1972), and references therein.

15. Cotton,F.A.; Walton,R.A. Multiple Bonds Between Metal Atoms (Wiley Interscience, New York, 1982), and references therein.

16. Hoffmann,R. Solids and Surfaces A Chemist's View of Bonding in Extended Structures (VCH, New York, 1988).

17. Matsumoto, K.; Fuwa,K. *J. Am. Chem. Soc.* 104, 897 (1982).

18. Newman, R.A.; Martin,D.S.; Dallinger,R.F.; Woodruff,W.H.; Stiegman,A.E.; Che,C.M.; Schaefer,W.P.Miskowski,V.M.; Gray,H.B. *Inorg. Chem.* 30, 4647 (1991).

19. Muraveiskaya, G.S.; Kukina,G.A.; Orlova,V.S.; Estaveva,O.N.; Porai-Koshits,M.A. *Dokl. Akad. Nauk SSSR* 226, 76 (1976).

20. Cotton, F.A.; Falvello,L.R.; Han,S. *Inorg. Chem.* 21, 1709 (1982).

21. Appleton, T.G.; Hall,J.R.; Neale,D.W. *Inorg. Chim. Acta* 104,19 (1985).

22. Yamaguchi, T.; Sasaki,Y.; Ito,T. *J. Am. Chem. Soc.* 112, 4038 (1990).

23. Steele, B.R.; Vrieze,K. *Trans. Met. Chem.* 2, 169 (1977).

24. Peterson,E.S.; Bancroft,D.P.; Min,D.; Cotton,F.A.; Abbott,E.H. *Inorg. Chem.* 29, 229 (1990), and references therein.

25. Zipp,A.P. *Coord. Chem. Rev.* 84, 47 (1988), and references therein.

26. Arrizabalaga, Ph.; Castan,P.; Laurent,J.P. *Chem. Phys. Let.* 76, 548 (1980).

27. Renn,O.; Albinati,A.; Lippert,B. *Angew. Chem. internat. Edit.* 29, 84 (1990), and references therein.

28. Barton,J.K.; Rabinowitz,H.N.; Szalda,D.J.; Lippard,S.J. *J. Am. Chem. Soc.* 99, 2827 (1977).

29. Matsumoto, K.; Takahashi,H.; Fuwa,K. *J. Am. Chem. Soc.* 106, 2049 (1984).

30. Matsumoto, K.; Takahashi,H.; Fuwa,K. *Inorg. Chem.* 22, 4086 (1983).

31. Sakai, K.; Matsumoto,K.; Nishio,K. *Chem. Lett.* 0, 1081 (1991).

32. Krogmann,K. *Angew. Chem. internat. Edit.* 8, 35 (1969), and references therein.

33. Keller,H.J. in, Extended Linear Chain Compounds, J.S. Miller, Ed. (Plenum Press, New York,1982), pp. 357-402.

34. Clark,R.J.H. *Chem. Soc. Rev.* 19, 107 (1990).

35. Balch,A.L. *Ann. N.Y. Acad. Sci.* 313, 651 (1978).

36. Papavassiliou,G.C. *J. Phys. Chem.* 10, 489 (1977).

37. Elding,L.I. *Inorg. Chim. Acta* 20, 65 (1976).

38. Mattes, V.R.; Krogmann,K. *Z. anorg. allg. Chem.* 332, 247 (1964).

39. Rimkus, V.G.; Preetz,W.Z. *Z. anorg. allg. Chem.* 0, 73 (1983).

40. Grabowski, A.; Preetz,W.Z. *Z. anorg. allg. Chem.* 0, 101 (1987).

41. Werner,A. *Z. Anorg. Chem.* 12, 51 (1896).

42. Cromer,D.T.; Waber,J.T. International Tables for X-ray Crystallography; Kynoch: Birmingham, England, 1974; Vol. IV, pp 72-98, 149-150.

43. Appleton,T.G.; Hall,J.R.; Neale,D.W.; Thompson,C.S.M. *Inorg. Chem.* 29, 3985 (1990).

44. Appleton, T.G.; Hall,J.R.; Neale,D.W.; Thompson,C.S.M. Rosenfeld,A.; Apfelbaum,H.C.; Blum,J.; Gibson,D. *Inorg. Chem.* 29, 3985 (1990).

45. Appleton, T.G.; Hall,J.R.; Hambley,T.W.; Prenzler,P.D. *Inorg. Chem.* 29, 3562 (1990).

46. Toftlund,H. *J. Chem. Soc. Chem. Commun.* 0, 837 (1979).

47. Simonsen, O.; Toftlund,H. *Inorg. Chem.* 20, 4044 (1981).

48. Bitha, P.; Morton,G.O.; Dunne,T.S.; Delos Santos,E.F.; Lin,Y.; Boone,S.R.; Haltiwanger,R.C.; Pierpont,C.G. *Inorg. Chem.* 29, 645 (1990).

49. Bruck, M.A.; Bau,R.; Noji,M.; Inagaki,K.; Kidani,Y. *Inorg. Chim. Acta* 92, 279 (1984).

50. Appleton, T.G.; Hall,J.R.; Ralph,S.F.; Thompson,C.S.M. *Inorg. Chem.* 28, 1989 (1989).

51. Hoch, J; Milburn,R.M. *Inorg. Chem.* 18, 886 (1977).

52. T.G. Appleton, *Inorg. Chem.* 23, 3521 (1984).

53. Barton,J.A. *Biochem.* 1, 1 (1992).

54. Katoh, M.; Miki,K.; Kai,Y.; Tanaka,N.; Kasai,N. *Bull. Chem. Soc. Jpn.* 54, 611 (1981).

55. Reis, A.H.; Peterson,S.W.; Washecheck,D.M.; Miller,J.S. *Inorg. Chem.* 15, 2455 (1976).

56. Wu, Li.; Schwederski,B.E.; Margerum D.W. *Inorg. Chem.* 29, 3578 (1990).

57. Al-Baker,S.; Dabrowiak,J.C. *Inorg. Chem.* 26, 613 (1987).

58. Kuroda, R.; Neidle,S.; Ismail,I.M.; Sadler,P.J. *Inorg. Chem.* 22, 3620 (1983).

59. Faggiani,R.; Lippert,B.; Lock,C.J.L.; Rosenberg,B. *Can. J. Chem.* 60, 529 (1982).

60. Appleton,T.G.; Hall,J.R.; Ralph,S.F. *Inorg. Chem.* 24, 4685 (1985).

61. Zemskov,S.V.; Ptitsyn,B.V.; Lyubimov,V.N.; Malakhov,V.F. *Russ. Journ. Inorg. Chem.* 12, 648 (1967).

62. Grinberg,A.A.; Ptitzuin,B.V. *Ann. inst. platine* 11, 77 (1933).

63. Groning,O.; Elding,L.I. *Inorg. Chem.* 28, 3366 (1989).

64. Groning,O.; Drakenberg,T.; Elding,L.I. *Inorg. Chem.* 21, 1820 (1982).

65. Teggins, J.E.; Milburn,R.M. *Inorg. Chem.* 3, 364 (1964).

66. Teggins, J.E.; Milburn,R.M. *Inorg. Chem.* 4, 793 (1965).

67. Ismail, I.M.; Kerrison,J.S.; Sadler,P.J. *J. Chem. Soc. Chem. Commun.* 0, 1175 (1980).

68. Poe, A.J.; Vaughan,D.H. *J. Chem. Soc.* 0, 2844 (1969).

69. Drougge, L.; Elding,L.I. *Inorg. Chem.* 27, 795 (1988).

70. Brown, C.; Heaton,B.T.; Sabounchei,J. *J. Organomet. Chem.* 142, 413 (1977).

71. Gamsjager,H.; Murmann,R.K. *Adv. Inorg. Bioinorg. Mech.* 2, 317 (1983), and references therein.

72. Welch,G.L.; Hamm,R.E. *Inorg. Chem.* 2, 295 (1963).

73. Hamm,R.E.; Kollrack,R.; Welch,G.L.; Perkins,R.H. *J. Am. Chem. Soc.* 83, 340 (1961).

74. Frank, M.J.; Huchital,D.H. *Inorg. Chem.* 11, 776 (1972).

75. Kukushkin,V.Y. *Zh. Neorg. Khim.* 33, 1905 (1988).